What Drives Isoprene in Tropical Australia?

Rebecca Leigh Wilson, MSPH

This thesis is submitted to

Macquarie University and The University of Edinburgh

for the degree of Doctor of Philosophy

Department of Environmental Sciences

School of Geosciences

July 2018

MACQUARIE University SYDNEY·AUSTRALIA

THE UNIVERSITY of EDINBURGH

Abstract

Isoprene is the dominant biogenic svolatile organic compound (BVOC) emitted from plants across the globe, with a mass of 400-600 Tg emitted annually. Its emission and chemical degradation plays a central role in the atmosphere, contributing to the formation of ground-level ozone and secondary organic aerosol. Tropical ecosystems contribute up to 75% of the global isoprene budget.

Seasonal isoprene emission patterns in tropical regions remains unclear, particularly when compared to the mid-latitudes. It was hypothesised that in tropical regions, isoprene would be consistent throughout the year. However, a 12-year record of satellite observations of formaldehyde (HCHO) over the Amazon basin showed that HCHO columns reduced by 20-40% each year during the wet-to-dry transition. This thesis verifies these observations and investigates the hypothesis with a long-term, ground-based measurement study in a rainforest environment, paying particular attention to this transition period.

To improve understanding of seasonal isoprene emissions patterns I conducted a measurement and modeling campaign in Far North Queensland to understand the drivers of isoprene emission in tropical Australia. A Fast Isoprene Sensor was installed in the Daintree Rainforest and I measured canopy-level isoprene concentrations over three years. They show that isoprene emissions follow a seasonal cycle, which differs from the Amazon. The measurements are compared against GOME-2B satellite observations and MEGAN and MLC-CHEM models to investigate factors driving emission patterns across several timescales.

Findings show that model bias decreases by over 10% when leaf area index varies in response to the growing season and the emission factor is optimised by time and season.

This is the first major BVOC study to be conducted in the Daintree, and is the first isoprene study in tropical Australia in over 20 years. The results presented in this thesis represent the first observations of seasonal isoprene emission patterns in Australia and provide an important contrast to other tropical ecosystems.

Declaration

I declare that this thesis is my own work and has not been submitted in any form for another degree or at any other University or institution. This thesis contains only original material. Any additional help received during the perparation of this work has been indicated in the 'Contributors' section.

Rebecca L. Wilson

Acknowledgements

First and foremost I would like to thank my supervisors Peter Nelson and Paul Palmer. I will always count myself lucky that I had two mentors to show me how good science is done, and your encouragement, patience, flexibility, and combined wealth of experience allowed me to grow in ways I wouldn't have had I only worked with one of you. Both of you extended yourselves to make this joint structure sucessful, and I'm truly grateful. Many thanks also go to Tony Morrison for selflessly taking time out of his own work to help me with mine. Field trips, equipment repairs, ideas, suggestions, and advice; the list is endless. This project would have certainly taken much longer without your invaluable assistance. To my examiners, thank you for taking the time to read this work. Finally, acknowledgement is due to the Department of Environmental Science at Macquarie and the School of Geosciences at Edinburgh, who worked together to bring this project from an idea into a reality with their financial support and did their best to make the transitions between continents as seamless as possible.

I've always joked that I should thank Qantas but really, this project would have been much more difficult without the help of many people. The Daintree Rainforest Observatory staff: Andrew Thompson, Johan Larson, and Peter Byrnes. Michael Liddell, Susan Laurance and Nico Weigand at James Cook University, thank you for your insights and knowledge of the region. And thanks for letting me store my gear when we were evacuated for Cyclone Ita. Ian Jamie, Soo Jean Park, and David Cameron, thank you for your assistance with the

Contents

List of Tables

List of Figures

Chapter 1

Introduction

Isoprene (2-methyl-1,3-butadiene, C_5H_8) is a colourless volatile liquid that is emitted into the atmosphere by many trees and shrubs. It is a basic building block of a family of chemicals known as terpenes, which, along with other plant-emitted alcohols, esters, carbonyls, and acids, are known collectively as biogenic volatile organic compounds (BVOC). BVOC emissions play important roles in plant health, metabolism, communication, and reproduction (Finlayson-Pitts and Pitts, 2000; Sharkey and Yeh, 2001; Sharkey et al., 2008). Went (1960) first presented evidence of biogenic emissions in a largely qualitative form, comparing the hazes above forests (Figure 1.1) to anthropogenic (smog) and natural sources (sea salt).
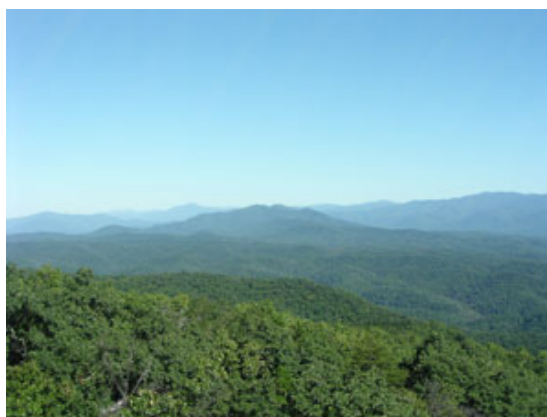
Figure 1.1: BVOCs create haze over the Smoky Mountains. *Photograph by U.S. National Park Service*

The emission and degradation of BVOCs plays a central role in trace atmospheric chemistry, contributing to both the formation and removal of pollutants and greenhouse gases such as ozone (O_3), carbon monoxide (CO), and methane (CH_4). Specifically, isoprene has been shown to have several influences on ambient air: it is a precursor to secondary organic aerosol formation (SOA) (Carlton et al., 2009; Claeys et al., 2004); it affects the hydroxyl radical (OH) balance (Lelieveld et al., 2008; Taraborrelli et al., 2012); and it can both promote and inhibit ground level O_3 formation, which in turn affects human health and local vegetation. In addition, its contribution to formation of SOA causes atmospheric cooling while the persistence of CH_4 causes isoprene to be an indirect contributor to global warming.

Forested areas dominate isoprene emissions, and hardwood trees such as oaks, poplars, and eucalyptus dominate global emissions (Finlayson-Pitts and Pitts, 2000). An estimated 400-600 Tg of isoprene are emitted annually across the globe (Guenther et al., 1995); the largest contribution of isoprene (up to 75%) comes from tropical forests (Guenther et al., 2006). However, the isoprene emission patterns of tropical forests are poorly understood, particularly in Australia, Africa, parts of Southeast Asia and globally across seasonal timescales. Due to its size and global interest in saving the Amazon rainforests, this region has been well documented (e.g., Kesselmeier et al., 2000; Rinne et al., 2002; Yañez Serrano et al., 2014, and others). Recently, there has been increased interest in other tropical regions, including Southeast Asia (Langford et al., 2010; Lim et al., 2011; Llusia et al., 2014; MacKenzie et al., 2011; Padhy and Varshney, 2005a,b; Tambunan et al., 2006) and Africa (Marais et al., 2014). BVOC emission patterns have been shown to differ between forests in the Amazon and Asia (Langford et al., 2010). In Australia, there are fewer isoprene emissions studies, and those that exist tend to focus on the mid-latitudes (He et al., 2000; Winters et al., 2009). To date, there is only one isoprene study in tropical Australia (Ayers and Gillett, 1988).

Isoprene emissions, background, and a site description and research plan are presented in this chapter. In Sections 1.1 and 1.2, the occurrence and function of isoprene is discussed, followed by a description of how it oxidizes in the atmosphere and a comparison of other ground-based canopy studies in tropical latitudes. The chapter concludes in Section 1.4 with a discussion of the major research questions and an overview of the thesis structure.

1.1 Background to Isoprene: Natural Occurrence and Function

1.1.1 Discovery

Guivi Sanadze first reported the biogenic emission of isoprene by plants grown in a greenhouse environment in the USSR in 1957 (Figure 1.2, Sanadze, 1957). Sanadze led a team of researchers in evaluating the volatile products emitted from acacia (*Robina pseudo acacia L.*), poplar (*Populus nigra L.*), willow (*Quercus iberica Stev.*), and box tree (*Buxus sempervirens L.*). Isoprene was identified and its emission was characterised as a light- and temperature- dependent process in these very early experiments. Reinhold Rasmussen independently corroborated Sanadze's findings in the United States in 1965 (Rasmussen and Went, 1965), and in 1970 isoprene was positively identified using mass spectrometry (Rasmussen, 1970).
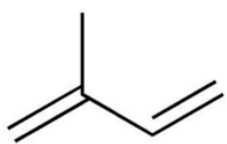
Figure 1.2: The structure of the isoprene molecule.

Isoprene's light and temperature emission dependence were confirmed in the 1970s and it was during this time that Went posed the question "what happens to

the 17.5 x 10^7 tons of terpene-like hydrocarbons or slightly oxygenated hydrocarbons once they are in the atmosphere each year?" (R. Kamens, UNC, personal communication, 2007). Went (1960) suggested that these biogenic compounds are responsible for the blue haze seen over forests in Appalachia, and to a lesser extent, in the western United States. They are also responsible for the haze over the Blue Mountains to the west of Sydney.

1.1.2   The Hows and Whys of Isoprene Emission

Isoprene is created within a plant and emitted by the isoprene synthase (IpS) enzyme acting on dimethylallyl pyrophosphate (DMAPP) (Sharkey et al., 2008; Silver and Fall, 1991) along the mevalonate (MEP) metabolic pathway (Schwender et al., 1997) and can make up to 2% of photosynthetic activity (Figure 1.3 Sharkey et al., 2008). Strong isoprene emitting species tend to be fast-growing dicots (e.g, poplars, willows, eucalypts) or monocots (e.g, reeds, Dani et al., 2014). Understanding a plant's regulation of isoprene emission necessitates understanding the regulation of the enzymatic pathways. While every plant has a MEP pathway, not every plant makes isoprene. Plants that do not make isoprene lack a gene that allows them to synthesise the IpS enzyme (Sharkey et al., 2005). Not every plant within the same family will emit isoprene, and there are no clear observable traits to definitively indicate isoprene emission, so classifying isoprene emitters and non-emitters without direct measurement is challenging (Pacifico et al., 2009).

There are several hypotheses to explain isoprene emission patterns among plant families. The studies that have looked at phylogenetic patterns have not reached consistent conclusions (Dani et al., 2014; Hanson et al., 1999; Harley and Monson, 1999; Monson et al., 2013; Sharkey and Monson, 2014). Monson et al. (2013) believes that the capacity to emit isoprene has been gained and lost several times throughout the evolutionary record. They suggest that the
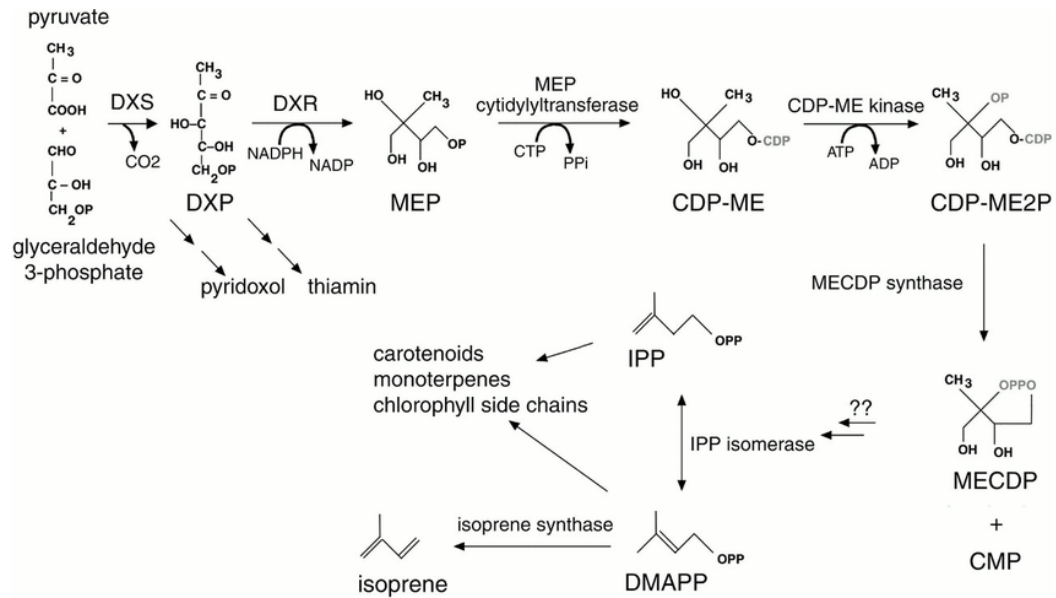
Figure 1.3: A schematic of the MEP pathway. *Image adapted from Sharkey and Yeh (2001).*

capacity was conserved in locations where it benefitted the plant most. Sharkey and Monson (2014) presents an alternative hypothesis, that plants gained the capacity to emit isoprene in one evolutionary change, and then progressively lost it through several different evolutionary occurrences. Dani et al. (2014) suggests that emission capacity occurs when a plant is capable of undergoing significant speciation, which generally occurs in long-lived plants that grow faster than most trees. Loreto and Fineschi (2015) suggest that examining the patterns of isoprene-emitting plants might yield some clues. For example, if one examines the plants that tend to emit isoprene (broad-leafed deciduous plants), one might find that these trees see more benefit to emitting during the growing season than trees where isoprene emission is low, such as conifers.

In addition to the capacity for isoprene emission, plants also differ in rates of emission. Emission rates are largely determined by plant species; however, growth and environmental factors are also heavily influential in determining how much a given plant emits. Such factors include plant and leaf age, and historic and current climatic conditions (Sharkey et al., 2008). Immature leaves are not capable of emitting isoprene; photosynthesis (commonly used as an indicator of

leaf maturity) typically commences some weeks before isoprene emission (Harley et al., 1994; Sharkey and Loreto, 1993; Sharkey et al., 2008). Wiberley et al. (2005) found that leaves that are grown under high temperature conditions will begin to emit isoprene several days sooner than leaves grown at a lower temperature. As leaves age, and near senescence, both their isoprene emission and rate of photosynthesis declined (Harley et al., 1994).

Isoprene is often emitted by plants that have high photosynthetic rates, which is a characteristic of plants that do not live in challenging environments, such as deserts. However, a leading hypothesis for why plants emit isoprene is that it protects the leaves against stress (Loreto and Schnitzler, 2010; Vickers et al., 2009). Isoprene emission activity has been shown to be largely resistant to the changes that drought stress can bring on a plant, as emissions continue even under conditions that cause photosynthetic capacity to deteriorate (Monson et al., 2007; Tingey et al., 1981). This indicates that isoprene might contribute to a plant's thermoregulation, since water stress can often lead to heat stress. However, isoprene emission is reduced in high CO_2 environments (Rosenstiel et al., 2003; Scholefield et al., 2004); trees grown in such environments have lower than average amounts of IpS, which can account for longer-term emissions reductions. Additionally, isoprene may not be emitted in plants that are adapted to stressful living conditions (e.g, arid regions).

In addition to a thermotolerance role, there are several other current hypotheses to explain why plants emit isoprene. In a review of the state of the science from a botanical perspective, Sharkey (2009) suggest several possibilities for why plants emit isoprene: it could serve as a metabolic relief valve for releasing phosphate that is "stuck" in dimethylallyl diphosphate (DMADP); a mechanism for dissipating energy; or serve to protect against damage from O_3, singlet oxygen (O^1D), and other reactive oxygen species (ROS).

Though the basic mechanisms of how isoprene is emitted are known, there

are still active lines of research for botanists to explain why isoprene is emitted (Sharkey, 2009). Sharkey (2009) states that current lines of inquiry should include topics such as why does isoprene respond so strongly to temperature and light; why does emission decline in high CO_2 environments; why are there diurnal and seasonal cycles; and why is isoprene only emitted by mature leaves. In addition, botanists are still interested in understanding how carbon moves through a plant to be finally emitted as isoprene; and understanding how the rate of synthesis is controlled by a plant.

These lines of questioning for botanists are all pertinent for tropical regions. While it is known that isoprene production is strongly dependent on the availability of sunlight and warm temperatures, both these criteria are present in abundance in tropical regions. Rainforests throughout Southeast Asia are undergoing rapid land-use changes, which will undoubtedly change the emission profiles of the region.

Diel and seasonal variation in the tropics is particularly intriguing. In the mid-latitude and polar latitudes of both hemispheres, there is a significant difference in hours of sunlight between summer and winter. This corresponds to warmer and colder temperatures and plants' growing seasons. In tropical latitudes, the temperatures are more constant year-round, and there is little change in sunrise and sunset times through the year. This gives rise to an almost continuous growing season, which in turn would support the hypothesis of year-round isoprene emissions. However, satellite studies over the Amazon indicate that isoprene emission may follow a seasonal cycle in a tropical environment (Barkley et al., 2009).

Ground studies from the region seem to reflect the same phenomenon (Yañez Serrano et al., 2014). However, studies from Borneo indicate that this is not a feature of those forests (Langford et al., 2010). There, isoprene emissions remain fairly constant throughout the year. One stark difference between these two

tropical ecosystems is that Borneo is a wet tropical rainforest that receives rainfall year-round, and the Amazon exhibits distinct wet and dry seasons. Differences in tree species between the two continents may also explain the difference in emission patterns. Though similar fractions of deciduous and evergreen plants are isoprene emitters, there are relatively few deciduous trees (e.g., maples, birches, poplars) anywhere in the tropics (Loreto and Fineschi, 2015). In Australia, there are almost no measurements of isoprene emission rates in the tropics. The only study that has been done in tropical Australia was over the course of a few days in 1988 (Ayers and Gillett, 1988). Inventories are usually comprised of observations from midlatitude species and extrapolated to tropical ecosystems (Emmerson et al., 2016; He et al., 2000), but current estimates remain significantly different from reported values (Emmerson et al., 2016; Guenther et al., 1995).

1.2   Isoprene in the Atmosphere

Once emitted into the atmosphere, isoprene's initial oxidation mechanisms are fairly well understood (Figure 1.4, Finlayson-Pitts and Pitts, 2000; Seinfeld and Pandis, 1997). The oxidation process begins when isoprene reacts with one of three compounds: $OH\cdot$, O_3, or nitrate (NO_3). In the first step of the oxidation process, isoprene is attacked at one of its two carbon double bonds (a total of four possible attack sites). The respective concentrations of OH, O_3, and NO_3 determines which species first reacts with isoprene, but OH is usually the first reactant. Subsequent additions of oxygen and NO produces one of six possible configurations of an alkoxy compound, which react further with NO. If O_3 is the initial reactant, the decomposition occurs through an ozonide pathway. Formaldehyde (HCHO), methacrolein (MACR), and methyl vinyl ketone (MVK) are the primary products of isoprene reacting with $OH\cdot$ or O_3. Isoprene reaction with NO_3 is slightly different; it leads to the formation of C5-hydroxynitrato carbonyls or

HCHO with a C4-nitrato carbonyl.
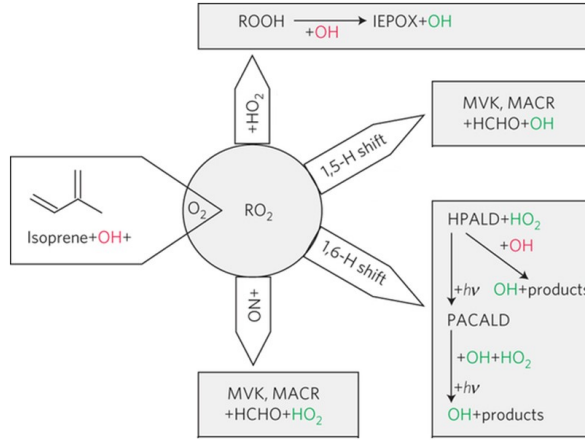
Figure 1.4: A schematic showing the pathways of isoprene oxidation and the final products. Red text indicates compounds that are lost in the reaction, green text indicates where compounds are re-formed. IEPOX indicates isoprene epoxydiol, MVK indicates methyl vinyl ketone, MACR indicates methacrolein, HPALD indicates hydroperoxy aldehydes, and PACALD indicates phenylacetaldehyde. *(Image adapted from Fuchs et al. (2013))*

Isoprene oxidation plays a significant role in rural and urban environments across the globe. Its significance in urban air pollution was found when atmospheric scientists sought to understand the precursors driving the formation of ground-level ozone, smog, and other secondary pollutants (Jeffries et al., 2013). As Jeffries states, 'Imagine [in the 1970s] having to tell [city planners] that they would have to spend [money] to reduce exposure to a gas that no one emitted and no one knew for sure how it came to be there.' Atlanta, GA, USA, serves as a classic example of local urban air pollution that is heavily influenced by the isoprene emission of surrounding forests (Chameides et al., 1988; Geron et al., 1995). There, as with other urban areas, oxides of nitrogen (NO_x) are present in excess due to anthropogenic emissions.

$$(R1)\mathrm{OH} + \mathrm{Isoprene}(^+\mathrm{O}_2) \longrightarrow \mathrm{RO}_2$$

$$(R2a)\mathrm{RO}_2 + \mathrm{NO} \longrightarrow \mathrm{RO} + \mathrm{NO}_2$$

$$(R2b) \mathrm{RO_2 + NO \longrightarrow RONO_2}$$

$$(R3) \mathrm{RO_2 + HO_2 \longrightarrow ROOH + O_2}$$

$$(R4) \mathrm{RO_2 + RO_2 \longrightarrow 2\,RO + O_2}$$

$$(R5) \mathrm{RO + O_2 \longrightarrow carbonyls + HO_2}$$

$$(R6) \mathrm{HO_2 + NO \longrightarrow NO_2 + OH}$$

$$(R7) \mathrm{OH + NO_2 \longrightarrow HNO_3}$$
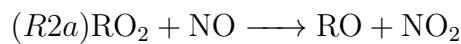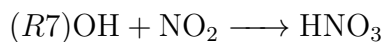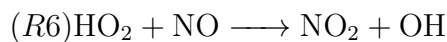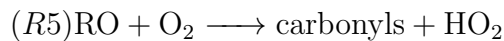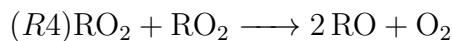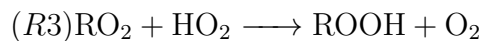
The reactions listed above summarise Figure 1.4, particularly the reaction after the initial oxidation (Barket et al., 2004). NO_x (NO + NO_2) is a combustion product and its presence or absence is a key determinant of the final ratios of isoprene oxidation products shown in Figure 1.4 and as R2-R4 in the reactions above. Concentrations emitted from tailpipes range from a few ppm to several hundred ppm, depending on the make and model of the vehicle, and its operating conditions (Turns, 1996). If isoprene begins to oxidize in an urban (high NO_x) area, its first reaction product, a reactive oxygen species broadly classed as RO_2, reacts with NO (R2a), producing NO_2. The NO_2 quickly photolyses and combines with O_2 to form tropospheric O_3 (Harley and Monson, 1999). Though classed as a secondary air pollutant because it is formed, rather than directly emitted, O_3 is a powerful greenhouse gas. High O_3 is related to increased global warming (Forster et al., 2007). Increased levels of O_3 have been positively correlated to hospital admissions, particularly for cardiopulmonary complaints (Bell et al., 2005, 2004; Goldberg et al., 2001), and has been shown to damage plants by reducing photosynthetic capacity, decreasing growth rates, and lowering crop yields (Booker et al., 2009; Wang et al., 2007).

Isoprene and other BVOCs in urban areas are precursors to the formation of peroxyacetyl nitrate, which is a component of photochemical smog (PAN, Fis-

cher et al., 2014; Seinfeld and Pandis, 2006). It is a reversible reaction of the peroxyacetyl radical with NO_2:

$$CH_3C(O)OO + NO_2 + M \longleftrightarrow PAN + M \,,$$
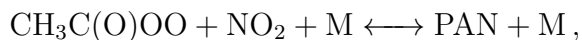
where M is usually either N_2 or O_2. In a modeling study combining global ground measurements, Fischer et al. (2014) reports that isoprene is responsible for 37% of the global PAN budget. Isoprene is the largest contributor; no other VOC contributes more than 10%. PAN has a highly variable lifetime (between 3 hours and 13 days), which enables it to serve as a reservoir for NO_x (Seinfeld and Pandis, 2006). PAN is primarily thermally and photolyticially degraded; warmer temperatures leading to lower concentrations and cooler temperatures contribute to higher PAN concentration (Pippin et al., 2001; Talukdar et al., 1995). If it is transported aloft (into lower temperatures) after formation, it is possible for PAN to be transported long distances before degradation, which in turn releases NO_x into airsheds where it is not typically found, such as remote or forested locations.

When isoprene is emitted into and oxidizes in a rural environment, where low NO_x regimes prevail, the effects are quite different. First, isoprene oxidation in a low NO_x environment will often reduce tropospheric O_3. This is because RO_2 will react with itself (R4) or with O_3 when NO is reduced or absent (Harley and Monson, 1999).

Where high NO_x environments can cause isoprene to be a precursor to photochemical smog, low NO_x environments can cause it to be a precursor to secondary organic aerosol (SOA). This is because, in the absence of NO_x, the reaction rates of 1st degree products are slower, allowing time for particle condensation (Kroll et al., 2006). The homogeneous nucleation of isoprene yields very low levels of SOA: only ∼2% of the original mass will end up as aerosol (Lee et al., 2006). However, catalysing the reaction with an acidic seed does yield aerosol growth

(Czoschke et al., 2003). Cloud chamber studies, using conditions typical of the Amazon, have estimated that SOA formation from isoprene could contribute up to 1.6 Tg/year, which would constitute up to 20% of the biogenic contribution to the global aerosol load (Lim et al., 2005). The SOA originating from isoprene oxidation products is hygroscopic in nature, and can serve as cloud condensation nuclei (CNN). This is important for global climate change as numbers of CCN can affect cloud formation and rainfall patterns.

In rural airsheds, isoprene and CH_4 can often be found together. Similar to isoprene, the first reactant in the oxidation process of CH_4 is generally $OH^\cdot$, however the reaction rate constant of CH_4 with $OH^\cdot$ (k=6.40 x 10^{-15} cm^3 $molecule^{-1}$ s^{-1} at 298 K Atkinson, 2003) is much slower than isoprene (k = 101 x 10^{-12} cm^3 $molecule^{-1}$ s^{-1} at 298 K Seinfeld and Pandis, 2006). As a result, isoprene is comparatively a much stronger driver of tropospheric chemistry than CH_4, and can indirectly influence the decay rates of CH_4 as well as CO concentrations in the atmosphere (Guenther et al., 1995; Sanderson et al., 2003; Seinfeld and Pandis, 1997). This is vitally important in the tropics, as the atmosphere in the tropical latitudes is where 80% of the global methane burden is removed (Monks et al., 2009).

The ability to understand and replicate the processes controlling BVOC emissions and their ultimate fate in the atmosphere is necessary for understanding future conditions and climate change. However, there are still significant uncertainties associated with emissions of isoprene and other BVOCs (Monks et al., 2009) . Globally, isoprene emission estimates have reached a precision of approximately a factor of two, but for any given time and location, that uncertainty can be as much as a factor of five (Guenther et al., 2006). Uncertainties associated with mono- and sesquiterpenes are larger, and vary by individual compound (Monks et al., 2009). Monks et al. (2009) states that the tropics are critical for climate, due to the high irradiance and humidity found in these latitudes. These

uncertainties have an impact on emissions predictions, which in turn has a limiting effect on the ability to predict SOA, aerosols, and other GHGs and estimate their impact on regional air quality and larger climate changes (Monks et al., 2009).

The primary suggestion to bound these uncertainties is additional observational studies, with an emphasis on variation in spatio-temporal scales (Monks et al., 2009; Pacifico et al., 2009). These observations, in combination with satellite observations and model studies, provides an integrated approach that improves understanding of the mechanisms driving BVOC emissions, fate, and transport. An integrated approach improves climate models, and allows researchers to address concerns about air quality, the impacts of land use change and shifting agricultural practices, and biogenic response to climate change (Laothawornkitkul et al., 2009; Monks et al., 2009).

1.2.1   Field Studies of Isoprene

Due to its prevalence, isoprene is the focus of many field studies. Its spatio-temporal and genetic specificity also means that in order to gain a comprehensive understanding of global emissions, many studies are needed. The majority of field studies occur in the mid-latitudes of the northern hemisphere, spanning a few days to a few weeks. On the shortest of timescales, a plants responsiveness related to isoprene emissions can change within a matter of minutes (Pugh et al., 2011). Laboratory and field studies also indicate that isoprene emissions are driven by circadian rhythms, that is, isoprene emission is not 'switched on' as soon as threshold temperature and radiation level are reached (Hewitt et al., 2011). Instead, emission rates rise in the morning, peak at midday, and decrease in the afternoon. In the mid-latitudes and further pole-ward, isoprene emission patterns follow a plant's growing season. Plants begin to emit a short time after bud burst in the spring (Pressley, 2005). In Australia, studies also tend to be cen-

tered around the mid-latitudes, specifically the eucalypt forests of southeastern Australia (He et al., 2000; Winters et al., 2009). These studies are important as eucalypts are strong emitters of isoprene, and their emission patterns are still very poorly captured by global emissions models (Emmerson et al., 2016). Emmerson et al. (2016) states that this is because emission factors for *Eucalyptus* were calculated using an enclosure measurement of young trees, where field measurements show that the emission rates of mature trees (seven years old) are several times lower than younger trees (two years old).

There is a growing interest in longer-term studies in order to understand how isoprene changes seasonally, as leaves and trees mature, or in response to long term environmental stresses, such as drought. These studies can help improve air quality forecasts where BVOC-induced ground-level ozone is a problem, improve model performance, and give insight into plant response to land use and climate change. This will then change the chemical balance of regional airsheds around the world. Elevated CO_2 levels, and changed growing conditions can affect isoprene emissions across a plant's lifetime, and increased plant stress in the form of droughts and severe weather events also affect plant productivity and isoprene emission (Loreto and Fineschi, 2015; Sharkey et al., 2008). Pressley (2005) published the longest-running isoprene data set, from Michigan, USA, which spans four years. Pressley collects isoprene flux samples throughout the growing period, as isoprene emission effectively ceases after leaf senescence each year. During the growing season, they observed high fluctuations between day-to-day observations at this northern hardwood forest. In a similar vein, Potosnak et al. (2014) conducted a seasonal study of isoprene emissions to validate an oak-dominated forest. The longer time series allowed for a study of the longer-term sunlight impacts. The occurence of a drought during the study also allowed for a different, and valuable data set to test the model.

Due to a relative lack of accessibility and infrastructure, there are fewer stud-

ies focused on tropical ecosystems than mid-latitude and tundra environments, even though tropical forests contribute up to 75% of global emissions (Guenther et al., 2006) and drive a significant portion of the tropospheric chemistry of the tropical latitudes (Guenther et al., 1999). Isoprene emissions estimates over the tropical regions are frequently inferred from satellite retrievals of total columns of HCHO, which will be further discussed in Section 1.2.2. Inferring emissions from tropical regions can be challenging due to the complex interplay between biomass burning, biogenic emissions, and climate, as well as the dynamics of the Intra-tropical Convergence Zone (ITCZ) and El Niño Southern Oscillation (ENSO) (Barkley et al., 2009, 2008).

However, there are still several canopy-scale field studies of tropical ecosystems, summarised in Table 1.1. Geron et al. (2002) did leaf-level studies on 20 of the most abundant plants at a lowland rainforest station in Costa Rica. Rinne et al. (2002) show above-canopy data from the wet to dry (WtD) transition season over a 3-day period over the Amazon, with mixing ratios of 4-5 ppb. Kuhn et al. (2002) conducted a similar study in a different part of the forest during the same season, and found mixing ratios nearly double that amount. A more recent study by Yañez Serrano et al. (2014) is the first seasonal study over the Amazon, stretching for two periods during the wet and dry seasons. While this is an important study, providing some longer-term continuity of record and establishment of emissions profiles at that new site. Yañez Serrano et al. (2014) observe a distinct seasonality, which echoes satellite observations; however, this study did not include the transition seasons, where previous investigation of satellite observations showed intriguing results (Barkley et al., 2009).

1.2.2 Satellite Studies

Satellite observations provide an alternative method to quantify global isoprene emissions. In particular, they are essential to the observation of isoprene in loca-

Table 1.1: Over-canopy Measurements of Tropical Isoprene

Location	Forest Type	Season	Study Length	Concentration/Flux*	Instrument	Study
Tapajos, Brazil	terra firme rainforest	WtD	3 days	4-5 ppbv	FIS	Rinne et al. (2002)
Jaru-Rondonia, Amazonia	tropical rainforest	WtD	unknown	9.00 ppbv	GC-FID, GC-MS	Kuhn et al. (2002)
Sarpiqui, Costa Rica	lowland tropical wet	dry	3 days	2.2 mg C m^{-2} h^{-1}	GC-MS	Geron et al. (2002)
ATTO, Manaus, Amazonia	terra firme rainforest	dry	10 days	4-6 ppbv	PTR-MS, GC-FID	Yañez Serrano et al. (2014)
TT34	terra firme rainforest	dry	94 days	2.8 ppbv	PTR-MS	Jardine et al. (2011)
K34, Manaus, Amazonia	lowland rainforest	dry	20 days	3.4 ppbv	solid sorbent, GC-MS	Kuhn et al. (2007)
C14	terra firme rainforest	wet	21 days	6-7.5 ppbv	solid sorbent, GC-MS	Kesselmeier et al. (2000)
ATTO, Manaus, Amazonia	terra firme rainforest	wet	14 days	1-2 ppbv	PTR-MS, GC-FID	Yañez Serrano et al. (2014)
Danum Valley, Malaysia	wet rainforest	dry	17 days	1.5 ppbv	PTR-MS	Langford et al. (2010)
Danum Valley, Malaysia	wet rainforest	dry	30 days	2.5 ppbv	PTR-MS	Langford et al. (2010)

* Average daily maxima

tions inaccessible to surface measurements. Earth observation satellites, such the European Space Agency's Global Ozone Monitoring Experiment (GOME) satellite, provide meteorological, trace gas, and aerosol data to researchers on a 3-day cycle (Figure 1.5 De Smedt et al., 2008, 2012, 2015). It is difficult to directly observe isoprene by satellite, but formaldehyde (HCHO), one of isoprene's reaction products, is a weak absorber of the wavelengths monitored by the satellite and it has a known lifetime, which makes it possible to derive the original emissions. The yield of HCHO is approximately 0.3 ppbv/ppbv isoprene emitted in a low nitrogen oxide (NO_x) environment, and given respective compound lifetimes ($\sim$1.8 hours for isoprene, $\sim$3 hours for HCHO), the emission rate at a given location can be inversely modeled using satellite observations. This method has uncertainties such as biomass burning (production of HCHO), high winds (displacement errors or 'smearing'), and the satellites cannot observe below clouds (cloud cover must be <40%). Efforts are made to constrain these errors (Marais et al., 2012), as HCHO satellite retrievals are important tools to estimate emissions in locations where ground-based data is sparse or impossible to obtain.
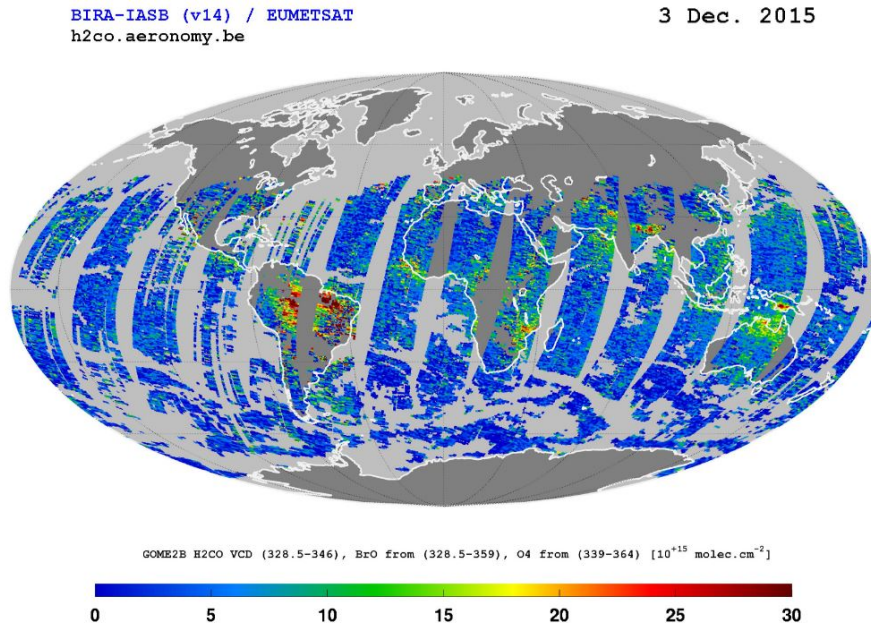
Figure 1.5: Columns of HCHO, as observed from the GOME-2B satellite. *Image from TEMIS*

Extensive work to quantify long-term isoprene emissions over the entire Amazon using satellite measurements has been done by Barkley et al. (2009, 2008). Initially, work was done to understand the net fluxes over the entire Amazon basin (Barkley et al., 2008). Over the Amazon, ground-based *in situ* studies are sparse, resulting in a challenging environment to study region-wide fluxes. Satellite data poses additional challenges due to significant biomass burning that occurs on a regular basis, and retrieval errors from the satellite data itself (Barkley et al., 2008). The retrieved satellite data was paired with the limited observational data as well as estimates from the Model of Emissions of Gases and Aerosols from Nature (MEGAN) model. Barkley et al. observed a strong seasonality in the *in situ* observations that the model was not able to capture well. When the modeled emissions were linearly regressed against observed satellite HCHO columns, the temporal variation was captured well, however the spatial variation was poorly represented. The model was found to generally over-predict emissions, particularly in the western part of the Amazon (where there is less biomass burning) during the dry season (when there are higher temperatures and light levels). Barkley et al. (2009) further explored the temporal variability in an analysis of 12 years of satellite observations over the Amazon. Barkley et al. (2009) demonstrates that on a seasonal time scale, variation in HCHO columns over the Amazon basin reflect variations in the isoprene mixing ratio (Figure 1.6). The analysis shows a reproducible annual minimum in the transition between the wet and the dry season, with a 20-40% reduction in these months (Barkley et al., 2009). However, the transition from the dry to wet seasons does not show the same dramatic reduction.

The original hypothesis as to why this reduction occurs was that though the trees in the rainforest are green year-round, an annual leaf flushing occurs in preparation for the dry season. Analysis of NASA's Moderate Resolution Imaging Spectroradiometer (MODIS) Leaf Area Index (LAI) and Enhanced Vegetation
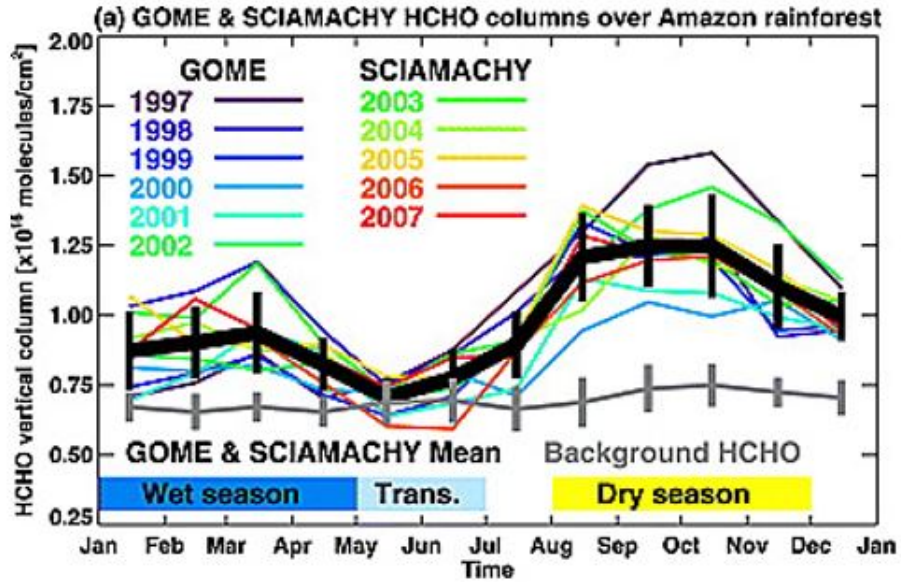
Figure 1.6: Plot showing satellite data indicating a shutdown of isoprene emissions over the Amazon Rainforest *(image reproduced from Barkley et al. (2009))*

Index data over the Amazon show significant leaf flushing during the wet-to-dry transition, indicating the trees' preparation for warmer, sunnier conditions (Myneni et al., 2007). This seasonally-driven annual leaf turnover, and subsequent new growth, accounts for 30% of HCHO column variability found in satellite data (Barkley et al., 2009). It is also possible that this leaf cycle regulates the wet season, as well. Myneni et al. (2007) report that increases in leaf evapotranspiration at the end of the dry season appears to drive changes in surface air buoyancy, thus increasing the likelihood of convection and rainfall. Another hypothesis is that trees adapt their LAI in response to environmental conditions, optimizing for the available sunlight and soil moisture (Caldararu et al., 2012).

Africa is a significantly under-represented continent in the realm of tropical studies, and an analysis of the satellite measurements has only recently been completed (Marais et al., 2014). Marais et al evaluated the HCHO columns derived from the Ozone Monitoring Instrument (OMI) satellite (Marais et al., 2014). They found a strong seasonality in the savannas surrounding the equator, and a much weaker seasonality within the equatorial forests. The OMI-derived

HCHO emissions were found to be approximately twice as high as the direct measurements (from two campaigns), though it was acknowledged that one of the campaigns was over vegetation that contained a relatively low fraction of isoprene-emitting species (Harley et al., 2003; Serça et al., 2001). The other reference of direct measurement, an aircraft study, had a larger sampling footprint and corresponding variability in emissions (Greenberg et al., 1999). This could be a factor in the discrepancy between *in situ* and satellite-derived isoprene measurements.

Southeast Asia represents an important area of study, as rapid land-use change is changing the biogenic emissions profile in a substantial way. However, deriving isoprene emissions from satellite data is a challenge here as there is significant biomass burning, which confounds the data. There has also been significant land-use change: forests have been converted to palm oil plantations at a rapid rate (Stavrakou et al., 2014) and cropland in China is being converted to tree plantations, increasing the regional isoprene load (Geron et al., 2006). In addition, rapid industrial growth in India, China, and the rest of Southeast Asia has changed the aerosol loading in the region, causing dimming of incoming radiation and changing cloud cover patterns (Stavrakou et al., 2014). This dimming has some effect on isoprene emissions, as its manufacture is dependent upon photosynthetically available radiation (PAR) levels. Stavrakou et al. (2014) compared GOME HCHO columns against modeled output constrained by a single field campaign. Like other tropical regions, it was found that the model overpredicted satellite-derived emission estimates in the equatorial forests of Malaysia and Indonesia. However, in India and China, where the aerosol loading is more variable, the estimates were less consistent, first underpredicting and then overpredicting. There was an observed cooling episode across the Asian continent during that time.

1.3 Emissions Inventories and Chemical Modeling

Emission models are an important tool to understand biogenic emission patterns on a global scale. By fitting together physical and chemical processes, it is possible to present a detailed, cohesive picture of biogenic emissions and atmospheric conditions to make predictions about future conditions with a high degree of confidence.

Biogenic emissions models, which aim to replicate the interactions between the atmosphere and the terrestrial biosphere, are classified as either multi-layer canopy models or big leaf models. Multi-layer models explicitly solve for CO_2, energy exchange, and chemical transport and integrate emission fluxes across all layers to determine total flux (Leuning et al., 1995). These models provide detailed information about parameters typically measured at the leaf level, as well as intra-canopy behaviour (Dai et al., 2004). However, this is computationally expensive and often necessitates a reduction in either spatial coverage or time. Alternatively, big leaf models incorporates all properties of a canopy (from ground to the top of the canopy) into a single leaf to calculate flux (Dai et al., 2004; Dickinson et al., 1998). By lumping parameters into coupled equations, big leaf models are less computationally intensive for the same space and time requirements. Their primary shortcoming is that they must make assumptions about the vertical profile of a canopy and other leaf-level parameters (Dai et al., 2004).

One of the most widely-used multi-layer emissions models is the Model of Emissions of Gases and Aerosols from Nature (MEGAN) model (Guenther et al., 2006, 2012). MEGAN uses base emissions from different ecosystems (classified as plant functional types) and constrains them with local environmental factors. This is considered a 'bottom-up' method for building models, as the base emissions are extrapolated from available field and laboratory studies, and estimated

where none exist. MEGAN can also be simplified by parameterizing the results of the multi-layer model into a big leaf version. As discussed in Section 1.2.2, isoprene emission estimates over the tropics are frequently inferred from satellite observations (Pacifico et al., 2009), but this can be difficult due to retrieval errors and biomass burning, which can be widespread. The meteorological intricacies of the Intertropical Convergence Zone (ITCZ) and El Niño/Southern Oscillation (ENSO) makes modeling tropical climates difficult as well (Barkley et al., 2009, 2008).

MEGAN has been found to have a higher estimate of isoprene fluxes across the tropical latitudes in comparison to studies using inverse models based on satellite observations or concentration estimates (Barkley et al., 2008; Marais et al., 2014; Stavrakou et al., 2014). Though some of the differences can be attributed to the fundamental differences between bottom-up versus top-down approaches, there are other factors that could explain the differing estimates across continents. In the Amazon, MEGAN was found to poorly capture the seasonal emission cycle, though it did a better job in the dry season than other parts of the year (Barkley et al., 2008). In Africa, the equatorial forests were found to have the strongest positive bias compared to the other plant types in the study, such as savanna (Marais et al., 2014). One reason for this overestimation could be that plant- and canopy-level emission data for African vegetation is quite limited, and extrapolations have been made from other continents (Guenther et al., 2006, 2012). The sources of emissions overestimations are more uncertain in Southeast Asia. This is a result of there being relatively few *in situ* studies in the region, and rapid land-use changes introduce significant uncertainties (Stavrakou et al., 2014). In addition, industrialisation is changing the aerosol loading and cloud cover patterns across India and China, which are not always represented in meteorological data sets that are paired with MEGAN. However, a more recent study has indicated that satellite studies, as a whole, underestimate isoprene

emissions (Gu et al., 2017).
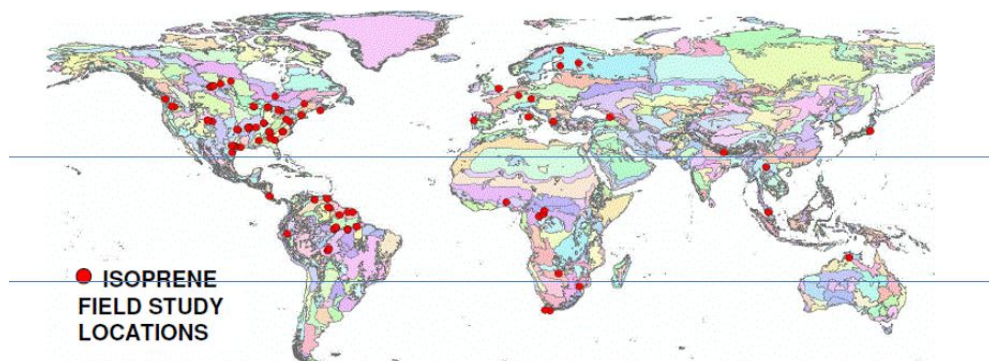
Figure 1.7: Map indicating study sites used to develop MEGAN. Horizontal lines indicate the Tropics of Cancer and Capricorn. *(Image reproduced from Guenther et al. (2006))*

As MEGAN relies on field observations to build its emissions profiles, it suffered from the same lack of field studies discussed in Section 1.2. Figure 1.7 shows the locations of the field observations used to build the original MEGAN model. North America and Europe have the highest concentration of studies, followed by South America. While the amount of observational data to develop the updated model is greatly expanded (Guenther et al., 2012), observations from Africa, Australia, and parts of Southeast Asia remain underrepresented.

The MEGAN estimates across Australia remain largely uncertain. The first iteration of the model (Guenther et al., 2006) contained only one study from the Australian continent (Ayers and Gillett, 1988) (Figure 1.7). The Ayers and Gillett study occurred over a 5-day period in the grassy region to the west of Darwin, Australia. The second iteration of MEGAN (Guenther et al., 2012) draws from a more robust data set to estimate emissions by Australian trees. However, a recent study shows that MEGAN estimates across Australia could differ from observations by as much as a factor of six, despite the incorporation of additional observations (Emmerson et al., 2016). This is likely due to the fact MEGAN was developed using leaf-enclosure measurements from trees in the

Northern Hemisphere, and trees that were young. Eucalypts have been shown to have a decreasing isoprene emission along the tree's lifetime, so the overall age of trees in a canopy is an important consideration for an emissions profile. In the Australian tropics, the emissions profile remains totally uncharacterised. Given that MEGAN overestimates emission rates in tropical rainforests on other continents compared to the satellite observations discussed in Section 1.2.2, it is reasonable to hypothesize that this is the case in Australia as well. However, there have been no field or laboratory studies to date of isoprene emission of Australian tropical trees, so it is unknown how they compare to species used in the characterisation of the plant functional types used in MEGAN.

1.4   Research Questions and Study Structure

Although we have a good understanding of isoprene emission patterns in temperate and boreal forests, our understanding of tropical emissions patterns, especially on a seasonal scale, is more limited. Fundamental questions remain unanswered, including: does the seasonal variation observed via satellite over the Amazon reflect ground-level emissions patterns? If ground-based observations do reflect a seasonally-based change, what processes –botanical or environmental –are driving this change? Are emission patterns the same across all continents in the tropics? If there are seasonal patterns, how can they best be modelled? In this thesis I will address elements of these questions by collecting ground-based measurements in a rainforest environment and comparing the findings to an emissions model to understand its drivers and which components affect performance.

In Chapter 2, I discuss the instrument setup and methodology of the fieldwork component of this research. I present a full site description, comprising of a description of the forest itself and the local and regional atmospheric drivers. Then the following hypothesis is addressed:

- **The Fast Isoprene Sensor can be adapted to run unattended on a long-term basis, and collect concentration measurements as well as flux measurements.**

I show the process of adapting the FIS to successfully operate on a largely-unattended basis at the site. This is achieved through a combination of adapting the FIS power supplies to conserve oxygen by reducing its operating times and making use of bi-hourly automatic calibrations to form a continuous zero correction that can adjust for diurnal temperature fluctuations. The instrument adaptation, from this work, along with a method to prevent FIS operation without sufficient O_2, have been shared with the instrument manufacturer. They are now offered as a standard feature or as an option for researchers interested in similar long-term installations (Hills, personal communication, 2015).

Barkley et al. (2009) states that isoprene emissions in the Amazon decrease annually during the WtD transition season ($\sim$ March - June) due to rapid leaf flushing in preparation for the warmer temperatures during the dry season. However, there was only sparse *in situ* data to refer to, and no canopy-level data to confirm the hypothesis (Barkley et al., 2009). From their work, I am testing the following hypotheses:

- **There is a seasonal emissions cycle in the Daintree Rainforest**

- **The seasonal emissons cycle follows a pattern similar to that observed in the Amazon.**

In Chapter 3, I present the data collected from the FIS and use it to test these hypotheses. A seasonal measurement and modeling study was conducted at the field site across several years, paying particular attention to the WtD transition period. These ground-based observations are then compared against satellite column observations to evaluate goodness-of-fit and whether column variability is reflective of ground-level variability at this site.

The results from the field measurement site are compared against two emissions models in Chapter 4–MLC-CHEM and a custom-built MEGAN-style model. This model is used instead of the full MEGAN model to allow for greater specificity of local conditions, and greater control over the individual elements that drive variations in emissions. I show that measured seasonal patterns of isoprene emissions are reflected in the modelled environment, and explore the hypotheses:

- **Differences in isoprene emission between Amazonian and Southeast Asian rainforests can be explained by differences in emission rates.**

I describe how the model is built, and conduct a battery of sensitivity tests to elucidate model performance. Following that, the hypothesis is tested by evaluating model output across several timescales to understand how well it follows seasonal trends, in comparison against a base-case scenario.

In Chapter 5, I summarise the research findings and discuss their implications towards the current understanding of seasonal patterns of isoprene emission in tropical forest. The thesis is then concluded with a discussion of areas for further research in the field.

1.4.1   Organisation, Logistics, and Thesis Structure

This study was designed as a joint degree program between Macquarie University (Sydney, Australia) and the University of Edinburgh (Edinburgh, Scotland), where the project would be co-managed by supervisors at each location. The research plan was structured to take advantage of the respective areas of expertise at each location and allowed me a much wider exposure to different ideas. As part of the terms of the agreement, I had to divide my time between each university, and move between them at scheduled times determined at the outset of the study. This dictated the workflow, as some tasks were location-specific.

The first year was spent at Macquarie, which also served as the location for all field- and labwork, since the study site was in Queensland. During this time, I modified the FIS for remote operation in the rainforest and the field study began approximately six months into my degree plan. This plan was somewhat delayed due to the failure of a photomultiplier tube, which prompted additional instrument testing after its replacement. After deployment of the FIS at the DRO, I returned to the field site approximately every five weeks for routine maintenance of the FIS. The FIS also required several repairs during this initial data collection period. Between field trips I also began learning the code I would need to process the data.

During the second year, I moved to Scotland and began processing the data that I had collected. It was intended that data would be collected on my behalf while I was away, but James Cook University was constructing new lab space and accommodation, which made the power supply unreliable. Given that the transition season was the primary period of interest, it was decided that I should return to Australia from March through May and conduct a series of intensive field studies, where I would be on hand to monitor progress and do any necessary repairs on the spot. In addition to this, it was decided to add a secondary method of data collection to have quality assurance on the data from the FIS. Three separate trips were planned for this period. The first was halted after three days due a cyclone, when the area was evacuated to nearby Cairns. The remaining two trips ran to completion. The FIS was left in the field after my return to Scotland, but due to continuing maintenance issues, it was decided by myself and my supervisory team to stop data collection, bring all equipment back to Sydney, and wait for my return.

The first half of year three was spent in Scotland. While there, I finished learning how to use all the modeling tools required and finished analysing the data collected during the first two years of the study. After I returned to Australia,

the data collection goal was to fill in the gaps remaining from the first two years of study. A series of three intensive campaigns were planned and completed periodically over nine months during my third year. Finalising the analysis and fitting all the data and model results together completed the study.

Chapter 2

Site Description and Methodology

Field measurements lay the foundation for understanding trace gases and the role they play in the atmosphere. The links between concentrations of these gases and major environmental challenges over the past 40 years is well documented (Hartmann et al., 2014). *In situ* measurements across several spatial and temporal scales are imperative to monitor short- and long- term changes in trace compounds and provide a reality against which a model's predictive power can be tested. Trace gases, including VOCs, can be measured from the ground-based laboratories (including mobile laboratories and ships), balloon- and air-borne measurement platforms, as well as satellite observations.

This chapter shows the development of the experimental method, with a focus on the long-term monitoring campaign. First, a site description is presented in Section 2.1, with descriptions of major drivers of the Australian tropical climate and local meteorology presented in Sections 2.3 and 2.3.1, respectively. Following that, the Fast Isoprene Sensor (FIS) is presented in Section 2.4, and I show how it was adapted to operate in a remote, humid tropical environment. A discussion of using concentration measurements instead of fluxes is presented

in Section 2.6, and the field deployment settings are described in Section 2.7. The analysis methodology is described in Section 2.8, including an analysis of performance in air conditioned and non-air conditioned settings. Following this, the methodologies of comparative methods and data are presented. Section 2.9 details the cartridge sampling methodology, with pre-deployment testing results presented in Section 2.10. The chapter closes with a description of satellite and GEOS-Chem retrieval methods in Section 2.11.

2.1   The Daintree Rainforest

Figure 2.1: Map of the Wet Tropics of North Queensland. Cape Tribulation is indicated by the pin. *(Image courtesy Google Maps)*

The Daintree Rainforest is the largest continuous rainforest in Australia, with an area of 12,000 km^2. The forest is part of the Wet Tropics of North Queensland (Figure 2.1), a geographically, meteorologically, and anthropologically complex region that is the most biodiverse area on the continent. The land where the Daintree is located has sustained a forest for approximately the last 110 million years, since the Cretaceous Age, and Tracey (1982) classifies it as a complex Mesophyll Vine forest type 1A (Russell, 1985). It contains: "30% of the marsupial

species, 60% of the bat species, 25% of the rodent species, 40% of the bird species, 30% of the frog species, 20% of the reptile species, 60% of the butterfly species, 65% of the fern species, 21% of the cycad species, 37% of the conifer species, 30% of the orchid species, and 18% of Australia's vascular plant species" currently documented (UNESCO, 2014). The Daintree and surrounding forests contain the oldest vegetation types in Australia, some dating to more than 65 million years ago (Keto and Scott, 1986). Of the 19 primitive plant species still found on the planet, 12 are located in this area. What remains of the original forest covers 0.3% of Australia's land mass, approximately 70% of which is uncleared old growth forest (as documented since European settlement). The remaining 30% of the Wet Tropics region has been cleared, resulting in significant fragmentation of the accessible low-elevation and tablelands forest (Turner, 2001). The low-lying areas, in particular, were logged from the 1930's - 1980's; some of these areas have since been re-forested (Stork and Turton, 2008).

In 1988, the Wet Tropics of North Queensland was added to the UNESCO World Heritage Listings (UNESCO, 2014). The forest extends to the surf (and in some places, into it), where it meets the Great Barrier Reef, making this the only place in the world where two World Heritage Sites abut one another. Most of the land parcels (70%) in the region are protected by UNESCO, and the majority of remainder is protected by other groups, including the state of Queensland, the Wet Tropics Management Authority, and the Douglas Shire Council. The region was also named an Indigenous Protected Area (IPA) by the Australian Federal Government in 2013.

Indigenous populations have lived in the Daintree for approximately 40,000 years, which makes them the oldest rainforest-dwelling culture in the world (UNESCO, 2014). The local aboriginal groups utilize small, local fires for several cultural practices (Hill and Davis, 1999, 2003). The total biomass burned in any given year is ~1 hectare (ha), but these fires are small and do not impact the

environment on a regional scale (Hill and Davis, 1999, 2003).

The Wet Tropics still represent one of the most intensely productive corners of Queensland; tourism is one of the dominant industries (Stork and Turton, 2008). Most of the tourism impacts to the area are in the use of walking trails, camping areas, and water sources (creeks and rivers). Land that has been cleared for conversion to farm and ranch land is primarily located in tablelands and lowland rainforest. This has scattered some endemic floral and faunal species, and fractured native forest paths (Stork and Turton, 2008). The parts of the forest that retain primary growth are largely rough terrain that is difficult to access.

2.2   The Daintree Rainforest Observatory

Figure 2.2: The Daintree Rainforest Observatory.

This study was conducted at the Daintree Rainforest Observatory (DRO, 16°06' 14.8"S, 145°26' 58.0" E), a research station owned and operated by James

Cook University (Cairns, Australia), approximately 150 km north of Cairns (Figure 2.2). It is one of the few areas of lowland rainforest remaining that has not been subjected to logging activity. Though generally in the Daintree Rainforest, the parcel of land on which the DRO sits is not formally included as part of the World Heritage Site. Thus, it is not subject to direct management by UNESCO (Stork and Turton, 2008). The nearest town is Cape Tribulation (pop. 330), located 1.5 km to the north. The observatory is situated approximately 1 km inland from the coast.

A primary feature of the DRO is a canopy crane (Liebherr 91EC, figure 2.3a) that was installed in 1998 (Stork, 2008). The crane allows access to approximately 1 ha of forest canopy via a gondola (Figure 2.3b) that is lifted from the ground and can drop anywhere along the arc of the crane jib. The crane sits on a slope about 40 m above sea level and 300 m from the forest edge. A small enclosed shed and a covered, open-air staging area are located at the crane base–both were replaced during a site upgrade in 2014. The buildings are not air conditioned; however, there is a small thermostat-controlled roof fan in the enclosed shed to regulate temperature. All structures onsite are powered by diesel generator which is located near the office and living spaces outside the forest. Equipment can be moved to the base of the crane along a small gravel track either by foot or a motorised all-terrain vehicle.

The hectare of land surrounding the canopy crane supports nearly 1000 trees (comprised of 78 species), many of which are endemic to the area (Observatory, 2014). Canopy height is irregular, measuring between 25-35 m. Of the identified species, only two have been targeted as a subject in a prior isoprene study, both of which were conducted outside tropical Australia (Padhy and Varshney, 2005a). DRO staff conduct a quinquennial census of the trees in the reach of the crane with a measurement of >10 cm diameter at breast height (dbh). The most recent census was completed in 2014 (Observatory, 2014). The top five species (25.9%

(a) A canopy crane allows for sampling within and above the canopy. The author is standing on the platform collecting samples. *(Photograph by Andrew Thompson)*

(b) The gondola permits access to approximately 1 ha of forest.

of the total surveyed) represented in this hectare are:

1. *Cleistanthus myrianthus* : 91 trees

2. *Myrstica globosa ssp muelleri* : 61 trees

3. *Alstonia scholaris*: 46 trees

4. *Syzygium graveolens*: 45 trees

5. *Normanbya normanbyi*: 44 trees

Forty nine trees in the plot are unidentified.

2.3   Australian Climate and Weather

Northern Australia, from the Kimberley region in Western Australia to north Queensland in the east, experiences a tropical climate (Köppen Am/Af), with distinct wet and dry seasons (Figure 2.4). In the tropical latitudes, the climate is governed by the summer Indo-Australian Monsoon, ENSO, and the Madden-Julian Oscillation (MJO, Figure 2.5).
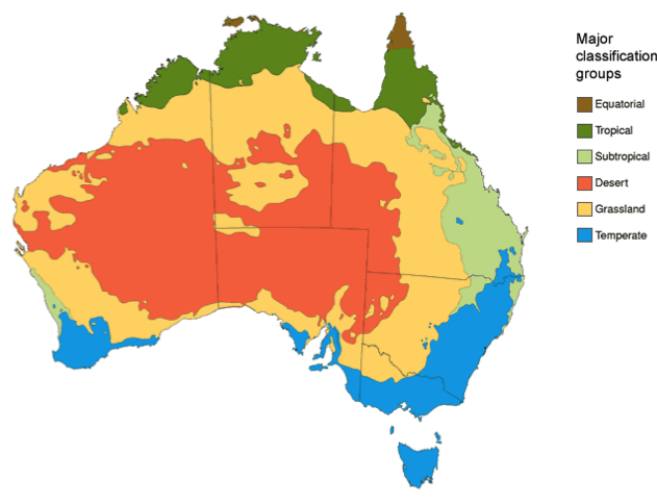
Figure 2.4: Australian climate zones, using a modified Köppen classification system. *(Image courtesy Australian Bureau of Meteorology)*

The Indo-Australian Monsoon is the main climate driver between the months of December and April. Colloquially known as "the wet", the monsoon brings heavy rainfall across the far north of the continent. Throughout most of the year, the prevailing wind is from the east or southeast. As summer approaches, winds shift to the northeast. This causes the formation of a low pressure system, and a trough that stretches across the continent. Moist air moves in from the oceans, creating conditions that facilitate widespread heavy rainfall. The trough sometimes moves back out to sea during the season, which provides a break in the rain.

The El Niño/Southern Oscillation (ENSO) is the second major forcing mechanism affecting tropical Australia. Anomalously warm sea surface temperatures in the eastern Pacific Ocean, off the coast of Peru (El Niño), accompanies high air surface pressures over the western Pacific ocean. This leads to a drier than average wet season in Tropical Australia during the summer months (November-April), and a later onset of the wet season. El Niño winters (May-October) are dry and cool. In contrast, anomalously cool temperatures (La Niña) correspond with low air surface pressures over the western Pacific Ocean, a wetter than average wet season with an earlier onset than usual. La Niña winters are typically

mild.
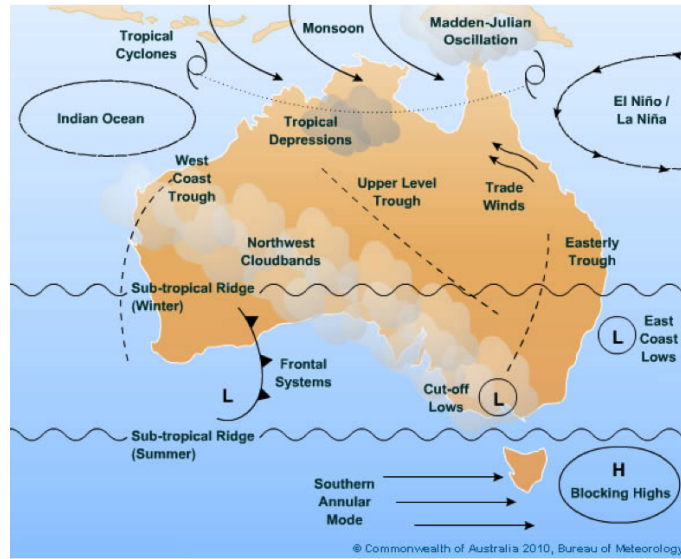
Figure 2.5: Primary meteorological factors driving Australian climate *(Image courtesy Australian Bureau of Meteorology)*

The Madden-Julian Oscillation (MJO), the third major climate driver, affects intraseasonal variability in the tropical atmosphere (Zhang, 2005). It influences rainfall variability over Pacific Islands and tropical Asia. Due to the fact that it has an interaction with ocean-atmosphere processes, there is some indication it may contribute to the evolution of ENSO. A distinct feature of an active MJO is a strong westerly wind, which runs counter to the easterly trade winds that typically dominate the region's wind pattern. At the surface, it features a large center of strong, deep convection (the "active phase"), flanked to the east and west with weak, deep convection (the "inactive" or "suppressed" phases). Globally, the active phases are easiest to identify in the eastern Indian and western Pacific Oceans, where there is a large "warm pool" to facilitate convection. The MJO is similar to ENSO in that although it is named an oscillation, the occurrence of active periods is not regular. Active periods can occur in a given location between anywhere from 30-100 days (Salby and Hendon, 1994). The MJO may also be influenced by ENSO, since ENSO affects size and location of the "warm pool".

2.3.1 Local Meteorology

The Daintree Rainforest is a tropical climate, and is affected by the forcing agents described above. The local microclimate is characterised by seabreezes with a diurnal cycle prevailing. Air temperatures are moderate compared to inland, as is common for coastal environments. Seasons are roughly divided between wet (Jan-Mar) and dry (Jun-Oct) separated by transitions (Apr-May, Nov-Dec). Sunlight hours are relatively constant during the year, with only 2 hours difference between the summer and winter solstices (Table 2.1). Average temperatures (Figure 2.6a) exhibit some seasonality; the average high temperature in the summer months (Dec-Feb) is $\sim 32°$C, and the average winter high (Jun-Aug) is $\sim 25°$C.

Table 2.1: Sunrise and Sunset at Cape Tribulation, QLD

Date	Sunrise	Sunset	Solar Elevation
June 21	06:47	17:57	50.58°
December 21	05:46	18:51	82.57°

Annual rainfall rates exhibit a distinct seasonality, with 70% of the annual rainfall occurring in the wet season, between January and March (Figure 2.6). During the transition to the dry season, rainfall amounts decrease sharply before reaching a minimum between the months of June and October. Humidity increases during November and December, with occasional heavy showers in the late afternoon and evening. Though the site is coastal, and experiences typical sea breeze conditions, the majority of rainfall occurs around sunset and during the overnight hours (Figure 2.7). However, there is significant variability within this valley (Figure 2.6b). For instance, eight years of data collection at the DRO has shown an average rainfall of $\sim$5700 mm per year, while the nearest Bureau of Meteorology station, 1.2 km north of the observatory, reports only $\sim$4900 mm. The difference between the 8-year average and the climatological averages are even greater, with the Bureau of Meteorology reporting only $\sim$4000 mm per year. The greatest discrepancy between the two is found during the wet sea-
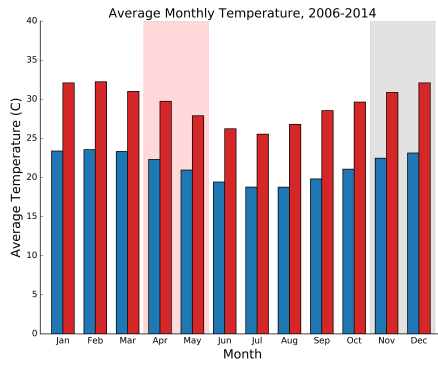
(a) Average monthly temperatures at the DRO. Red bars indicate average highs, blue bars indicate lows.
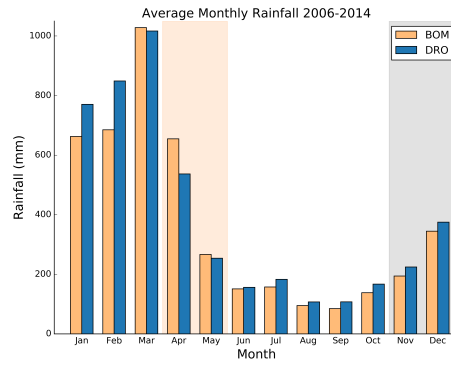
(b) Rainfall over the DRO and Cape Tribulation. The blue bars indicate rainfall measured at the DRO. The yellow bars indicate rainfall at the nearest BOM site (1.5 km north).
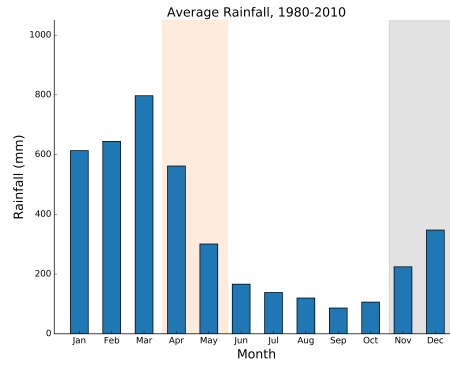
(c) Climatological monthly rainfall amounts (mm) in Cape Tribulation, QLD, recorded at the BOM station.

Figure 2.6: Climatological rainfall and temperature for the DRO. The areas shaded pink indicates the wet-to-dry transition season. The areas shaded gray indicates the dry-to-wet transition.*(Cape Tribulation data courtesy Australian Bureau of Meteorology)*

son. The differences in rates are attributed to the valleys and peaks along the coast, with similar variability in rainfall reported at other sites (M. Liddell, JCU, personal communication, 2013).

Like rainfall, the local wind patterns also exhibit a seasonality (Figure 2.8) Wind speed and direction are averaged over hourly intervals, and the period during which data was collected for the study is presented here. Annually, the predominating wind is from the SSW, with a sea breeze in the afternoon. As the
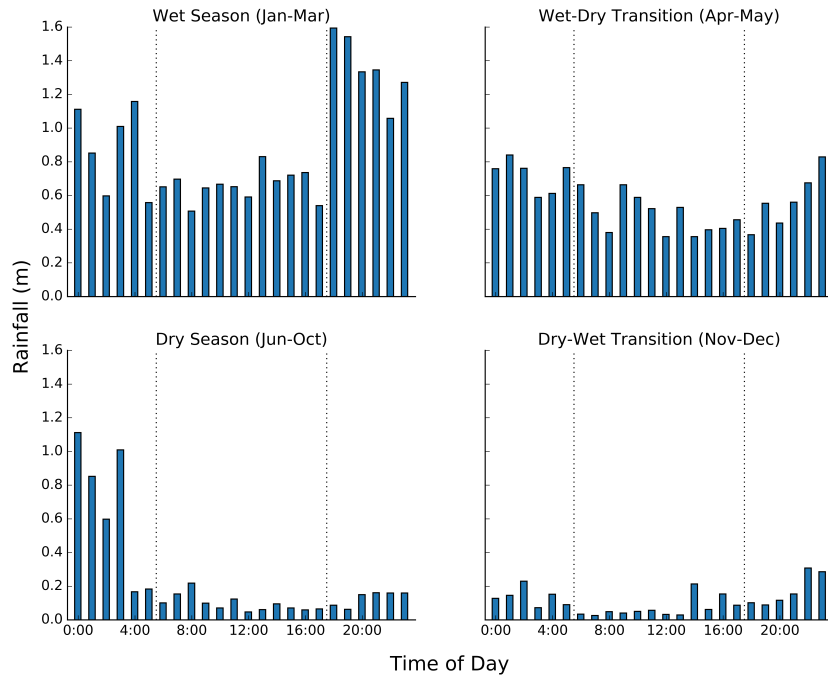
Figure 2.7: Average hourly rainfall over the DRO, grouped by season. Lines indicate 6:00 and 18:00 local time.

seasons shift from wet to dry, the wind changes, and shows a slightly stronger offshore component. It then settles into a similar pattern during the dry as seen during the wet. Finally, during the transition from dry to wet seasons, there is a much stronger offshore component.

The region also lies in the path of tropical depressions and cyclones, which typically occur during the summer and autumn (December-May). Major cyclones that have affected the area in the past include Rona (2/1999), Larry (3/2006), and Yasi (1/2011). The most recent cyclone to affect the area was cyclone Ita, which made landfall near Cooktown (30 km north of the study site) on 11 April 2014 and disrupted one of the field trips for this research. The DRO sustained minimal damage in the storm.

(a) Wet Season (JFM)

(b) Wet to dry transition (AM)

(c) Dry Season (JJASO)

(d) Dry to wet transition (ND)
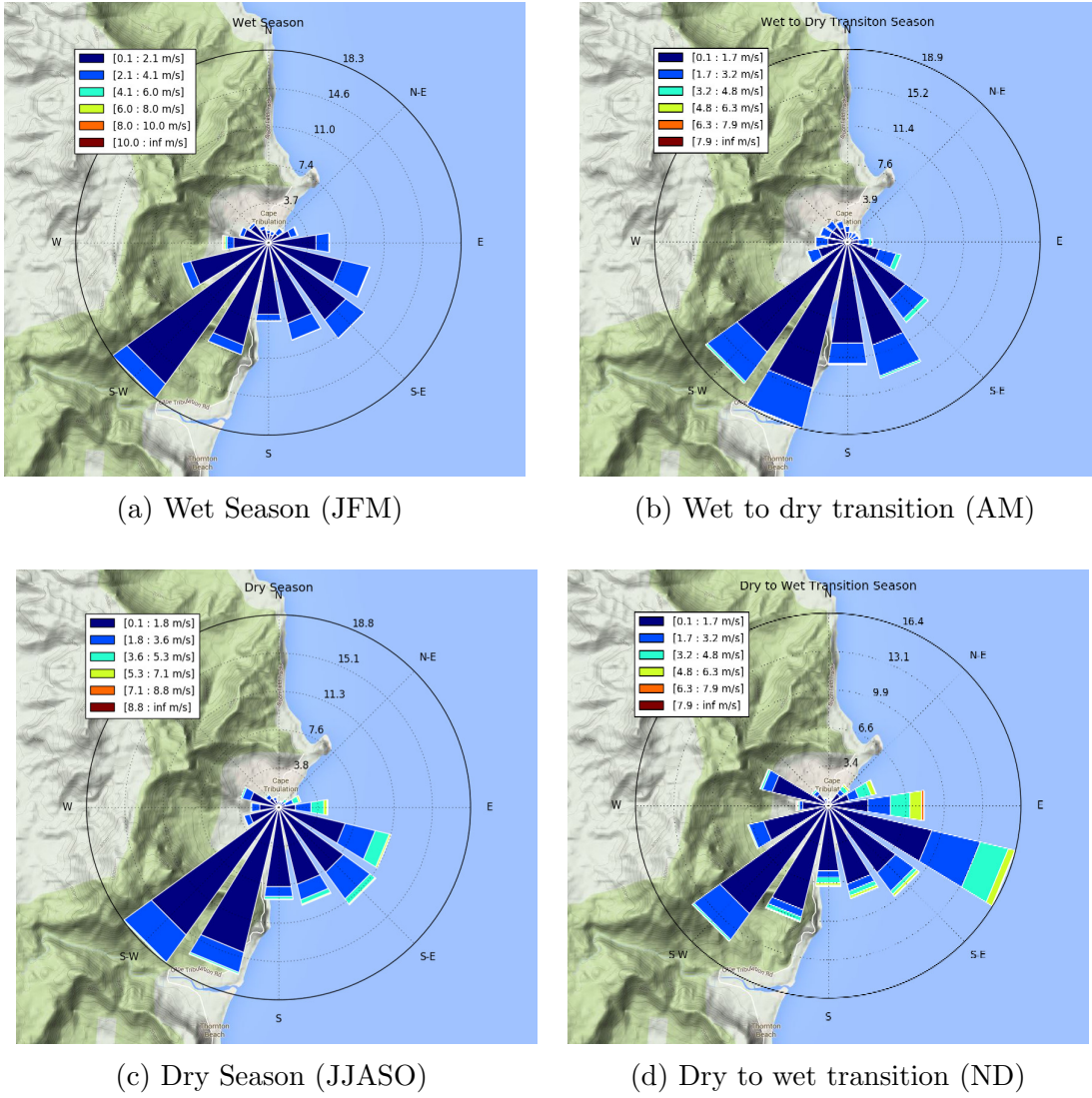
Figure 2.8: Average winds (m/s) at the DRO, grouped by season *(Background maps courtesy Google Maps.)*

2.4 The Fast Isoprene Sensor

Isoprene may be measured in several ways, including spectrometry, chemical ionisation mass spectrometry, chemiluminescence, and gas chromatography (Heard, 2006). Most of the instrumentation used in these methods are large, require mains power and a temperature-controlled environment, and are intolerant of the temperature and humidity extremes that are present in the rainforest. The Fast Isoprene Sensor (FIS) is a real-time detection system that uses chemiluminescence to measure isoprene by reacting it with an excess of ozone. This system

was developed by Alan Hills (Hills and Zimmerman, 1990), and, based on its settings, allows for the detection of isoprene from individual leaves up to canopy-level fluxes. The FIS is best used in environments with low anthropogenic influence, as other alkenes, particularly propene, can confound the signal. Monoterpenes and non-alkenes will also confound the signal, but at a significantly lower rate than isoprene at the wavelengths monitored by the FIS (Hills and Zimmerman, 1990).

The rapid response time of the FIS, which can be as short as 0.1 sec, and capacity for continuous measurement are in line with the capabilities of a Proton Transfer Reaction-Mass Spectrometer (PTR-MS)– a popular instrument for monitoring isoprene. While a PTR-MS has been used in similar short- and long-term studies in tropical ecosystems (e.g., the OP3 study in Borneo and the ATTO site in Brazil (Langford et al., 2010; Yañez Serrano et al., 2014)), it was unsuitable for this study primarily because its power consumption exceeded the amount allotted to us at the DRO. The FIS was identified as a suitable substitute for the following reasons:

1. The FIS is tolerant of generator-supplied power,

2. While the FIS does provide a more stable response when operated in air-conditioned areas, this is not a requirement for operation; and

3. The FIS has also been used successfully at other long-term measurement sites (Potosnak et al., 2013; Pressley, 2005).

To measure isoprene concentrations, the FIS draws sample air into a reaction cell chamber. In this chamber it is mixed with ozone-rich air, which reacts with isoprene and any interfering compounds which may be present; light is emitted as a consequence of these reactions. These photons are counted, averaged across a given timescale, and recorded in an external program. The impact of these confounding compounds is discussed fully in Section 2.4.1.

Ozone is supplied by an ozone generator that operates simultaneously with the FIS. Oxygen at 50 pounds per square inch (psi) is supplied to the FIS in order to maintain a pressure differential on the mass flow controllers (MFCs; BOC Gas, Australia). The oxygen is then routed to the ozone generator, and is returned to the FIS as ozone-rich air. After it is mixed with sample air in the reaction cell chamber and the isoprene reacted out, the sample + ozone passes through a catalytic converter which converts the ozone back in to oxygen, then is pumped out of the system as waste air.

Every two hours, the system goes into an autocalibration mode. In this mode, two other air supplies are used: The FIS can be supplied with isoprene from a standard tank (4.1 ppm isoprene in a balance of N_2, Scott-Marrin, Inc, Riverside, CA, USA) and a 'zero air'. This is air from nearby the FIS, of the same temperature and humidity as the sample air, that is passed through the catalytic converter to strip out any compounds that might react with ozone prior to entering the reaction cell chamber. The autocalibration is completed over the course of nine minutes every two hours, and consists of the following steps, forming a standard addition calibration:

1. sample + zero

2. standard + zero

3. sample + standard

Each step is held for three minutes. When the nine minutes are complete, the system returns to sampling mode.

2.4.1   Confounding Compounds in the FIS

The FIS is optimized to detect isoprene through its use of O_3 as a reactant and the selectivity of the photomultiplier tube (PMT) to detect photons in the

500-nm region (Hills and Zimmerman, 1990). Isoprene's response with O_3 is higher than other alkenes, as well as its efficiency for producing light within the range the PMT is set to detect. However, the FIS will detect anything with a double carbon bond, which has the potential to interfere with the measurement of isoprene. Table 2.2 shows the FIS relative response (RR) to other compounds, in decreasing order. Compounds with a RR less than 0.1 are not included here.

Table 2.2: Relative Response Factors of Alkenes in the FIS and Their Estimated Contribution

Compound	Relative Response Factor	Estimated Contribution
Isoprene	1.0	
Propene	1.0	<1%
Methyl Vinyl Ketone (MVK)	0.4	~10%
Methacrolein (MACR)	0.4	~10%
2-Methylpropenal	0.19	
Ethene	0.15	
2-Methyl-3-Buten-2-ol (MBO)	0.15	nil
Dimethyl Sulfide (DMS)	0.12 (0.54)*	<1%
3-Butene-2-one	0.12	

* indicates with (without) a DMS filter on the input line. A DMS filter was not used in this research.
(Table reproduced from Hills and Zimmerman (1990))

Propene (RR = 1.0) and ethene (RR = 0.15) are byproducts of combustion, with highly variable concentrations ranging from ppt-ppb. Concentrations can be higher in the tropics due to biomass burning (Hewitt, 1998). 1000-2500 ppt and 100-500 ppt ethene and propene, respectively, were observed in a boreal forest in Finland in March and September– months where daylight hours are similar to that found in the tropics ($\sim$ 12 hours Hakola et al., 2006). Seasonal differences in ethene concentrations were likely due to the source of the air masses, with those coming from remote areas cleaner. In addition, Hakola et al. observed higher concentrations during periods of lower daylight, reflecting the photochemical nature of the reaction. In the tropics, where hours of daylight are more consistent, a lower seasonality would be expected. Though the DRO is quite remote, there are still cars and cargo ships in the vicinity. If the propene concentration is estimated

at the high end of the Arctic estimates, this is 0.0025 ppb, which would affect FIS measurements at a fraction of a percent.

Methyl vinyl ketone (MVK) and methacrolein (MACR) are two intermediate reaction products from the oxidation of isoprene. Yañez Serrano et al. (2014) found mixing ratios up to 2.80 ppb (MVK + MACR). As a ratio of isoprene, MVK+MACR mixing ratios were 20% the level of isoprene within the canopy, rose to 30% above the canopy, and reached 50% at the highest levels measured (79 m). It would be reasonable to assume a MVK+MACR mixing ratio at 1/3 that of isoprene. As the two have different relative response factors, a conservative estimate would use the higher response factor. If, given any isoprene mixing ratio, there is also MVK+MACR at 1/3 the amount, and all of it reacted in the FIS at a RR of 0.4 (all MVK), that leads to a change in FIS response of 11%. Assuming a mass contains only MACR (RR of 0.25) leads to a change in FIS response of 7%. Therefore, it would be cautious to estimate isoprene mixing ratios as being ∼10% lower than reported by the FIS.

MBO (RR=0.15) is a compound readily emitted by conifers (Goldan et al., 1993). Since it was first discovered, its presence has been documented in several field studies, in northern hemisphere pine forests (e.g., Geron et al., 2016; Karl et al., 2012). There are two pines native to Australia: the hoop pine and the bunya pine. The hoop pine is found in dry rainforests and is not in the same taxonomic family as northern hemisphere pines. The bunya pine is found across Queensland, but its presence in the wet tropics is quite restricted. It is only found in two locations, at altitudes > 500 m (CSIRO). As such, the estimated contribution of this compound is negligible. Mango is another tree which has been observed to emit MBO (Jardine et al., 2013). However, no mangoes are found in the hectare surrounding the canopy crane (Observatory, 2014).

DMS (RR = 0.12,0.54) is the most abundant sulfur compound emitted into the atmosphere. The largest source of DMS is marine emissions by phytoplank-

ton, which could be a consideration given the DRO is a coastal site bordering the Great Barrier Reef. Its lifetime is short, between 11 min and 46 h (Marandino et al., 2013). Shipboard measurements taken off the Great Barrier Reef show measurements between 150-450 ppt (Marandino et al., 2013). As this FIS is not equipped with a filter for DMS, the RR factor would be 0.54, but even with the assumption of the highest end of the estimate, this would affect FIS measurement by a factor of $< 1\%$.

2.5 FIS Pre-deployment Testing and Modifications

In order to ensure that the FIS would be able to run autonomously in the field for up to six weeks at a time, several instrument modifications were required. The primary issues to be addressed were oxygen consumption and protection from the elements–weather and pests.

Ants and rodents were two invaders of concern at the field site. Several species of ant live in the area, but two are likely to be found in the vicinity of the FIS and sampling line: a green ant (*Oecophylla smaragdina*), a harmless species which can be found climbing along the length of the sampling line, and a red ant (*Wasmannia auropunctata*) that is attracted to electrical equipment and could build a nest inside the FIS, given the opportunity. Rodents in the area are capable of chewing through any exposed tubing or wiring, and seek refuge in dry areas during the wet season. The first instrument shed where the FIS was housed showed signs of prior rat activity. Some equipment was damaged while the FIS operated out of this building, but no data was lost. A replacement shed was constructed in March 2014; there were no indications of rodent presence for the remainder of the field studies.

To combat these threats, a stainless steel case was designed and commissioned to house the FIS (Samuelson, Sydney, Australia). This case was fitted with Swagelok ports to allow for sample and exhaust lines to be delivered into and out of the FIS without propping the case open. The case was also fitted with two 120 mm, 240 V fans (Jaycar YX2514, Sydney Australia), oriented so air flowed through the case at a rate of 3.0 m^3/min. The intended configuration of the box is that the FIS and ozoniser are stacked on top of one another and the box is latched closed. Data is recorded on a computer located outside the box. A window allows for monitoring of the system without opening the box. The fans are located in the top half of the case; thus the instrument that is on top experiences greater cooling. When the FIS and ozoniser were stacked on top of one another inside the closed case, the heat generated by the ozoniser caused the interior temperature to exceed 50°C within 30 min., which irreversibly damaged the photomultiplier tube (PMT). A second tube was installed, and a second set of 120 mm fans were installed. The FIS and ozoniser were then tested in various configurations within the case to find an arrangement that would not cause a significant rise in interior temperature and subsequent failure of FIS parts.

2.5.1   Temperature tests

Temperature trials were conducted to determine the rate of heating of the FIS PMT under various configurations within the exterior case. Tests were conducted on Macquarie University campus, first in a lab where the temperature is maintained at 22° C, and then in a temperature-controlled room maintained at 37° C. The ozoniser was the primary generator of heat in the system (Figure 2.9) and the photomultiplier tube (PMT), located within the FIS, is the most sensitive component. Irreversible damage is caused when the PMT is operated or stored at temperatures exceeding 50° C. A temperature sensor was attached to the exterior of the PMT, and temperatures were recorded every five minutes. In order

to prevent damage to any of the instrument components, tests were stopped and the configuration declared unworkable if and when the PMT temperature reached 45° C. The FIS system was tested under three different configurations:

1. The ozoniser stacked on top of the FIS (Figure 2.9, blue line)

2. The FIS was placed inside the case and the ozonizer kept outside (Figure 2.9, green line)

3. No case used (Figure 2.9, red line)
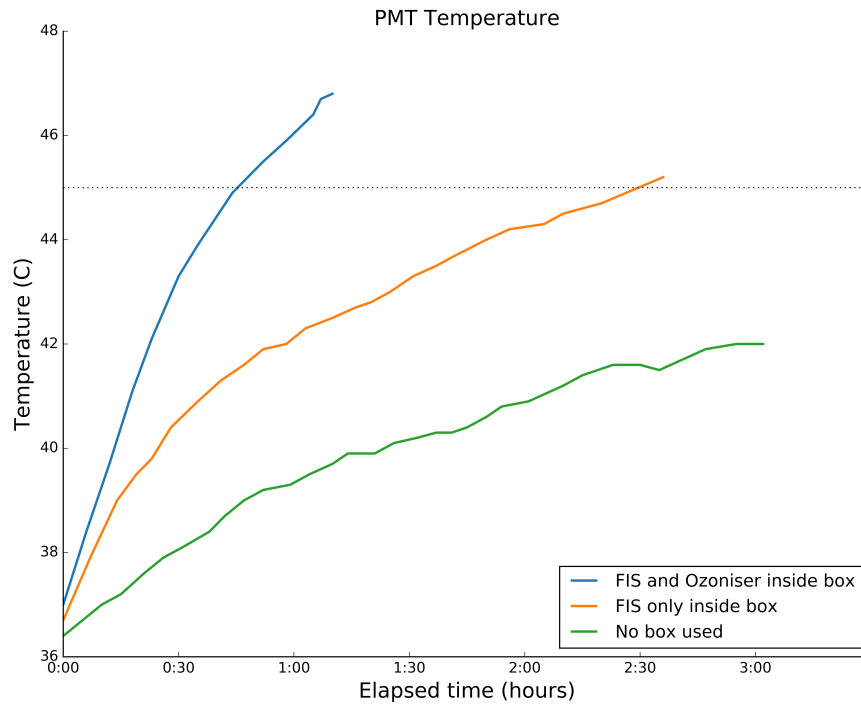
Figure 2.9: The results of the temperature trials with various fan configurations. The blue line indicates the PMT temperature when the FIS and ozoniser were both running inside the protective case; the green line indicates the PMT temperature when only the FIS running inside the case, with the ozoniser outside, and the red line indicates the PMT temperature when no box was used. Trials were stopped when the PMT temperature reached 45°C, indicated by the horizontal dotted line.

Testing the system with the FIS stacked on top of the ozoniser was deemed unnecessary because that is what caused the initial PMT failure. Evaluating the

data from this configuration showed the PMT failed within 30 minutes. The two configurations with equipment enclosed in the box were tested with no fans running, two fans, and finally four, shown in Figure 2.9. This was tested in order to determine whether the fans were capable of cooling the system at all. When those configurations failed, running the system outside was tried, though it was never considered as a long-term experimental setup because it offered no protection to the FIS. However, this was the most successful configuration.

Configurations where the ozoniser was on the bottom, blowing exhaust onto the FIS, all saw steadily rising PMT temperatures. The fans were capable of slowing the rise in temperature, but not controlling it, or maintaining equilibrium at an acceptable temperature. When each component of the FIS system was placed in the box separately, temperatures were controlled with 4 fans running. However, temperature control was only achieved near the threshold where the PMT sustained damage.

A test on the successful configuration was repeated in April 2013 at the DRO in the instrument shed that housed the FIS at the base of the canopy crane. The FIS performed reasonably well in the field; the PMT temperature stabilised between $40°$ C and $45°$ C, but it was unknown how the FIS would fare in a place where the daytime high can easily reach $35°$ C, and the instrument is not continuously monitored. The decision was made to remove the top portion of the protective case and build a replacement constructed from snake- and rat-proof stainless steel wire mesh, and lined with flyscreen to deter ants and other insects. The frame was secured to the base with wire loops, and the flyscreen attached with duct tape. This open-air housing remained in place until April 2014, when the construction of a new shed on the site and shorter measurement campaigns made such precautions unnecessary.

2.5.2 FIS Modifications to Conserve Oxygen

The FIS was required to run autonomously in the field for as long as possible. This was a challenge because the FIS requires a continuous oxygen supply. The oxygen is used to generate a clean source of ozone and the mass flow controllers (MFCs) within the FIS require pressure from a gas supply for proper operation. Under continuous operation, the FIS consumes approximately one standard G-size bottle of oxygen per week. Liquid oxygen (LO_2) is a possible substitute for gaseous O_2 for long-term deployments (Hills, 2013), but given the large size and relative difficulty of transporting and maneuvering LO_2 tanks, this option was dismissed. Through two modifications, the operation time of the FIS was extended from one week to five.

First, oxygen supplies were doubled by teeing together two tanks to supply the FIS in parallel (Figure 2.10), which extends the operation time from one to two weeks. Second, a method was developed to discontinue measurements with the instrument at night and thus conserve oxygen. An exterior timer (Omron H5S-WFB2) was added to FIS so that the ozoniser only ran 7.5 hours per day (25 minutes of each hour for 18 hours). The timer controlled the ozoniser power supply and a solenoid valve at the base of the ozoniser O_2 input line (Figure 2.11). Oxygen tanks were changed every five weeks in order to prevent the FIS from running on empty tanks, and to provide a few days' buffer to allow for inconsistencies in filling by the supplier, or minor leakage that could occur during storage.

When the timer was in the 'on' mode, the FIS functioned normally. When it was switched 'off', the ozoniser powered down and the solenoid valve closed. This resulted in no oxygen flow through the system and no ozone supply to the FIS reaction cell. The pressure requirements of the mass flow controllers within the FIS were maintained, as the supplied oxygen runs into the FIS before being

Figure 2.10: The two oxygen tanks are joined in a T, which then continues inside to the FIS. The arm sections of the lines are Swagelok stainless steel, and the main body of the line is 1/4" teflon encased inside a flexible steel plumbing line. All joins are tested for leaks every 5 weeks when tanks are replaced. The entire assembly is then covered in plastic to protect from rain.

routed to the ozoniser. During the time period that the ozoniser is powered down, ambient air from the top of the tower continues to flow through the FIS. The PMT output from this sample air are recorded, but are not included in the data analysis. The timer was set to collect data for 25 minutes of every hour (hh:50 - hh:15), then powered off for the remainder of the hour. Setting the timer to include the top of the hour allowed for the inclusion of automatic calibrations when they occurred, while still giving several minutes for ozone flowing through the system to 'scrub' any compounds that might have accumulated on the reaction cell glass in the previous 35 minutes. At night, the ozoniser was shut down between 22:00 and 4:00 local time (AEST). Data collection started before dawn every morning in order to capture any sunrise emissions that may occur and allow for seasonal changes in sunrise and sunset times without re-programming the timer.

Figure 2.11: The solenoid valve at the base of the O_2 input line controls the flow of oxygen into the ozoniser.

2.6 Concentrations and Fluxes

Accurate instrumental measurement of isoprene in the atmosphere is an essential component of this study. The FIS was selected for its low detection threshold, high sensitivity, and its tolerance of the conditions and pre-existing infrastructure at the field site. Though the focus of this research was on above-canopy concentrations, the FIS is able to determine concentrations all the way down to leaf-level by changing flow and integration period settings (Hills, 2013). The integration periods, ranging from 0.5 to 5.0 seconds, means that it is possible to capture very small scale variations as well as isoprene fluxes.

Concentrations and fluxes are related quantities, where concentrations commonly have units of molarity, mass/mass, or parts per million volume and fluxes include a time and area component to the quantity. This transforms the scalar concentration quantity into a vector. There are several methods to calculate fluxes of trace gases; the most direct of which is this eddy covariance (EC) method

(Langford et al., 2009). The EC method directly determines flux by calculating the covariance of a compound's mixing ratio and the vertical wind speed (Guenther and Hills, 1998; Rinne et al., 2002).

Since its development, the FIS has been utilised for flux measurements in many different applications. For example, Zimmer et al. (2000) used an FIS to characterise isoprene emission from oak leaves. It has also been used to determine above-canopy isoprene fluxes in several locations across the globe (Apel et al., 2002; Baker et al., 2005; Potosnak et al., 2013, 2014; Pressley, 2005). In addition, Exton et al. (2010) have developed a method that utilises the FIS in a marine environment. The capability for the FIS to be used in a concentration-measuring capacity was evaluated in a prior study (Barket et al., 2001). In this evaluation, the FIS was found to perform the worst in the late afternoon and early evening, when isoprene production had diminished, and concentrations were below 0.5 ppb.

Instrument zero drift was identified as a second source of discrepancy between FIS measurements and isoprene concentrations. Barket et al. (2001) concluded that instrument zero should be calculated several times a day (Barket et al., 2001). These discrepancies were of particular importance as the diurnal heating of the instrument shed caused substantial changes to the instrument zero throughout the day due to changing ozoniser performance.

A test of FIS accuracy and precision was conducted across a range of instrument settings to understand the components of instrument noise. Since there was no PTR-MS available to directly compare measurement output, the results are compared against the findings of Hayward et al. (2002) and further statistical measures to distinguish changes in isoprene concentration from instrument noise is presented. The results of this testing will be applied to the Daintree measurements in Chapter 3.

2.6.1   Setup of Calibrations

To evaluate the level of noise present in the FIS system, and to determine if any settings were more or less prone to noise, a comprehensive set of calibrations was conducted, both in the lab and in the field. These calibrations were conducted across all measurement settings in order to determine if one setting performed substantially better or worse than any other. Two settings were varied for this calibration: the O_2 flow and the reaction cell flow.

The O_2 flow setting determines the amount of ozone-rich air available to mix with sample air by rate of flow of oxygen from the supply tanks into the ozone generator and back into the FIS, where the ozone-rich air is mixed with sample air and the resulting photons are counted. Flow was measured between 600-800 standard cubic centimetres per minute (SCCM) in 50 SCCM increments. 800 SCCM is the recommended flow and it is recommended to not go below 600 SCCM as that could cause the ozone generator to become supply-starved and shorten its life span (Hills, 2013). There was benefit in investigating how variations in this flow affects the FIS as operating with a reduced O_2 flow can extend the life of supply tanks by as much as a week in the experimental configuration described in Section 2.5.

The reaction cell flow was tested between 3.0 and 4.5 standard litres per minute (SLPM) in 0.5 SLPM increments. These settings encompass rates suitable for leaf-level measurements at the low end and those used for canopy-scale flux measurements at the upper end. Taken with the O_2 flow, a total of 16 settings combinations are included in the analysis. Each calibration was conducted with isoprene standard flows of 0.0, 3.0, 6.0, 9.0, 12.0, 15.0, and 19.0 sccm, corresponding to concentrations of 0 to 23 ppb.

The photon counts recorded by the data collection program were converted to concentrations (in parts per billion) across all files at all flows. Measurement

began one minute after the isoprene flow rate changed, to allow time for the instrument response to stabilise, and ended 30 seconds before the standard flow changed to the next value. For each flow rate, a mean photon value was calculated as well as two standard deviations and the noise statistics (NS), as described by Hayward et al. (2002) for use with the PTR-MS—another instrument that uses count data as part of its measurements.

2.6.2 Noise Statistics and Normalcy of Responses
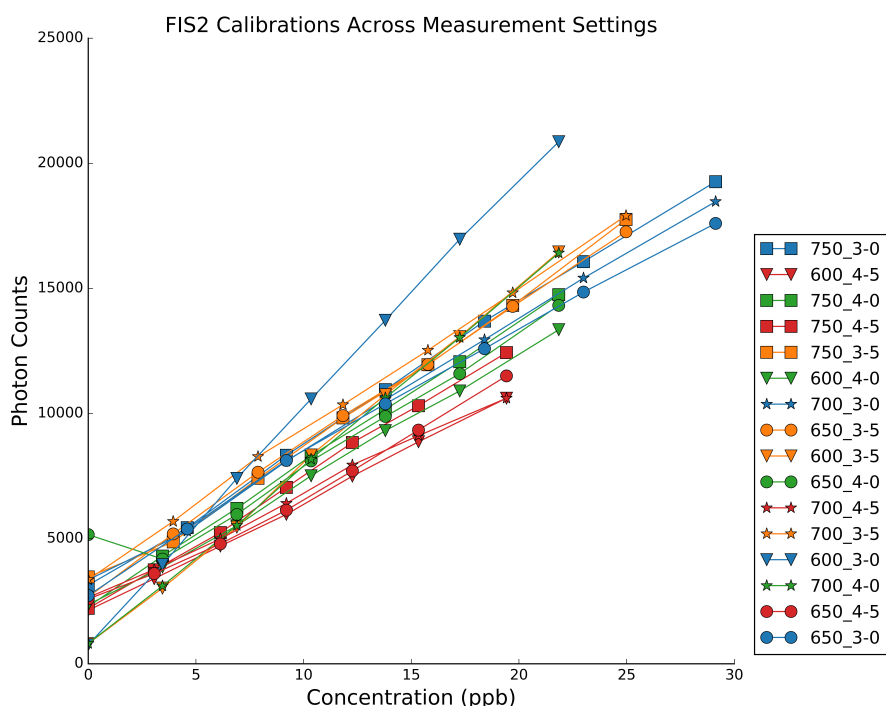
Figure 2.12: FIS calibrations across all measurement settings. The x-axis indicates isoprene concentration (ppb), and the y-axis indicates photon counts. Individual plots indicate mean response of 5-second sample integrations for a minimum of 3 minutes. Plot colour indicates the Reaction Cell flow (in standard litres per minute), and the marker shape indicates O_2 flow (in standard cubic centimetres per minute).

Figure 2.12 shows the calibrations cluster according to their reaction cell flow, and an increasing mean photon value with increasing O_2 flow. Patterns can be discerned according to colour (indicating the same reaction cell flow) or marker
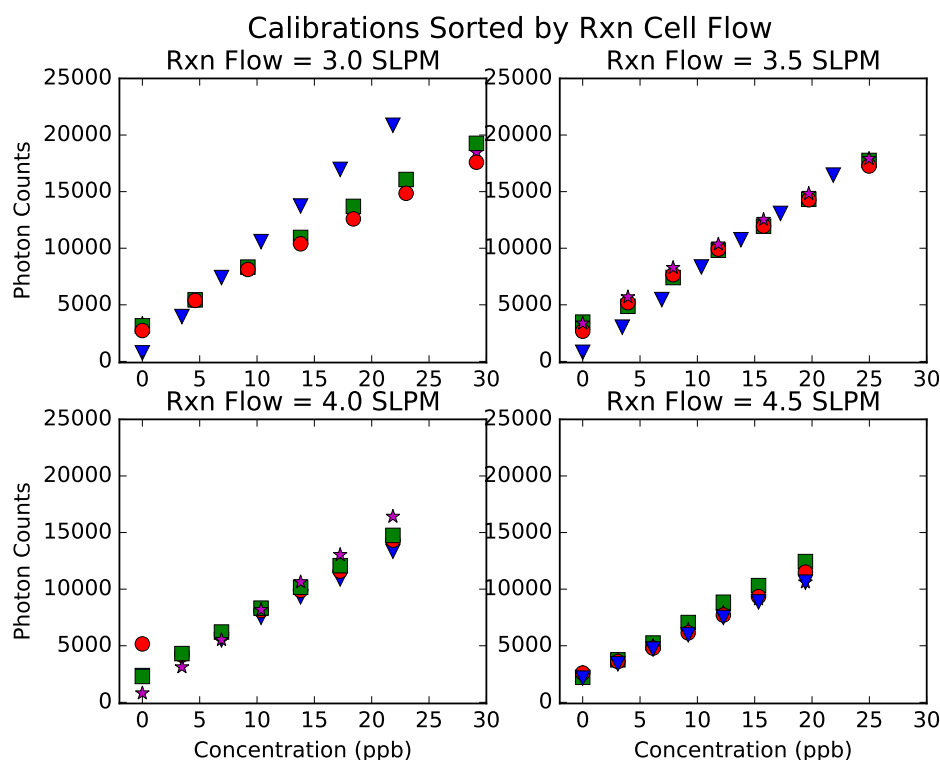
Figure 2.13: FIS calibrations sorted according to reaction cell flow. O_2 flow rates are indicated as: blue triangle (600 sccm), red circle (650 sccm), magenta star (700 sccm), and green square (750 sccm).

type (indicating O_2 flow). The slope along the 3.0 SLPM reaction cell/600 SCCM O_2 flow combination, which was the lowest flow rate combination of all possible settings, differs to the other combinations. Figure 2.13 shows the average photon count per ppb as grouped by reaction cell flow. The photon counts decrease with increasing reaction cell flow rates, as would be expected with a shorter overall residence time. This decrease is slightly countered with increasing O_2 flow (more ozone is available to react with the isoprene), but the effect is most pronounced in the lower reaction flow rates. At a reaction cell flow rate of 4.5 SLPM, which is used in this study, the effects of different O_2 on photon counts is not significant.

Hayward et al. (2002) did similar work with a PTR-MS, performing a series of calibrations at different mixing ratios to challenge the assumptions of a linear response at low concentrations, and the need for calibration of the instrument at all. This work was then used to determine how much of the instrument response

was due to noise, and how much could reasonably be attributed to a diurnal cycle. This work was further applied when the instrument was used to measure concentrations of isoprene in Borneo on the OP3 campaign. Within this work, Hayward, et al derives a noise statistic (Eq. 2.1), that enables the standard deviation for any mean signal to be predicted on the spot. They define the noise statistic (NS) as:

$$NS = \frac{meansignal(cps)}{\sqrt{meansignal(cps) * dwell(s)}} \,, \tag{2.1}$$

where *meansignal* indicates the average response of the instrument in counts per second (cps), and *dwell* is the amount of time (in seconds) the sample spends in the reaction chamber. Noise statistics were calculated for each of the FIS flow rates at each setting and are presented in Table 2.3, grouped by reaction cell flow and O_2 flow. The Gaussian column in the table shows the percentage of measurements that should lie beyond each NS, and the calculations show the percentage of FIS measurements that lie beyond the NS. Taken as a whole–these measurements include all flow rates–the noise statistic clearly does not describe FIS behaviour, as the spread of measurements is much larger than the NS would predict at all levels, though the effect is particularly pronounced along the tails (beyond +/-2NS).

Table 2.3: Noise Statistics along Reaction Cell and O_2 Flow Rates (per Hayward (2002)),

Noise Statistic	Gaussian	Sorted by Rxn (SLPM)				Sorted by O_2 (SCCM)			
		3.0	3.5	4.0	4.5	600	650	700	750
%n >mean + 0.5NS	30.9	38.95	40.83	37.5	39.85	39.464	40.91	38.87	37.9
%n <mean - 0.5NS	30.9	40.82	40.44	39.92	40.43	39.64	39.73	40.71	41.53
%n >mean + NS	15.9	30.09	31.57	27.2	29.63	29.213	31.53	29.28	28.48
%n <mean - NS	15.9	32.72	31.49	30.0	31.104	30.191	31.53	31.63	31.96
%n >mean + 2NS	2.2	16.86	18.84	12.93	15.132	15.539	17.86	15.22	15.14
%n <mean - 2NS	2.2	18.92	18.24	15.13	13.87	14.144	17.96	17.34	16.71

All calibrations at each flow rate were then tested for normal distribution using (Table 2.4).

The majority of settings combinations show a non-Gaussian distribution at the 0 SCCM flow rate where only zero air and ozone are in the reaction cell. Zero air is manufactured on the spot, within the FIS, by passing ambient air through an intake port in the FIS, that is scrubbed by a catalytic converter at a temperature of 125 °C, then passed into the reaction cell where it is mixed with ozone. The cause of this variation is unclear; it was seen both in the laboratory and in the field measurements. This result prompted a derivation of an alternative method to calculate the zero drift throughout the day, discussed in Section 2.8.

As seen in Table 2.4, FIS stability increases with the addition of isoprene. Standard flow rate is indicated in the table, as different settings give different mixing ratios for the same flow rate. The FIS becomes unstable again at the highest of flow rates (19 SCCM). The manual indicates 20 SCCM as the highest recommended flow rate setting for the isoprene standard; at this setting the mass flow controller is completely open and not restricting the amount of air flowing through (Hills, 2013). This is likely to explain the lack of consistency in results at 19 SCCM. However, since this corresponds to a concentration between 19.42 ppb and 29.13 ppb, it is safe to disregard these results as they are much higher than would be observed in ambient conditions.

Table 2.4: Normalcy of FIS Response During Calibrations

Standard Flow Rate	Gaussian	Not Gaussian
0 SCCM	6	10
3 SCCM	12	4
6 SCCM	15	1
9 SCCM	13	3
12 SCCM	14	2
15 SCCM	12	4
19 SCCM	7	9

(SCCM indicates standard cubic centimeters per second of flow in the FIS)

To further describe the distribution patterns of individual flow rates, a quantile-quantile plot was made for each calibration. The plot for a reaction cell flow rate of 4.5 SLPM and 700 SCCM is shown, as that is the setting combination that was used in this study. This particular instrument setting is normal for all flow rates, except the 0 SCCM. Due to this, it was decided to calculate a zero from the isoprene sample mode, which has a much smoother response. This is elaborated on further in Section 2.8

2.7   Instrument Setup in the Field

The FIS was deployed at the Daintree Rainforest Observatory (DRO) in April 2013. It was installed in the instrument shed at the base of the canopy crane, approximately 100 m into the forest (Fig.2.15). A 1/4" teflon sampling line was encased in a UV-treated PVC hose (Pope 12 mm x 15 m, model 1011581) and installed up the crane mast. The inlet sat at a height of 35 m, approximately 5-10 m above the canopy. The inlet was fitted with a 2 μm filter to prevent spiders and insects from entering the line, and the assembly was further protected from wind and rain by a stainless steel bowl (Sunbeam, Figure 2.16). Inside the shed, the FIS was configured for long-term unattended operation. Since the sampling line was longer (50 m) than the maximum sample line length recommended in the manual (7.62 m), a scroll pump (Varian IDP2, Lexington MA) was fitted to the back of the system to aid the internal pump with pulling sample air down the line. Sample residence time inside the sampling line was approximately 2 seconds. Data was recorded and stored externally (LabVIEW), and the file was backed up every 24 hours.

An automatic standard-addition calibration program ran every two hours, including during sleep mode. The calibration began with three minutes of zero air–air of the same temperature and relative humidity as the sample air, but
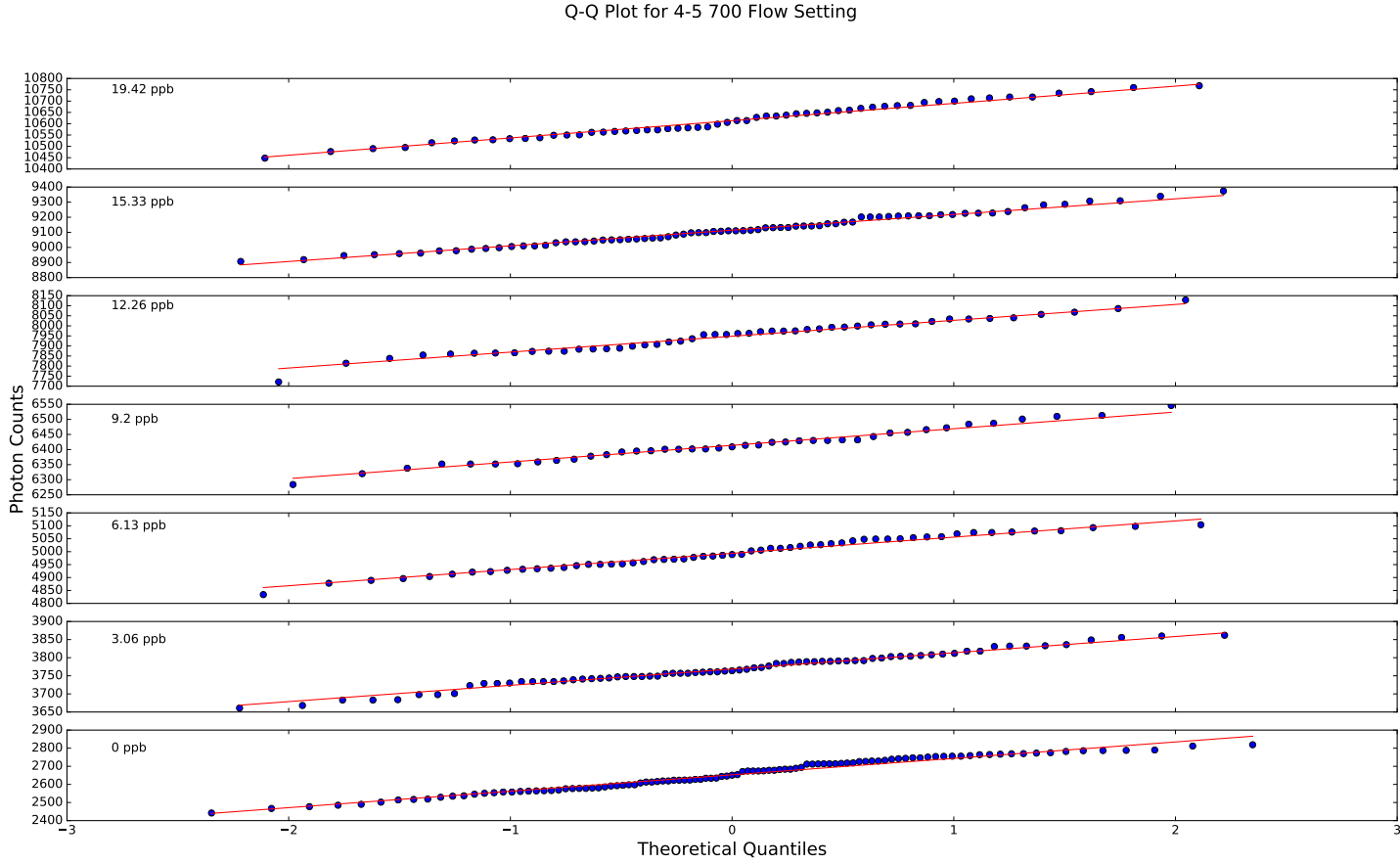
Figure 2.14: Quantile-Quantile plot of FIS calibration. Reaction cell flow rate = 4.5 SLPM, O_2 flowrate of 700 SCCM. The dots mark the measured photon counts and the red line indicates a best fit, as calculated from the mean and standard deviation.

passed through a catalytic converter to remove isoprene. After that, there were three minutes of zero air mixed with bottled isoprene standard in a balance of nitrogen (Scott-Marin, Riverside, CA, USA). Finally, the zero air was turned off and the isoprene standard air was added to sample air for three minutes. After the completion of the calibration, the FIS returned to sampling mode.
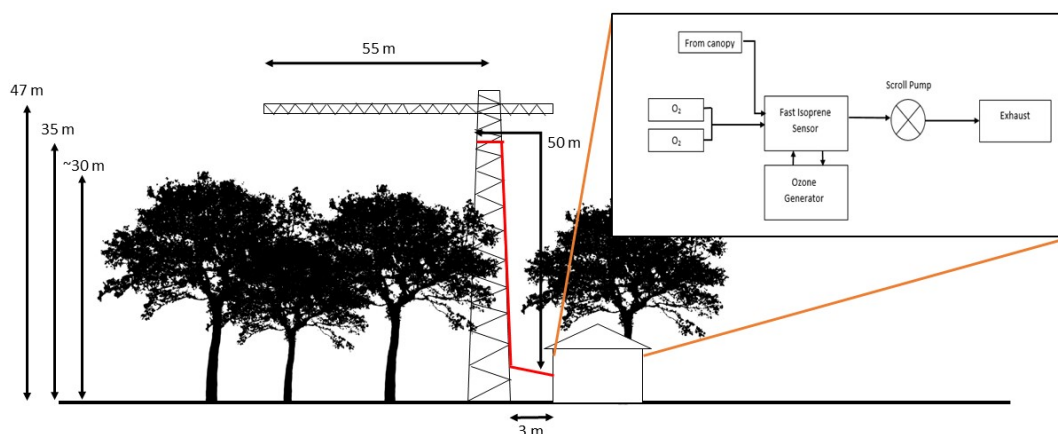
Figure 2.15: Schematic of the sampler setup. The sampler line (in red) sat approximately 5-10 m above the canopy height. Inside the shed, the FIS measured isoprene pulled down from above the canopy.

Figure 2.16: The inlet of the sampling line, protected from wind and rain by a stainless steel bowl.

2.8 FIS Data Analysis

FIS data were processed over several steps, with slight modifications performed when required in individual files, discussed in Chapter 3. The basic steps are outlined below, then individual components are addressed more thoroughly in the subsections that follow.

For each file, a database was created to house the measurements and convert photon counts to concentrations in bulk while maintaining the integrity of the original files. First, the day of the year for each measurement was calculated from the file name and the elapsed time recorded within the file, and added to the database. Next, the average photon count was calculated for the isoprene standard plus zero automatic calibration setting. This value served as a calibration factor which was applied to the hour on either side of the calibration, e.g. the 8:00 a.m. calibration applied to all samples taken between 7:00 and 9:00 a.m. Finally, the data collected during times when the FIS was idle were removed.

2.8.1 Zero Determination

As discussed in Section 2.6.2, the zero calculated during calibration periods was not always an accurate reflection of the actual instrument zero. To accommodate for this shortcoming, a dynamic zero was calculated for each hour and applied to data collected during that time. This dynamic zero was determined by calculating the average sampled photon counts between 5:00 and 5:05 and 21:00 to 21:05. The slope between these two values was then applied to each hour through the day. The 5:00 and 21:00 times were used as they were both well before dawn and after dusk, so no isoprene is being manufactured. In addition, it falls within the operational times of the FIS under long-term unattended sampling conditions.

This method was tested on data collected at Macquarie University, then applied to two case studies using data from the DRO that show the improved

fit of the dynamic zero in different sampling conditions. As discussed in the following sections, the resulting zero value calculated from this method provides a better fit for the data than the zero value that is measured during the automatic calibration.

2.8.2 Impact of Air Conditioning on FIS Performance

The performance of the ozoniser in the FIS system is strongly dependent upon the operating temperature and the maintenance of a consistent temperature across the entire measurement period (A. Hills, UCAR, 2013, personal communication). These requirements could not be met at the DRO due to amperage and noise limitations on the instrument shed. FIS performance under the recommended operating parameters and field conditions were compared; concentrations were calculated using the method outlined in the operating manual and the method described above, respectively.

Figure 2.17 shows the results of using both the method outlined in the FIS manual and the method developed for this study to derive isoprene concentrations from photon counts on a single set of data. In the box plot, the two approaches overlap between 6am and 6pm, and the IQRs completely merge from 11am-3pm, which is the time of peak isoprene emission.

The primary difference between these two approaches is the concentrations overnight. There are some points of agreement between them (e.g., the evening of 26 Nov.), but in general the method used in this study underreports the isoprene in the air. This is due to the fact that the zero calculation method used in this study sets a zero before dawn and after dusk, when isoprene is no longer produced. A scatter plot of this same data (Fig. 2.18) elaborates on this further. This plot shows a direct comparison of the two isoprene calculations, along with a linear fit and R^2 value. When all data points are considered, the correlation is
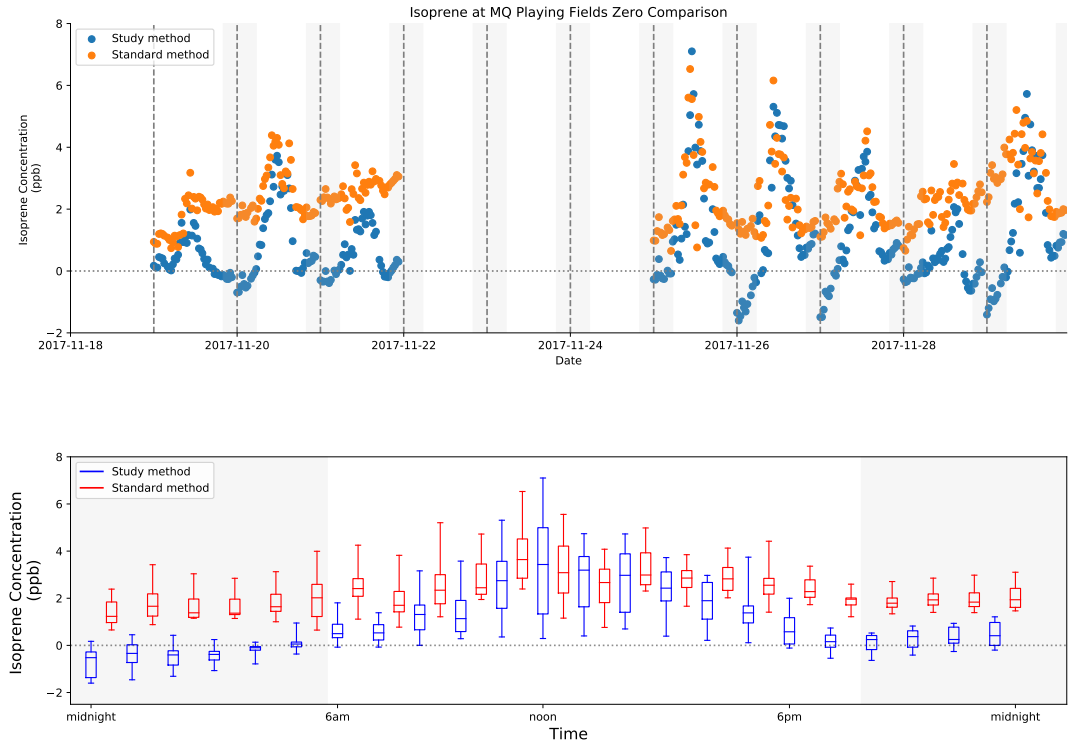
Figure 2.17: A comparison of isoprene calculations using the standard method in the FIS manual and the method used in this study. Grey areas indicate overnight hours.

almost 1:1, but there is an offset; the zero calculation used in this study leads to an underestimation of isoprene by 1.47 ppb. When the overnight data is removed (18:00-6:00, plot not shown), the correlation remains the same and the offset decreases to -1.11 ppb. The R^2 improves by 3%. The Spearman ranking shows a moderate correlation (r_s=0.53, p=1.43 x 10^{-27}), where the Pearson ranking shows a strong correlation (r=0.68, p=1.62 x 10^{-49}).

However, there are also several important differences between the Sydney site and the DRO. First, the Sydney site is inland and the DRO is coastal, so there is no sea breeze to advect the isoprene to another area. In addition, a collapsing boundary layer in the overnight hours further traps any unadvected isoprene to this location. Figure 2.19 shows the wind profile at the DRO in the late afternoon and early evening hours (16:00-20:00) for the years 2013-2015. This winds shift from onshore to offshore by noon, and pushes unreacted isoprene out of the area
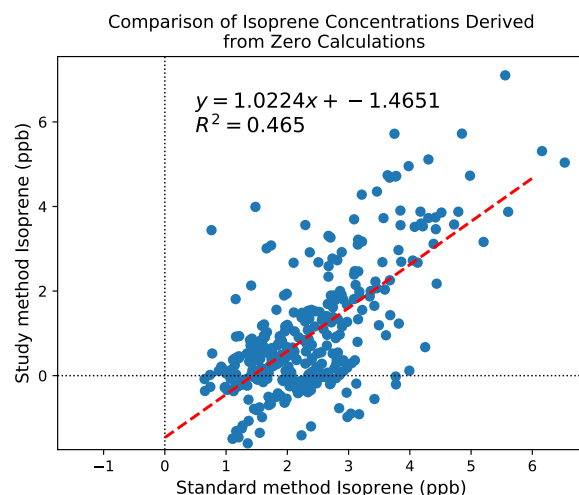
Figure 2.18: Plot of isoprene calculation using the process described in the FIS manual vs. the method used in the study.

throughout the afternoon. This pattern persists until the sun goes down and the winds become light (<0.8 m/s) and shift to come from the south southwest. They remain light throughout the night. A third possible effect on the zero calculations is the humidity. One of the suggestions for successfully running the FIS is that the sample air and zero air need to be at the same temperature and humidity (Hills, 2013). This requirement was difficult to meet as the sampled air was above the canopy and the zero air was taken from within the canopy. In addition to having slightly different temperatures and humidities, the coastal air was high in salts which necessitated more frequent cleaning of the FIS lines than the manufacturer recommendation.

A second difference between the site at Macquarie University and the DRO is their proximity to traffic. The Macquarie site is located near a major highway in an urban setting and the DRO is rural, with little traffic. As discussed in Section 2.4.1, the FIS also detects propene and other compounds found in vehicular emissions. This contributes to the concentrations observed by the FIS at this site. The presence of vehicular emissions can be observed on solid sorbent cartridges, and will be discussed more fully in Sec. 2.10.1.
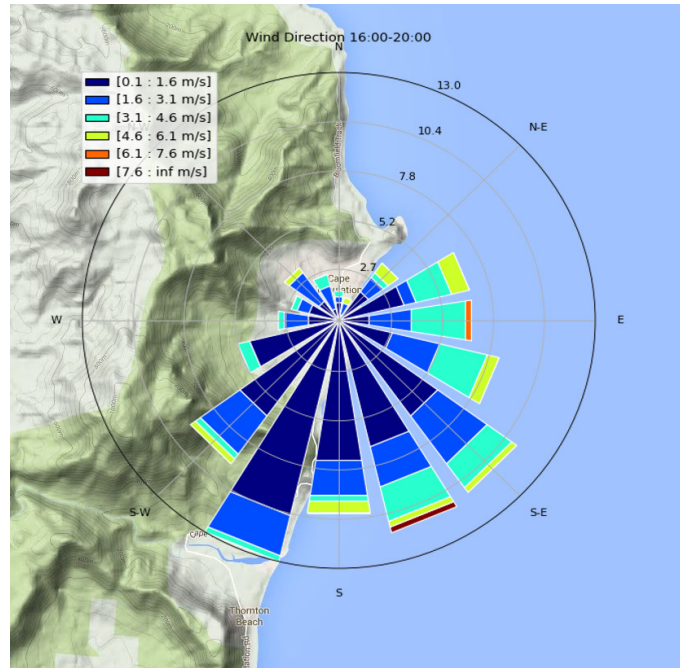
Figure 2.19: Wind direction and speeds at the DRO in the late afternoon and early evening hours, 2013-2015.

2.8.3 Case Study: Stable FIS Data

In this example, we examine the behaviour of FIS2 in April-May 2015. This was the first DRO deployment of this machine, and it sampled isoprene from above the tree canopy for several days (27 April-2 May) before sampling from within the canopy (2-4 May). On 4 May the sampling lines were returned to their original above-canopy configuration. Figure 2.20 shows the hourly average photon count taken by FIS2 during the campaign. Average sample photon counts are shown in blue, and the average photon count of the FIS zero from automatic calibrations are indicated by red. The calculated hourly zero is indicated by the green line and overnight hours are shaded gray.

From this plot, several points are evident. First, the average 'zero' photon count is consistently higher than the average sampled photon count during the overnight hours. This is true both early in the sampling period, as well as later in the series, when the FIS undergoes a baseline shift. Applying these zero values to the sampled photon counts would result in negative concentrations during the

overnight hours across all days. Second, the zero value shifts throughout the daytime hours and is inconsistent from day to day. For example, on April 29, the average zero count stays very close to the average sample counts, which would indicate isoprene concentrations at or near zero. However, the following day the zero does not vary greatly throughout the day, leading to an indication of a higher daytime concentration. Conversely, the calculated hourly zero shows a smoother response across all days, and consistently yields an expected diurnal response. It is also capable of taking instrument drift into account. This is evidenced by the shift during the overnight hours of May 3-4: the diurnal shape the following day is preserved.
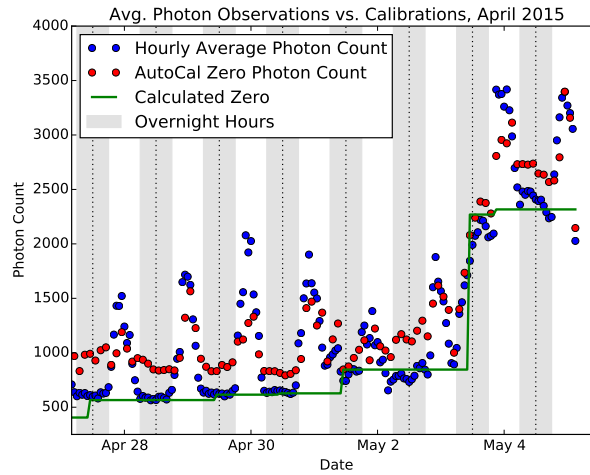
Figure 2.20: A figure showing the photon counts of FIS2 throughout data collection in April 2015.

2.8.4   Case Study: Unstable FIS Data

The August 2015 data from FIS2 shows how the hourly zero approach features in a more unstable sampling pattern. In this case (Figure 2.21), there were more baseline shifts throughout the study period. The autocalibration zero values (red) re-set each time sampling was stopped to do a full calibration, and the sampling average photon counts (blue) took on an arc shape, though there were still diurnal cycles apparent during the daytime hours. The hourly zero line

(purple) was clearly able to capture this cycle while still allowing for instrument drift.
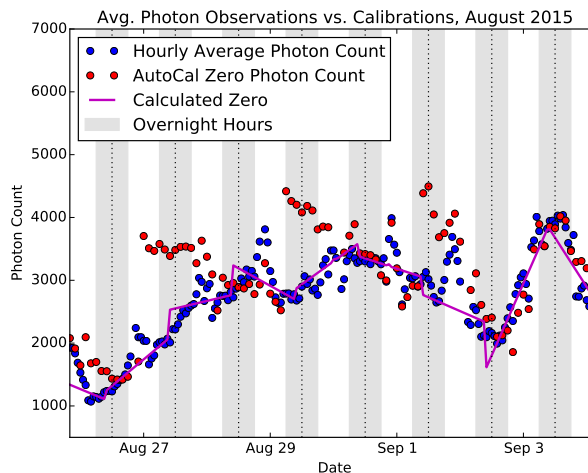
Figure 2.21: A figure showing the photon counts of FIS2 throughout data collection in August 2015.

2.9   Solid Sorbent Sampling

Though this study is primarily directed at understanding the seasonal changes of isoprene over a tropical forest, compounds are not emitted in isolation. In addition to isoprene, hundreds of other VOCs are emitted by plants, and a basic insight into what is emitted in the Daintree Rainforest is lacking. Trees that are low emitters of isoprene are often high emitters of other compounds, such as monoterpenes, and knowing the balance of these compounds contributes to a broader understanding of the emission profile of the forest. Collecting whole air samples also provides an opportunity to assure that the measurements of the FIS were accurate.

Broad-spectrum atmospheric sampling is generally accomplished in one of several ways. One method requires air to be collected whole and stored in a large stainless steel canister or teflon bag for later analysis by gas chromatography. Another method makes use of passive samplers to collect broad-spectrum atmo-

spheric data on sorbent materials. These have the benefit of being both portable and relatively inexpensive. However, in order to collect enough material to analyse, the filters must be exposed for an extended period of time, and as such; do not present a snapshot of emissions.

A third method, used in this study, actively samples air by drawing it through glass or stainless steel tubes fitted with solid sorbent beds that capture targeted compounds. There are several beds available, such as carbon-based materials with a high surface area (>1000 m^{3}g^{-1}) that can collect multiple compounds, and polymers with small surface areas (<50 m^{3}g^{-1}), capable of trapping specific compounds. These beds can be used singly or in succession to optimise for particular sampling requirements.

Dunne et al. (2018) reference specific issues when attempting to compare isoprene measurements collected using different techniques. Specifically, they cite the use of non-equivalent certified standards, non-equivalent sampling and averaging times, and non-equivalent calibration methods. Several steps are taken in this study to mitigate these issues. First, the same tank is used to make calibration standards for both the FIS and solid sorbent cartridges, so any discrepancies of the tank from the stated concentration are consistent across techniques. Second, the measurement averaging time for the FIS is five seconds, and the measurement period for the cartridges averages 30 minutes. Therefore the FIS measurements are averaged to specifically match the sorbent cartridges. Third, though the calibration approaches are not similar, efforts are made to diminish error with the solid sorbent cartridges. Isoprene calibrations are drawn through the sorbent tubes and desorbed in the same manner as the samples, instead of directly injecting a standard onto the GC column. Therefore, any incomplete desorptions or other handling issues will also apply to the calibrations.

2.9.1   Equipment and Sampling Method

BVOC samples collected on the solid sorbent cartridges were analysed using gas chromatograph-mass spectrometer (GC-MS) system (Shimadzu GCMS-QP 2010, Kyoto, Japan) fitted with a thermal desorption system (Shimadzu TD-20) and a 30 m, 0.25 um RTX-5 Sil MS capillary column (Restek Corp., Bellefonte, PA, USA). Ultrapure helium was used as the carrier gas throughout the study. The TD-20 has a thermo-module to cool the trap tube, so refrigerants are not required. As the temperature increases in the desorption process, high volatility (low boiling point) compounds separate from the sorbents early in the chromatographic analysis and larger, less volatile compounds appearing later in the analysis.

Supelco Carbotrap 300 (Sigma Aldrich GB) cartridges, packed with Carbotrap C, Carbotrap B, and Carbosieve SIII, were used in this study. Carbotrap C captures C3-C20 compounds, Carbotrap B targets C5-C12 compounds, and Carbosieve SIII traps C2-C5 compounds. All three sorbents are hydrophobic, making them suitable for humid environments–an important consideration for working in the Daintree. The U.S. Environmental Protection Agency (EPA) Method TO-17 provides a comprehensive plan for collecting and analysing VOCs with cartridges, which has been validated by extensive testing (Agency, 1999).

The cartridges used in this study are not especially suited to capture the compounds that can interfere with isoprene measurements, discussed in Sec. 2.4.1 (Table 2.2). MBO is the only compound that they can detect. Propene and ethene are both too volatile. MVK and methacrolein can be quantitatively measured using Tenax TA, but this is not an optimum product for the measurement of isopren. However, the sorbents in Carbotrap 300 are capable of capturing mono- and sesquiterpenes, including α-pinene, β-pinene, d-limonene, eucalyptol, and citronellol.

Cartridges were conditioned for 120 minutes at 350°C and 50 mL/min in

an ultra-pure helium carrier gas prior to the commencement of pre-deployment testing discussed in Section 2.10.1 and again before transport to the DRO. When transported to and from the lab, cartridges were stored in an opaque plastic container in an insulated bag. Cartridges were refrigerated immediately after sample collection and a cold pack was added to the insulated bag to keep samples cool during transport.
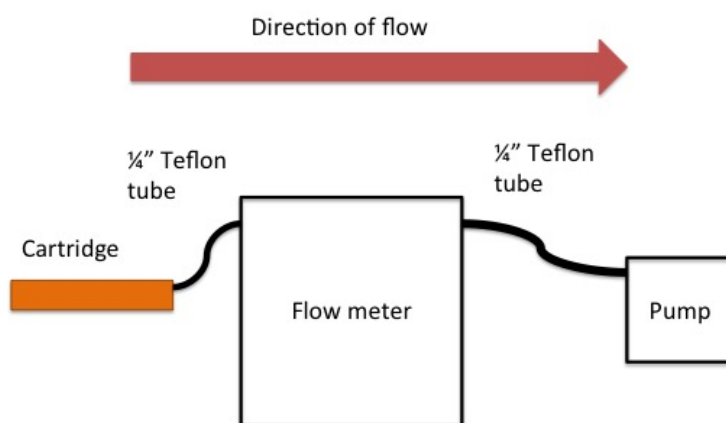
Figure 2.22: The setup of the cartridge sampling apparatus. Air flow indicated by arrow.

At the DRO, samples were collected at a height of 35 m, above the rainforest canopy and in close proximity to the inlet line for the FIS. Duplicate samples were taken, according to the schematic (Figure 2.22). A volume meter (Dry Gas Test Meter, DC-1A, Shinagawa Corp., Tokyo, Japan) and a battery-operated personal sampling pump (Airchek Sampler, Model 224-PCXR7, SKC Inc., PA) were fitted behind the cartridge. This setup was used at ground level for sample collection during pre-deployment testing.

2.9.2 GC-MS Analysis Method

To prepare samples for analysis, they were first removed from refrigeration and allowed to come to room temperature. Once they reached room temperature, they were dried by passing 3L of argon (Ar) through them at a rate of 0.5L/min. After that, the samples were thermally desorbed from the cartridge (flow rate of 60 mL/min for 5 min), then injected onto the column at 24°C, with the oven set at 29°C (3 mins). The oven then increased in temperature to 200°C at a rate of 8°C/min where it was held for an additional 3 mins to conclude the analysis. Chromatographic peaks were identified by matching retention time, mass spectrometer signal and fractionation patterns to an isoprene standard, which will be discussed below. The mass spectrometer scanned between 35 and 400 amu beginning 20 seconds into the chromatographic program, in order to allow any remaining water to pass through without detection. Peaks were identified at a voltage of 70 eV. Though MVK and methacrolein are present in environments where isoprene is also found, the detection limit of these two compounds was not determined for the GC system.

2.9.3 Calibration Protocol

The GC-MS was calibration was calibrated with isoprene throughout the analysis process. Four calibration cartridges of either 2 ppb, 4 ppb, or 8 ppb isoprene were randomly placed among each batch of cartridges to be analysed. In addition to this, every fifth cartridge in a batch was a laboratory blank. This ensured that any background changes that might occur during an analysis could be tracked.

Calibration cartridges were built using a dilution of isoprene standard (4.1 ppm in a balance of N_2, the same as was used to calibrate the FIS) and filtered bottled air (BOC, Sydney, Australia). The two components were mixed in a gas dilution calibrator to the above-specified concentration, and as shown in Fig.

2.23, a sample of the output mixture was pulled through a cartridge arranged with a dry gas meter and pump behind to mimic field conditions.
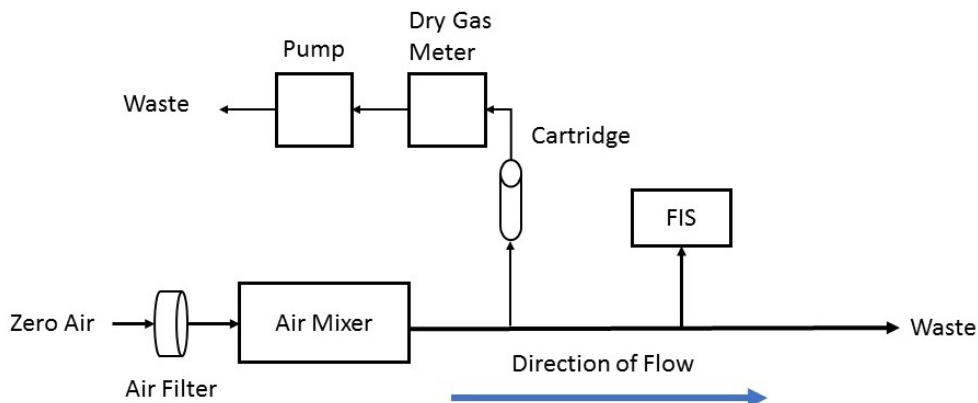
Figure 2.23: The setup for testing the cleanliness of the zero air. Direction of flow indicated by blue arrow.

2.10   Cartridge Pre-Deployment Testing

Prior to their use in the field, the solid sorbent cartridges were subjected to analysis and testing to ensure their performance out in the field; the results are presented below. First, their breakthrough threshold was tested in a laboratory setting. Then, their performance was tested against FIS measurements collected at one of the atmospheric monitoring stations in the Sydney metro area operated by the New South Wales Office of Environment and Heritage (NSW OEH)

Determination of Breakthrough Threshold

Cartridges were tested in a laboratory environment to determine their breakthrough threshold, the largest volume of air that could be sampled on one cartridge without saturating the sorbents. To conduct the test, isoprene-rich air was mixed in a gas dilution calibrator (model 4010, Sabio Engineering, Round Rock, TX, USA) from 4.1 ppm isoprene (in a balance of nitrogen) and filtered zero air

(BOC, Sydney, Australia) to a 1/1000 dilution, yielding 4.1 ppb. As shown in Fig. 2.24, this air was sent to waste, and a tee was inserted along the output line to sample from. The sample line contained two cartridges in series, and a sampling pump pulled the isoprene-rich air through them. 1, 5, 10, and 20 L of air were pulled through the cartridges.
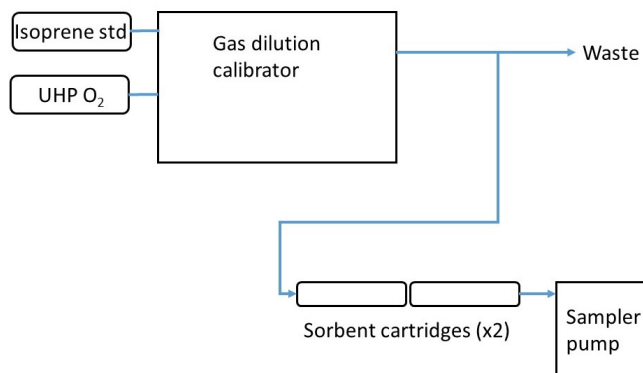
Figure 2.24: Schematic of cartridge breakthrough testing.

Samples were analysed using the GC-MS using the method described above. Figure 2.25 shows the results of this test. The front cartridge (left) shows the isoprene peaks associated with the volumes tested. The right panel shows the second cartridge in the series. Isoprene elutes at ~45 seconds, so only the first two minutes of the analysis are displayed for brevity. These results clearly indicate that there was no breakthrough at any of the tested volumes and a sample volume of 20L will provide sufficient material to detect a clear peak using the analysis method.

2.10.1 Outdoor Testing at NSW OEH

In preparation for deployment at the DRO, a preliminary comparison of FIS data and solid sorbent cartridges was undertaken at the NSW OEH atmospheric monitoring station located on the grounds of Macquarie University (33° 45' 57"

Solid Sorbent Cartridge Breakthroughs
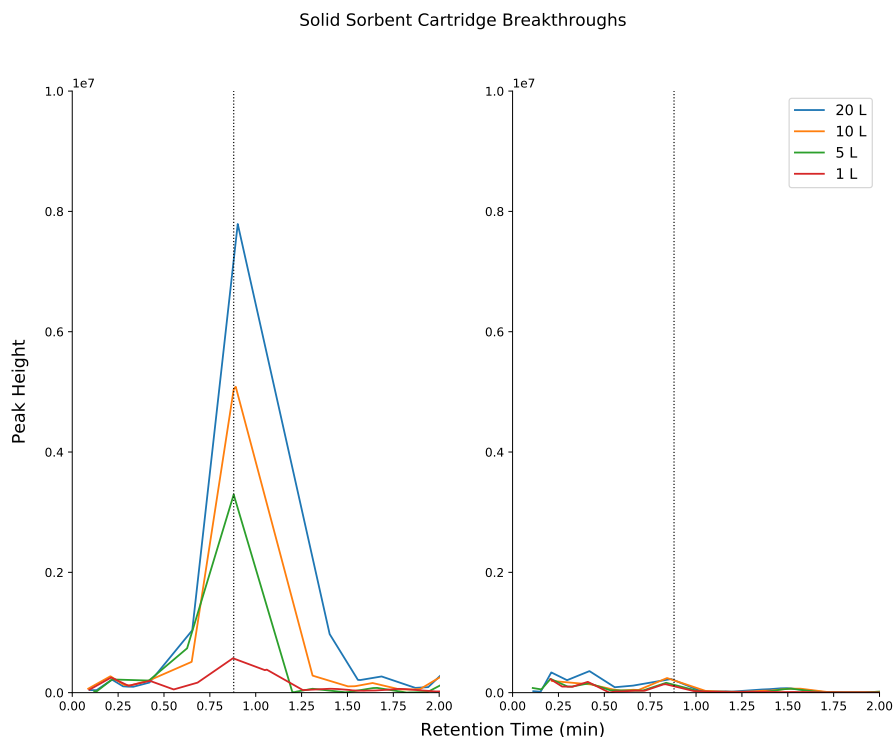
Figure 2.25: Results of breakthrough testing. The front sorbent tube is on the left, the back is on the right. Vertical line indicates isoprene, which peaks at ∼45 seconds.

S, 151° 7' 3" E). Samples were collected both in daylight hours and after sunset to quantify performance and correlate measurements at a variety of times. Results of this analysis are shown in Fig. 2.26.
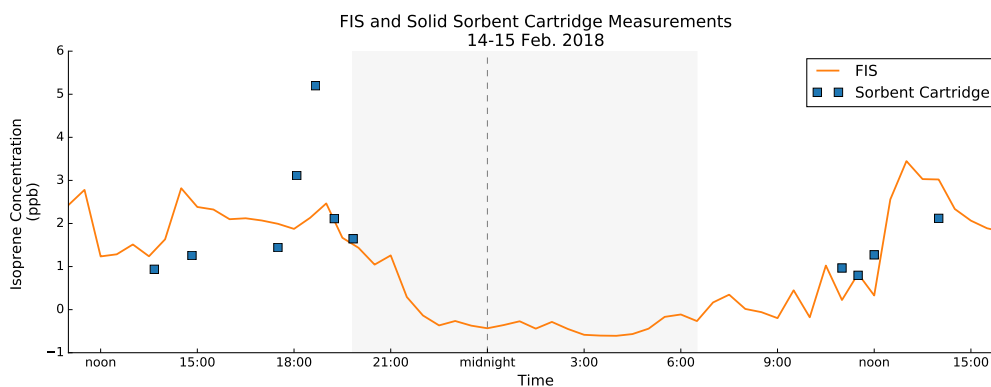
Figure 2.26: Time series of FIS data compared to solid sorbent cartridge measurements. FIS concentrations reported in 30-minute averages, cartridge measurements plotted at the midpoint of their measurement period. Shaded area indicates overnight hours.

The results presented in Fig. 2.26 show a close agreement between the FIS

and solid sorbent cartridge measurements, particularly in the evening and the morning where the difference between measurement techniques is within 13% of one another for both periods. Afternoon solid sorbent samples collected between 12:00 and 18:00 showed isoprene concentrations, on average, 40% lower than FIS concentrations, indicating that other compounds may have influenced the FIS measurements. This is a possibility as the OEH site is within 1 km of a major highway, and chromatograms show traces of fuel compounds (e.g., long-chain hydrocarbons, toluene). Chromatograms also indicate the presence of monoterpenes; eucalyptol dominates in this location.

2.11 Comparison of FIS Data to Other Sources

2.11.1 Satellite Data

There have been major advances over the past 20 years in the use of satellites to detect trace tropospheric gases from space. Satellite data products are a powerful complement to traditional ground-based networks due to their extensive spatial coverage and their ability to show the regional impacts of anthropogenic pollution and biogenic emission events (Duncan et al., 2014). These satellites measure the density of molecules in a column of air below them and, provided there is little chemical transformation or transport, the column measurements can be used to calculate the column abundance of the compound of interest. However, satellite data products are not without their limitations. They are only able to provide the number density of a compound in a complete column of air, so there is no information about its vertical distribution. In addition, the ability to detect any compound is associated with the cloud cover in the area. Clouds interfere with the detection of surface-level pollutants, and satellites will only be able to detect the number densities of compounds that are above them (Hoff and Christopher,

2009).

The detection of VOC emissions–including isoprene–carry additional challenges. As it is difficult to directly measure VOCs by satellite, formaldehyde (HCHO), is used as a proxy (Chamides and Lodge, 1992). However, the variability of HCHO column density has been correlated with the variability in isoprene emissions and, due to their short chemical lifetimes ($\sim$1 hr for isoprene and $\sim$3 hrs for HCHO), the horizontal distribution of HCHO is due to the distribution of VOC sources rather than the effects of transport (Duncan et al., 2014; Millet et al., 2008; Palmer et al., 2003, 2006).

Another challenge in using HCHO satellite products is the data have large spectral and computational uncertainties associated with them (Duncan et al., 2014), despite their relative abundance and clear absorption spectra(De Smedt et al., 2008). HCHO, which absorbs in the ultraviolet (UV) range, has a low optical density when compared to other UV absorbers (e.g, NO_2 and BrO), so the signal to noise ratio of measured radiance limits the detection of HCHO (De Smedt et al., 2008). To reduce the impact of this limit, a daily radiance spectra from the equatorial Pacific Ocean is used as a reference. The region selected is assumed to have a low and stable HCHO column (Stavrakou et al., 2009). Other compounds fall into the HCHO fitting interval, including O_3, NO_2, and BrO. Reference spectra for these compounds are included in the fitting procedure (De Smedt et al., 2008).

A method exists of inferring isoprene emissions from spectroscopic HCHO column measurements, which has been used successfully in tropical ecosystems over the Amazon, Africa, and Australia (Barkley et al., 2012, 2008; De Smedt et al., 2008; Palmer et al., 2001, 2003). This approach quantifies isoprene by treating HCHO as a high yield product of BVOC oxidation with column density variability due to variability in emissions. From the assumptions and limitations described above, a multi-step process converts the raw observations into a vertical

column density (VCD) that can be mapped, though it also introduces further uncertainties from the fitting algorithm (Bucsela et al., 2013; Leue et al., 2001).

Retrieval and Use

HCHO retrievals from the GOME-2 instrument aboard the Meteorological Operational satellite-B (MetOp-B) satellite were used in this study. Launched on 17 September, 2012, into low polar orbit, GOME-2 detects solar backscatter in the UV-Visible spectrum and has a spatial resolution of 40 x 80 km and swath of 1920 km (De Smedt et al., 2012). This wide swath is achieved by GOME-2 operating in tandem with its sister instrument (another GOME-2) aboard the MetOp-A satellite (Callies et al., 2000; EUMETSAT, 2015). This will continue until the MetOp-A can no longer provide reliable data. Level 2 data which has been processed to remove instrument artefacts such as duplicate data and synchronization frames, and includes calibration coefficients and sensor units, was used in this study.

In the GOME-2 satellite, HCHO columns are derived from radiance observations using a two-step process known as the differential optical absorption spectroscopy (DOAS) technique. The HCHO data averaged over a 24-hour period in a 2x2.5° window (16°-18°S, 145°-147.5°E) were collected for 2013-2015, including periods when ground-based measurements were not being made. The satellite passes at approximately 9:30 am local standard time and has a the revisit of approximately 3 days. Days with no overpass or cloud cover in excess of 40% were not included in the study. This left approximately 140 days/year (38%) available for this study–146 days in 2013, 140 in 2014, and 147 in 2015.

In order to facilitate a 'like to like' comparison of FIS measurements and the GOME HCHO VCDs, the isoprene mass fractions measured with the FIS (hourly average) were converted to an estimated HCHO yield and resulting column density (VCD_m). Assuming that isoprene is evenly mixed throughout the boundary

layer, it is possible to integrate the number concentration of isoprene along the height (z) axis (Eq. 2.2) to yield an estimated VCD (VCD_m , Eq. 2.3). This can then be compared against the GOME-2 column density, VCD_s (Seinfeld and Pandis, 2006).

$$\Omega = \rho_{sfc} \int_0^\infty e^{\frac{-z}{H}} dz \tag{2.2}$$

$$\Omega = -\rho_{sfc} z_{scale} (e^{\frac{-z_{max}}{z_{scale}}} - e^{\frac{-z_{min}}{z_{scale}}}) \tag{2.3}$$

In this expression, Ω is the estimated VCD, ρ_{sfc} is the average measured isoprene mass fraction multiplied by the density of the air column, z_{scale} is assumed to be the boundary layer height (estimated here at 1500 m), z_{min} is the minimum height (0 m), and z_{max} is the Kármán line, the boundary between the atmosphere and space (10^5 m).

The total error in the GOME-2 measurements is calculated on a per-pixel basis, and incorporates both random and systemic sources as discussed above (De Smedt et al., 2008). However, the number calculated from this should be considered an upper limit of the error. De Smedt et al. (2008) states that for large numbers of pixels, the slant column random error is less than 2%. However, when individual pixels are considered, the total error is approximately 70%, with random error as the dominant source. Errors from subtracting out the background HCHO concentration (using the reference area) range from 5% to 12%. Error from slant columns and air mass factor uncertainties are equivalent in the tropics, and range from 10% to 20%. In total, the error for monthly means is between 20% and 40%. (De Smedt et al., 2008)

Figure 2.27 shows the fitting window used for the satellite products in this study. The DRO is in the upper left hand corner of the window. This was selected as this is the natural boundary of the grid cell in the GOME-2 product. Though the DRO is situated in the corner of the cell, the forest in this cell is still part
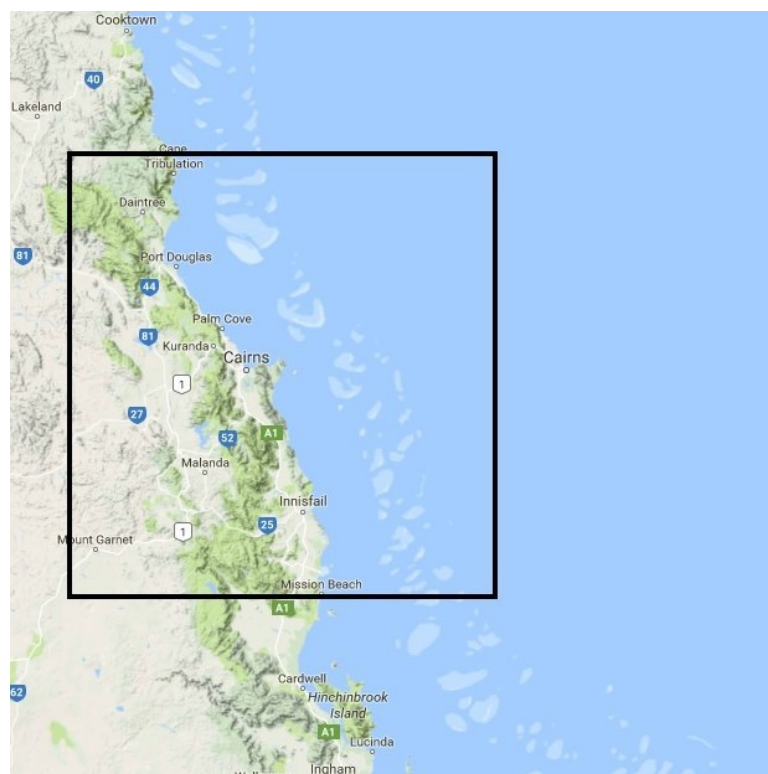
Figure 2.27: The 2°x 2.5° satellite window used in this study, 16°-18°S, 145°-147.5°E.

of the Wet Tropics of North Queensland management area and is subject to the effects of diurnal sea breezes. Neighboring cells were considered, but were rejected on the grounds of either being overwhelmingly comprised of water and therefore not representative of terrestrial isoprene emissions (north), or containing mostly grass and ranch land and not inclusive of forest emissions (east). As the satellite observation occurs at 9:30 am local time, substantial mixing has not yet occurred, and the predominant winds are from land to sea, so this grid cell also captures advection.

2.11.2 GEOS-Chem Model Data

As discussed in Chapter 1, global 3-D emissions and chemistry models provide an important insight into emissions patterns by fitting together physical and chemical processes into a cohesive picture of biogenic emissions processes. Like

satellites, they provide a spatial continuity that fills the gaps in ground-based measurement networks, and supply chemical and transport estimates in locations where observations are sparse or difficult to obtain. In addition, they serve as the primary tool for chemical forecasting.

GEOS-Chem, a global 3-D chemical transport model, combines assimilated meteorological data from NASA's Goddard Earth Observation System (GEOS) MERRA-2 with emissions, photochemistry, and deposition modules to form a comprehensive meteorological-chemical model (Bey et al., 2001). Model resolution is 0.5° x 0.625°, with 72 vertical layers. Gas-phase tropospheric chemistry is solved using KPP (Damian et al., 2002), and MEGAN supplies isoprene emissions data (Guenther et al., 1995, 2012).

Data Retrieval and Use

In this study, GEOS-Chem v10-01 was used to generate isoprene data for comparison to FIS measurements and output from other models. Like the GOME-2 observations, GEOS-Chem data from 2013-2015 was generated, regardless of whether or not FIS measurements were collected for the corresponding time. The model was initialised 6 months prior to the period of interest in order to reduce the effects of initial conditions. Data resolution was 2° x 2.5° , fitted to the same grid cell latitude and longitude as the as the satellite data in 1-hour time steps. 47 vertical layers were generated as part of the output, but only surface level data was used in this study. FIS measurements are compared to isoprene model output in Chapter 3, and other outputs (e.g., NO_x, O_3 and HCHO) were used as supplementary data points for the models as described in Chapter 4 as they required these inputs to successfully run and these species have never been measured at the DRO.

In the following chapter, these methods are applied to a multi-year data set collected at the DRO between 2013 and 2018. The data includes three years of

FIS measurements which are analysed across seasons and compared to satellite observations and GEOS-Chem output. In addition, the results of a solid sorbent cartridge study undertaken in March 2018 are presented and analysed.

Chapter 3

Results of the FIS Field Measurement Campaigns in the Daintree Rainforest

The results of three years of FIS measurements at the Daintree Rainforest Observatory (DRO) are presented and discussed in this chapter. In Section 3.1, the timeline for data collection is introduced, followed by a summary of the results in Section 3.4. Interannual variability is discussed in Section 3.5 and results for individual years are then shown in Section 3.6. The results are then compared to GOME-2B satellite observations in Section 3.7 and GEOS-Chem model output in Section 3.8. The chapter concludes with a summary of the key results in Section 3.9.

3.1   Data Collection Schedule

Isoprene data were collected for a total of 176 days between 2013 and 2018 (Table 3.1) during all four seasons. As the primary focus of this campaign was to measure the emission patterns during the WtD transition, there are measurements for this

season across three years. Dry season data (Jun-Oct) is available for two seasons
(2013 and 2015); DtW transition season data (Nov-Dec) is available for 2015 only
and wet season data was collected in 2018.

Table 3.1: Sampling Days at the Daintree Rainforest Observatory

Year	2013	2014	2015	2018	
	24 Apr - 24 May	28 Apr - 9 May	24 Apr - 4 May	14 Mar - 22 Mar	
	24 May - 11 Jun	10 Jun - 24 Jun	25 Aug - 3 Sep		
	28 Jun - 13 Jul		8 Dec - 20 Dec		
	28 Aug - 12 Sep				
	4 Oct - 31 Oct				
Totals	105 days	29 days	34 days	8 days	**176 days**

The Fast Isoprene Sensor (FIS) was installed at the Daintree Rainforest Ob-
servatory (DRO) in April 2013. The FIS was configured for long-term, unat-
tended sampling (discussed in Ch. 2) with a shutdown procedure to conserve
oxygen during overnight hours (21:00-05:00). DRO staff periodically checked on
the instrument to ensure its continued operation. Data, stored locally, were col-
lected from the site once every 4-6 weeks when the oxygen cylinders were changed
and regular maintenance occurred. Several mechanical and power-related issues
developed when running the FIS remotely; this led to some gaps in the data
which are addressed in the individual analyses in Section 3.6.

In 2013, sampling during the WtD and dry season occurred from 24 Apr–31
Oct (Table 3.1). The commencement of work at the University of Edinburgh was
concurrent with major renovations at the DRO, which prevented measurements
being collected during the wet season 2013–2014. FIS sampling was stopped
due to the lack of a continuous and stable power supply during that time. In
2014, measurements were taken during three trips in April and May in order
to have data from the WtD season. The first campaign was aborted when the
area was evacuated due to Cyclone Ita (landfall 12 Apr 2014 22:00 AST), but the
other two were carried to completion. Continued remote sampling was attempted
throughout the dry season (10 Jun-24 Jun), but the decision was made to cease

unattended operation after a major instrument failure. Final measurements were collected during longer, attended campaigns in Apr–May, Aug–Sep, and Dec 2015 (Table 3.1). These dates were selected in order to provide additional observations during the WtD transition season and fill in data gaps from previous years' data collection periods. Additional data was collected in Mar 2018 in order fill the gap in wet season data and conduct a solid sorbent cartridge study to clarify isoprene concentrations in the evening and nighttime hours.

3.2 Determination of Isoprene Concentrations from Photon Counts

3.2.1 Zero Calculation

As discussed in Ch.2, baseline zeroes were calculated by taking the average sample value from 5:03-5:08 and again at 21:03-21:08. These five-minute blocks coincided with when the FIS was running during unattended operation and allowed the same zero calculation to be used for every data file in the study. The two average values were set as baseline zeroes, and the difference between them was divided by 16 and fractionally applied as the zeroes throughout the day (the hourly zero).

The implementation of this approach requires an assumption that isoprene concentrations are at or very near zero at these two times every day. This assumption is feasible because the crane and the FIS are located 1.4 km from the ocean (Fig. 2.1). Thus, there is a continual influx of isoprene-poor marine air, particularly in the afternoon and evening hours, when the sea breeze pushes in air from offshore. In the early morning, isoprene emission has not occurred for several hours, and the time selected is prior to sunrise. This assumption was supported with the analysis of solid sorbent cartridge measurements. Sorbent sampling included collecting samples from late afternoon through sunset and

into the overnight hours. The results of this portion of the study are presented in Sec. 3.3.

## 3.2.2   Steps to Convert Photons to Concentrations

All FIS photon counts were recorded in Labview and several steps were required to convert counts to concentration. First, the data were put into a database in order to preserve the original text file. The day of the year was calculated from the file name and applied to each line in the file. Next, the calibration factor was derived from the average photon count during the 'zero + standard' timestep of the autocalibration. This occurred for 3 minutes of the 9-minute autocalibration sequence, but only the last 2.5 minutes was used in order to allow the FIS response to stabilise. This calibration factor was applied to the hour before and after the calibration in question. The FIS calibrates every two hours; i.e. the calibration factor from a 14:00 calibration was used between 13:00 and 15:00 on that day. These calibrations are marked by the peaks in Fig. 3.1a.

The photon response factor was calculated from the linear regression equation such that:

$$RF = (Calfactor - HourlyZero)/(IsoStd), \qquad (3.1)$$

where RF (photon counts per ppb) is the response factor, $IsoStd$ (ppb) is the amount of isoprene standard added to the system during the autocalibration (Hills, 2013), and $Calfactor$ (photon counts) is the average photon count for the automatic calibration, applied to $\pm$ 1 hr from when it was measured. $HourlyZero$ (photon counts) is the interpolated zero photon count.

The final isoprene concentration was calculated as shown in Eq. 3.2. $IsoConc$ gives the final concentration in parts per billion (ppb), $Photon$ is the photon count for a 5-second measurement interval, and RF is calculated from Eq. 3.1.
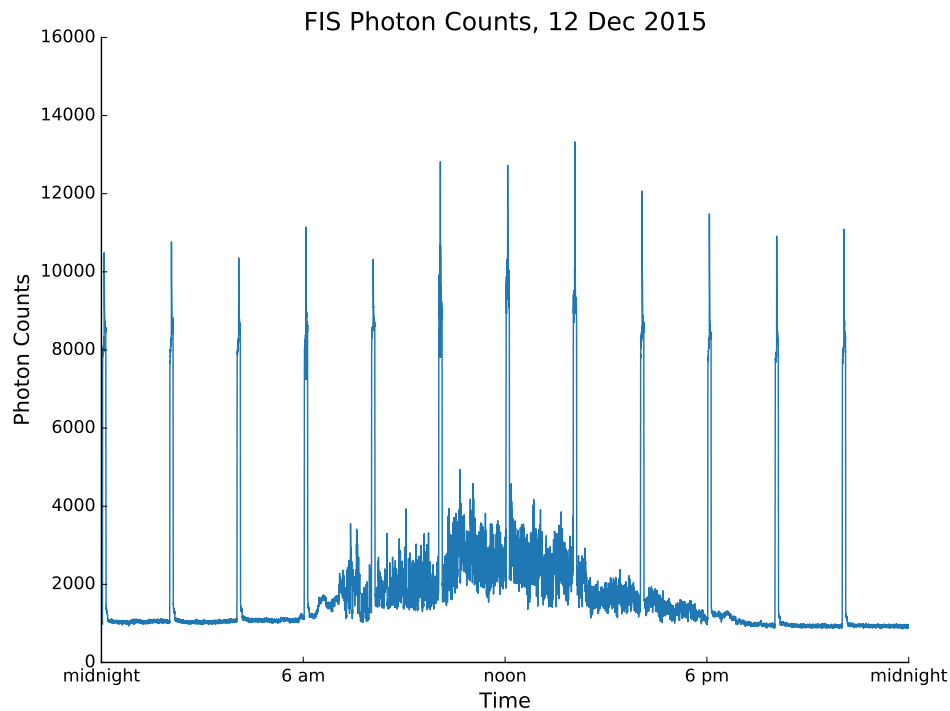
(a)
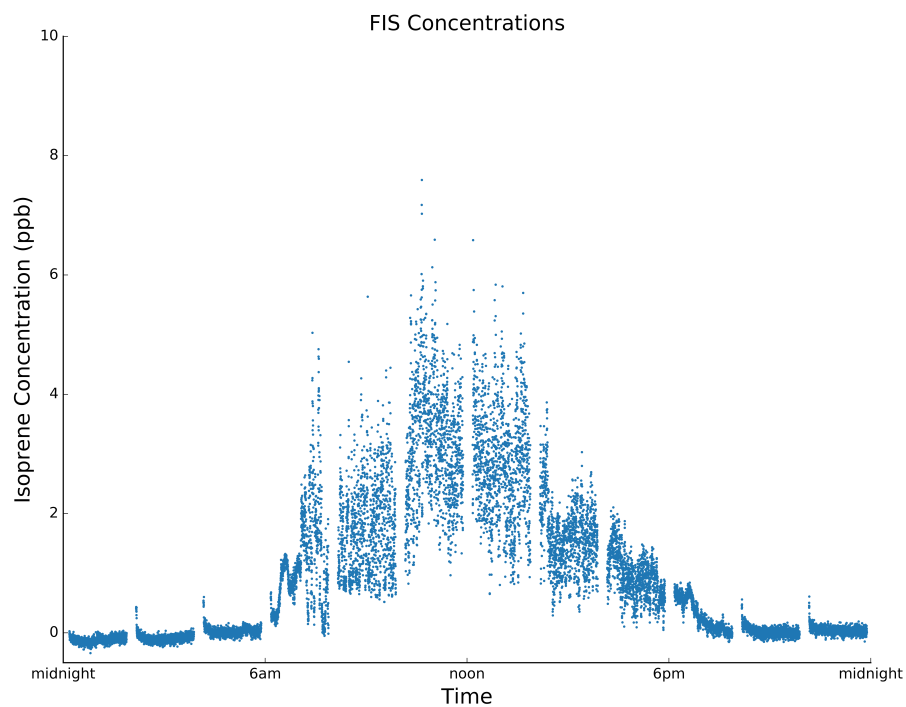
(b)

Figure 3.1: An example of a typical 24-hour sample of raw data (3.1a). The peaks throughout the day are automatic standard-addition calibrations that are used to determine the concentration for the hour before and after their occurrence. Calibration concentrations have been removed from the final data set (3.1b). Each point represents one 5-second measurement interval.

$$IsoConc = IsoStd \frac{(Photon - HourlyZero)}{(Calfactor - HourlyZero)} \tag{3.2}$$

This step was applied to all data as a database command to an entire file, which could range from a few hours to several weeks in length. In the unusual case that a complete set of observations were not available, data were occasionally processed in smaller time steps of an hour or less. This generally occurred when sampling was stopped to do a full calibration or other regular maintenance. Since the zero calculation required samples from both morning and evening, it could not be calculated if only one was present. The missing value is taken from the neighbouring file (the 05:00 zero from the first file and then the 21:00 zero from the second) and applied to the file in question. The isoprene concentration is then calculated as normal. The calibration factor occasionally required similar handling, but if there were no available calibration or zero data, the time period was left blank and the corresponding isoprene concentration was not calculated. Figure 3.1b shows the final isoprene concentration with calibration peaks removed.

3.3   Results of Cartridge Sampling

In order to assess the quality of the FIS measurements, a field campaign incorporating solid sorbent cartridges was conducted in March 2018. The cartridges were used to measure isoprene and monoterpenes throughout the day and into the overnight hours following EPA Method TO-17 (Agency, 1999). Method details, data collection and analysis procedures were described in detail in Ch. 2, and will be summarised here. Following that, the FIS and measurements will be presented and compared. Finally, there will be a discussion of the nighttime sampling portion of the campaign.

3.3.1 Data Collection and Analysis

Solid sorbent cartridges were transported from Sydney to the DRO in order to collect complementary measurements to the FIS. Prior to departing Sydney, the cartridges were conditioned for 120 minutes 350°C and 50 mL/min in an ultrapure helium carrier gas. They were transported in the author's checked luggage to the DRO. After the sample had been collected, cartridges were immediately stored inside an opaque container and refrigerated. The samples were brought back to Sydney in an insulated bag with cool blocks as part of the author's carryon luggage and immediately taken to the laboratory refrigerator at Macquarie University, where they were stored until analysis.

The sample set contains two field blanks–one stored in the DRO refrigerator immediately upon arriving, and one stored with all other cartridges and added to the refrigerator last, upon the completion of sampling. In addition to this, a field blank was collected every 10th sample. These blanks were carried to the top of the crane, opened and immediately closed, then refrigerated with the rest of the samples. 20L of air was collected in each cartridge over a period of ∼30 min.

Solid sorbent cartridge measurements were collected in fair and overcast conditions from the top of the crane tower, within 0.5 m of the FIS inlet. No sampling occurred in rainy conditions as climbing or being on the tower was prohibited due to safety concerns. Every 2nd–3rd sample was collected in duplicate in order to calculate error.

3.3.2 Results from FIS and Cartridge Measurement Campaign

The results of the 2018 measurement campaign are presented in Fig. 3.2. FIS measurements are shown in blue, solid sorbent cartridge measurements are indi-

cated in orange. The FIS data is presented as 30-minute averages–either hh:00-hh30 or hh:12–hh:30 and hh:30–hh:59, depending on whether or not there is a calibration in that hour. Cartridge data is plotted at the midpoint of the sample period. Days are separated by dashed lines and overnight hours are shaded in gray. The relative percent difference of the duplicate samples was calculated using the equation:

$$RPD = \frac{x_1 - x_2}{\overline{X}} \,, \tag{3.3}$$

Where x_1 and x_2 represent the duplicate samples and $\overline{X}$ is the mean of the samples. The calculated precision was applied to samples collected within two hours of the duplicate. The majority of errors were within 60% of one another and a small number were in excess of 120%. As shown in the plot, cartridge measurement tracks closely to FIS response, with only one outlier (on 16 Mar) that does not have error bars that cross the line of FIS concentrations.
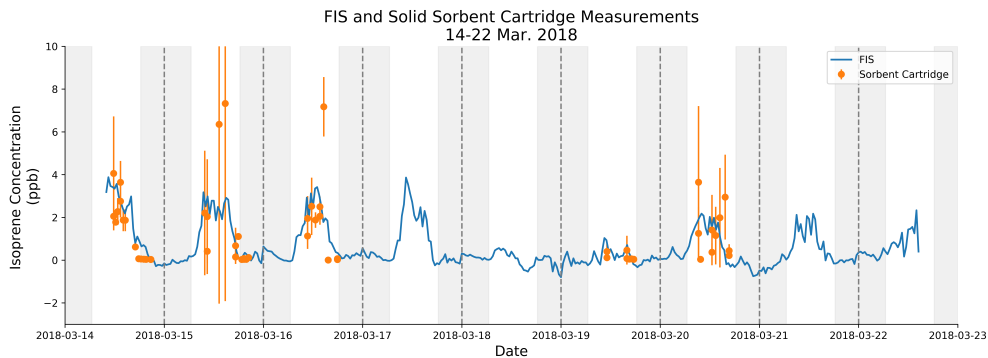

Figure 3.2: Time series of 2018 FIS and solid sorbent cartridge data. FIS concentrations reported in 30-minute averages, cartridge measurements plotted at the midpoint of their measurement period. Days are separated by dashed lines, and evening hours are denoted by the shaded areas.

A direct comparison of FIS and cartridge measurements is shown in Fig. 3.3. Here, the FIS measurements have been time-matched to coordinate with the times that sample collection took place. The figure shows good agreement between the measurement techniques, with a 1:0.87 correlation and an offset of 0.04 ppb.

These results clearly indicate that the isoprene detected by the FIS matches what is measured with the solid sorbent cartridges. Other compounds that are known to contribute to isoprene signal in the FIS (e.g., MVK or methacrolein, see Ch.2) were not detected in these samples, so it is unlikely they are contributing to any difference in responses.
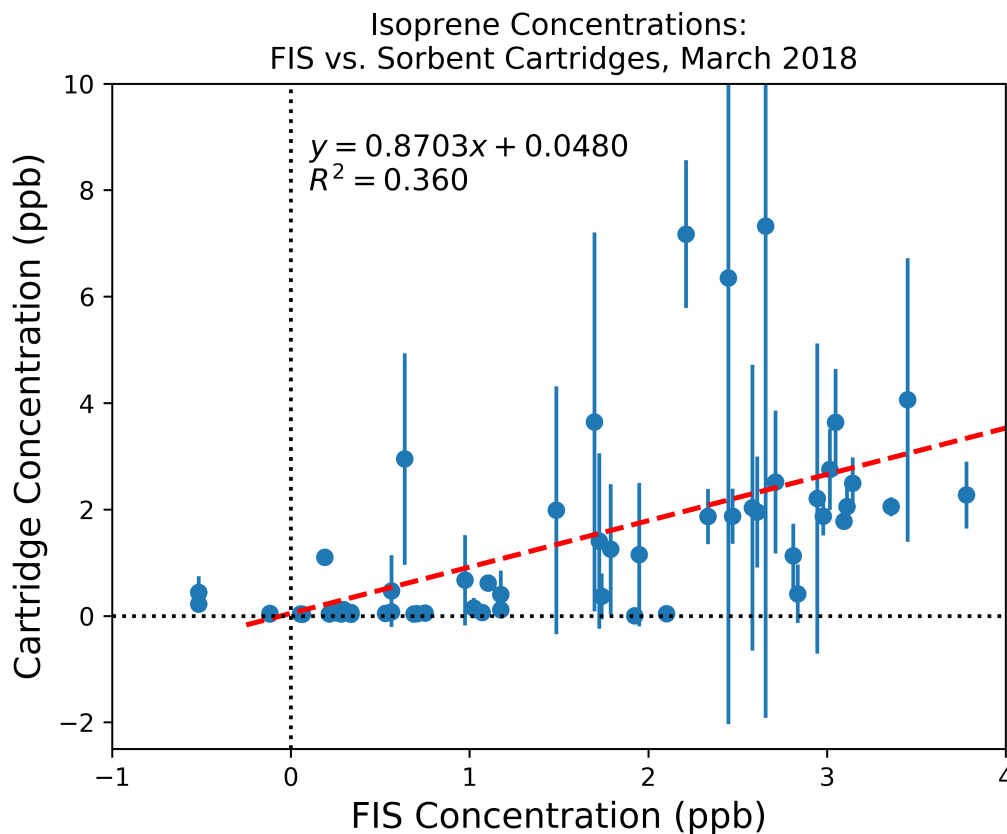

Figure 3.3: Scatterplot of solid sorbent cartridge data compared to FIS observations. FIS measurements are the average concentration time-matched to the cartridge measurement sampling times. Line of best fit shown in red.

In their analysis of BVOC measurement techniques, Dunne et al. (2018) found a 20% difference between results when comparing PTR-MS isoprene measurements and solid sorbent cartridges analysed by GC-MS. They found a correlation of 1:1.23 and an intercept of 0.31 ± 0.10 ppbv (Dunne et al., 2018), with the best agreement in midday, no significant correlation in the early morning (05:00-10:00) and a slope of 1.18x + 0.41 in the evening and overnight hours, indicating that other compounds were contributing to the PTR-MS signal, and the

relative contribution was highest in the evening. The results from the Daintree are similar to these and other findings reported in the literature, which include slopes of 0.79-2.15 and offsets up to 0.39 ppb (Dunne et al., 2018, and references therein).

3.3.3   Results of Nighttime Sampling Campaign

One focus of this field campaign was to collect solid sorbent samples as late as possible (up until 21:30) in order to provide secondary measurements and justify the zero calculation throughout the study. Continuous sampling from 17:00-20:30 or 21:00 occurred on three clear nights in this study; sampling ended at approximately 18:00 on overcast evenings.
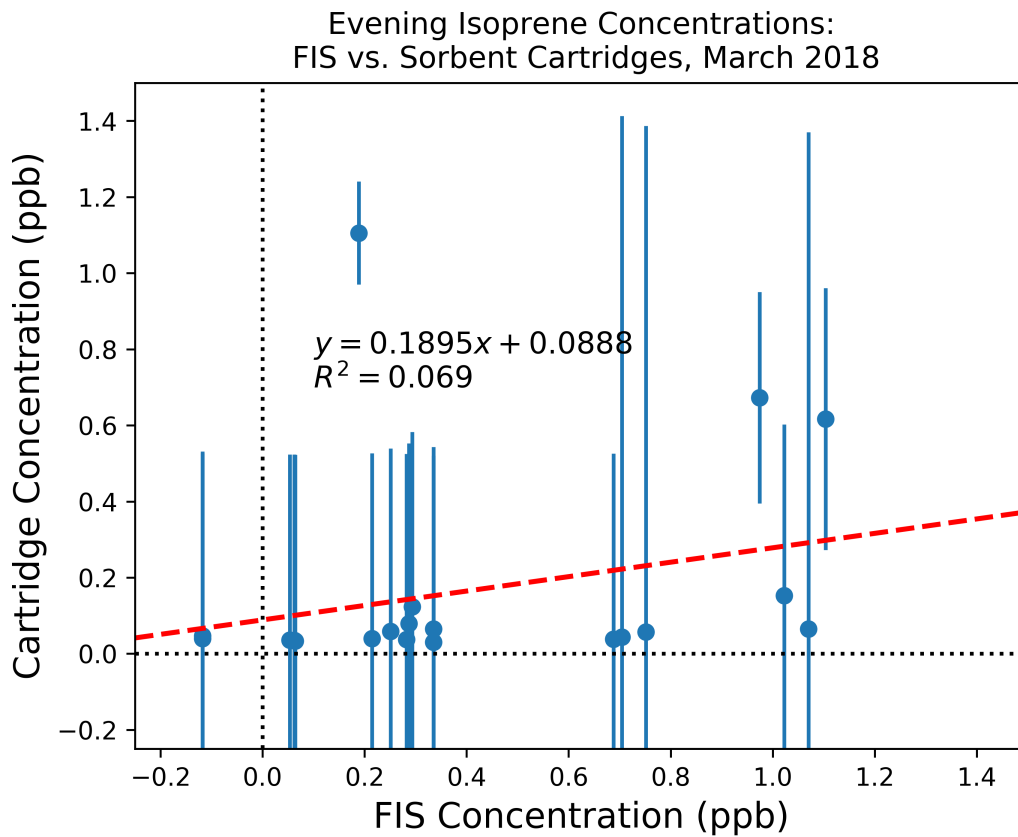

Figure 3.4: Scatterplot of solid sorbent cartridge data compared to FIS observations between 17:00-21:00. Line of best fit shown in red.

Figure 3.4 shows a comparison of FIS and solid sorbent cartridge measure-

ments at the DRO between the hours of 17:00 and 21:30 across all days in the study where evening cartridge measurements occurred. In contrast to Fig. 3.3, this plot shows a more biased response, with a 5:1 correlation between the FIS and cartridge measurements. Like Figs. 3.2 and 3.3, the errors are generally large because the average concentrations are less than 1 ppb and when that is used as the denominator in the error calculation, even small differences between the concentrations in the duplicate samples will cause the error to exceed 100%. Though the R^2 of the nighttime averages is only 6%, all but two of the error bars cross the line of best fit and half of them have an average difference of <0.25 ppb.

3.4 Summary of Results from Ground-Based Measurements

Isoprene concentrations across the measurement time period show regular variations that can be attributed to seasonal periods of growth. Table 3.2 summarizes the mean concentrations (ppb) of isoprene for the times 12:00-15:00 across all sampled seasons. The results from this data set show that concentrations reach a maximum in the DtW transition (late spring-early summer), and are at a minimum during the dry season, which corresponds to the winter months. Isoprene concentrations were highest in 2015 and lowest in 2013.

Table 3.2: Isoprene Concentrations Measured Between 12:00-15:00 at the DRO from 2013-2015

Season	Height (m)	Isop (ppb, 12:00-15:00)
2018 Wet	35	1.29 ± 0.31
2013 WtD	35	0.21 ± 0.03
2015 WtD	35	1.42 ± 0.05
2013 Dry	35	0.36 ± 0.03
2015 Dry	35	0.94 ± 0.08
2015 DtW	35	1.52 ± .09

As discussed above, FIS isoprene measurements were collected for 29 days

in 2014. The FIS also experienced several failures throughout these field studies due to a manufacturing defect that led to cracked ozonizer tubes (Figure 3.5). As it failed, the sensitivity of the FIS decreased to 10 % of normal. The raw data from the most successful measurements is shown in Figure 3.6, but the data set was not deemed reliable enough for inclusion in any further analyses.

Figure 3.5: Damage to the ozone generator, discovered during a refurbishment.

All hourly isoprene concentrations for the measurement campaigns are shown in Fig. 3.7. Seasonal variation is observable in 2015 (Fig. 3.7b), with annual minima in the dry season. These results show that the WtD season emission pattern in the Daintree differs from the ground-based and satellite observations reported from the Amazon in Yañez Serrano et al. (2014), Barkley et al. (2008) and others, which show annual minimum isoprene emissions occurring during the WtD transition period. They are closer to measurements from Asian forests (e.g., Langford et al. (2010)), which show little variation in concentrations throughout the year.

These results are reflected in Fig. 3.8, which shows box plots of hourly concentrations by year and season between 6:00 and 18:00. There is a clear diurnal variation, and the seasonal variation is apparent as well. With the exception of
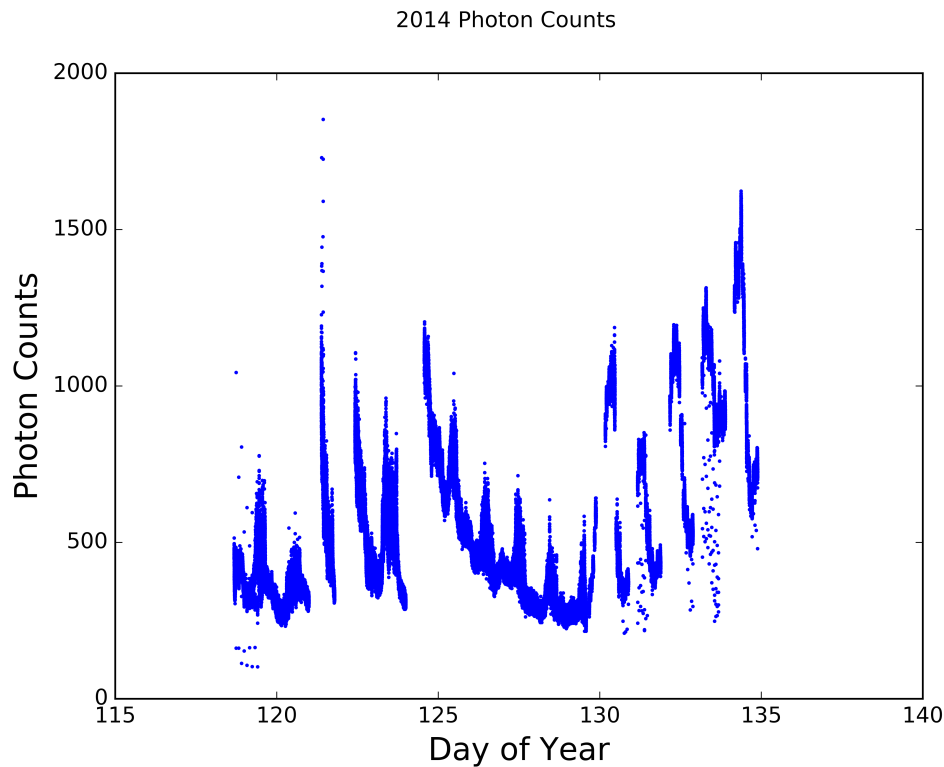
Figure 3.6: Plot showing the photon counts measured by the FIS in 2014. Each point represents a 5-second measurement period.

2013, isoprene concentrations peak at an average of 1.5 ppb during the 12:00–15:00 hours in the WtD transition season in 2015, but are only 0.2 ppb during the same time and season in 2013. During the dry season, isoprene concentrations reach a maximum of approximately 1 ppb between 12:00–15:00. The DtW transition season shows the highest daily average isoprene concentrations, with average peaks of 1.5 ± 0.09 ppb between 12:00-15:00.

Figure 3.9 shows a comparison of FIS measurements to net radiation for the three measurement campaigns. The FIS measurements are presented as hourly averages and grouped annually. Of the three measurement campaigns, the highest R^2 occurs in 2018. This is likely because these measurements occurred during only one season. The poorest R^2 occurs in 2013, which had the most measurements and the most data collected during three seasons. 2013 had the most days under cloudy or overcast conditions (<400 W/m^2), which explains why it had the lowest average peak concentration values presented in Table 3.2.

FIS Measurement Data Set
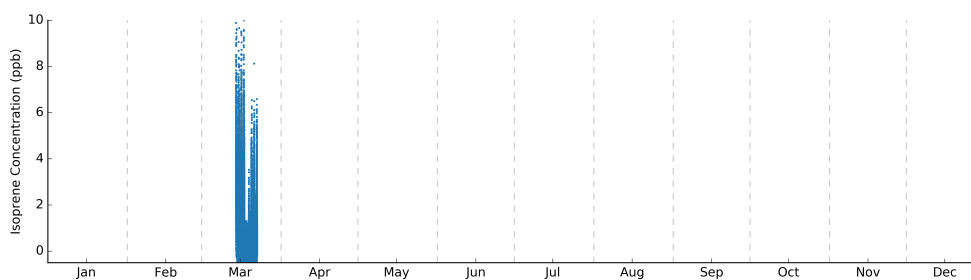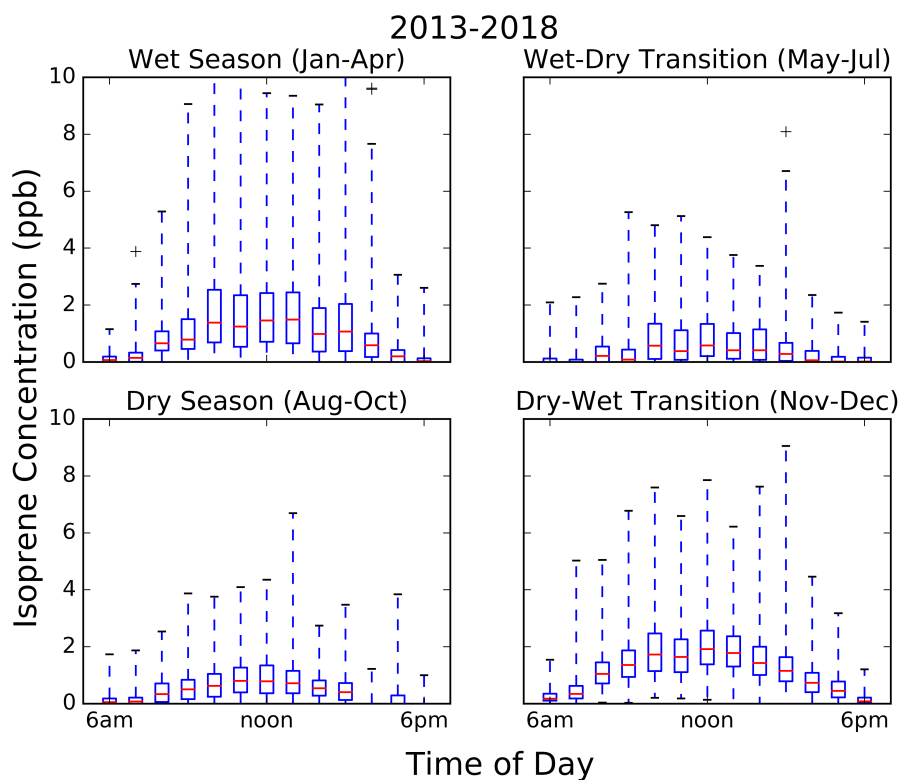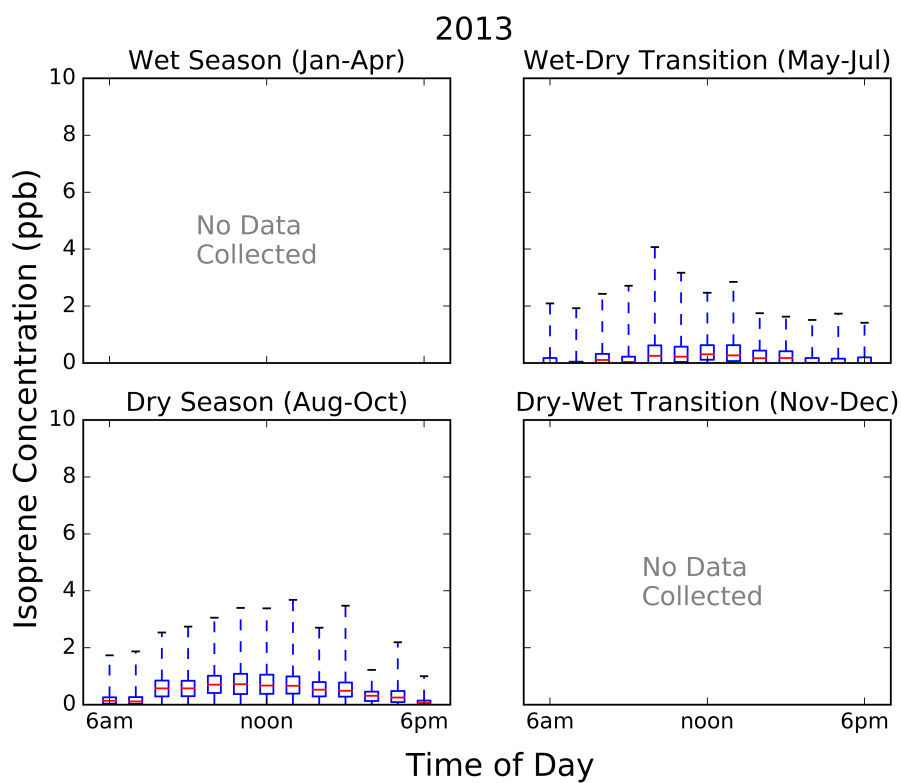

(a)

(b)
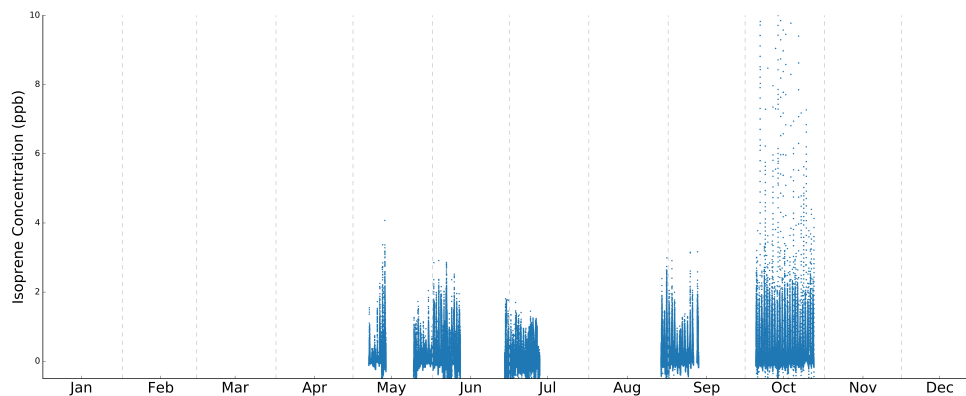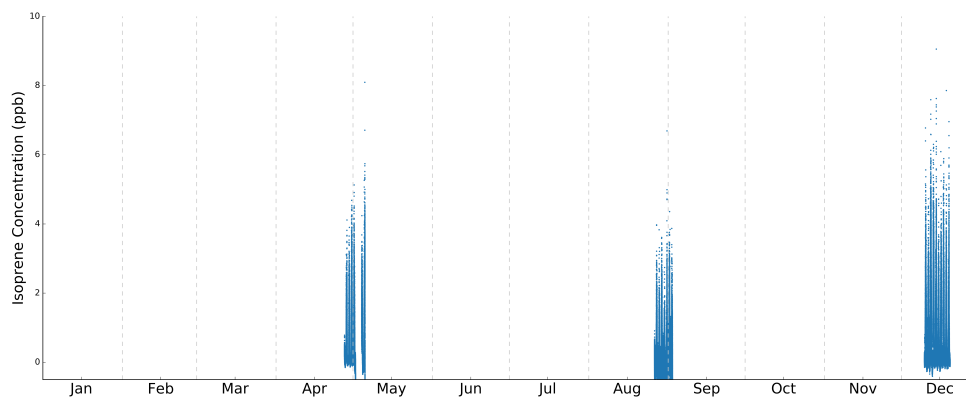
(c)

Figure 3.7: Plot showing all DRO isoprene concentration measurements with an averaging time of 5 seconds. Figure (a) is for the 2013 measurement season, (b) shows 2015, and (c) shows 2018.
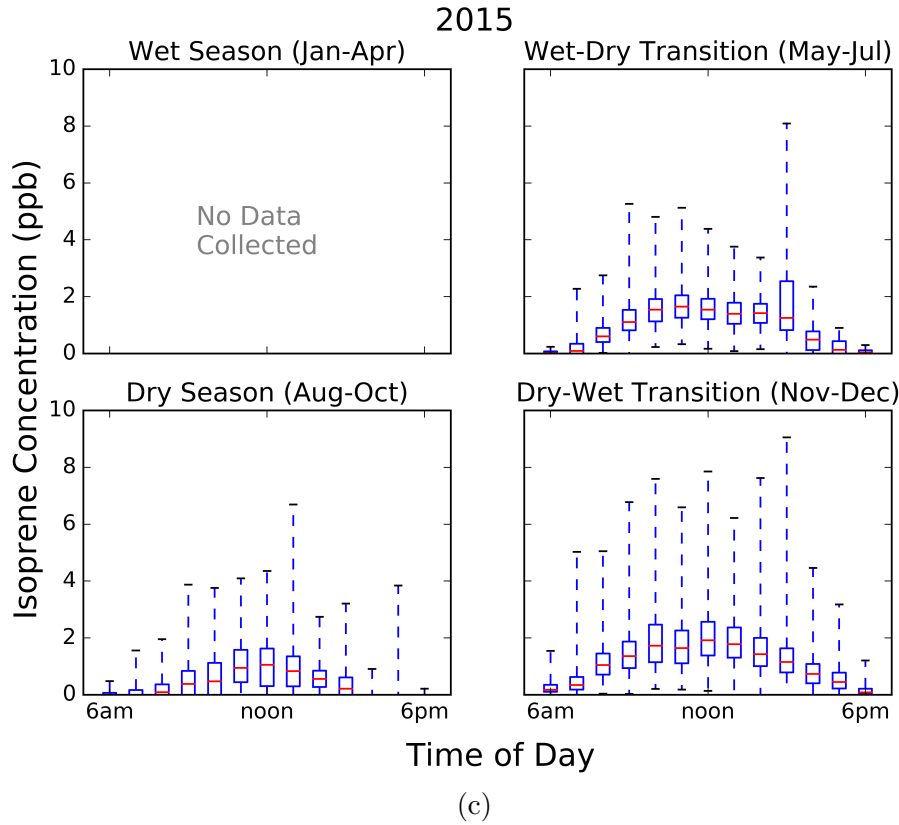
2013-2018

(a)

2013

(b)

Figure 3.8: Hourly average isoprene concentrations (ppb), averaged over a season.

A comparison of these results to other ground-based studies in the tropics (Table 1.1, Ch. 1) shows some similarities. Because the wet and dry seasons in the Daintree do not occur in the same months of the year as the Amazon, seasonal behaviour is being compared rather than specific calendar months. There is only one Amazonian study that covers multiple seasons in one site in one year (Yañez Serrano et al., 2014). This study occurs at the Amazonian Tall Tower Observatory (ATTO), 135 km NE of Manaus, Brazil. Yañez Serrano et al. (2014) report average above-canopy peak mixing ratios of 2.39-6.13 ppb in the wet and dry seasons, respectively.

In the Daintree WtD season, the maximum mean concentration is 1.42 ± 0.05 ppb, with an upper quartile of ~ 2.25 ppb between 12:00 and 15:00. However, the maximum reported concentration in all three years is variable, ranging from 4 ppb in 2013 to more than 6 ppb in 2015. Two Amazonian canopy-level studies

(a)

(b)

(c)
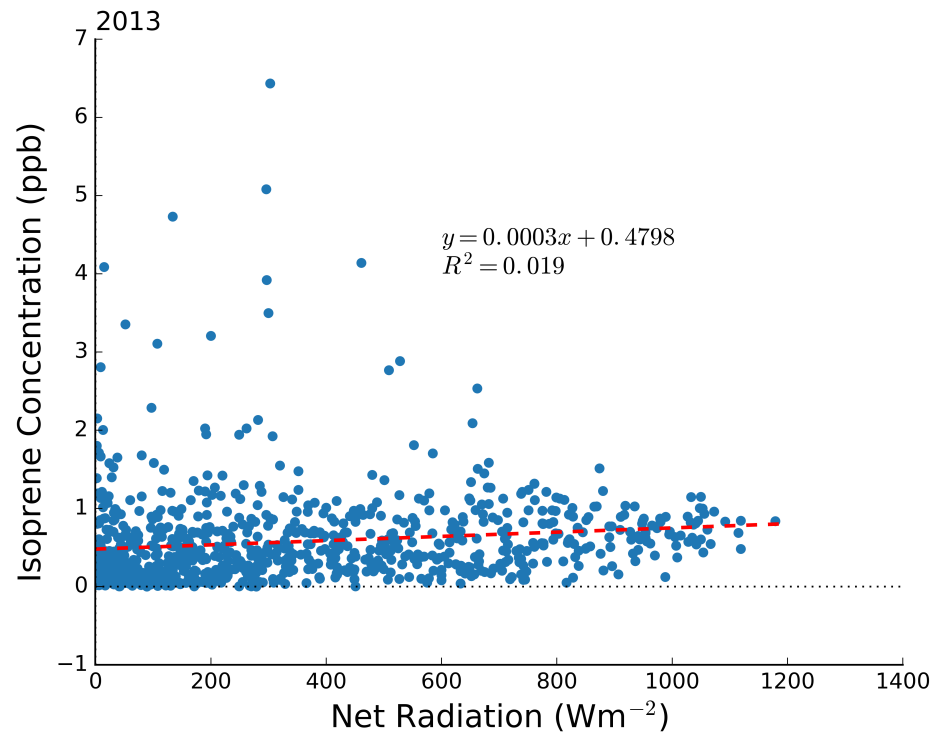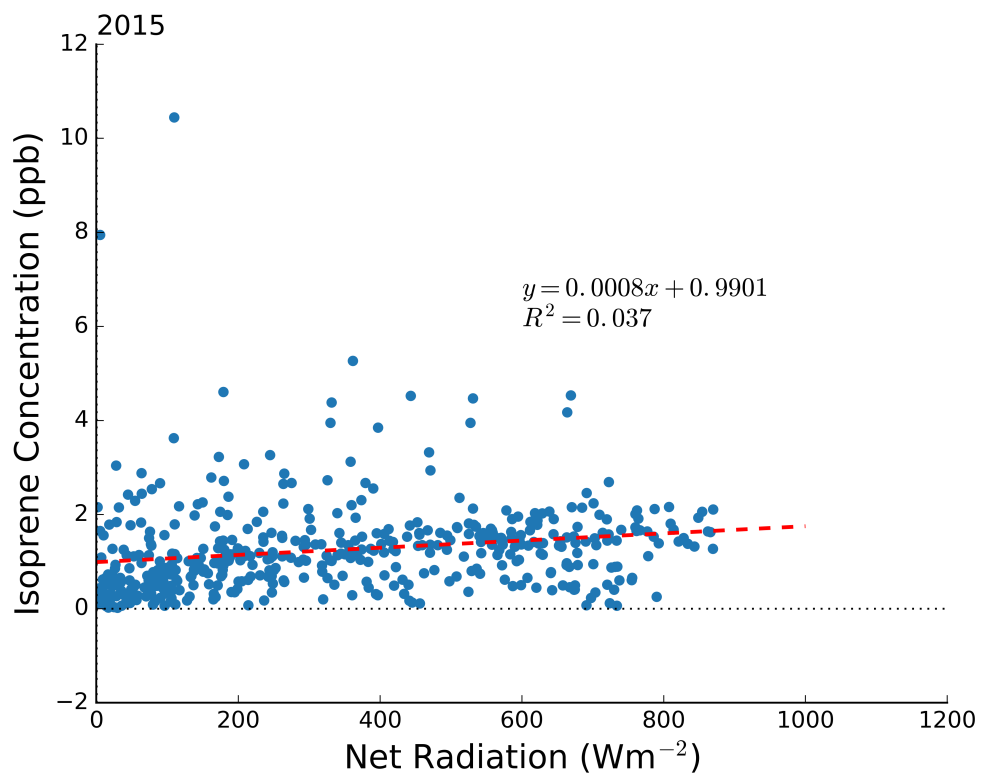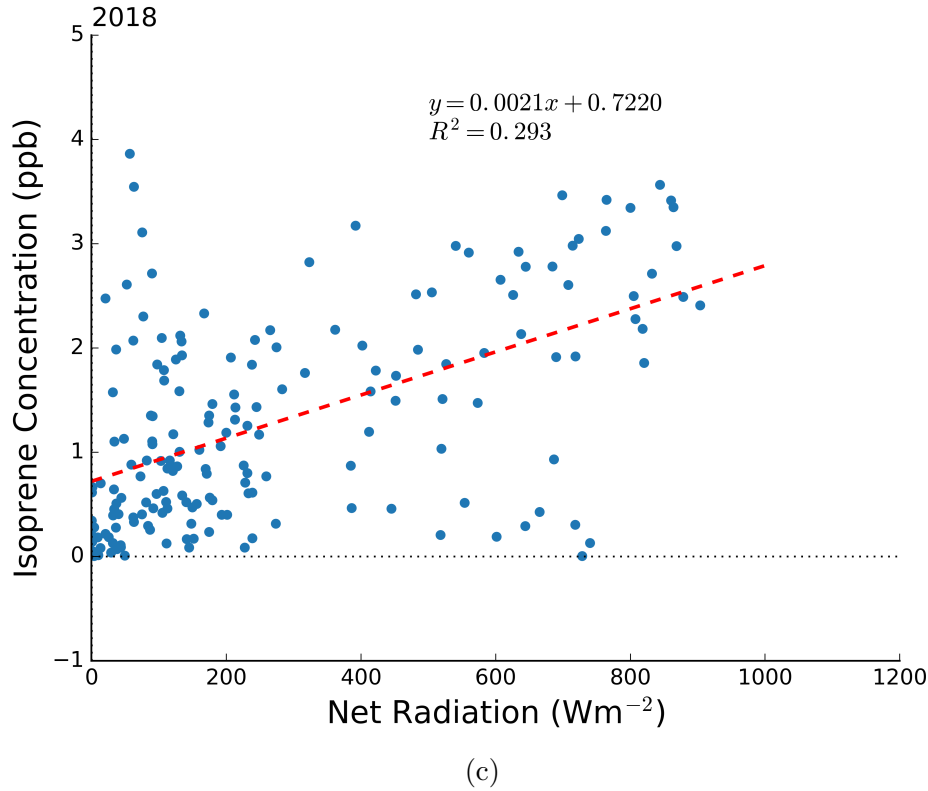
Figure 3.9: Hourly isoprene measurements compared to net radiation.

report data from the same season (Kuhn et al., 2002; Rinne et al., 2002). Rinne et al. (2002) observe mixing ratios of 4-5 ppb, and in a different part of the forest, Kuhn et al. (2002) reported 9.00 ppb, nearly twice the value reported by Rinne, et al. Still, even the lower value is 2 times greater than the interquartile range for the same season in the Daintree.

In this study, isoprene concentrations were observed to be at a minimum during the dry season, with a significant difference between 2013 and 2015. In 2013, the 12:00-15:00 mean is 0.36 ± 0.03 ppb, while the 2015 mean is 0.94 ± 0.08 ppb. The maximum observed concentrations in both years were 4-6 ppb. The majority of the dry season data in this data set comes from 2013; measurements were collected for only a 10-day period in 2015. There are several tropical canopy level studies to compare during the dry season; Amazon canopy studies span from three days (Geron et al., 2002) to three months (Yañez Serrano

et al., 2014). Mixing ratios reported from the Amazon range from 2.8-6 ppb in different parts of the forest, in different years (Geron et al., 2002; Jardine et al., 2011; Kuhn et al., 2007; Yañez Serrano et al., 2014). Like the WtD transition, the concentrations measured in the Daintree Rainforest are approximately half those measured in the Amazon. However, the Daintree measurements are in much closer alignment with isoprene measurements from Borneo. Langford et al. (2010) reported concentrations of 1.5-2.5 ppb in a Malaysian rainforest during the dry season. The difference in these measurements and those originating from Amazonian studies were noted, and attributed to the lack of a marked seasonality in Borneo (Langford et al., 2010).

In the DtW season, there are no tropical canopy studies with which to compare the findings presented here. There are some Amazonian wet season studies, one of which reports peak mixing ratios of 2.39 ppb above the canopy (38m) at the ATTO site (Yañez Serrano et al., 2014), which is twice the peak mixing ratio observed in the Daintree. Another reports a canopy-level (30m) peak mixing ratio of 7.5 ppb at a site 50 km NW of Manaus, Brazil (Kesselmeier et al., 2000). Additionally, Muller et al. (2008) have reported modeled Amazonian isoprene emissions using MEGAN to be 2-5 times lower in the wet season than the dry. If concentrations in the wet season are consistent with those observed in the DtW season, then the Daintree difference between dry and wet season emissions would be at the lowest end of that range.

These results also have several implications for emissions modeling. As discussed in Ch. 1, the MEGAN model has a positive bias across tropical latitudes, with factors driving this overestimation differing across continents (Barkley et al., 2008; Marais et al., 2014; Stavrakou et al., 2014). Given that the concentrations reported here are near the bottom of the range of observations in Amazonian forests across all seasons, MEGAN is likely to overestimate emissions here as well. Like Africa, one reason for this overestimation is that plant-level emission

data for this region is quite limited. Another reason for this overestimation is that this site and much of the Daintree is coastal, which has been cited as a region with significant uncertainties in the understanding of BVOC production and chemistry cycles (Exton et al., 2014).

3.5   Interannual Variability in the Wet-to-Dry Season

In addition to seasonal trends, the number of samples and length of time represented in this data set allows for a discussion of possible drivers of variability. As discussed in the previous section, these variabilities are observed in both seasonal and interannual perspectives. Comparing results interannually shows variability (Figure 3.10), and satellite data corroborates FIS measurements indicating that isoprene emission are occuring during the WtD season. The relationship between isoprene emissions and plant stress, the presence of mature leaves, and environmental conditions was discussed in Chapter 1; these influence of these factors on concentrations measured in the Daintree are examined here.

3.5.1   Leaf Area Index

The Leaf Area Index (LAI) is one factor that could explain the seasonal variation seen in Figures 3.7 and 3.8. The LAI describes the one-sided green leaf area per unit ground surface area associated with a tree (m^2/m^2), though it is often averaged across a canopy. The index is used as an indicator of plant productivity and evapotranspiration and it is generally positively correlated with isoprene emissions. Though trees are green throughout the year in the tropics, studies show seasonal scale variation of LAI (Myneni et al., 2007). These LAI variations will have an effect on the seasonal emission rates of isoprene, and are hypothesized to
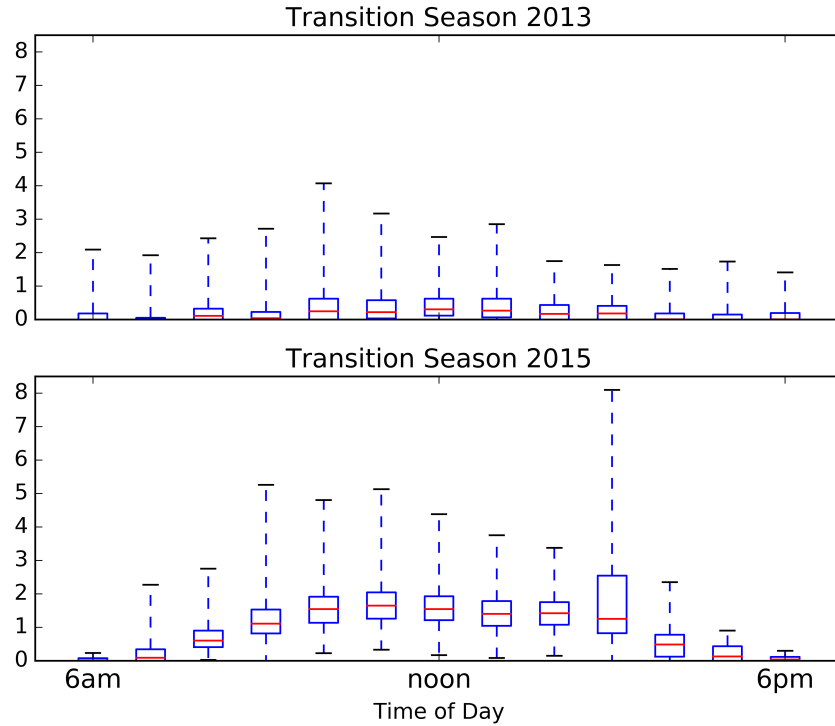
Figure 3.10: Isoprene concentrations during the WtD transition seasons

be one of the drivers affecting the annual minimum seen in the Amazon during the WtD transition season (Barkley et al., 2009). Though Gulden et al. (2007) observes a near-linear relationship between LAI and modelled isoprene emissions, a more recent study shows LAI is a very weak driver of modelled isoprene inter-annual variability in the continental United States (Tawfik et al., 2012). Tawfik et al. (2012) attributes this difference to an indirect response of soil moisture, which was not explicitly uncoupled from LAI in the model used in the earlier study.

All measurements made at the DRO to date indicate that the LAI of the Daintree is lower than the Amazon (Liddell and Laurance, 2015; Pokorska et al., 2012). There is only one published ground-based value (3.9 Pokorska et al., 2012) though the measurement season is not reported. Additional measurements are in the 'upper 3's to lower 4's' (S. Laurance, JCU, personal communication, 2014). By contrast, LAI estimates from the Amazon range from 4.0-5.5 (Myneni

et al., 2007). This difference could be attributed to the growing patterns in the Daintree, which has been previously damaged by cyclones (S. Laurance, JCU, personal communication, 2014). The Daintree Rainforest has a broken, uneven canopy, which is a lasting impact of cyclone damage. The effects of cyclones and hurricanes on forested areas have been shown to persist for decades (Chi et al., 2015). The Wet Tropics region, including the entire Daintree Rainforest and this site, has been described as 'hyper-disturbed', as there are always some areas of the rainforest recovering from a cyclone, flood, or fire (Bellingham, 2008; Turton, 2008).

Though topography plays a key role in enhancing or restricting storm impacts, larger trees tend to be more affected than smaller ones in the same vicinity (Ostertag et al., 2005; Staben and Evans, 2008; Turton, 2008). Large, flat leaves tend to be defoliated more frequently, on account of an increased aerodynamic drag in high winds (Herbert et al., 1999), but other plant traits, such as wood density, leaf thickness, and prior damage, contribute to a tree's resilience (Curran et al., 2008; Ostertag et al., 2005). While de-foliated branches will recover quickly, broken branches, uprooting, and fallen trees have longer-term effects on forest structure, such as a lower canopy height (Webb et al., 2011).

3.5.2   Water Availability and Drought

Water availability also has an effect on isoprene emission rates, and drought in particular. In addition, cyclones have been shown to alter existing moisture regimes (Laurance et al., 2002). Figure 3.11 shows the rainfall patterns in the five months leading up to and including the WtD transition season, and compares the rainfall for a given month to the climatological average. In the period leading up to the 2013 measurement season, 1499 mm of rain fell in the five months prior (Nov 2012–Mar 2013), making it the driest of the wet seasons (Figure 3.11a). However, this year received the most rainfall (1155 mm) during the WtD tran-

sition. The beginning of 2015 was characterised by a very strong El Niño cycle. 2021 mm of rain fell in the five months before the 2015 WtD transition, and then decreased sharply; the DRO received only 382 mm of rain during the WtD transition season (Figure 3.11b).

Several studies have investigated the relationship between soil moisture and isoprene emissions, though the majority are concerned with the impact of drought (Gu et al., 2006; Huang et al., 2014; Potosnak et al., 2013) . As mentioned in Ch. 1, isoprene emission activity is largely resistant to the changes that drought stress bring to a plant, even when photosynthetic activity begins to deteriorate (Monson et al., 2007; Tingey et al., 1981). Overall, a decrease in soil moisture can reduce global isoprene emissions by 20% (Muller et al., 2008), though Niinemets (2010) suggests that short-term droughts have no effect on isoprene emissions. Tawfik et al. (2012) shows soil moisture to be one of the largest drivers of interannual variability of isoprene emissions in the continental United States; soil moisture was responsible for 5-15% of interannual variability, depending on region.

An unpublished thesis by Daniel Zweekhorst attempted to quantify the role of soil moisture at the DRO for the year 2013 (Zweekhorst, 2014, unpublished thesis). He concluded that soil moisture did not play a strong role in isoprene variability at the DRO, though he did not include any interannual comparisons. This remains an area for future work at this site.

3.5.3   El Niño

El Niño in Far North Queensland is marked by a significant absence of rain during the wet season (Dec-Feb, Figure 3.12). Rainfall normalises during the WtD transition, with rainfall generally within 10% of the climatological average, while the rest of the eastern half of the continent experiences dry conditions. Dryer than average conditions generally return in the dry season (Aug), and
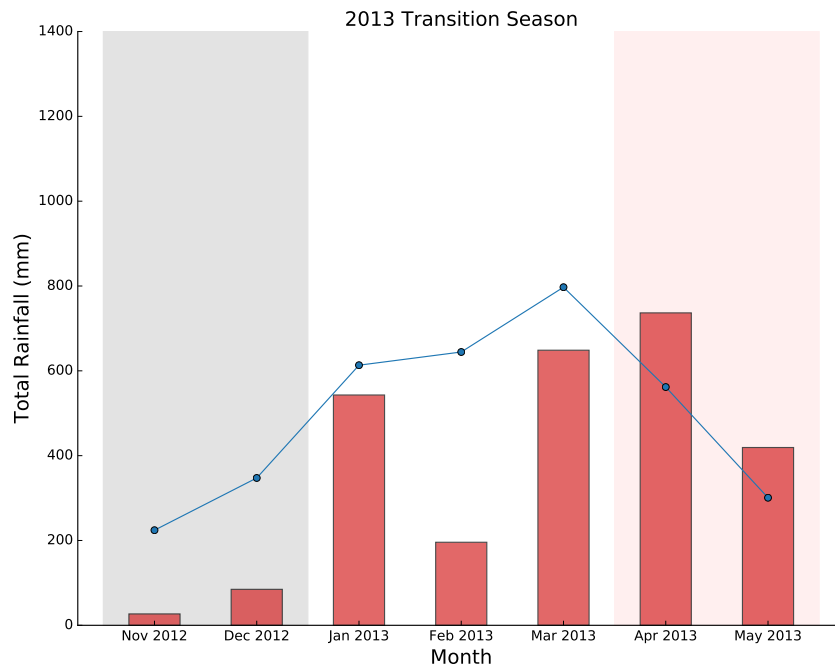
(a)
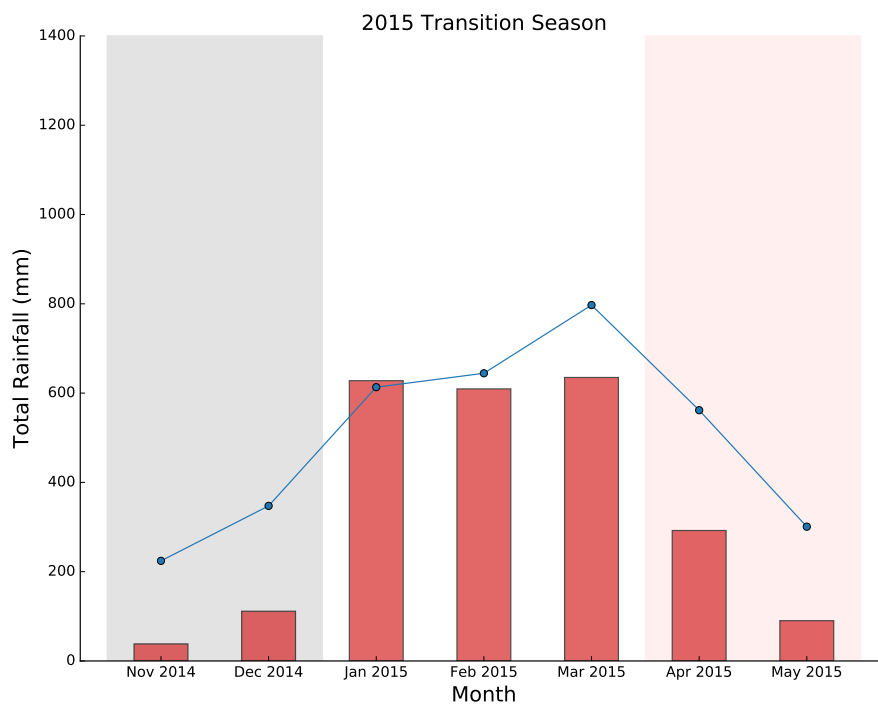
(b)

Figure 3.11: Total rainfall in the months leading up to each measured wet-to-dry transition season. Bars indicate total rainfall at the DRO, and the line indicates the climatological average (1980-2010). The gray shaded area indicates the WtD season and the red shaded area indicates the WtD season. Climatological temperature data is not available for this site.

prevail through the remainder of the year. These conditions can be seen in 2015 (Fig. 3.11b), particularly when compared to 2013.
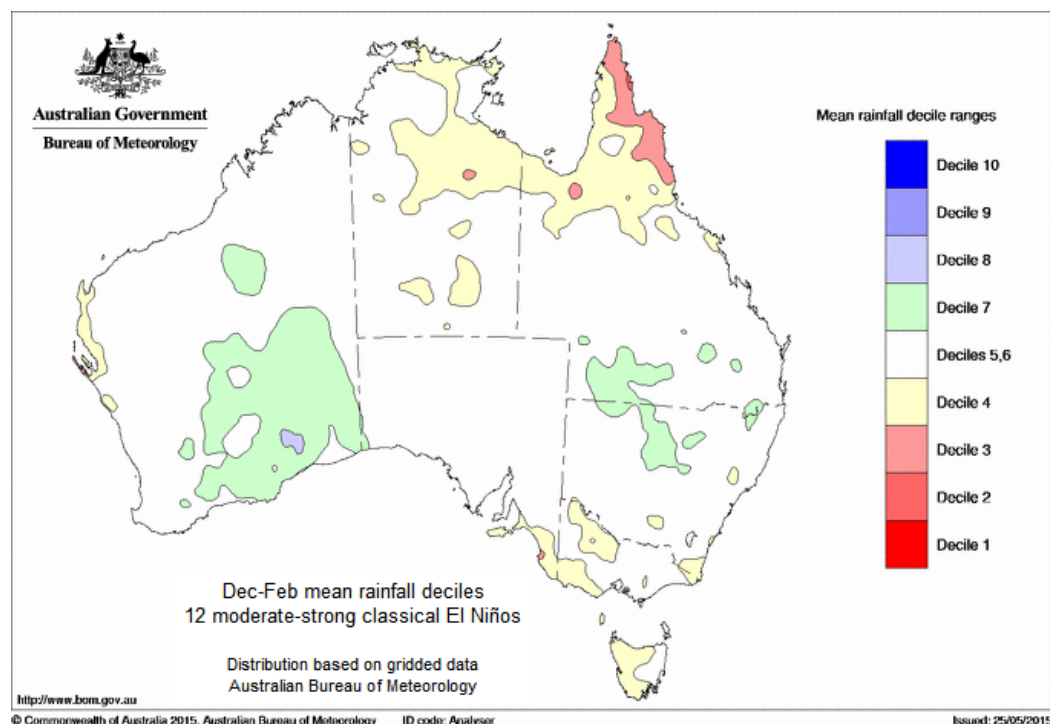
Figure 3.12: Rainfall departures from climatological average between Dec-Feb during moderate-strong El Niño. Green-blue areas indicate wetter than average; yellow-red indicates lower than average. *(Image courtesy Australian Bureau of Meteorology)*

3.6 Results from Individual Measurement Campaigns

3.6.1 2013 Results

The 2013 data set has the most coverage of all three years, spanning 105 days. The FIS was installed in the Daintree on 24 April 2013, and ran until 31 October 2013. However, there are several gaps in the data set, primarily due to instrument failures.

Figure 3.13 shows the isoprene concentrations (ppb) measured at the DRO

Figure 3.13: FIS measurements of isoprene concentrations (ppb) for the year 2013. Each point represents a 5-second measurement period.
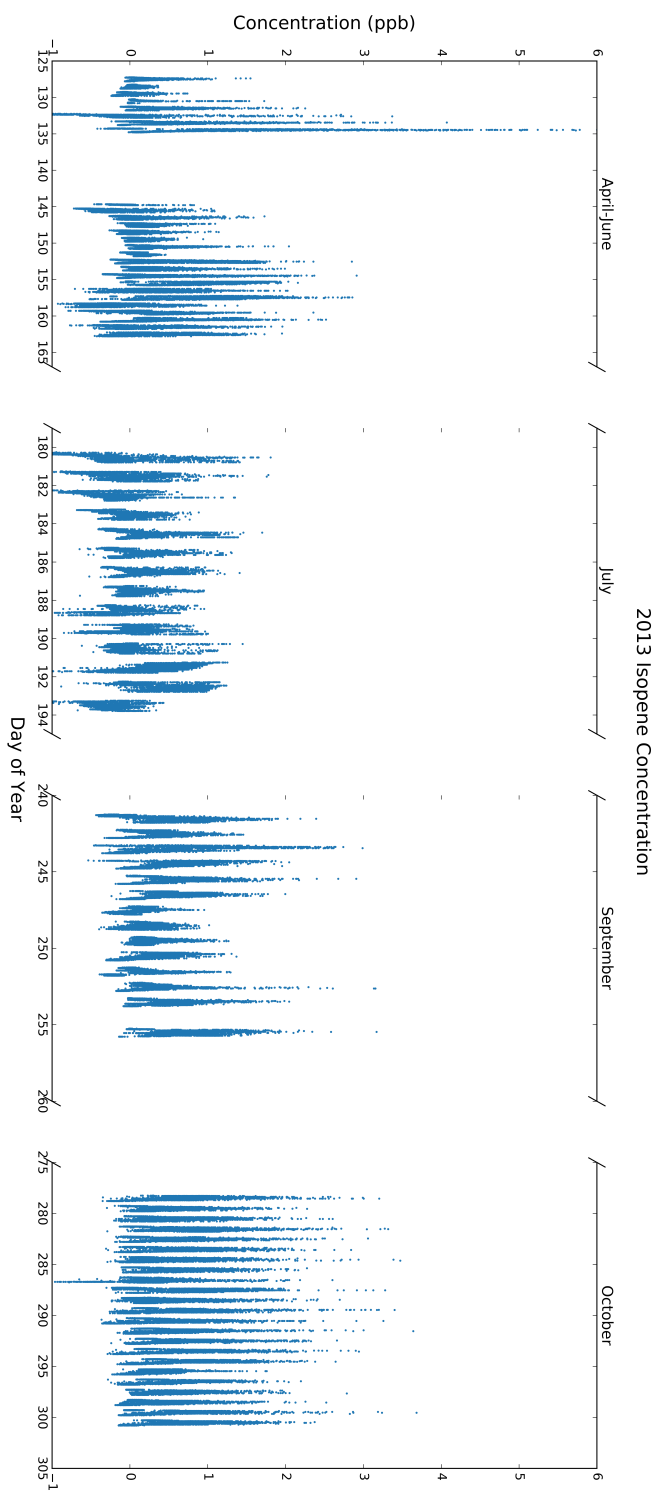
in 2013. The highest concentrations are in May-June and October, where daily maximum concentrations are ~ 3 ppb, and the lowest are in July, where the daily maxima are 1-2 ppb. There are some days, particularly in July, where the concentrations are <0, but they are artefacts of the process of converting from photon counts and concentrations, and occur either before sunrise or after sunset. The relationships between isoprene concentration, temperature, and net radiation are shown in Figure 3.14. Temperatures are shown along the x-axis, with net radiation indicated by the color bar. With a few exceptions, concentrations are mostly at or just above zero when radiation is the lowest (<200 W/m^2). Concentrations rise above 1 ppb when temperatures are high and there are full sun conditions (net radiation >800 W/m^2).
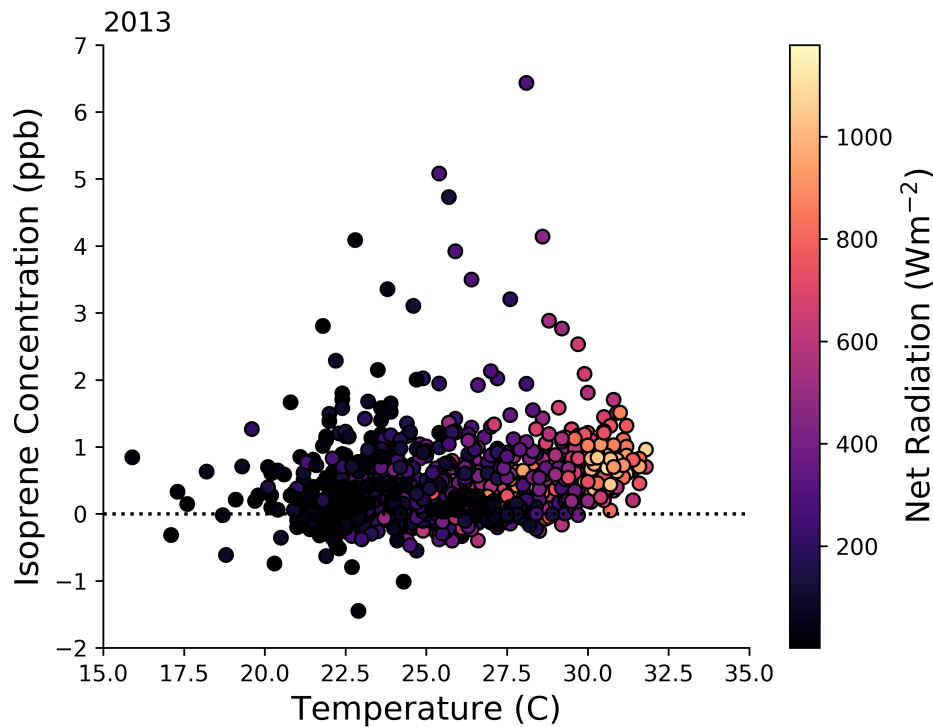

Figure 3.14: Scatterplot of hourly FIS measurements as a function of temperature and net radiation. The color bar indicates net radiation (W/m^2).

3.6.2   2015 Results

The 2015 dataset is comprised of three intensive field campaigns (Table 3.1), which ran 24 hours a day for periods of 10 days to 2 weeks; isoprene concentrations are shown in Figure 3.15. The sampling periods for this season were identified as ideal opportunities to address the project aim of measuring isoprene emissions across all seasons, while adding to the WtD transition season measurements.
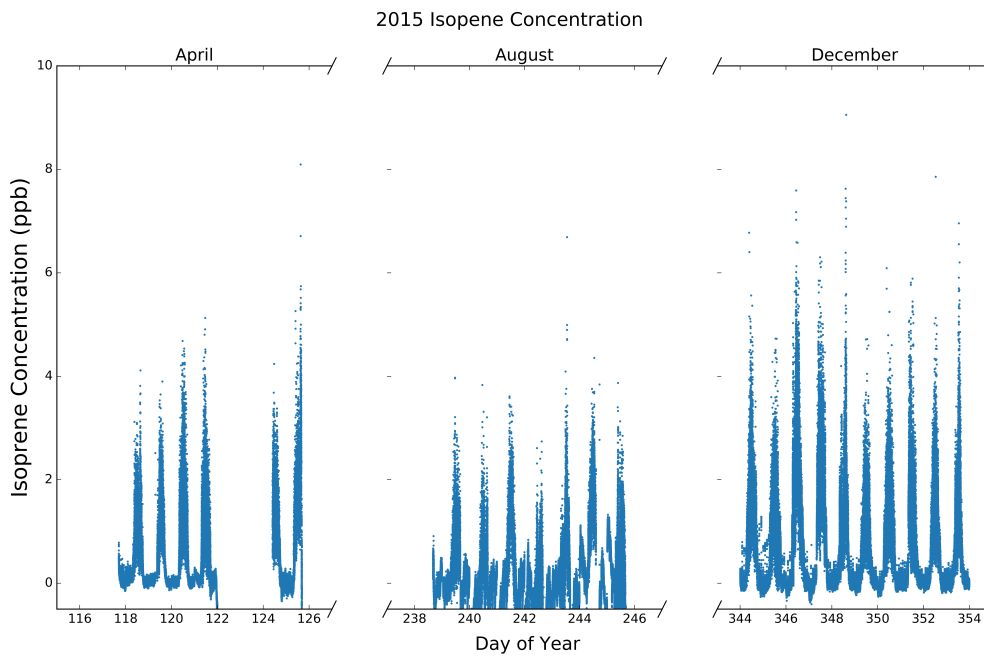
Figure 3.15: Isoprene concentrations measured by the FIS in 2015 with an averaging interval of 5 sec.

Figure 3.16 shows the 2015 measured isoprene concentrations compared to net radiation and temperature. There is a clear relationship between temperature and net radiation for this data set, with isoprene increasing once temperatures are >26.5°C. This emission pattern is more temperature-driven, as emissions occur even when net radiation is low (i.e., overcast days).
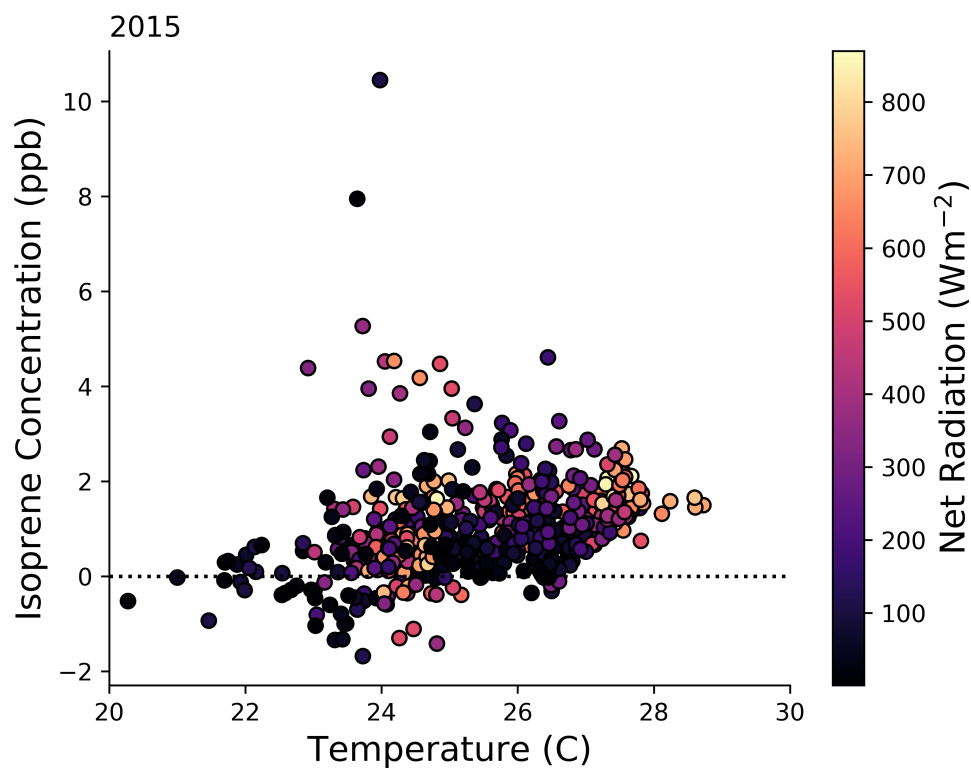
Figure 3.16: 2015 temperature and net radiation compared to FIS measurements; color bar indicates net radiation (Wm^{-2})

3.6.3   2018 Results

FIS measurements were collected from 14–22 March, 2018. The first half of the measurement period was clear and sunny, with maximum temperatures of 28-30° C. This was followed by 48 hours of continuous rain and overcast conditions. The final portion of the measurement period was mostly overcast, with intermittent showers. The time series plot of FIS measurements (in 5 sec. intervals) is shown in Fig. 3.17. These measurements show a clear response to the weather conditions, with the highest concentrations measured in clear, sunny conditions and the lowest daytime peaks on overcast days. These observations are further supported in Fig. 3.18, which show hourly average FIS concentrations compared to temperature and net radiation. Like the other years, there are some high concentrations (>2.0 ppb) in periods of low net radiation, but the majority occur in periods of high temperatures and full-sun conditions.
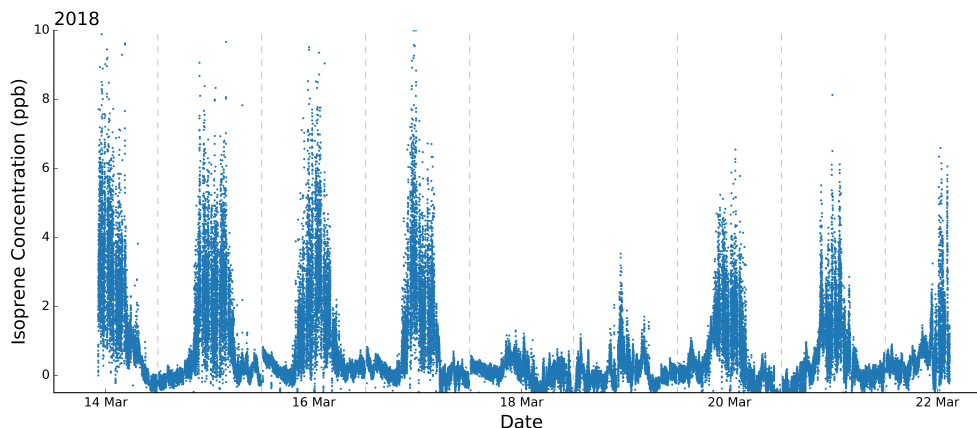

Figure 3.17: Plot showing the isoprene concentrations measured in 2018, with an averaging interval of 5 sec.
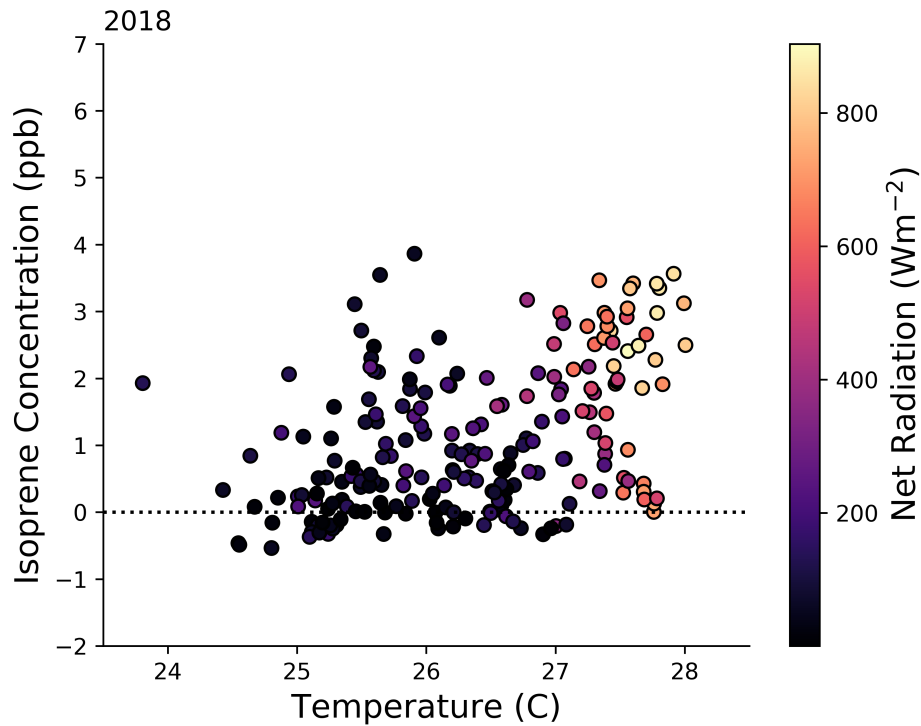
Figure 3.18: 2018 temperature and net radiation compared to FIS measurements; color bar indicates net radiation (Wm^{-2}).

3.7   Comparison of Ground-Level Measurements with GOME-2B Satellite Observations

As discussed in Ch. 2, satellite data products are complementary to conventional ground-based measurements due to their extensive spatial coverage and their ability to show the regional impacts of anthropogenic pollution and biogenic emission events (Duncan et al., 2014). FIS results were compared against observations derived from the GOME-2 instrument aboard the Meteorological Operational satellite-B (MetOp-B) satellite in order to assess fit and place the measurements in a more regional context.

The satellite passes over the DRO at approximately 09:30 local standard time once every three days. Days where cloud cover exceeded 40% are not presented in this analysis. In all plots, GOME-2 observations are compared against estimated

HCHO vertical column densities (VCDs) calculated from FIS observations using Eq. 3.4; the derivation of this calculation is described in full in Section 2.11.1.

$$\Omega = -\rho_{sfc} z_{scale} \left(e^{\frac{-z_{max}}{z_{scale}}} - e^{\frac{-z_{min}}{z_{scale}}} \right) \tag{3.4}$$

The equation converts measured FIS concentrations (hourly average) to an HCHO column, assuming a fully mixed boundary layer. This calculation was made for each hour, but in order to present a 'like to like' temporal comparison, the discussion regarding goodness of fit only considers the 9:00-10:00 hour to fit with the satellite observation time.
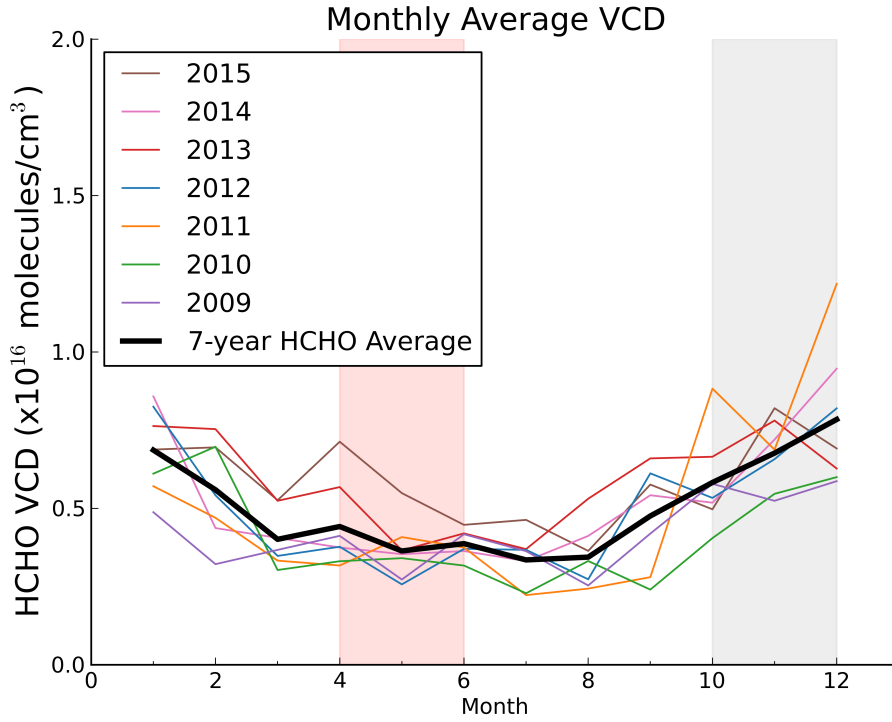
Figure 3.19: Average monthly VCDs (10^{16} molec/cm^2) of HCHO over the DRO from 2009-2015. Data from 2009-2012 is from the GOME-2A satellite, 2013-2015 data is from GOME-2B. The red bar denotes the WtD season, the grey area is the DtW season

Seven years of monthly average HCHO VCDs from the GOME-2 satellite are presented in Fig. 3.19. The WtD season is highlighted in red and the DtW season is marked in gray. As the GOME-2B instrument only became available in

Jan 2013, observations prior to that are from the GOME-2A instrument. From this figure, it is clear that while there is a seasonal emission pattern, there is no point where HCHO columns fall to background levels–the level of the global density of HCHO which is measured over an area in the remote Pacific Ocean, far from both anthropogenic and biogenic sources of HCHO. These observations are surprising, as it was expected that the lowest annual HCHO VCDs would approach background and it would occur during the WtD transition season, as has been observed in the Amazon (Barkley et al., 2009). Instead, as shown in the previous sections, isoprene emissions reach an annual minimum in the dry season, when temperatures and instantaneous PAR are at their respective minima.

Annual minima occur between May and August, though 2009 and 2012 show an increase in emissions from May to June. The highest emissions during the WtD season occur in 2015, which was when conditions were becoming favourable for El Niño formation. The lowest emissions occur during 2012, though the minimum occurs in May, with higher emissions in both April and June. The lowest consistent emissions across the entire season occur in 2010, which was the set up of one of the strongest La Niñas on record (Bureau of Meteorology, 2012).

3.7.1 Annual Overview of Satellite Observations of HCHO over the DRO

HCHO VCDs from each year that ground-based data was collected are presented in Fig. 3.20. These plots show the VCD for every day where an observation is available in the 3-year period, less days where cloud cover exceeds 40% ($\sim$ 140 days/year). The background HCHO VCD, taken from over the Pacific Ocean, is shown for reference.

Some of the trends observed in the ground-based measurements are also seen in Fig. 3.20. Both the 2013 and 2015 satellite observations show annual
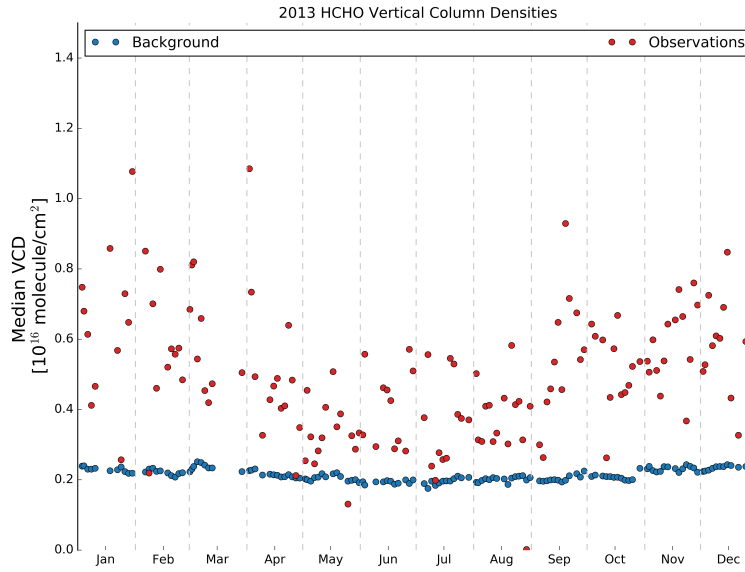
(a)
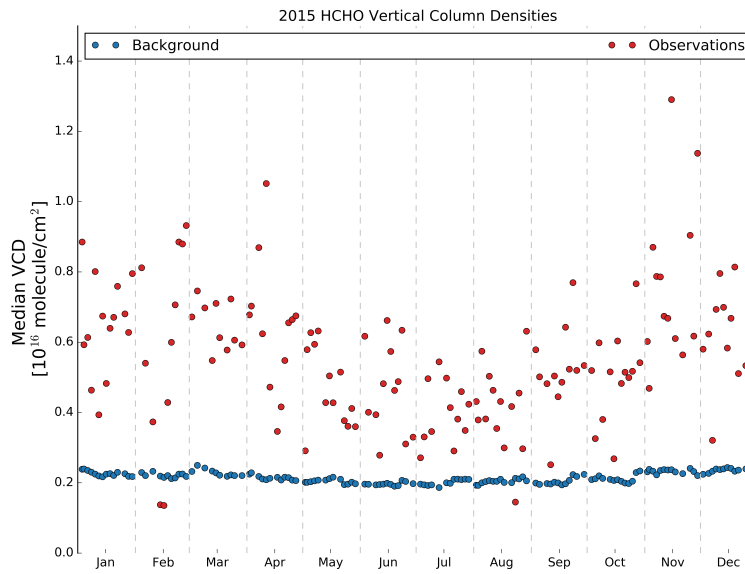
(b)

Figure 3.20: VCDs over the DRO during the measurement period. VCD median values shown in red, background values shown in blue.

minima in the dry season and maxima in the DtW and wet seasons. In addition, minima and maxima are similar in both magnitude and duration across both years. Individual years are discussed in more detail in the following sections, which include comparisons of observed VCDs with estimates of VCDs from FIS measurements.

3.7.2 2013 GOME-2B Satellite Observations

For each of the 2013 observations periods (Table 3.1), satellite observations of HCHO (upper panels) are compared to mean isoprene observations (lower panels) in Figures 3.21 and 3.22. In the upper panels, HCHO vertical column densities (VCDs) from the GOME 2/MetOp-B satellite are shown in orange (De Smedt et al., 2015).

Comparison of satellite data and observations have a 0.5 correlation for 2013; a time series comparison of the values is shown in Fig 3.23. In the figure, the measurements are time-matched–only those satellite observations that have corresponding FIS measurements for the same time ($\sim$ 9:30 LST) on the same day are shown. The fitting line shows a slope of 0.5, indicating that the calculated estimate is lower than the observation. Agreement between the observations and the estimates is the poorest in June 2013, where the observations differ from the estimates by >50% on some days. This discrepancy could be due to assumptions made in the calculation, e.g., that the isoprene concentration measured at a single point above the canopy represents a concentration throughout the mixing layer, or could be due to uncertainties in the satellite observations.

3.7.3 2015 GOME-2B Satellite Data

Figures 3.24 and 3.25 shows the comparison of isoprene observations with estimated VCD column values and the VCD measurements from the GOME 2
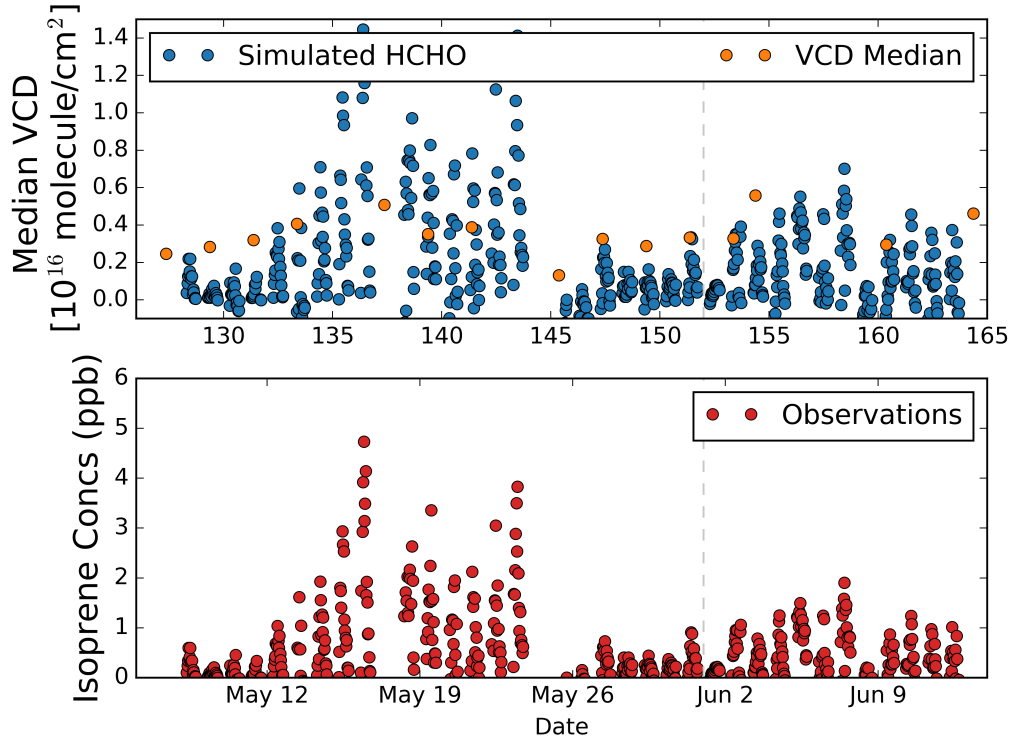
(a) May-June 2013
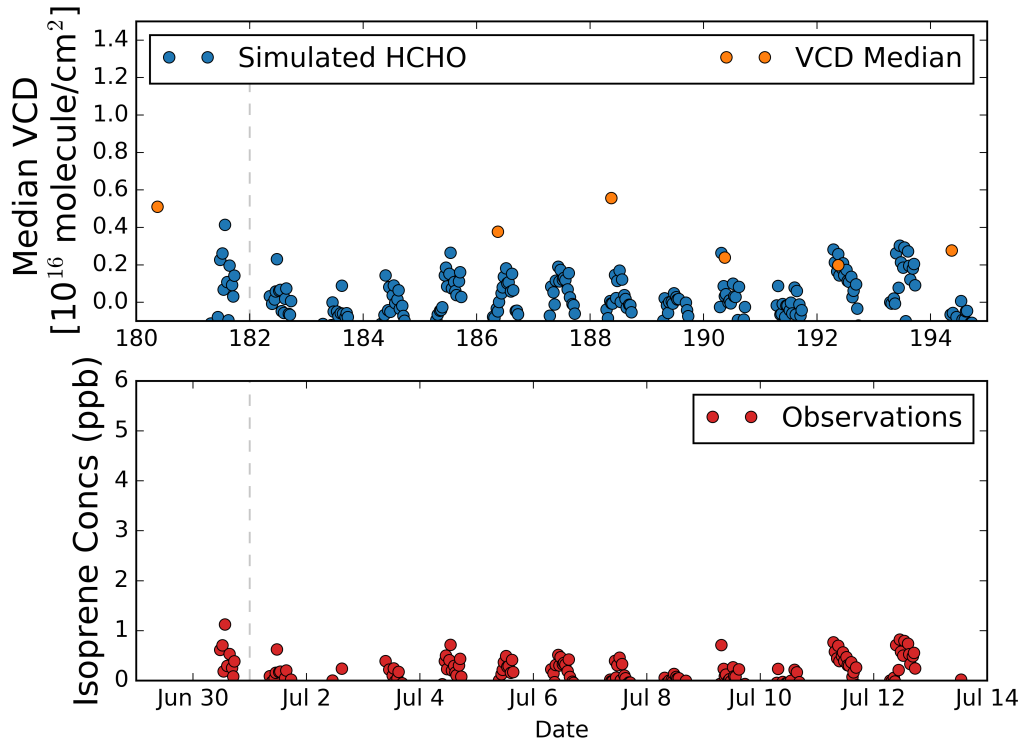
(b) July 2013

Figure 3.21: Top: The median VCD observations from satellite (orange, 1 measurement approximately every three days) and the estimated HCHO profile. Bottom: Isoprene observations, measured by the FIS (red, hourly).
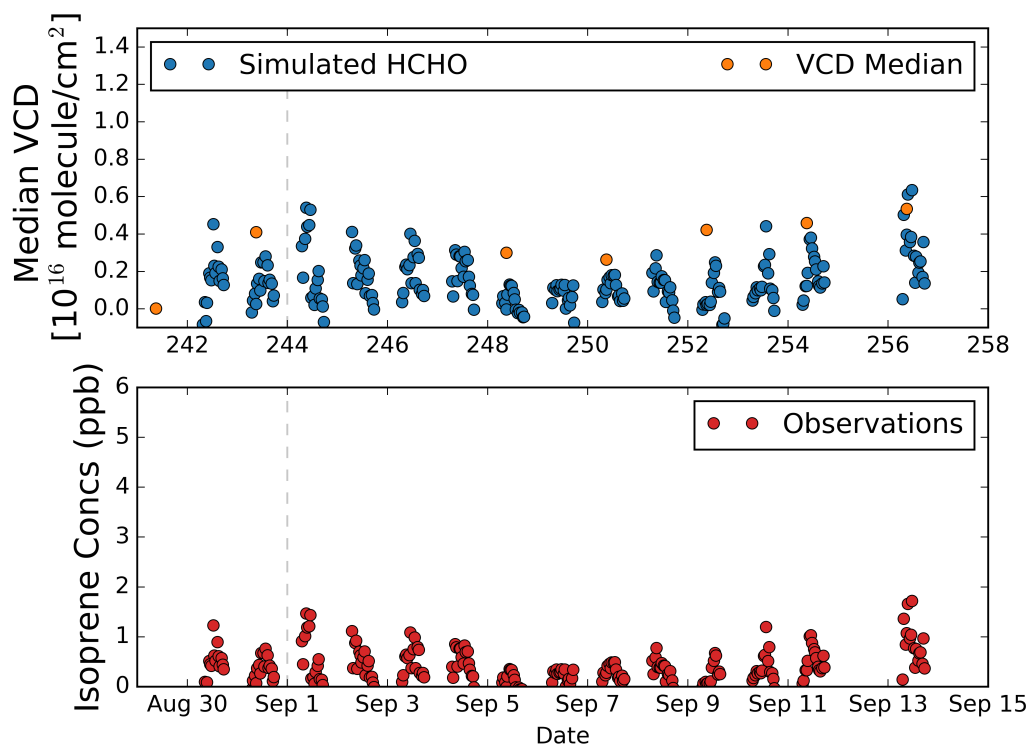
(a) September 2013
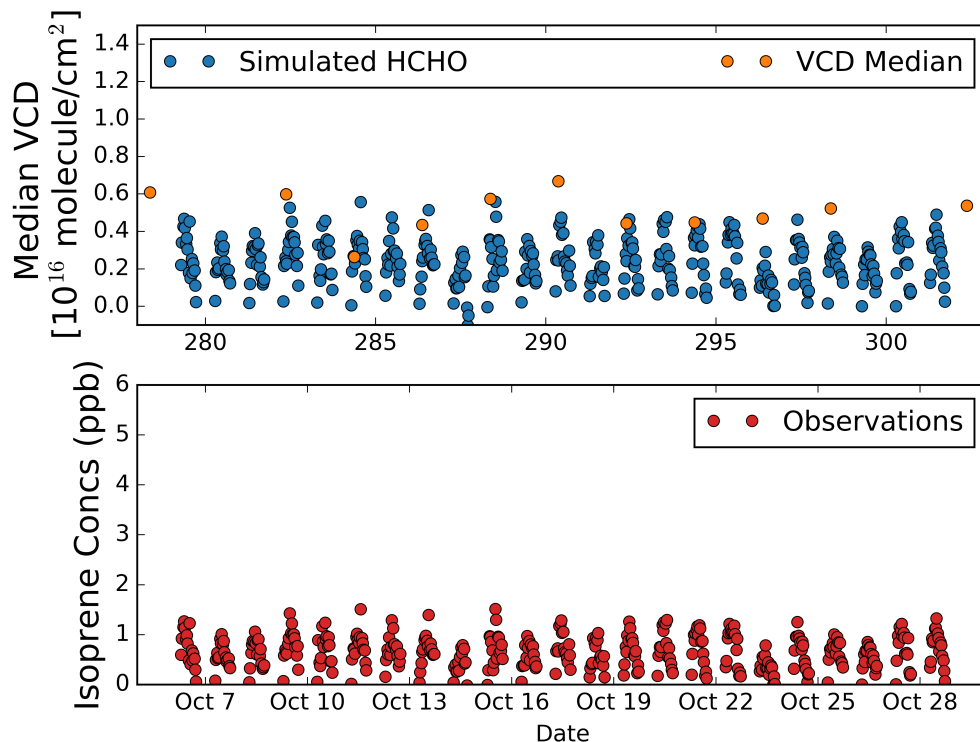
(b) October 2013

Figure 3.22: Top: The median VCD observations from satellite (orange, 1 measurement approximately every three days) and the estimated HCHO profile. Bottom: Isoprene observations, measured by the FIS (red, hourly).

Figure 3.23: Comparison of VCD estimates (from Eq. 3.4) and GOME-2B median HCHO VCDs. Only days and times where there are both FIS observations for the overpass time and day are included in the plot and line of best fit calculation.

satellite. The agreement between VCD estimates and VCD observations is the best of all three data sets, with differences of less than 10% in April and December. A scatterplot comparing the HCHO estimates to VCD observations is shown in Fig. 3.26. The slope for the 2015 observations is less than 2013, though this could be due to the fact that there are fewer observations here than in 2013. Like 2013, the discrepancies between estimates and observations could be due to either satellite uncertainties or estimate calculation assumptions.

(a) April 2015

(b) August 2015

Figure 3.24: Plots showing satellite data vs. measured isoprene concentrations. The upper panel shows an expected HCHO profile derived from the actual isoprene observations shown in the lower panel. The median VCD observation is shown by the orange points in the top panel.
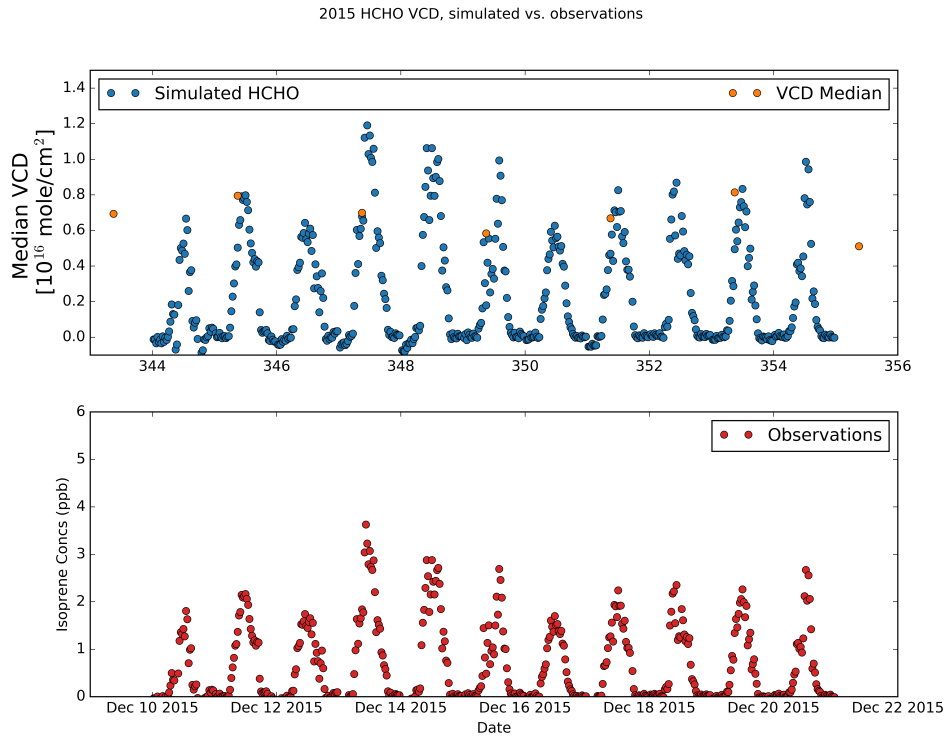
Figure 3.25: Plots showing satellite data vs. measured isoprene concentrations. The upper panel shows an expected HCHO profile derived from the actual iso-prene observations shown in the lower panel. The median VCD observation is shown by the orange points in the top panel.

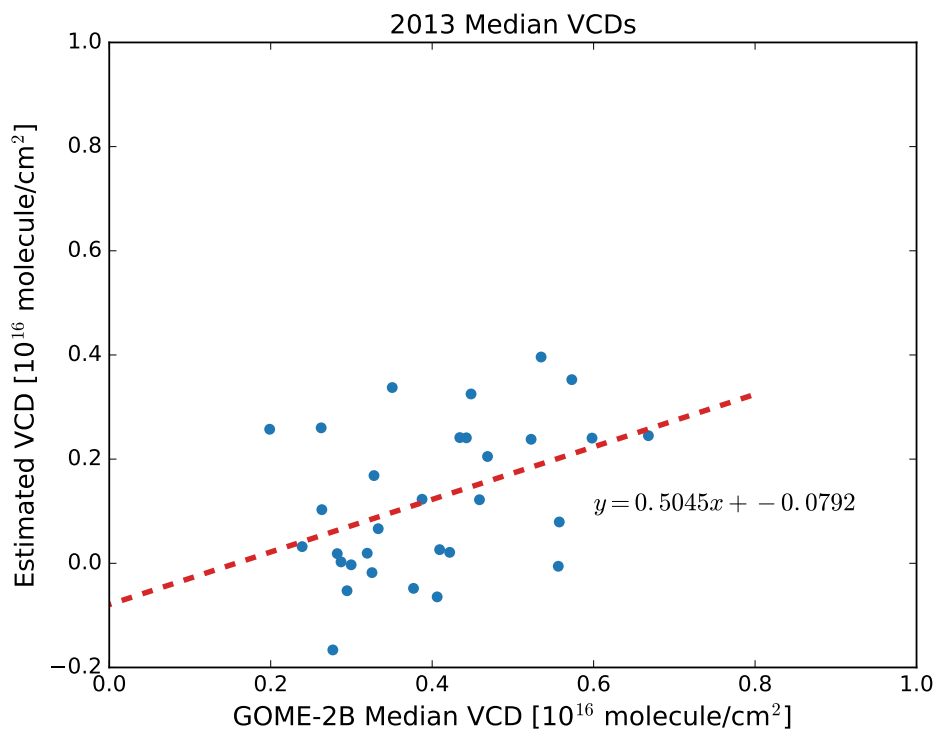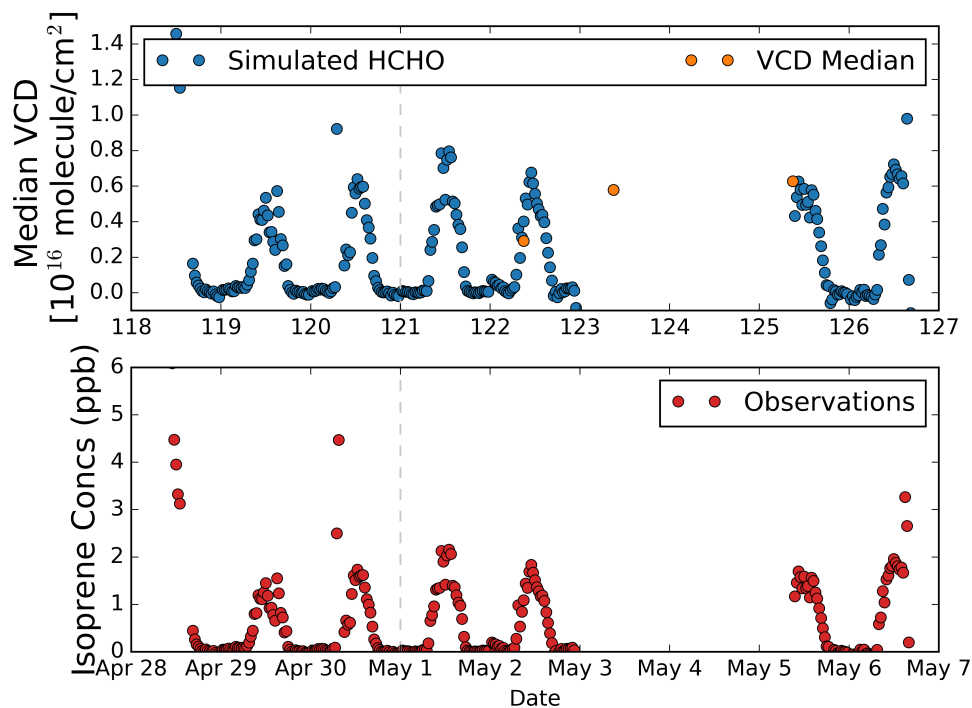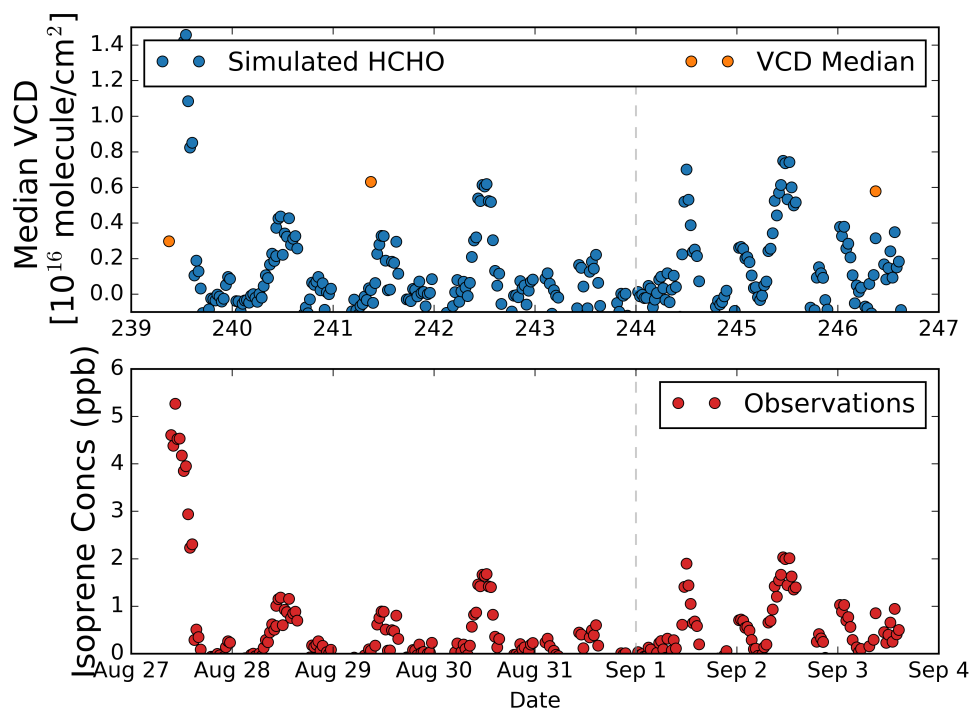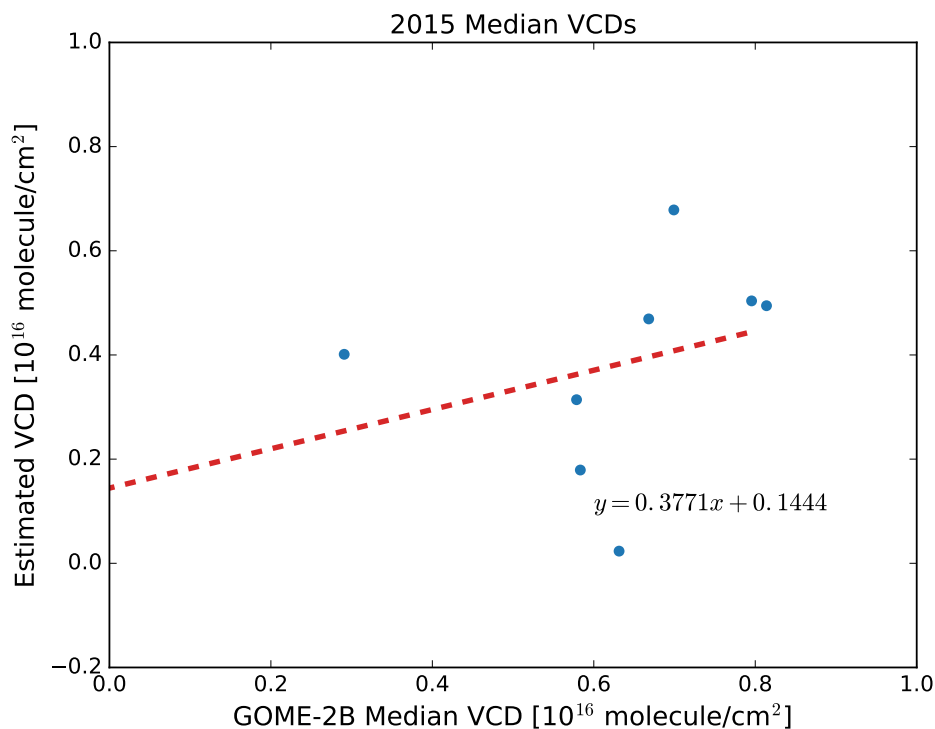Figure 3.26: Comparison of VCD estimates (from Eq. 3.4) and GOME-2B median HCHO VCDs. Only days and times where there are both FIS observations for the overpass time and day are included in the plot and line of best fit calculation.

3.8 Comparison of Results to GEOS-Chem Model Output

In order to understand the relationship between FIS measurements and model data, which will be explored further in the next chapter, the FIS results were compared to GEOS-Chem isoprene output.

Though each year was generated individually, all three were initialised 6 months prior to the period of interest in order to reduce the effects of initial conditions. Data resolution was $2°$ x $2.5°$, fitted to the same grid cell latitude and longitude as the satellite data in 1-hour time steps. Though the model generated data from 47 vertical layers from the ground level to the tropopause, only the bottom (ground) layer was considered here as that most closely matched where the FIS measurements occurred.

Since the model output is on a 2° x 2.5° scale and the FIS observations are point measurements, a few assumptions must be made to compare the two. First, the model output is assumed to be homogeneous across the entire box, and the point measurements are assumed to be representative of the entire area. This assumption is achieved somewhat because half the area under consideration by the model is open ocean, with significantly lower isoprene emissions than terrestrial biomes. The other assumption is that the meteorological conditions reported at the DRO are the same as the meteorological reanalysis data used in the model, and that any differences lead to negligible changes in model emissions. Finally, there is an assumption that the measured air is completely clean and free of any confounding compounds.

Ground-level isoprene concentrations were generated for 2013-2015 and the results are presented in Fig. 3.27. The results indicate that in 2013 and 2015, the FIS measurements are generally lower than the concentrations calculated in GEOS-Chem. In 2013, the FIS measurements are $\sim 50\%$ of GEOS-Chem estimates, regardless of time of year. In 2015, the discrepancy changes throughout the year. GEOS-Chem estimates exceed FIS measurements by a factor of 2-3 in the WtD transition, are nearly at parity in the dry season, and the GEOS-Chem estimates again exceed FIS measurements by approximately a factor of 2 in the DtW season.

A time-matched scatterplot of these output are presented in Fig. 3.28. This plot shows a direct, time-matched comparison of FIS measurements and GEOS-Chem estimates. The 2013 and 2015 measurement years are shown in left column and are combined in the lower right. The closest correlation between FIS measurements and GEOS-Chem estimates is in 2013, where the ratio between the two is 1:1.07. In contrast, the correlation in 2015 is slightly negative. Taken together, the correlation between FIS measurements and GEOS-Chem estimates is near zero.
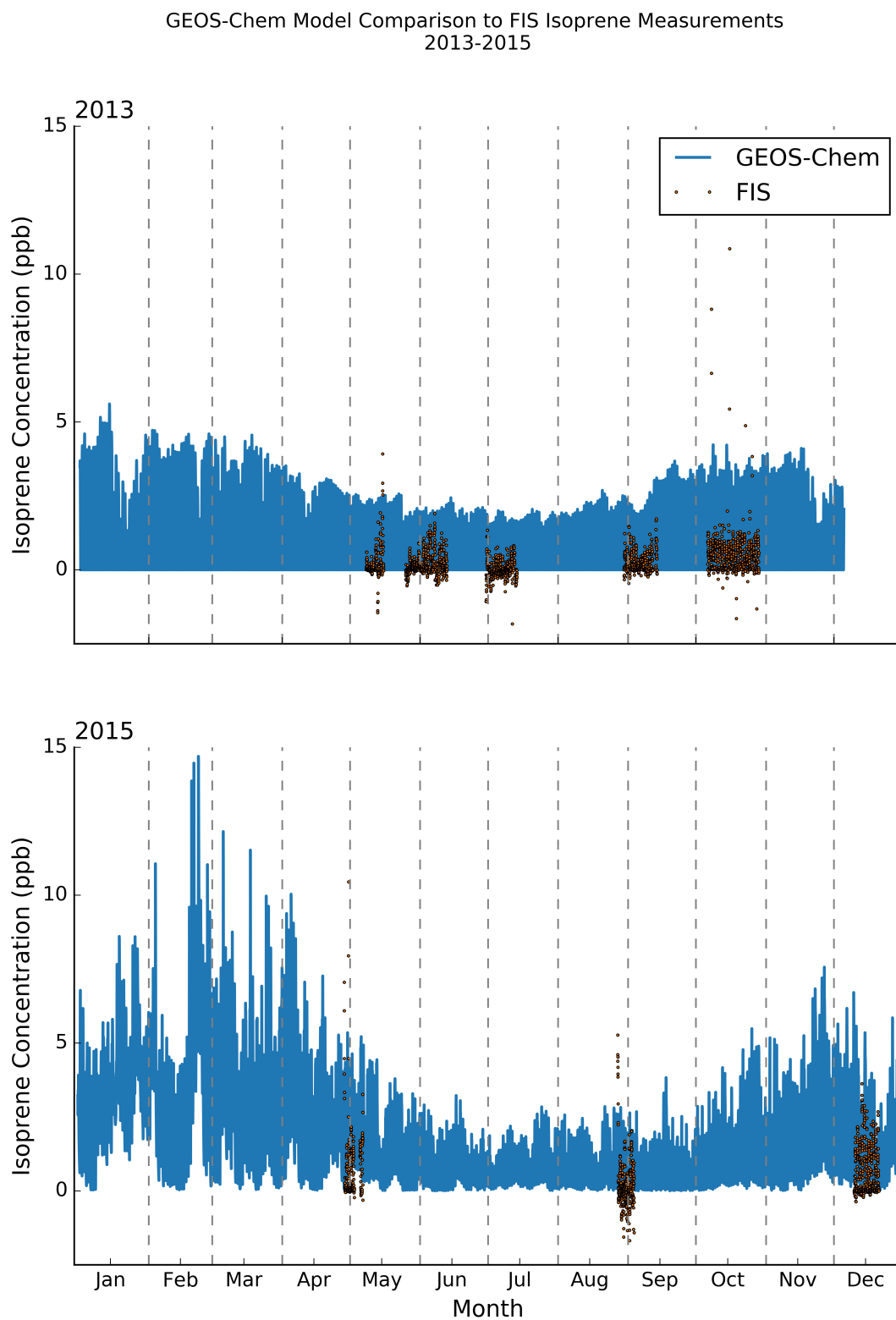
Figure 3.27: Time series of GEOS-Chem model estimates and FIS observations. Months are separated by the dashed lines.
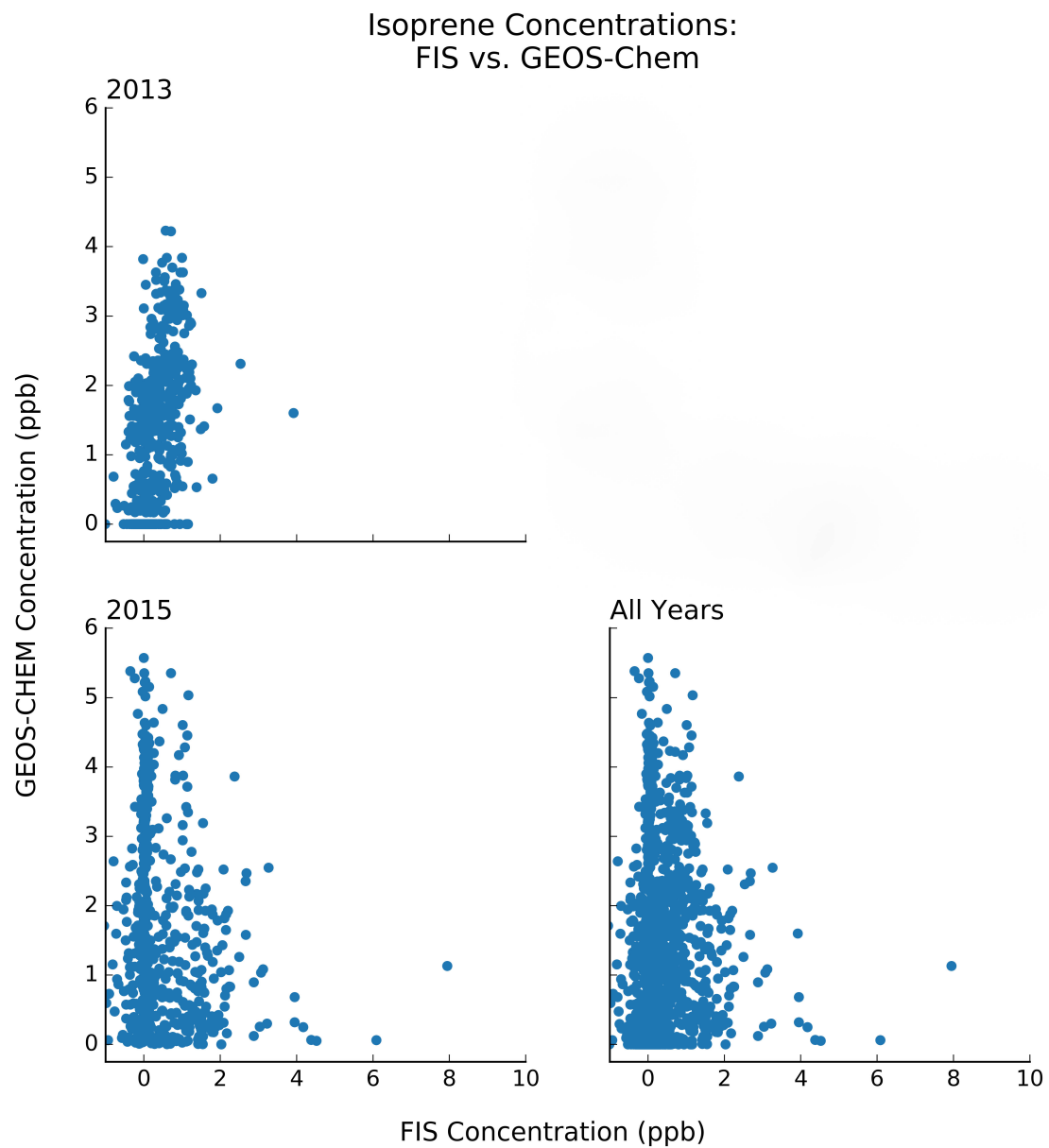
Figure 3.28: Scatterplot comparison of FIS observations and GEOS-Chem model estimates.

However, a near-zero correlation does not necessarily indicate that the FIS measurements and GEOS-Chem estimates are independent of one another. There are several factors that can account for the discrepancies between the two. First, the FIS is measuring isoprene over one area that, from a modeling perspective, can be considered a point source, while the model data presented covers a large area– $2°$ x $2.5°$, which is approximately 220 x 300 kms. The cell used in this comparison is $\sim$50% ocean, which moderates the isoprene concentration estimates reported by GEOS-Chem. Cities and grassland are also included in this cell along with other tropical rainforests that are further inland and not subject to the coastal conditions observed at the DRO. Finally, the tropical tree plant functional type that is used in GEOS-Chem was parameterized primarily from Amazonian measurements. As discussed in Sec. 3.5, emission rates suitable for Amazonian forests are likely not applicable for this particular forest.

Another source of discrepancy between the FIS measurements and GEOS-Chem estimates appears to come from night time observations. The 2015 data set, which has a negative correlation, includes night-time measurements. Conversely, the 2013 and 2014 data sets, which have positive correlations, do not include measurements between 21:00 and 5:00. Though other studies have reported observing isoprene in the overnight hours (e.g., Yañez Serrano et al., 2014), as was discussed in Ch. 2, local wind patterns at the DRO are offshore in the evening hours. This lead to a decrease of isoprene concentrations to at or near zero.

3.9 Key Results

In this chapter, the results from three years of field studies were presented and compared with GOME-2 satellite observations and GEOS-Chem model output to understand seasonal patterns of concentrations in the Daintree Rainforest. The FIS measurements were verified with a solid sorbent cartridge study which

additionally provided insights into isoprene concentration patterns in the early evening and overnight hours.

The findings from the FIS measurements showed that isoprene concentrations vary seasonally. However, unlike other tropical ecosystems that experience an annual minima during the WtD transition period, the annual minima in the Daintree occurred during the dry season, which corresponds with the winter months. Annual maxima occurred during the DtW transition, which corresponds to late spring and summer months. These findings were also observed in satellite observations and model output.

The solid sorbent cartridge study yielded interesting results into isoprene concentrations in the early evening and overnight hours. Other studies have shown variable isoprene concentrations overnight, but findings at the Daintree showed concentrations at or near zero. It is likely that this was due to the influence of wind patterns in the area–specifically the sea breeze. Further research into the wind patterns of the DRO and other coastal ecosystems is warranted.

In the next chapter, FIS results will be compared to model output data in more depth with an investigation into the strongest drivers of isoprene concentrations in the Daintree.

Chapter 4

Modelling FIS Data Using MLC-CHEM and MEGAN

In this chapter, the results presented in Ch. 3 are expanded upon and compared to two biogenic emissions models: MLC-CHEM and the Model of Emissions of Gases and Aerosols from Nature (MEGAN) model. MLC-CHEM is a stand-alone, single-column, multi-layer canopy exchange box model that is easily adapted for site-scale use. MEGAN is a state-of-the-science isoprene emissions model that has been widely adopted throughout the atmospheric chemistry community. MEGAN's driving equations are derived from satellite and *in situ* observations, and this research turns back to these roots to improve model performance in tropical ecosystems.

First, the models are described in Section 4.1, then a base-case analysis is presented in Section 4.2. An overview is presented for each model, then a seasonal analysis is presented. Within each season, a 10-day period is analysed before being placed into a season-long context. Following that, each model underwent sensitivity tests and simulations, the results of which are presented in Section 4.3. The models were not tuned to be site-specific in order to allow the results to be more broadly comparable to the findings in other tropical areas. Results

for these analyses are presented by model: MLC-CHEM results begin in Section 4.3.2 and MEGAN output is discussed beginning in Section 4.3.3. Model output is then compared to satellite observations in Section 4.4. The chapter concludes with a summary of key results in Section 4.5.

4.1   Model Descriptions, Input Parameters, and Supplementary Data

The MLC-CHEM and MEGAN models were selected for this research for their complementary approaches to analysing biogenic emissions: MLC-CHEM and MEGAN are multi-layer canopy models, though it is possible to parameterize the results from the multi-layer MEGAN model into a simplified big leaf model. As discussed in Ch. 1, multi-layer canopy models explicitly solve for CO_2, energy exchange, and chemical transport and integrate emission fluxes across all layers to determine total flux (Leuning et al., 1995). They provide details about parameters typically measured at leaf level as well as intra-canopy behaviour (Dai et al., 2004). In contrast, big leaf models incorporate all the properties of a canopy from the ground to the top of the canopy into a single 'leaf' to calculate flux (Dai et al., 2004; Dickinson et al., 1998). This makes it easier to calculate fluxes over greater areas and time scales.

MLC-CHEM is a stand-alone, single-column model based on the canopy exchange processes in the ECHAM5/MESSy model (Ganzeveld et al., 2010; Ganzeveld, 2002a). It is easily adapted for site-scale use and includes an explicit simulation of in-canopy processes. These processes include BVOC emissions, dry deposition of gases and aerosols, gas-phase chemistry, and turbulent exchange. MLC-CHEM also calculates both BVOC concentrations and fluxes at every time step and includes detailed chemistry, soil, and micrometeorological processing, which is often not available in a larger-scale model. Previously, MLC-CHEM has been

used to analyse components of atmosphere-biosphere exchange (Ganzeveld et al., 2006; Ganzeveld, 2002b; Seok et al., 2013) and land-use change in the Amazon (Ganzeveld and Lelieveld, 2004). For the first time, MLC-CHEM is being used to evaluate seasonal and annual cycles of emissions; this study represents an expansion of its capabilities.

The MEGAN model is one of the most widely-used multi-layer emissions models available (Guenther et al., 2006, 2012). MEGAN uses base emissions from different ecosystems (classified as plant functional types) and constrains them with local environmental factors. The base emissions are extrapolated from available field and laboratory studies, and estimated where none exist. However, MEGAN has a history of estimating higher emissions in tropical ecosystems compared to inverse models (Barkley et al., 2008; Marais et al., 2014; Stavrakou et al., 2014). Due to the paucity of field and laboratory emissions studies, only one field study from tropical Australia was used in the development of the original MEGAN model (Ayers and Gillett, 1988). Though the most recent version of MEGAN includes a more robust data set to estimate Australian emissions, emissions patterns over the Australian continent remain largely uncertain (Emmerson et al., 2016; Guenther et al., 2012). A canopy-scale model using the driving equations from MEGAN was built specifically for use in this project. Model isoprene emissions are calculated using the equations in Guenther et al. (2006), with OH chemistry and local meteorological effects included. This offline model allows for a more direct manipulation of input parameters to investigate the effects of particular drivers on emissions.

4.1.1 MLC-CHEM Input Parameters

The MLC-CHEM model space is defined by several parameters specified in the primary input file, summarised in Table 4.1. These include initialisation time and date, latitude, and land-use inputs to specify what percentage of model vegetation

is forest, grassland, and water. Additional time parameters include the number of time steps, the time lapse between calculations, and which time steps should be written to the output file. The latitude input adjusts sunrise, sunset, and hours of daylight for the specified time of year. No additional time for meteorological spin-up is required.

For this analysis, I initialised the model on 1 January each year (2013 and 2015). The latitude was set to -16 °, and the modelled area was set at 100% forested land. I did not scale the box to include the ocean as this model does not calculate marine emissions. Though they are not explicitly discussed here, this model did calculate biogenic NO emissions and foliage NO_x and HONO emissions. Gas-phase chemistry was based on an implementation of Carbon Bond IV (Ganzeveld, 2013; Yarwood et al., 2005). The isoprene emission factor was set at 8 μg C/g/hr, which was used in the Amazon in a previous study (L. Ganzeveld, WUR, personal communication, 2014). Soil moisture was set to 20%, derived from 2013 soil moisture data (Liddell, 2013) as the soil around at the DRO is known to be ~50% rock and the average soil moisture content was well above wilting point (P. Nelson, JCU, personal communication, 2015). Though soil moisture data is collected at the Daintree Rainforest Observatory (DRO), integrating it into the model was beyond the scope of the current study and has been identified as an area of future research.

Table 4.1: MLC-CHEM Input Variables and Base Case Settings

Variable	Initial setting
Number of Timesteps	105120 (1 year)
Length of Timesteps (s)	300
Write Frequency (1/n)	12 (every 30 min)
Surface Land Fraction (0-1)	1.0
Vegetation Fraction (0-1)	1.0
Forest Fraction (0-1)	1.0
Canopy Height (m)	30
Isoprene Emission Factor (μg C g^{-1} hr^{-1})	8

In addition to initial settings, MLC-CHEM accepts meteorological and chem-

ical input parameters on an hourly timescale. Meteorological inputs (temperature, wind, net radiation (shortwave + longwave)) are collected at the DRO by James Cook University (JCU) and made available as part of the Terrestrial Ecosystem Research Network (TERN, Liddell, 2013, 2014). Weather data from 2015 was obtained directly from JCU researchers (Liddell, personal communication, 2016). Chemical inputs (NO_x, O_3, and HCHO) were supplied by GEOS-Chem for this study as there are no current or historic above-canopy measurements of these gases available at the DRO. GEOS-Chem HCHO values were compared against satellite data as a common reference point to evaluate the values used here.

The upper boundary of the model was set at the mixed layer height. Since the height of the boundary layer has not been explicitly measured at this site, a diurnal cycle was constructed using estimates from GEOS-Chem. Though the model calculates isoprene concentrations below (7.5 m), within (22.5 m), and above the canopy (81 m, in the free atmosphere), FIS measurements were only taken above the canopy at a height of 35 m. Output between the 'within canopy' and 'above canopy' layers were scaled to calculate an estimated concentration at 35 m in order to allow for direct comparison of model output and FIS measurements.

4.1.2 MLC-CHEM Model Outputs and Calculation of Concentrations

BVOC emissions are calculated in MLC-CHEM using one of two modules, which can be specified in the input file. One calculates emissions based off the equations presented in Guenther et al. (G95, 1995). The other uses emissions calculations found in the MEGAN model (Guenther et al., 2006). The primary difference between these two approaches is that prior environmental conditions are considered in the MEGAN module. Though MEGAN is built as a big-leaf model (described

in Sec. 1.3), it is adapted for the leaf-scale calculations used in MLC-CHEM. The G95 module, used in this study, calculates leaf-level emission flux using radiation, temperature, leaf area index (LAI), and the structure of the canopy to calculate BVOC emissions:

$$F = D\epsilon\gamma\,, \tag{4.1}$$

where D is the foliar density (kg dry matter m^{-2}), ϵ is the emission factor (μg C m^{-2} hr^{-1} at standard conditions) and γ is an activity factor which accounts for deviations in PAR and leaf temperature from standard conditions. Emission factors are calculated for areas of low species diversity, and estimated for areas with high species diversity. γ is the product of two coefficients, for light (C_L, Equation 4.2) and temperature (C_T, Equation 4.3):

$$C_L = \frac{\alpha c_{L1} Q}{\sqrt{1 + \alpha^2 Q^2}}\,, \tag{4.2}$$

where Q = PAR flux (μmol m^{-2} s^{-1}), and $\alpha = 0.0027$ and $c_{L1} = 1.066$ are empirical coefficients. C_T is defined as:

$$C_T = \frac{exp\frac{\alpha c_{T1} Q}{RT_S T}}{1 + exp\frac{c_{T2}(T - T_M)}{RT_S T}}\,, \tag{4.3}$$

where T is the leaf temperature (K), T_S is the leaf temperature at standard conditions, R is constant (8.314 J K^{-1} mol^{-1}); $c_{T1} = 95{,}000$ J mol^{-1}, $c_{T2} = 230{,}000$ J mol^{-1}, and $T_M = 314$ K are all empirical coefficients.

MLC-CHEM output parameters include both atmospheric parameters (bulk Richardson number, mixed layer depth, eddy-diffusivity heat between crown and understorey layers) and fate and transport of several classes of compounds (isoprene, α-pinene, β-pinene, sesquiterpenes, carbon dioxide, and the hydroxyl radical). Outputs are provided for 3 layers: 7.5 m (soil layer), 22.5 m (crown layer),
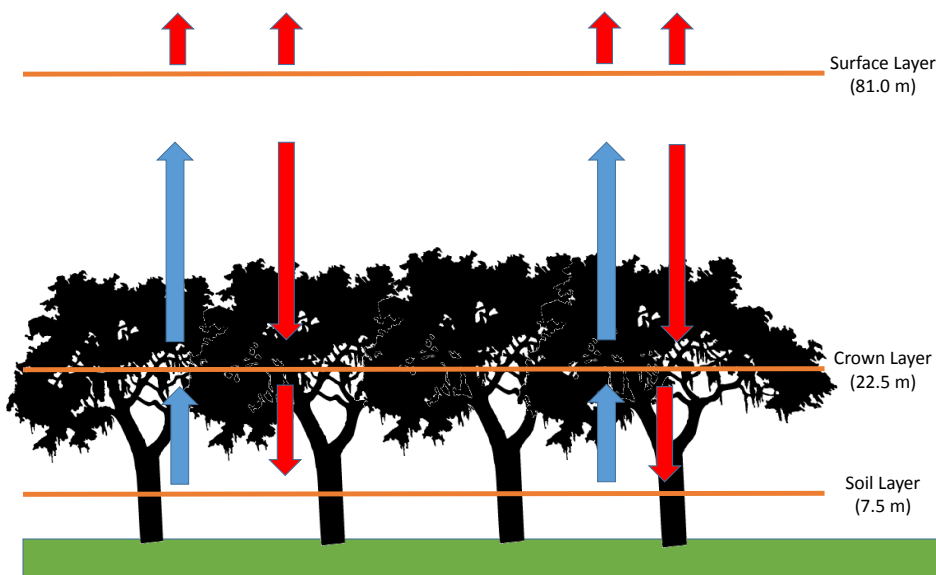
Figure 4.1: Schematic of the MLC-CHEM model. Emissions (blue arrows) originate in the foliated layers, and move into surrounding layers through mixing (red arrows). At the surface layer, the only emissions present are those that move into the layer. There, they are removed either through deposition or chemical oxidation.

and 81 m (surface layer) shown in Figure 4.1, except where parameters are not logical, e.g., there are no biogenic emissions in the surface layer. Since the heights reported in MLC-CHEM do not match with the measurement sampling height (35 m), results are scaled linearly using the following equation:

$$X_{35m} = \frac{1}{81.0 - 22.5}\left(X_{22.5m} - X_{81m}\right), \qquad (4.4)$$

where X is any value in the model at the height specified, and all Xs are the same parameter.

4.1.3 MEGAN Input Parameters

A canopy-scale, two-layer MEGAN-style model was developed for use in this study. This model simplified computations and allowed for easy manipulation of the modelled space to include or exclude individual features. Isoprene fluxes were calculated using the equations in Guenther et al. (2006). Specifically, emission

was calculated as

$$Emission = \sigma\gamma\rho\,, \tag{4.5}$$

where σ is the emission of a compound from the canopy at standard conditions (mg m^{-2}hr^{-1}), γ is an activity factor that accounts for changes from standard conditions (normalised ratio), and ρ describes production and loss within the plant canopy (normalised ratio, Guenther et al., 2006). The emission factor (EF), which is controlled in models with multiple ecosystems by the plant functional type, was initally set to 14, which is the basal emission factor for rainforests (Barkley et al., 2008; Guenther et al., 2006). In this study, ρ was set to unity. The value of γ is determined by several elements:

$$\gamma = \gamma_{CE}\gamma_{age}\gamma_{SM}\,, \tag{4.6}$$

where γ_{CE} considers the canopy environment, γ_{age} describes changes attributed to leaf age, and γ_{SM} addresses changes due to soil moisture. Like the MLC-CHEM model, soil moisture was included as a static variable derived from 2013 soil moisture data (Liddell, 2013) and the average soil moisture content for the study period was well above wilting point (P. Nelson, JCU, personal communication, 2015). The canopy environment is further described as:

$$\gamma_{CE} = C_{CE}\gamma_{PT} * LAI\,, \tag{4.7}$$

where C$_{CE}$ = 0.57 ensures that the emission activity achieves unity at standard conditions, γ_{PT} is the product of a temperature emission activity factor (γ_T) and a light activity factor (γ_P), and LAI is the leaf area index. The full MEGAN model utilises satellite observations to determine LAI, but for this offline version, LAI was kept constant for sensitivity testing and later varied using ground-based

observations (Liddell and Laurance, 2015). Advection, deposition, and multiple plant functional types were not considered in this treatment. Temperature and net radiation are the only meteorological inputs used in this model. OH concentrations were calculated along a diurnal cycle, using maxima reported in Vaughan et al. (2012) and references therein to estimate the validity of the calculations.

LAI from GEOS-Chem output data was used to calculate the LAI values used in this model. An algorithm was formulated from the GEOS-Chem LAI estimates and observational data served as a point of reference. (Liddell and Laurance, 2015). The GEOS-Chem HCHO values were compared against satellite data as a common reference point to check the validity of this approach.

4.1.4 MEGAN Model Outputs

Since this custom-built model was built solely for the examination of isoprene concentrations, that is its only output. First, gamma factors representing temperature and PAR changes are calculated, and losses from the OH oxidation of isoprene are subtracted out at a reaction rate of k=101 x 10^{-12} molec cm^{-2} s^{-1} (Atkinson, 2003). The resulting flux is then converted to a concentration to make it comparable to FIS measurements. This is done by first dividing the mass of emissions at each time step across the height of the boundary layer, which is parameterized from GEOS-Chem and scaled as

$$BL(t) = 1500\gamma_{P,t} + 577.98 \,, \tag{4.8}$$

where BL = boundary layer height (m), and γ_P is used as a surrogate for direct PAR measurements. 1500 m was the highest estimated BL, and 577.98 was the average overnight height. The resulting mass is then divided by the density of air, assumed to be 2.5 x 10^{25} molecules m^{-3}. Though air density is temperature dependent, an assumption of 25°C is reasonable for this location: the average high

temperature in winter is 25°C, and the average high in summer is 32°C. When calculated for 32°C, the change in density was <10% (see Ch.2 for a discussion of average temperatures at the DRO).

The boundary height represents a source of uncertainty in the model, both due to the lack of measurements to refer to and the complexity of the land surrounding the DRO–there are significant roughness and topological variation to the east and west of the site. The depth of the BL is seasonal and can be affected by events such as surface-based temperature inversions (Seidel et al., 2010). However, seasonal temperature variation at the DRO is low and surface-based inversions are typically shallow and occur less frequently in the tropics than more polar latitudes (Seidel et al., 2010). Cloudiness also affects the height of the BL, but this is accounted for by calculating BL as a function of PAR measurements. The parametrization described by Eq. 4.8 is a simple approach, but determining an accurate boundary layer parametrization for this dynamically complex site is beyond the scope of this study.

The background concentration of OH also represents a source of uncertainty in the model. The primary source of uncertainty comes from the fact that like other measurements, OH concentration measurements in the tropics are sparse compared to other locations on the globe (Vaughan et al., 2012). In addition, measurements are affected by local chemistry, e.g., pollution events as well as seasonal changes and there are very few measurements of clean, tropical environments on which to base an estimate. **?** observed two orders of magnitude difference between seasons in measurements in the Cape Verde Islands—the first seasonal tropical measurement of OH in a clean atmosphere, which makes it one of the only relevant points of comparison for this study. Though a single OH concentration is used throughout this study, adding in a seasonal factor might contribute to increasing agreement between model output and observations.

# 4.2 Base-Case Analysis of the MLC-CHEM and MEGAN Models

An analysis of model performance using the base settings is presented in the following sections. First, an annual overview is presented, then a 10-day period from each season is examined in detail.

4.2.1 Annual Overview

Figure 4.2 shows the output of year-long runs of the MLC-CHEM model. Distinct annual cycles are observable in all three years, with maximum concentrations in the dry-to-wet transition season (DtW, indicated by the red shaded area) and annual minima during winter, in the dry season. The highest concentrations occur in 2013. The modelled concentrations in 2013 show good agreement with observations for the months of June and July, but 2015 has the best fit with observations across multiple seasons. The poorest fits occur in October 2013, when MLC-CHEM indicates daytime maximum concentrations of 6-8 ppb, 3-4 times higher than observations.

Annual output from the MEGAN model from 2013-2015 is shown in Figure 4.3. The seasonal variations are quite small, with a difference of <1 ppb between daytime maxima in the wet and dry seasons. Model simulations provide a good fit for 2013 data, particularly in the latter half of the year. However, MEGAN underpredicts daytime maximum isoprene concentrations in 2014 and 2015 by a factor of 2-4.

The concentrations from the MEGAN base-case scenario differ from the findings of other studies. These studies have found that MEGAN consistently estimates emissions to be 20% higher than inverse model studies in the same region(Barkley et al., 2008; Marais et al., 2014; Stavrakou et al., 2014). Even with
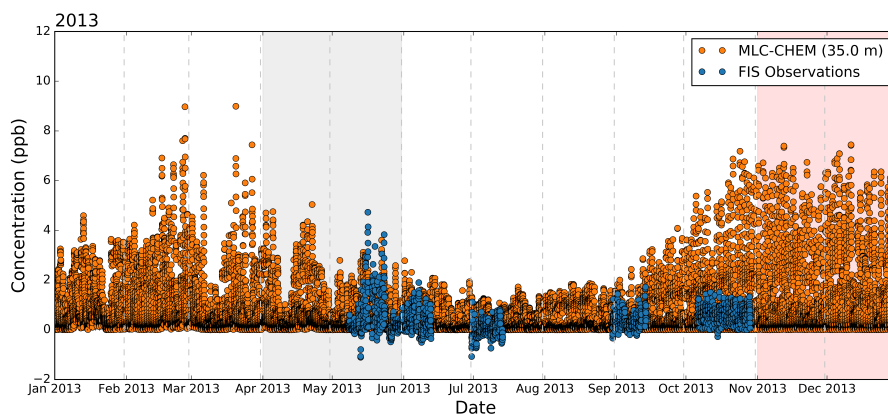
(a)
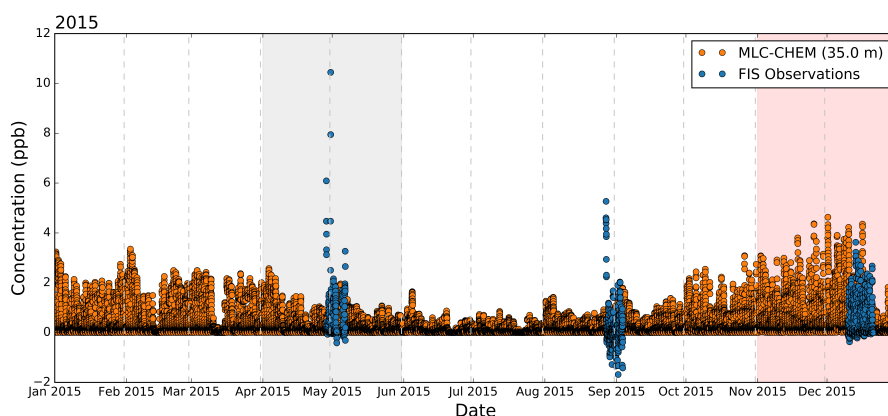
(b)

Figure 4.2: Plots showing the year-long MLC-CHEM model runs with hourly measured concentrations: a) 2013 and b) 2015. The gray shaded area indicates the WtD transition season, and the red shaded area indicates the DtW transition.

this difference, aircraft studies have found that both sets of estimates are below observational levels (Gu et al., 2017; Karl et al., 2007). No study has reported an underestimation; Langford et al. (2010) achieved a better model fit in Borneo only after lowering the isoprene base emission rate (BER). Given that the base-case in this study uses the default MEGAN BER, this underestimation is likely due to an excess of isoprene being removed via OH chemistry. The excess in the OH reactivity is observable through a 'double peak', where there is a peak in the morning followed by a u-shaped slump in concentrations in midday, followed by a second peak in concentrations in the afternoon. While it occurred throughout
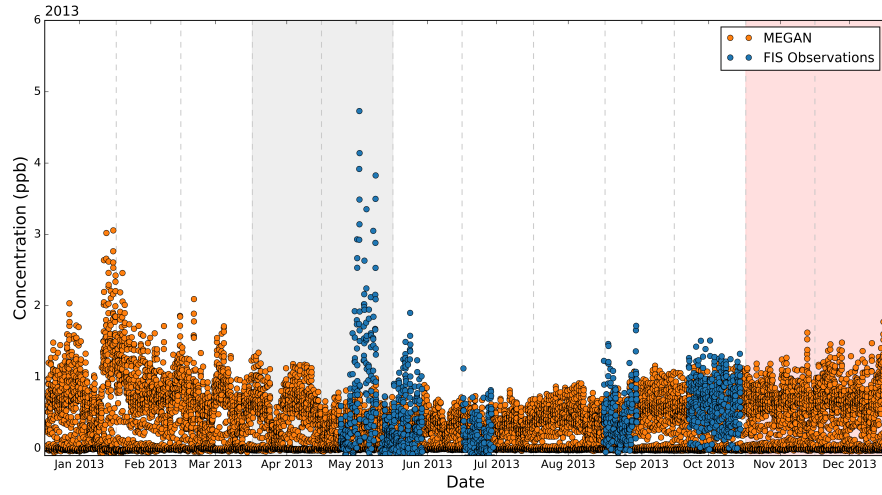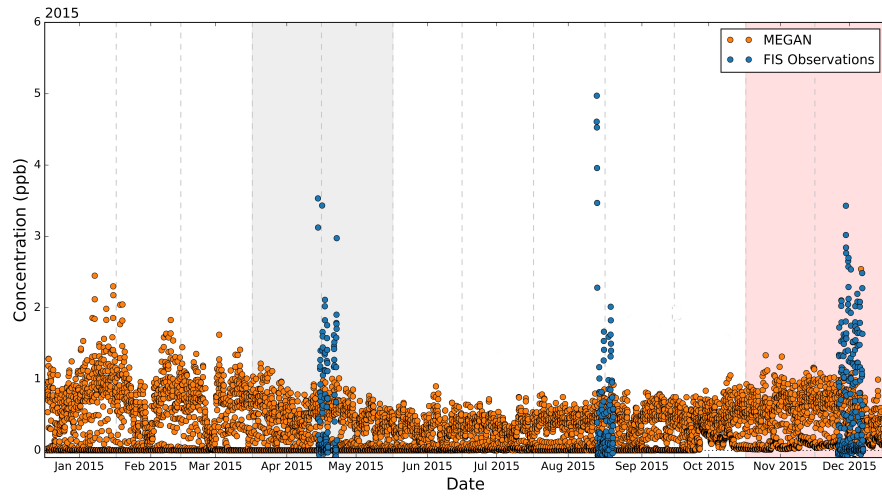
(a)

(b)

Figure 4.3: Plots showing the year-long MEGAN model runs with measured concentrations: a) 2013 and b) 2015. The grey shaded area indicates the WtD transition season, and the red shaded area indicates the DtW transition.

the year, it is most visible in the short-term time series plots discussed in the seasonal sections that follow.

4.2.2   Wet to Dry Transition Season

Since it was the focus of the study, the WtD transition season has the most observational data. The highest modelled concentrations for the WtD transition season occurred in 2013, where daily peak concentrations regularly approached 3 ppb and some days even exceeded 4 ppb, especially early in the transition season. In both 2013 and 2015, the concentrations show a general downward trend as the season progresses.

MLC-CHEM isoprene concentrations for the entire WtD transition season in 2013 and 2015 can be observed in Fig. 4.2. FIS observations, where they are made, are also displayed. As discussed above, the isoprene concentrations were higher in 2013 than 2015. Both years show a trend of decreasing concentrations through the progression of the season, which corresponds to an overall decrease in PAR and lower temperatures with the approach of Australian winter.

The best agreement between observations and modelled concentrations occurs in 2015, which could be due to several reasons. First, because there are fewer observations in 2015 than 2013, there is a smaller range of temperature and PAR combinations to make comparisons with. This is compounded by stable weather patterns that occurred during the measurement periods in 2015. Second, as discussed in Chapter 3, 2013 was the driest of all wet seasons, but the wettest of all observed WtD transitions. 2015 was the opposite: it had the wettest of all three wet seasons, and the driest WtD transition. A difference in soil moisture profiles may contribute to MLC-CHEM's ability to replicate observations, but an in-depth analysis of this aspect of forest dynamics is beyond the scope of this study.

In the WtD season, MEGAN output decreases in peak isoprene concentration as the season progresses, with maxima occurring at the beginning of the season. However, the model underestimates isoprene concentrations in comparison to FIS

measurements in both years. As this model output is from the base-case settings, there are several possibilities for this underestimation. First, the LAI could be too low. Second, the OH chemistry might be removing too much. Third, the emission factor could be set too low. Fourth, there might be an emission activity factor that is not captured by this model.

Few tropical field studies have collected samples in the WtD season, so model comparisons to *in situ* data are sparse during this season. Barkley et al. (2008) compared Amazonian field studies across multiple seasons to MEGAN output, one of which included data WtD season. MEGAN strongly over-estimated the measurements; the closest model iteration overestimated measurements by ~150%. A more recent study has included WtD season measurements, but the findings have not been compared to model output to date (Yañez Serrano et al., 2014).

MLC-CHEM model output of isoprene concentrations for the WtD season between 27 May and 7 Jun 2013, are shown in Figure 4.4. Figure 4.4a compares concentrations at a height of 35 m with FIS measurements in blue and MLC-CHEM output in orange. Precipitation and net radiation for the time period are presented in Figure 4.4b and modelled vertical movement and oxidation of isoprene is shown in Figure 4.4c. Positive values indicate an increase in isoprene concentrations, and negative values indicate a loss.

Figure 4.4a shows that agreement between FIS observations and model output improves with decreasing PAR. Model output and observations differ by <0.75 ppb on cloudy days (e.g, 29 and 31 May), whereas the difference is in excess of 2 ppb on days with full sun (e.g, 28 May and 1 Jun), where the model overestimates concentrations by 20-400%. This is reflected in Fig. 4.4c, where two of the four days with the strongest vertical motion (>1 ppb/hr, green line) also have the highest model output. Since this motion occurs early in the day, on both days where agreement is poor (28 May and 1 Jun), it indicates that the model boundary layer is either not rising quickly enough or early enough in the
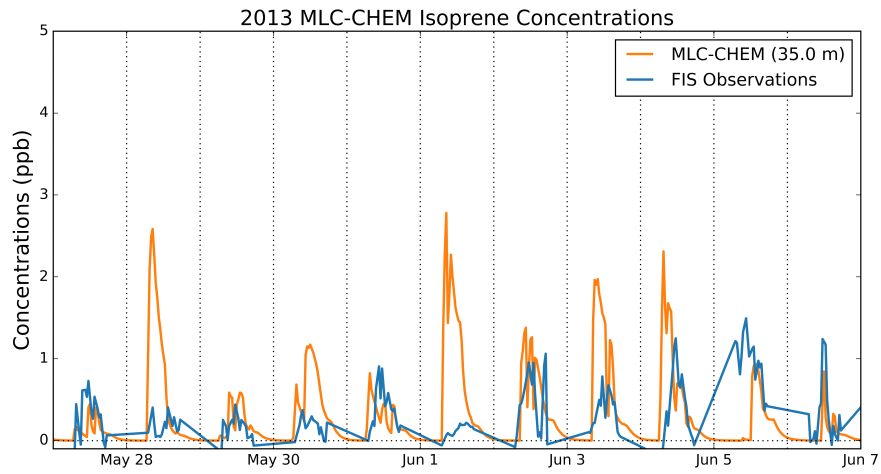
(a)
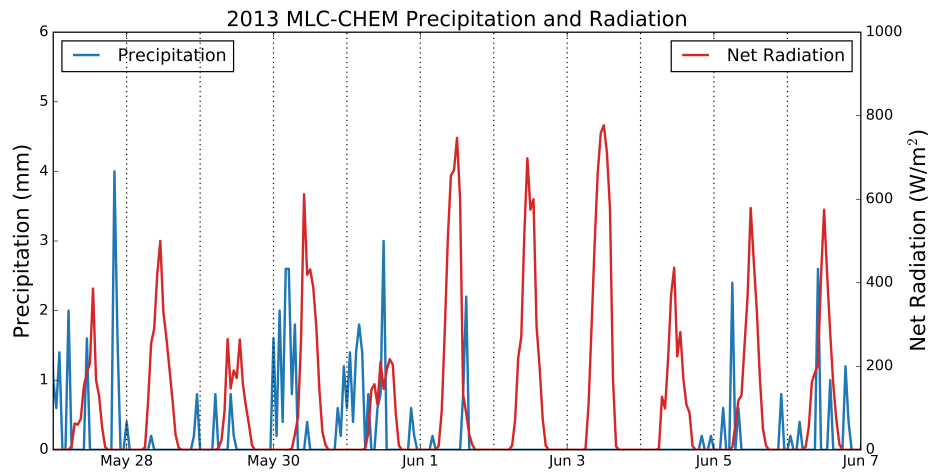
(b)
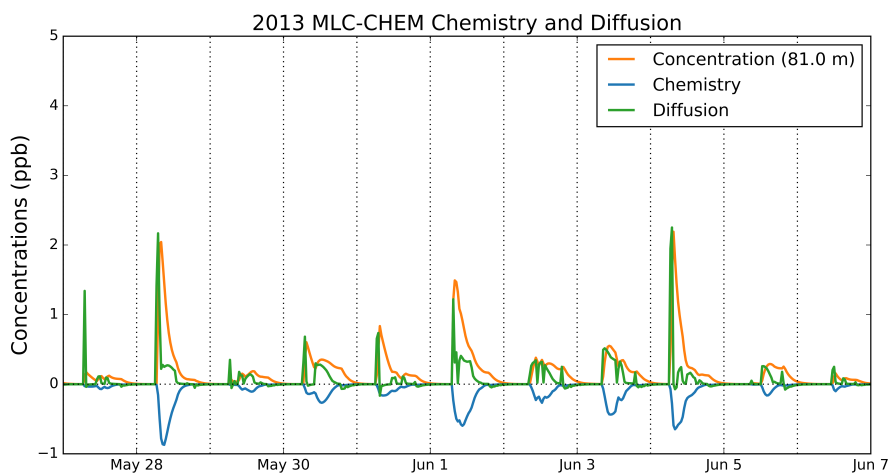
(c)

Figure 4.4: FIS observations and MLC-CHEM isoprene estimates during the WtD transition. Figure (a) shows the observed and estimated isoprene concentrations. Figure (b) shows net radiation and precipitation for the time period, and Figure (c) shows the movement of isoprene into the area, and its oxidation.

morning. This is supported by FIS measurements, which did not show strong increases in concentration in the early morning hours. The opposite is observed in the evenings where modelled isoprene tapers off, diffusing out of the 81 m layer just at or shortly after sunset.

The MEGAN isoprene output for a 10-day portion of the WtD season is presented in Figure 4.5. The PAR for the period is plotted in the top panel, the second panel shows the temperature, the third conatains γ_T and γ_{PAR}–the variation in emission activity due to temperature and PAR, respectively. MEGAN isoprene concentration output is in the bottom panel, compared against FIS measurements. Like MLC-CHEM, MEGAN performance is inconsistent across the time period; however, there are no days where MEGAN strongly over-estimates concentrations; the days with the poorest agreement (Jun 6 and 7) show an underestimation by MEGAN by up to 200% (1 ppb). The agreement between observations and modelled concentrations is better on days with lower PAR .

4.2.3 Dry Season

As discussed in Ch. 3, FIS measurement and satellite data indicated that the dry season has the lowest average isoprene concentrations in every year over the Daintree Rainforest, and these findings are replicated in both MLC-CHEM and MEGAN. The highest modelled concentrations occur in 2013, where peak daytime concentrations are $\sim$ 2 ppb through the season and begin to increase in September. Modelled concentrations diverge from FIS observations in October, when model results rise sharply to daily maxima 2-3 times higher than observations. Maximum daily concentrations are well below 2 ppb throughout the dry season in 2015 and increase in September to $\sim$ 2 ppb in 2015.

In the MEGAN model output for 2015, there is little variation as the DtW season approaches. The lower concentrations show a much closer agreement with
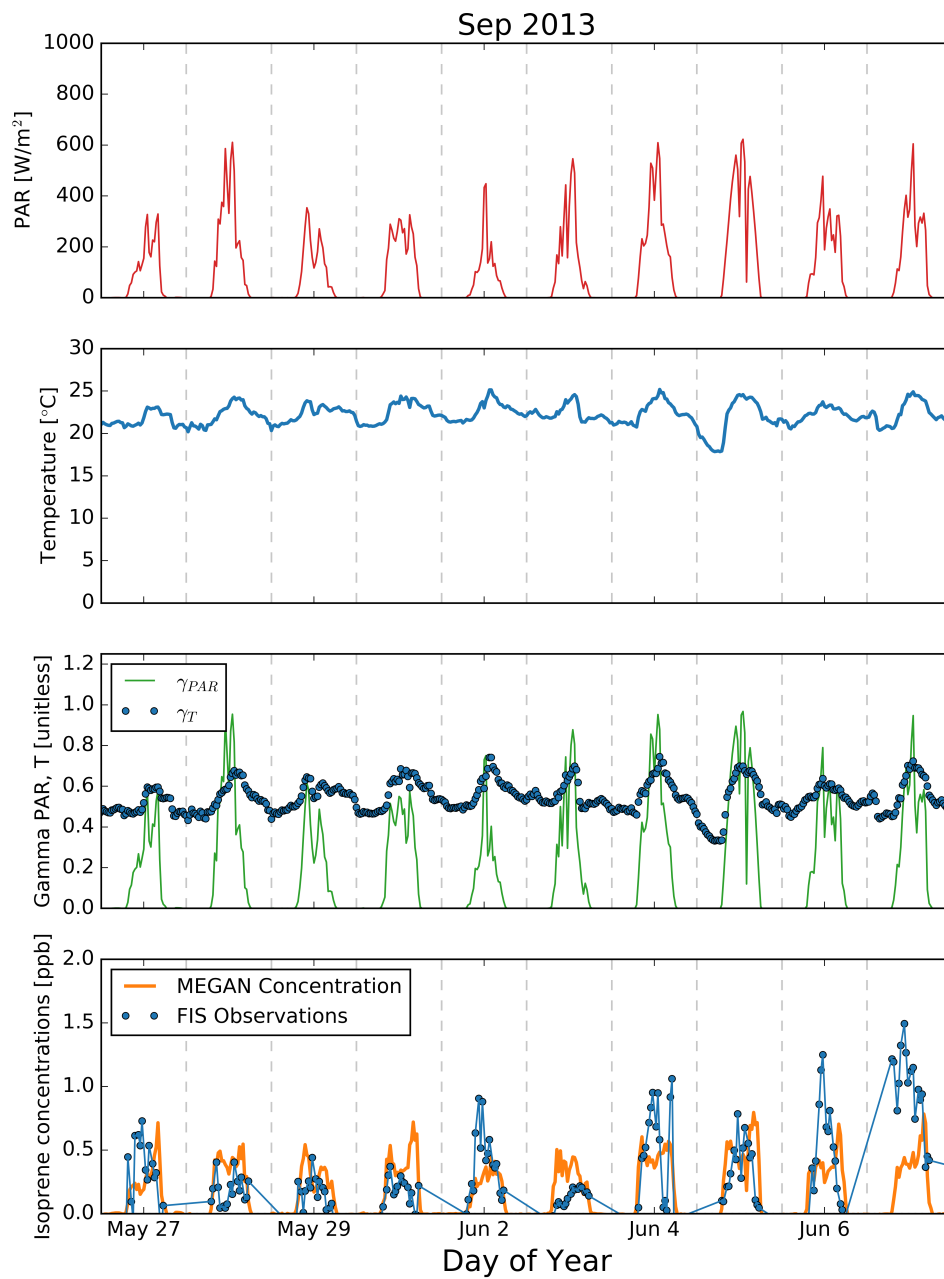
Figure 4.5: A comparison of FIS observations and MEGAN calculations during the 2013 WtD season. The top panel shows PAR for the period and the second shows temperature. The third panel shows γ_T and γ_{PAR}. Calculated concentrations are compared against FIS measurements in the bottom panel.

FIS measurements in October 2013, but isoprene concentrations are underestimated in June 2013 and August 2015. Langford et al. (2010) used MEGAN to model isoprene emissions over Borneo during Phase 2 of the OP3 campaign (OP3-III). They found the default BER to be too high for the area; utilisation of a BER from Amazonian measurement resulted in an emissions overestimation of >4 times their observations. In addition, though Langford et al. (2010) conduct their analysis with a static BER, they suggest that a variable BER might be more suitable for the site. These findings were corroborated in a Southeast Asia-wide study of land-use and climate change (Stavrakou et al., 2014). They observed that the default BER used in MEGAN resulted in an overestimation by a factor of 5, and when utilising a lower BER (6.6 mg m^{-2}h^{-1}), that overestimate fell to a factor of 3.3, in agreement with Langford et al. (2010)

Figure 4.6 highlights MLC-CHEM output over an 11-day period in the dry season. MLC-CHEM (Figure 4.6) over-predicts isoprene concentrations in every day but one, by as much as a factor of 4-6. The day with the best agreement is 5 Sep, which has the lowest PAR in the time series and is the only day where where there is rainfall during the day. Like the WtD transition, the days with the highest model overpredictions correspond to the days with the highest PAR.

The diffusion and chemistry for this time series in Figure 4.6c shows some changes from the WtD transition season. The early morning spike in isoprene concentrations is not a regular feature of the movement of isoprene into this layer. This is possibly due to the slightly cooler temperatures and later sunrise, which would cause the boundary layer to rise later in the morning compared to April and May. On the days where diffusion into the 35 m layer is high in the early morning, there is an equally fast oxidation (indicated by the blue line in Fig. 4.6c), which has a moderating effect on the overall concentration.

Figure 4.7 shows the MEGAN isoprene calculations for the 2013 dry season. Agreement between calculated concentrations and FIS measurements is inconsis-

(a)

(b)

(c)
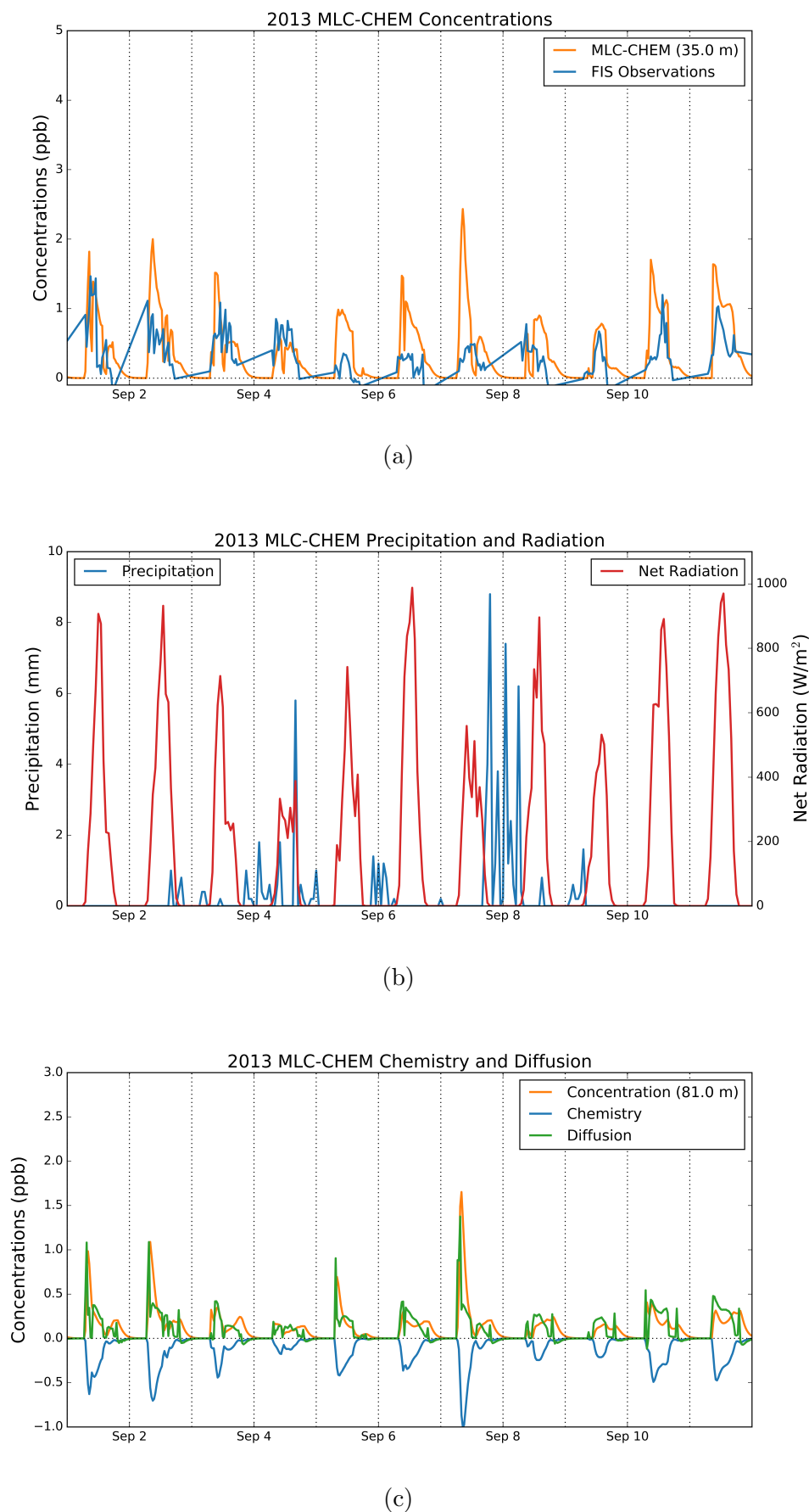
Figure 4.6: Plots showing the observations and MLC-CHEM modelled isoprene output during the dry season: (a) observed and estimated isoprene concentrations. (b) net radiation and precipitation for the time period, and (c) the movement of isoprene into the area, and its oxidation.
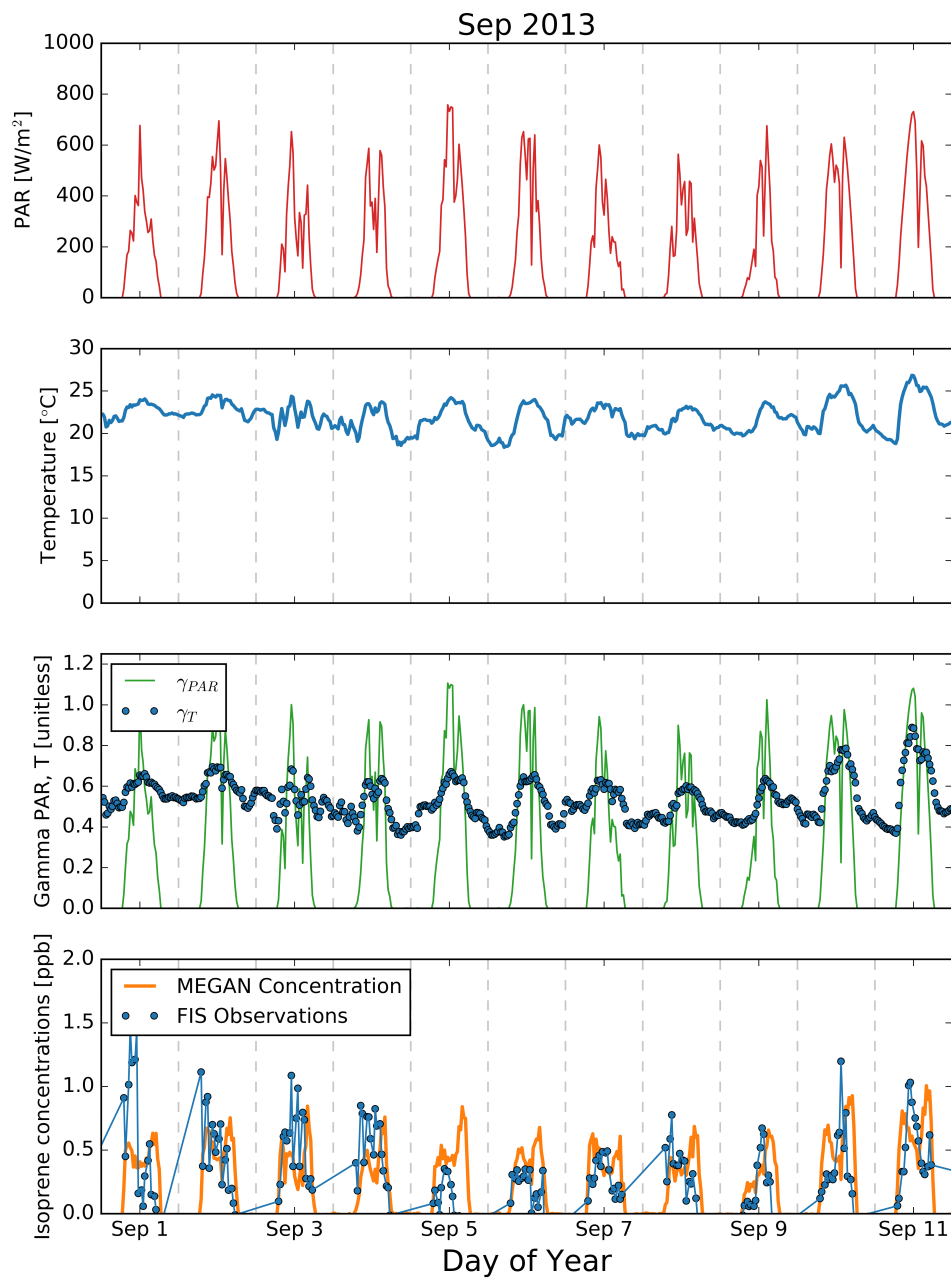
Figure 4.7: A comparison of FIS observations and MEGAN calculations during the 2013 dry season. The top panel shows PAR for the period and temperature is presented on the second panel. The third panel shows γ_T and γ_{PAR}. Calculated concentrations are compared against FIS measurements in the bottom panel.

tent; there are no significant over- or underestimations in the model calculations, but the modelled concentrations are slower to increase than the measurements indicate. This is particularly noticeable on 9 and 10 Sep where the isoprene concentrations peak in the afternoon and the model peaks occur two hours later. Like the WtD season, the days with the best agreement between observations and modelled concentrations occurs when the daily maximum PAR is below 600 W m^{-2}.

4.2.4   Dry to Wet Transition Season

In both MEGAN and MLC-CHEM, the conditions which begin late in the dry season persist throughout the remainder of the year. Like the previously discussed seasons, MLC-CHEM isoprene concentrations in 2015 are lower than 2013. Model output concentrations are not available for the last week of 2015 due to meteorological equipment failures, as MLC-CHEM relies on this input for its calculations. Interannual variation in the MEGAN concentration calculations yields daily maxima between 1-2 ppb in 2013 and under 1 ppb in 2015. These lower concentrations are likely due to two elements: 1) El Niño, which caused an increased cloudiness throughout 2015 (Figure 4.8); and isoprene removal through OH chemistry.

FIS concentration measurements were taken in the DtW transition season in 2015 and MLC-CHEM isoprene concentration output shows several features that are not replicated in observational data. First, modelled concentrations persist into the overnight hours, and do not reach zero until well after midnight the following day. Second, the timing of the onset of isoprene formation in the morning is inconsistent. On days where there is a spike in concentrations in the morning (e.g., 10 Dec,16 Dec), the model matches observations in the onset of diurnal isoprene emission, though the boundary layer has not begun to rise, as described above. On days where no such spike occurs, the model lags behind observations by as much as 2 hours. Finally, there are days where the model
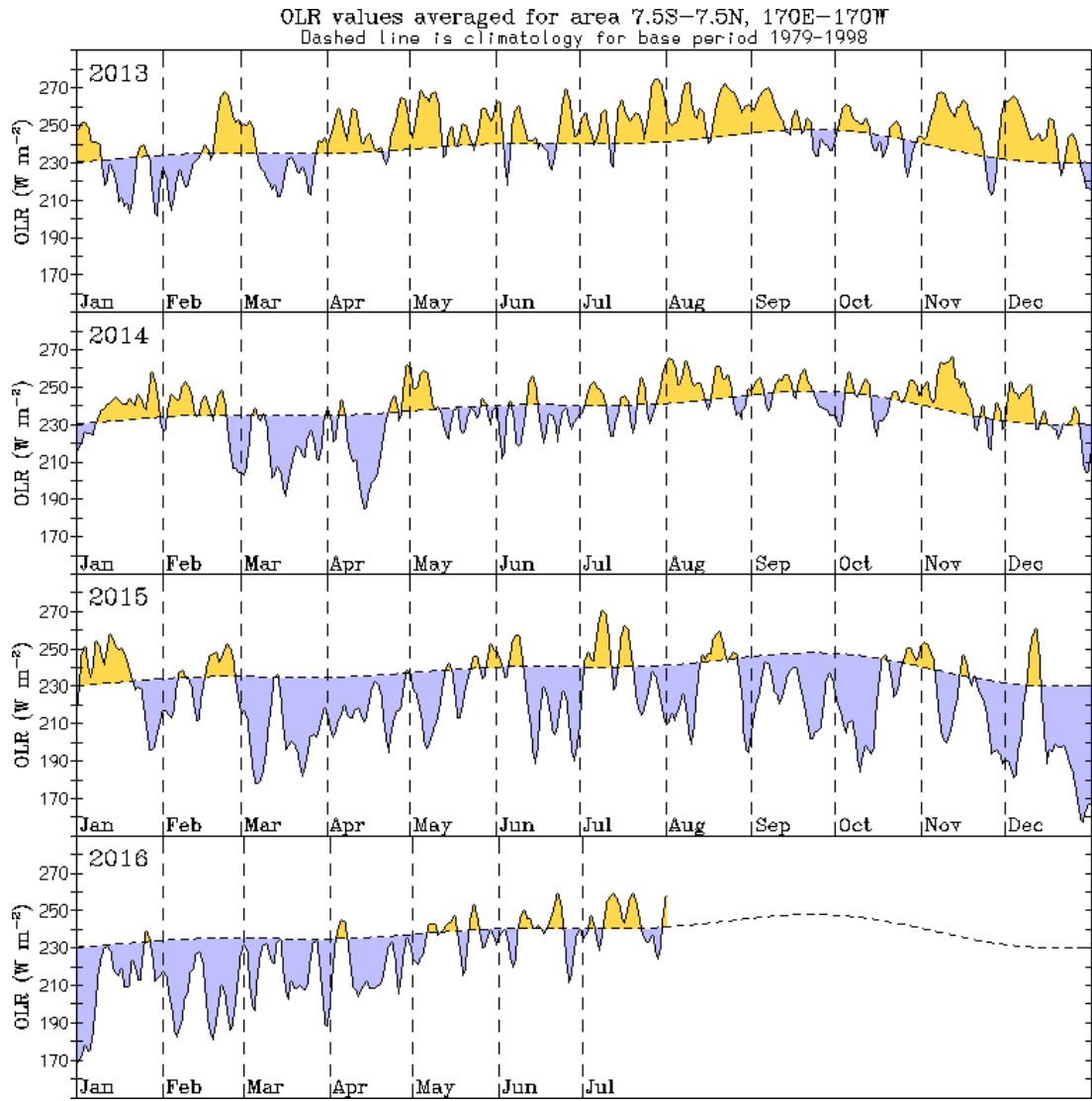
Figure 4.8: Plot showing departures from average outbound solar radiation (OSR), 2013-mid 2016. Yellow shaded areas indicate higher OSR (fewer clouds); purple shaded areas indicate lower OSR (more clouds). Dashed line indicates climatological average. *(Image courtesy Australian Bureau of Meteorology)*

strongly over-predicts (10 and 16 Dec) and underpredicts (13 and 14 Dec) isoprene formation. The over-predictions occur on the days with the highest direct PAR and temperature, and the underpredictions occur on days with the lowest directly measured PAR; there was not enough net radiation on these days for the drivers to initiate isoprene production. The contribution of diffuse PAR to isoprene emissions have not been estimated for this model.

A comparison of FIS measurements to the MEGAN model is shown in Fig.

(a)

(b)

(c)

Figure 4.9: Plots showing the observations and MLC-CHEM isoprene estimates during the dry-to-wet transition season. Figure a shows the observed and estimated isoprene concentrations. Figure b shows net radiation and precipitation for the time period, and Figure c shows the movement of isoprene into the area, and its oxidation.
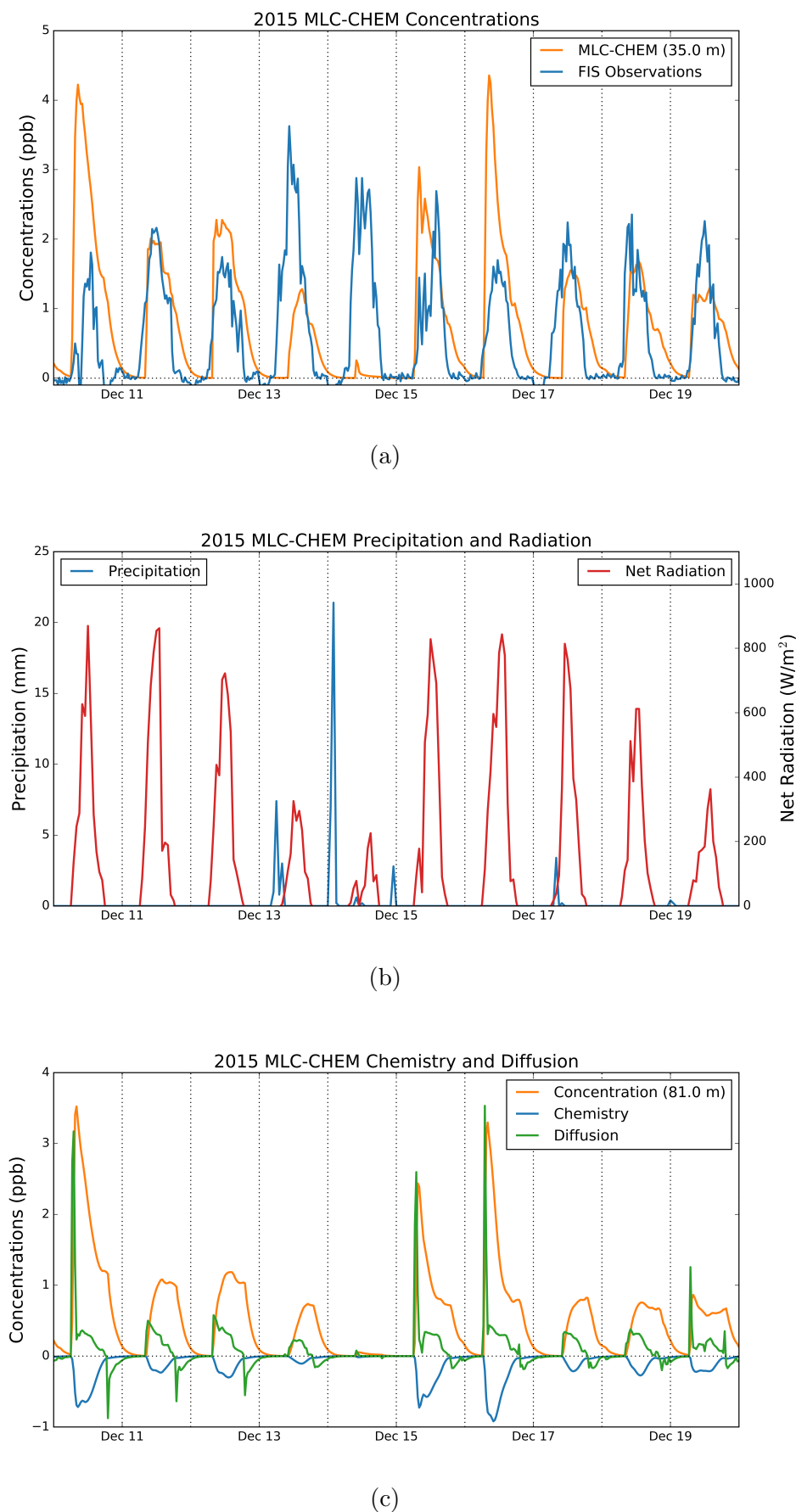
4.10. The MEGAN output consistently under-predicts isoprene concentrations by 50-200%. The presence of double peaks in the majority of this time period (see bottom panel) indicates that the OH chemistry, derived from observations from Borneo, is not reflective of conditions in the Daintree.

4.3 Description of Model Sensitivity Analysis and Scenarios

In order to understand the relationships between model inputs and the outputs they generate, both models underwent a series of sensitivity tests to understand how individual parameters drive isoprene concentrations with a goal of improving the fit between observed concentrations and model output. The models were not tuned to be site-specific in order to allow the findings to be more broadly comparable to the results in other tropical ecosystems.

4.3.1 Description of Sensitivity Tests

The first aspect of model behaviour taken under consideration was the role that NO_x and O_3 inputs play in the calculation of isoprene concentrations in the MLC-CHEM model. MEGAN was not tested in this way because it does not make use of these compounds when calculating above-canopy isoprene loss through chemical reaction. The base case used 2014 meteorological data with hourly inputs of O_3 and NO_x from GEOS-CHEM. The test case used the same meteorological inputs, and then O_3 and NO_x were each held to a flat rate: the median value from 2014. Above-canopy isoprene concentrations were compared for each case to determine if there were any changes to model chemistry from holding these compounds at a constant value.

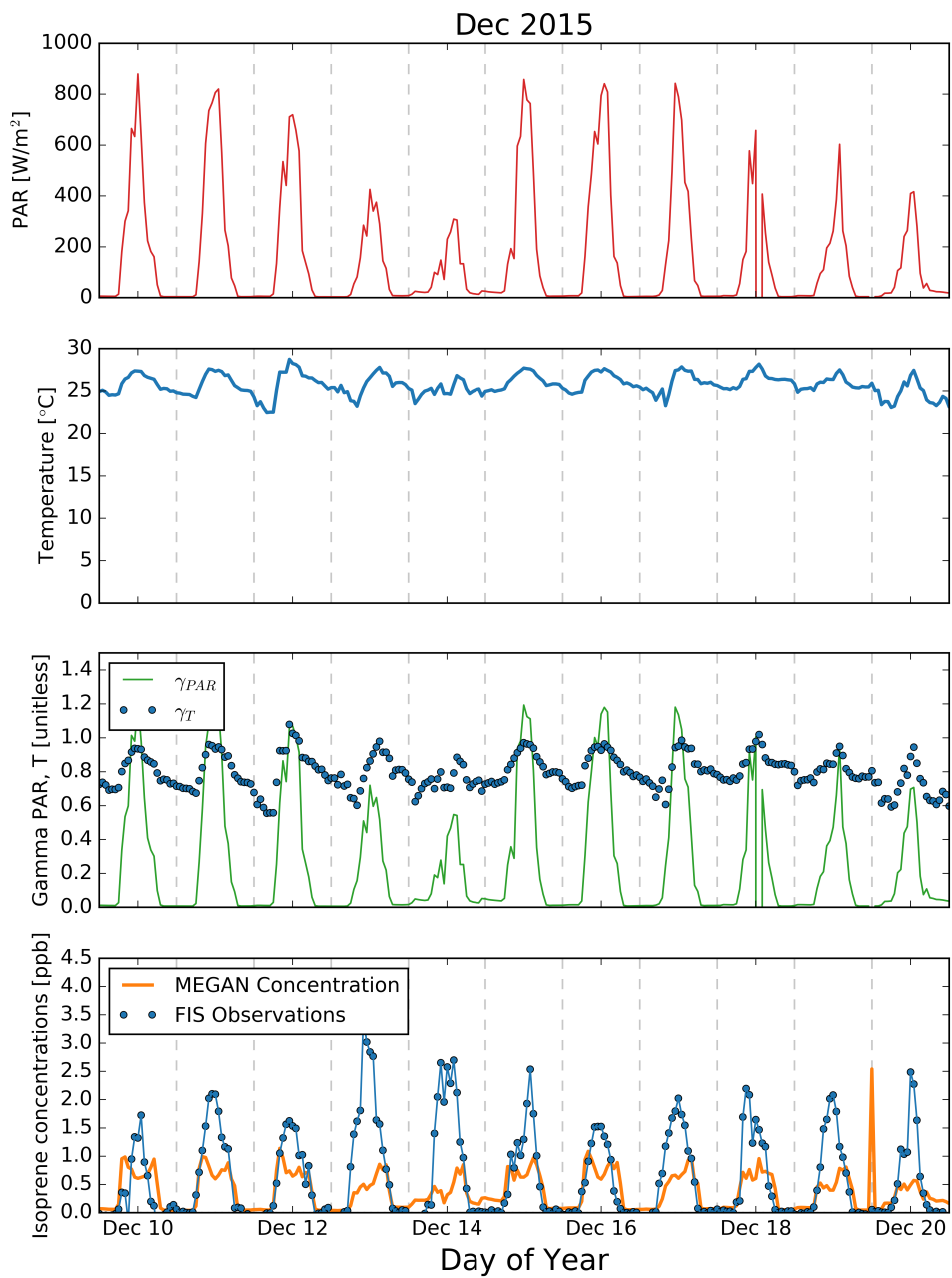LAI was the second model input tested in the sensitivity analysis. Given

Figure 4.10: A comparison of FIS observations and MEGAN calculations during the 2015 DtW transition season. The top panel shows PAR for the period and the second shows the temperature. The third panel shows γ_T and γ_{PAR}. Calculated concentrations are compared against FIS measurements in the bottom panel.

its direct role in calculating γ_{CE} (Equation 4.7), LAI has the potential to be a strong driver for changes in seasonal isoprene emission in the Daintree Rainforest. Though tropical forests are evergreen, the LAI typically follows a seasonal growing pattern. This variation has been hypothesized to be the driver of seasonal isoprene variation over the Amazon (Barkley et al., 2009); a more recent hypothesis suggests that trees expose newer leaves that are initially poorer emitters of isoprene, optimizing for the available sunlight and soil moisture (Caldararu et al., 2012). In order to understand how changing LAI would change isoprene concentrations in this model, the LAI was 1) halved, and 2) doubled, from the published Daintree Rainforest LAI of 3.9 (Pokorska et al., 2012).

Following the initial sensitivity tests, several scenarios were investigated (Table 4.2). Scenario S0 refers to the 'base case' which was described above; each subsequent scenario was added cumulatively to the model. First, LAI changed from a constant value to input data that is reflective of the annual growing season (S1). GEOS-Chem output, fitted to conform with published measurements, was used for LAI input (Liddell and Laurance, 2015). Second, EFs were investigated, following the observation that agreement between observations and MEGAN model output improved in Southeastern Asian rainforests when the EF was reduced (S2, Langford et al., 2010; Marais et al., 2014). Finally, the OH concentration was modified. The concentration measured over Borneo was utilised in S0, but significant variation has been observed across tropical forests as OH recycling and environmental factors are taken into consideration (Stone et al., 2011; Vaughan et al., 2012).

Table 4.2: Cases for Calculating Isoprene Concentrations

Name	Description	Period
S0	MEGAN and MLC-CHEM 'base case'	2013-2015
S1	Same as S0, with LAI reflective of annual growing season	2013-2015
S2	Same as S1, with base emission factor reduced	2013-2015
S3	Same as S2, with OH concentration modified to reflect other studies	2013-2015

Model bias for S0 and S3 were calculated for each of the model years using the following equation:

$$bias = 100\frac{1}{n}\sum \frac{Q_i^m - Q_i^o}{max(Q_i^m - Q_i^o)}\,,\qquad (4.9)$$

where n is the number of samples, Q^m is the modelled concentration at a given time step, and Q^o is the observed concentration for the same time step.

4.3.2   Sensitivity Analyses of the MLC-CHEM Model

A baseline model was run in order to provide a point of comparison for the sensitivity tests. Figure 4.11 shows hourly FIS measurements in comparison to hourly MLC-CHEM concentrations at a height of 35 m, colour-mapped according to net radiation. Both the 2013 and 2015 plots show a low R^2 value, which, when paired with a positive Spearman ranking (2013 S = 0.37 , p = 5.98 x 10^{-40} ; 2015 S = 0.36 , p =3.28 x 10^{-26}), indicates that the relationship between these two sets of data are likely not linear.

As shown in Fig. 4.11 MLC-CHEM has a tendency to overpredict concentrations when PAR is low. When the time series are examined (see figs 4.4,4.6, and4.9), the timing is early in the morning, between 8-10 am. This is likely due to the growth rate of the boundary layer in the morning–the concentration is dependent upon the height of the boundary layer. Thus, a 1-hour spike in the early morning hours indicates that isoprene emissions begin before the boundary layer begins to rise. This occurs again in the late afternoon in the 2015 plot; there are several points that indicate the presence of isoprene in the model which is not replicated in the observational data. One possibility for this occurrence is the complex topography of the site: the sun moves behind hills in the late afternoon, diffusing the remaining light. This alters the measured isoprene emission rate, but this diffusion is not accounted for in the MLC-CHEM model. Another
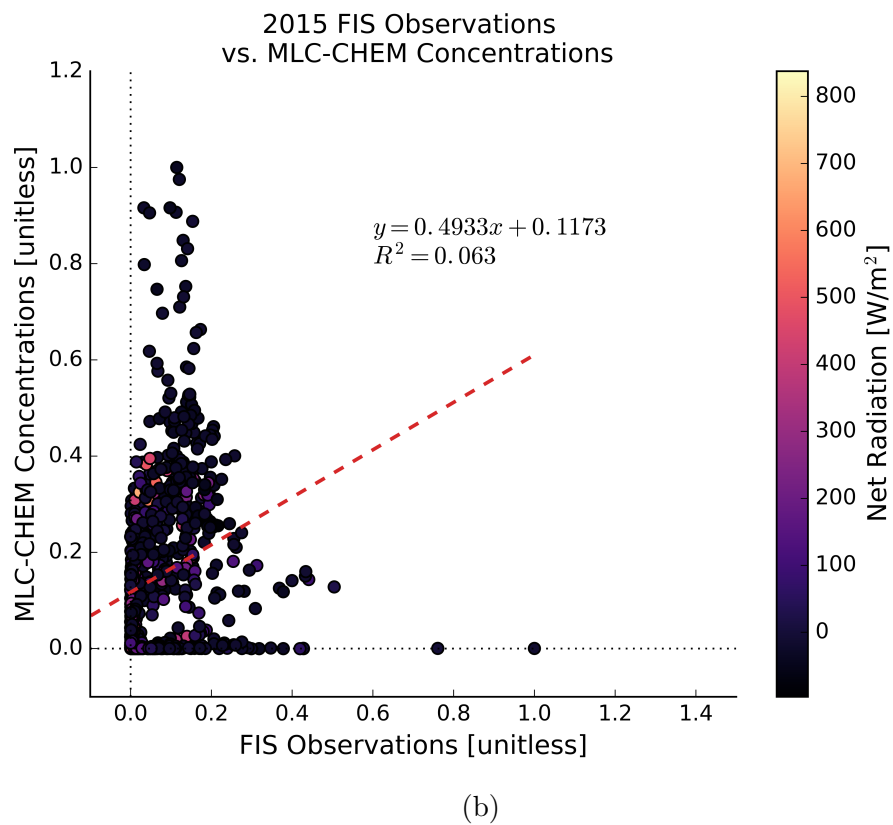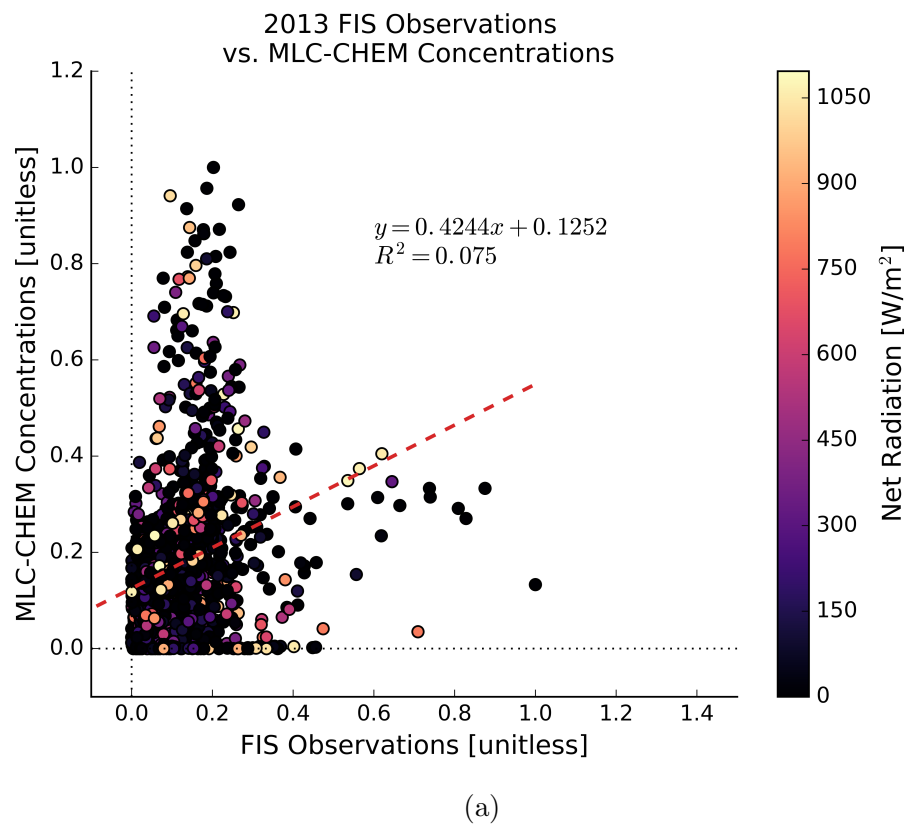
(a)

(b)

Figure 4.11: Plots showing FIS observations compared to MLC-CHEM estimates in 2013 (top), and 2015 (bottom). Colours are mapped according to time of day.

possibility is that the model is not accurately capturing the wind direction.

Model isoprene emissions, as described in Section 4.1.2, are based on both light and temperature. These equations are derived from field and greenhouse measurements made with an early-model FIS and described in Guenther et al. (1993). Guenther et al. (1993) compared isoprene emissions to leaf temperature and found some dependence on plant enzyme activity until ~35° C, after which emissions began to decrease. They also found that isoprene emission increased linearly with increasing PAR until a saturation point (Guenther et al., 1993).

A comparison of isoprene concentrations with PAR values for the year 2015 is shown in Figure 4.12, where measured concentrations are shown in orange and modelled with MLC-CHEM in blue. These results are similar to those found by Guenther et al. (1993), where there is an increase with increasing PAR. However, because this plot shows concentrations and not leaf-level emissions, the clear linear relationship is not as apparent. Modelled concentrations in excess of 1 ppb when PAR is low ($<$200 W/m^2) is likely due to boundary layer effects or cloudiness that is not accurately captured by the model. There are also times where modelled PAR is high ($>$400 W/m^2) and isoprene is at or near zero. This is likely due to the opposite effect–isoprene concentrations being low as the boundary layer grows in height in the morning.

Figure 4.13 shows the results of the MLC-CHEM O_3 and NO_x sensitivity tests. These were conducted in order to determine if holding these two compounds to a constant value affected isoprene concentrations. The base case used 2014 meteorological data with hourly inputs of O_3 and NO_x from GEOS-Chem. The test case used the same meteorological inputs, and then O_3 and NO_x were each held constant, at 27.42 ppb and 0.12 ppb respectively, which is the median value from 2014. Above-canopy isoprene concentrations were compared for each case to determine if there was any effect to holding these values constant. Comparing the isoprene outputs for the two different cases yields a 1:1 correlation and an R^2
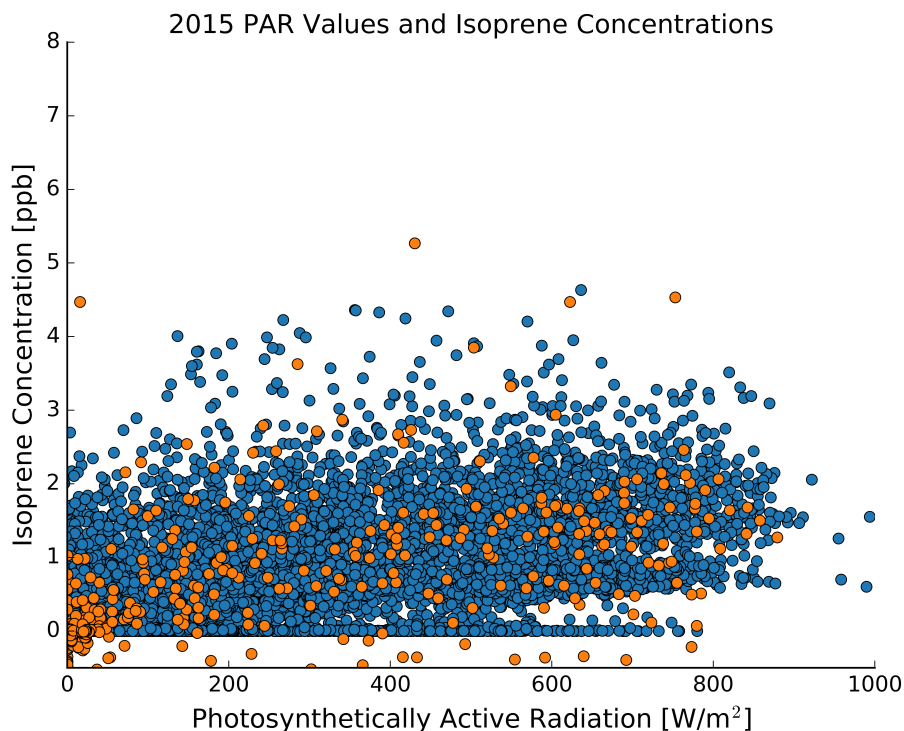
Figure 4.12: A comparison of 2015 measured (orange) and modelled (blue) isoprene concentrations and PAR.

of 1.0, which indicates that there was no change in isoprene concentrations when either NO_x or O_3 was held to a flat rate. Because this test shows that using a constant value for NO_x or O_3 has no effect the isoprene chemistry, it is possible to use constant values when O_3 and NO_x inputs from GEOS-Chem are unavailable.

The second sensitivity test conducted on the MLC-CHEM model was a variation of the LAI in order to verify that changing the LAI would result in a linear scaling of the isoprene concentration and that there would be no points where isoprene emissions reached a saturation point due to LAI. This test was important due to the necessity of accurately replicating an annual seasonal cycle with a paucity of ground-based LAI measurements at the DRO. The results of this test in all three model years is quite consistent (Figure 4.14). The effect of 0.5 LAI from the base case, from 3.9 to 2.0, shows that above-canopy isoprene concentrations decrease to $< 50\%$ of their original value. 2013 is an exception, and the change is $> 50\%$. However, all three years have $R^2 > 0.9$. The right column

(a)

(b)
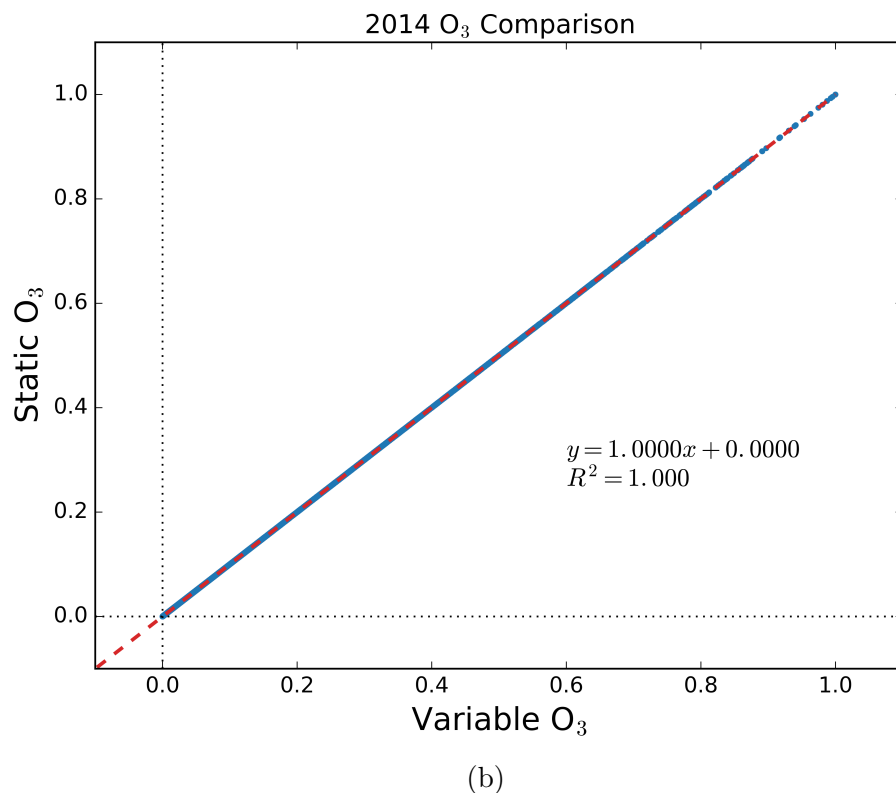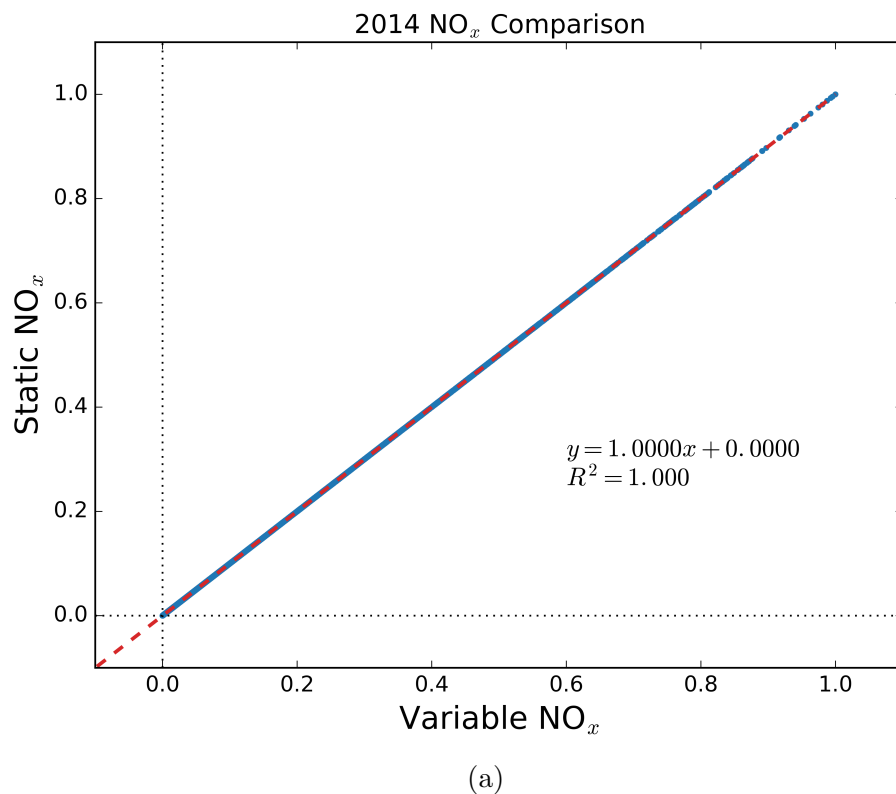
Figure 4.13: Time-matched concentration-concentration plot showing a comparison of MLC-CHEM isoprene concentration estimates when either NO_x and O_3 are held to a constant value instead of when constant and hourly NO_x and O_3 concentrations are used instead of hourly data in the input files. Hourly data is from GEOS-Chem; the static value is the annual average value from the GEOS-Chem data. Figure 4.13a compares constant and hourly NO_x concentrations on isoprene concentrations, and Figure 4.13b compares constant and hourly O_3 concentrations.

shows the results of doubling the LAI, from 3.9 to 8.0. These results are similar, though opposite, to what is seen on the left. Doubling the LAI increases the above-canopy isoprene concentrations by a factor of 1.5, with a very good agreement between the two cases. Again, the R^2 value > 0.9. Halving and doubling of the LAI does not correspond to an equal change in concentration because the concentration in MLC-CHEM takes chemical transformation, vertical movement and deposition into account when deriving these values.

Figure 4.15 shows the results of applying the scenarios in Table 4.2 to the MLC-CHEM model for 2015. Only S1 and S2 were used in MLC-CHEM because OH reacts with mono- and sesquiterpenes in addition to isoprene in this model, so the amount available to react with isoprene is already reduced. Varying LAI in MLC-CHEM has a strong effect on isoprene concentrations: the shape of the concentration profile changes entirely and annual maxima shift from Dec-Jan to May-Jun. The maximum concentrations nearly triple, from $\sim$5 ppb in Dec 2015 in S0 to $\sim$14 ppb in Apr 2015 under S1. One of the factors contributing to the increase in concentration is the high overnight concentrations. Most nights from Jan-Oct show a moderate overnight isoprene concentration, which occurs here when the diurnal supply of OH is exhausted. This then pushes the concentration on the following day higher than it would be otherwise. However, this is not reflected in FIS observations, which show isoprene concentrations decreasing to zero overnight. The effects of a variable LAI also dominate other contributors to isoprene concentration; lowering the EF (S2, Figure 4.15c) shows no change from S1. The model bias in the S2 scenario is 8.3%. Though this appears to be an improvement on the S0 scenario, it is due to a strong model over-estimation of concentrations in Apr-May, then a strong underestimation in Dec. Similar changes in model bias were observed in other years. The S0 bias in 2013 was 26%, and was nearly unchanged in S2, where the bias was 22%.

LAI = 2.0

2013 LAI Comparison

$y = 0.5345x + 0.0053$
$R^2 = 0.960$

(a)

LAI = 8.0

2013 LAI Comparison

$y = 1.5038x + -0.0558$
$R^2 = 0.965$

(b)

(c)

(d)
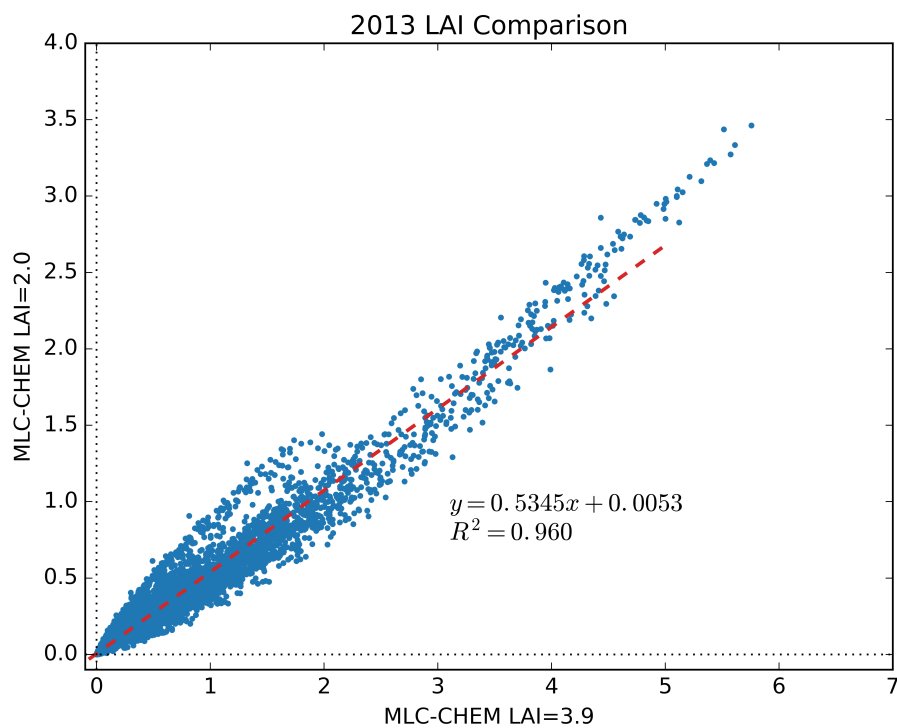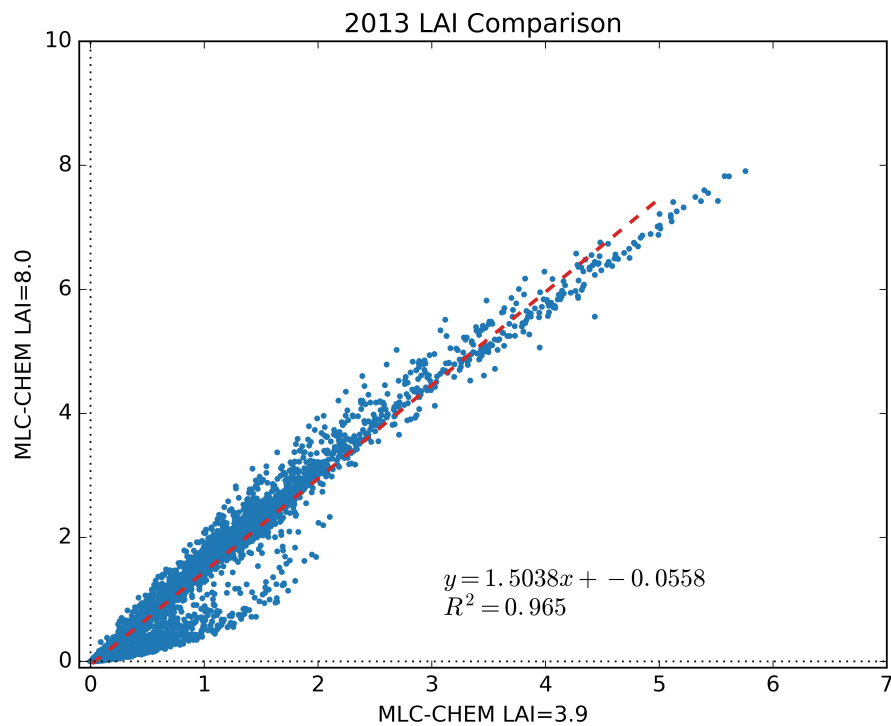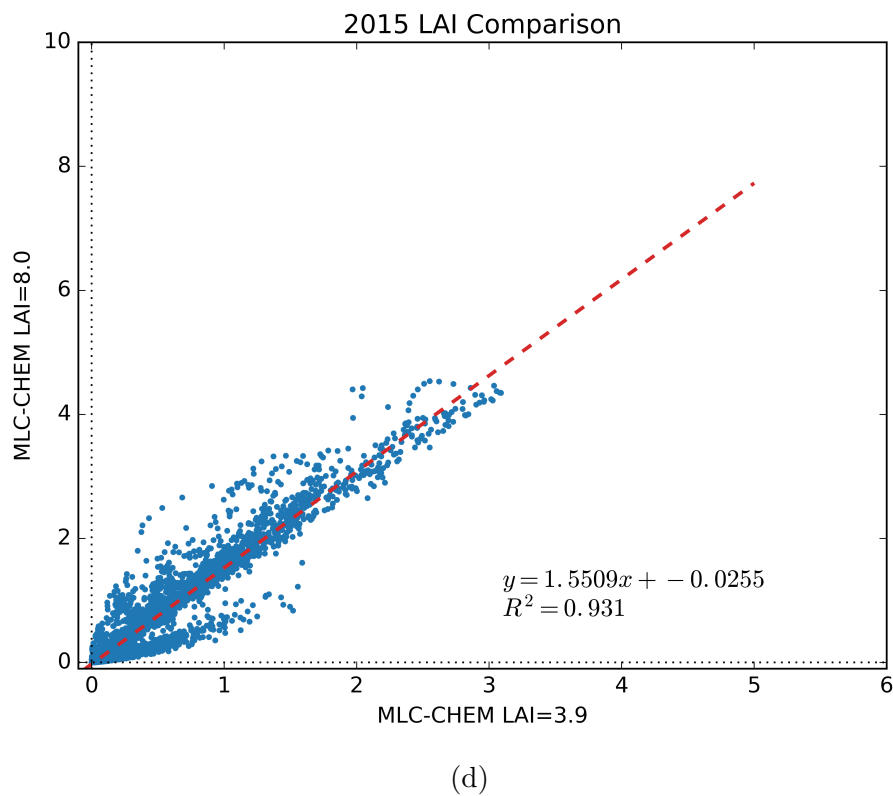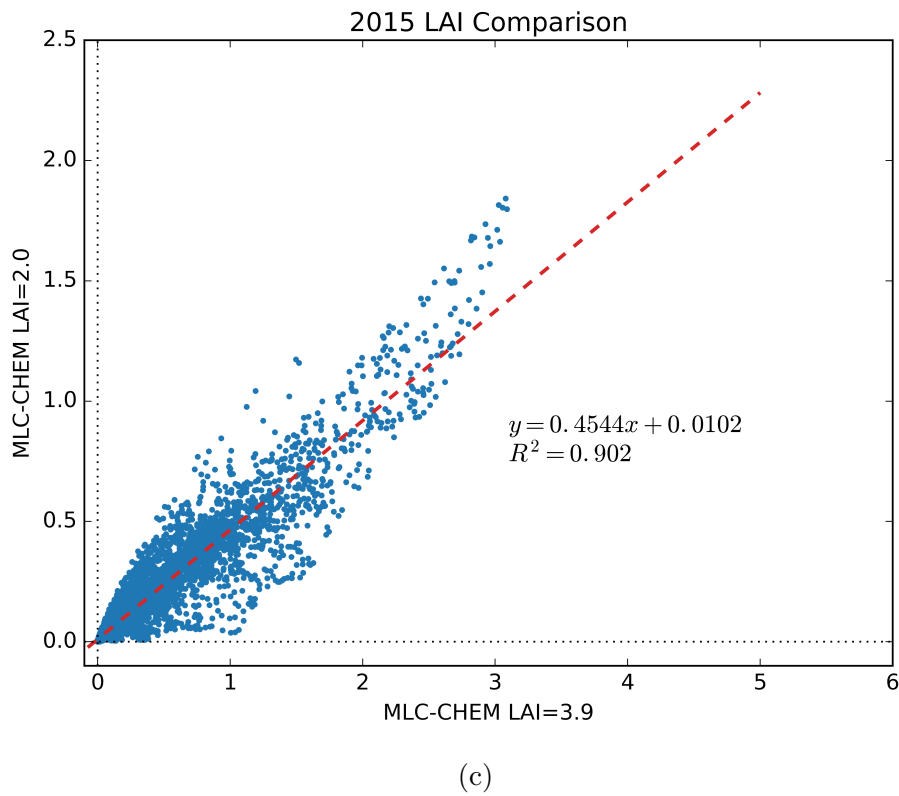
Figure 4.14: A comparison of MLC-CHEM above-canopy isoprene concentrations at different LAIs. Plots showing the effect of lowering the LAI by half (3.9 to 2.0) across all model/observation years are shown in a, c; the effect of doubling the LAI (3.9 to 8.0) in b,d.
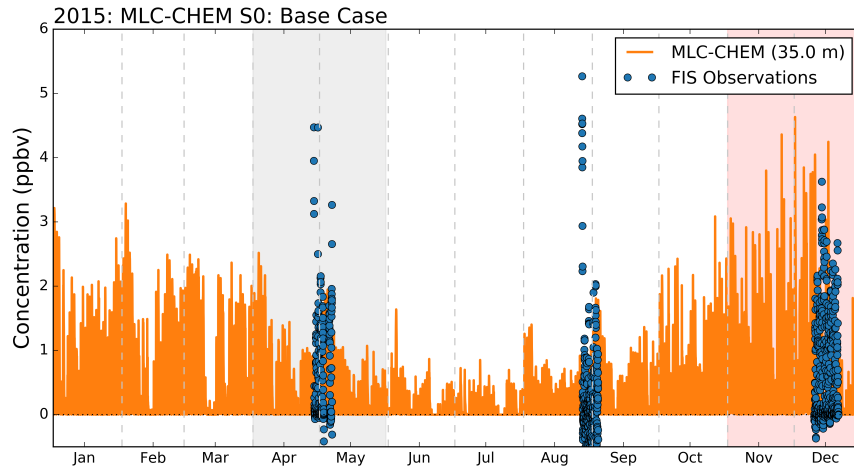
(a)
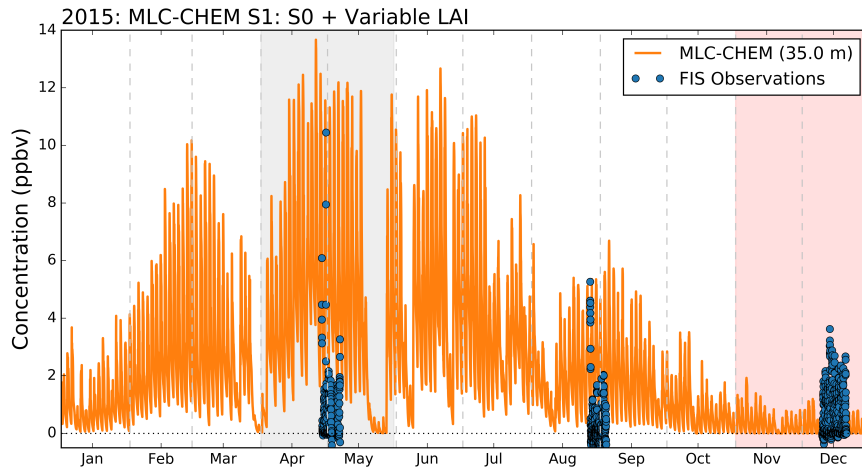
(b)
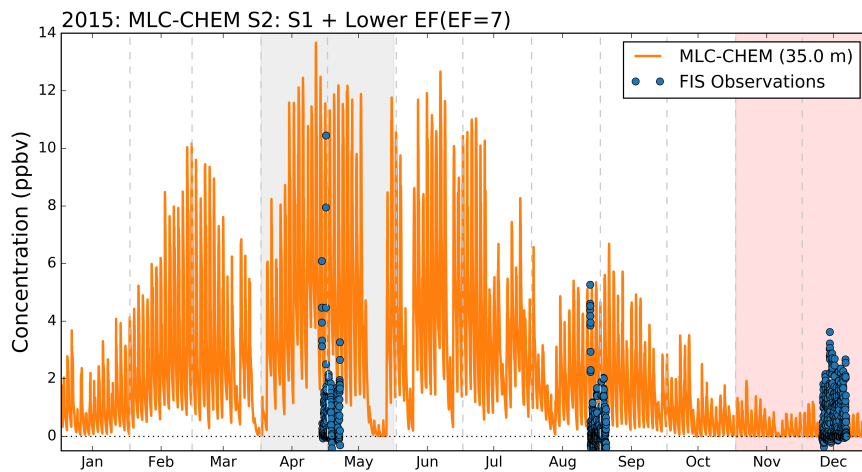
(c)

Figure 4.15: Changes to MLC-CHEM model, after the application of different scenarios. The gray region indicates the WtD transition season, the region in pink represents the DtW season.

4.3.3 Sensitivity Analysis of the MEGAN model

Figure 4.16 shows the results of the base case comparison of FIS measurements to MEGAN calculated concentrations. The 2013 data set shows a very flat response from the FIS, with the bulk of measured concentrations rarely exceeding 0.4, and much higher relative modelled concentrations. This flat response could be due to the strength of the outliers, which in 2013 occur when there is a low PAR (200-400 W/m^2), and a high observed isoprene concentration, which is not replicated in the model. However, there is a slightly positive Spearman rank correlation (S = 0.1955, p=8.48 x 10^{-9}), indicating that there is some relationship between FIS observations and modelled concentrations, but it is not perfectly monotonic. When combined with the low R^2 value, the Spearman ranking indicates that the relationship is positive, but not linear. The 2015 data set has a higher R^2 value than 2013, and a stronger positive Spearman rank correlation (S = 0.57, p = 5.04 x 10^{-36}). It also has several outliers similar to 2013 set, where high FIS observations are not replicated in modelled output. The poor fit of both plots could be due to the static LAI not sufficiently describing forest emissions behaviour during some seasons, a poor replication of boundary layer dynamics, or the OH chemistry mechanism removing not enough or too much isoprene.

The equations used to represent isoprene emission in the full MEGAN model, as described in Guenther et al. (2006), represent a refinement of the original equations described in Guenther et al. (1995) and extended in Guenther et al. (1999). In addition to supplementary equations describing plant type, leaf age, and several other climatological and environmental factors, the original two equations are supported by four others which are used to calculate empirical coefficients that rely on previous environmental conditions (24 and 240 hours prior) for their calculation. The model used in this research simplifies this somewhat by only considering the previous 24 hours.
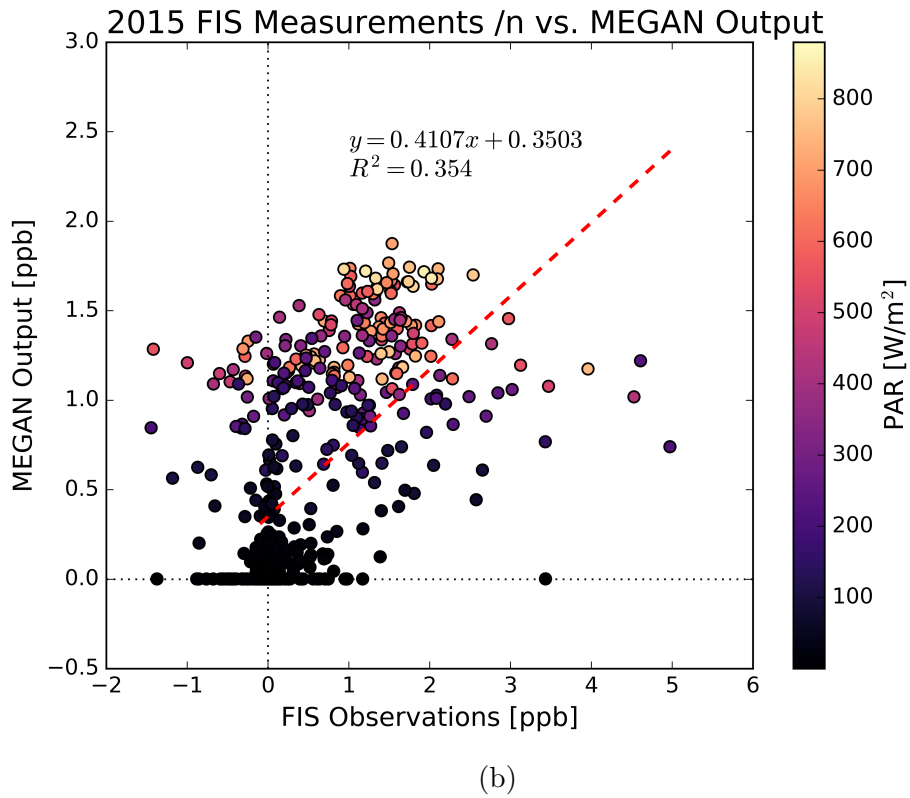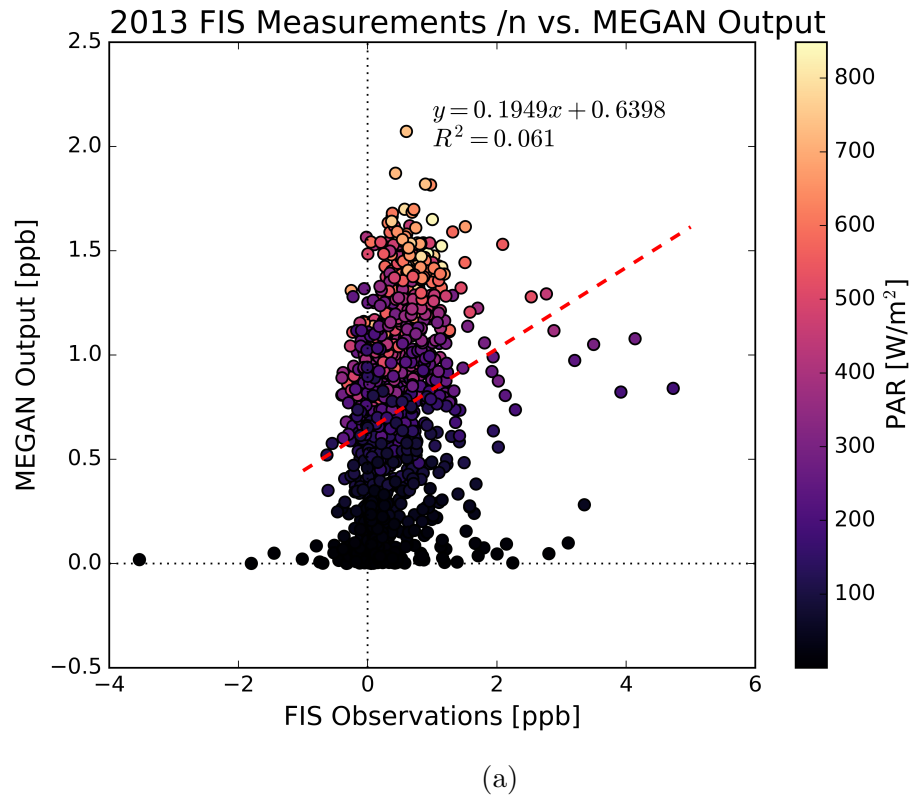
(a)

(b)

Figure 4.16: Plots showing normalised FIS observations compared to MEGAN calculations in 2013 (top), and 2015 (bottom). Colours are mapped according to PAR. the dashed line indicates the line of best fit.
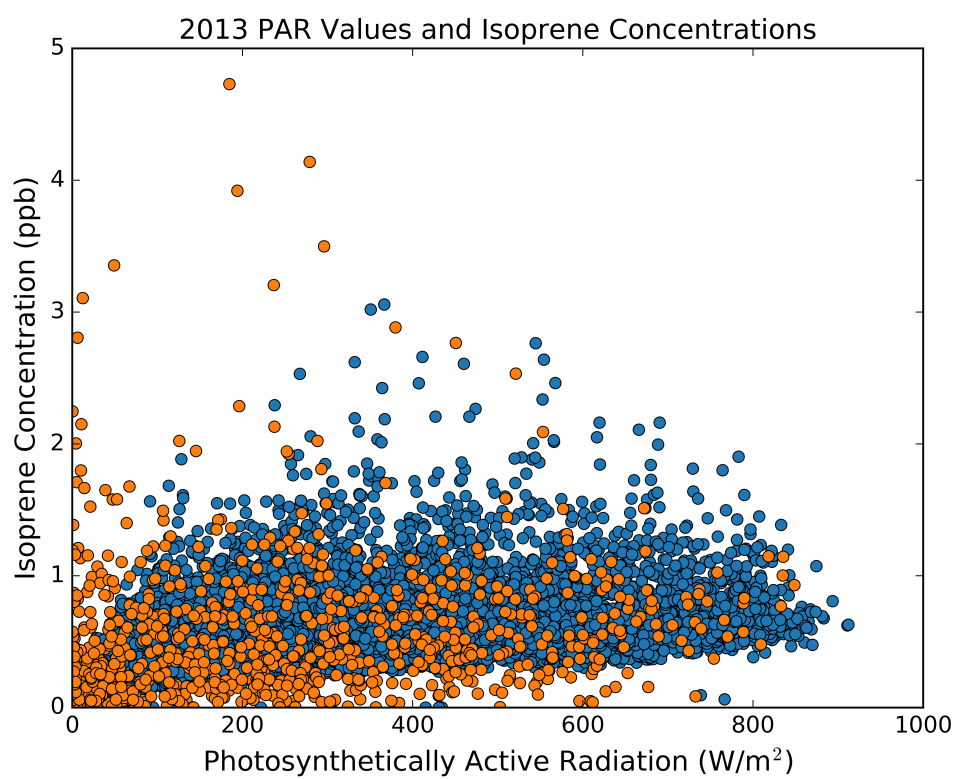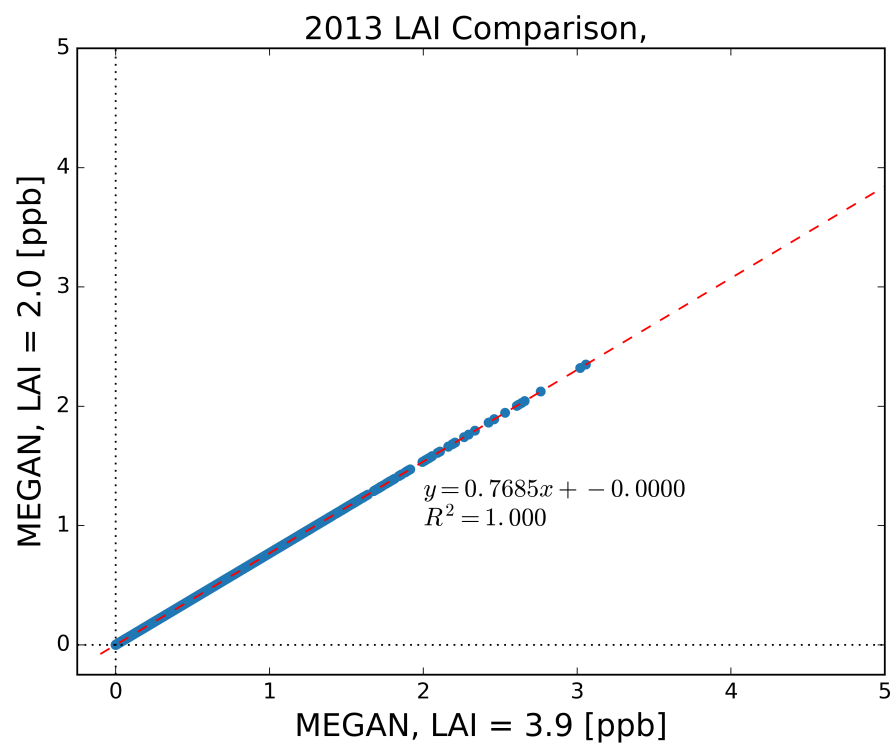
Figure 4.17: The relationship between PAR and isoprene concentrations for the year 2013. Observations are indicated in orange, model output is shown in blue.

Figure 4.17 shows a comparison of PAR and isoprene concentrations in 2013. MEGAN output is in blue and FIS observations are rendered in orange. These results show a clearer increase in isoprene concentrations with increasing PAR than the MLC-CHEM results discussed in Sec. 4.3.2. Though there is a boundary layer that grows and collapses throughout the day, there are no model results showing isoprene concentrations >1 ppb when PAR is <200 W/m^2, nor concentrations at or near zero when PAR is >400 W/m^2. However, there is a significant presence of isoprene observations that are at or near zero at higher PAR values, which indicates that there are other processes occurring at this site that are not captured well by the model.

Figure 4.18 presents the effect of varying LAI within the MEGAN model environment. Like the MLC-CHEM tests, this was done to understand if there was any point at which the isoprene response would saturate and flatten or if there was a minimum threshold below which the model would be starved for input due to the influence of LAI. The change in concentrations has a perfect correlation ($R^2 = 1.0$). This is because vertical motion and deposition are not considered in this particular model. Doubling the LAI (from 3.9 to 8.0) causes only a slight increase in concentrations (a slope of 1.1). Lowering the LAI has a stronger effect; the slope decreases to 0.76.

Finally, the effects of varying the emission factor (EF) was tested. A selection of 2015 MEGAN runs using different emission factors from 8-100 x 10^{-3} mg/m^{2}hr are shown in Figure 4.19, along with their best fit line and R^2 value. These results show an increasing correlation with increasing EF, with a 1:1.04 correlation at an EF of 85. However, this improvement in correlation comes at the cost of the intercept. The intercept steadily increases along with correlation, which indicates that the modelled isoprene will typically not reach zero. This is important, as it was shown in Ch. 3 that concentrations at or near zero are observed after sunset at this site.

LAI = 2.0

(a)

LAI = 8.0

(b)

2015 LAI Comparison,

$$y = 0.7685x + -0.0000$$
$$R^2 = 1.000$$

(c)

2015 LAI Comparison,

$$y = 1.1102x + -0.0000$$
$$R^2 = 1.000$$

(d)
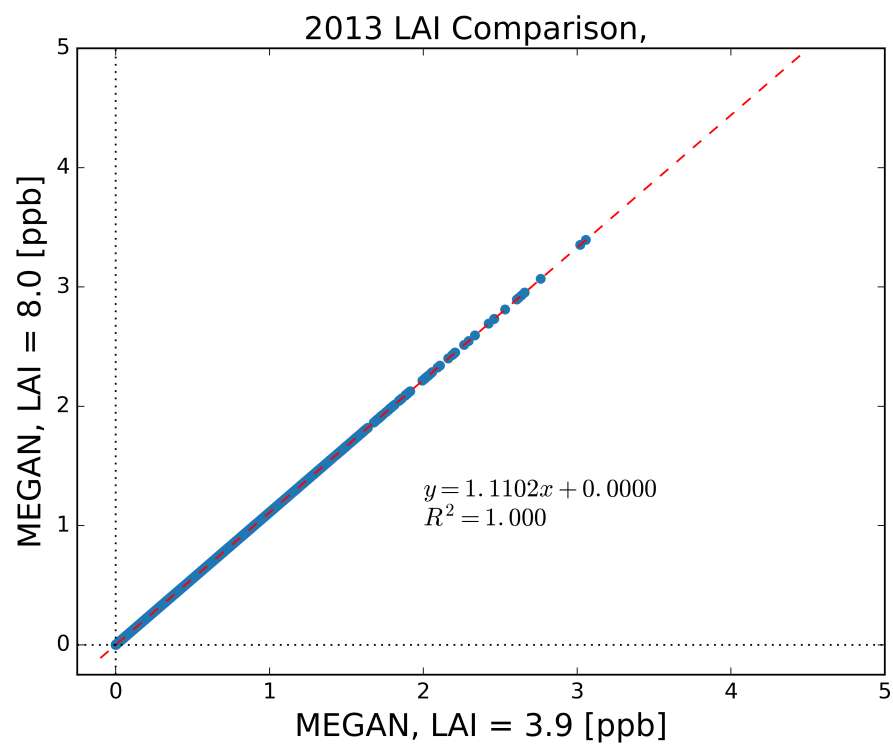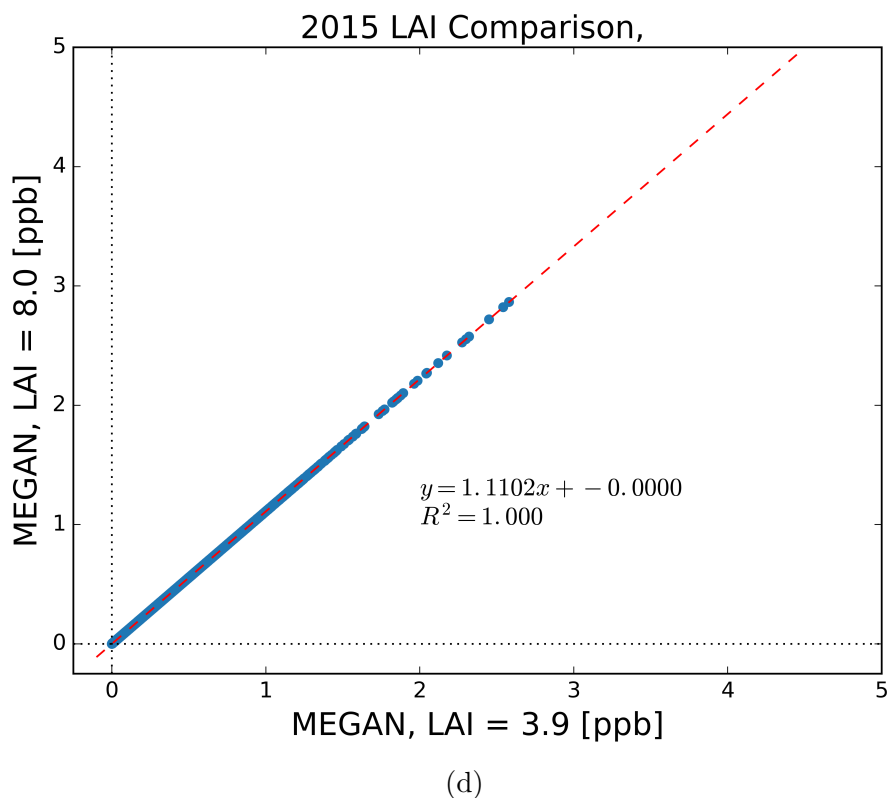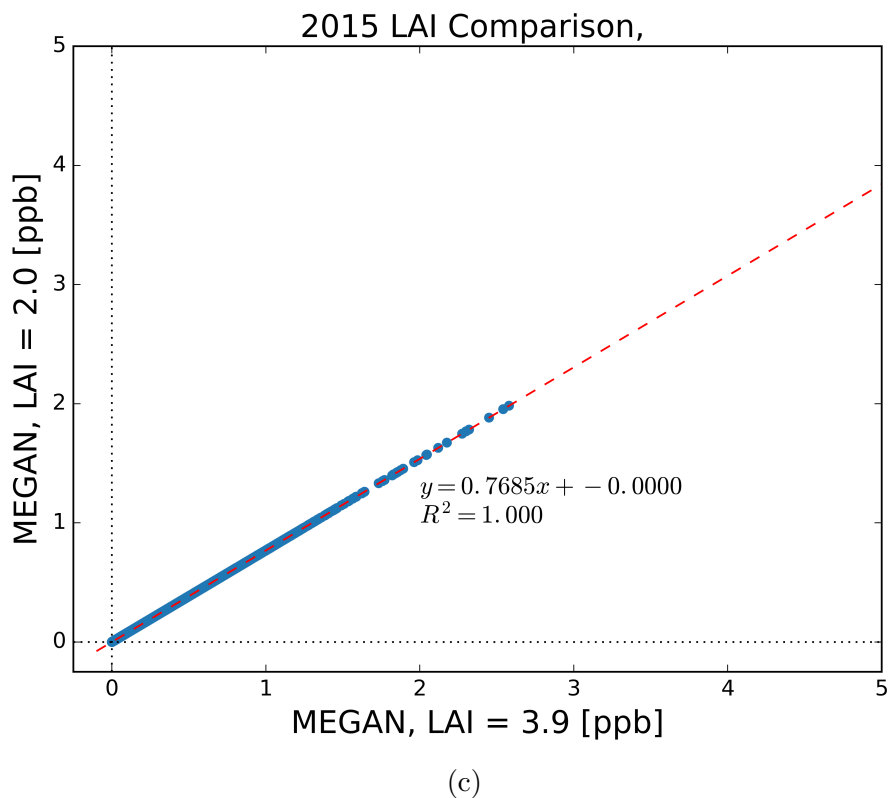
Figure 4.18: A time-matched concentration-concentration plot comparing MEGAN-derived isoprene concentrations at different LAIs. The x-axis represents isoprene concentration output when LAI is held to the published value of 3.9, and the y-axis shows the time-matched concentration when the LAI is either lowered by half (3.9 to 2.0) across all model/observation years are (shown in a, c) or doubled (3.9 to 8.0; in b,d).

$$y = 0.0979x + 0.1366$$
$$R^2 = 0.225$$

(a)

$$y = 0.3059x + 0.4268$$
$$R^2 = 0.225$$

(b)

(c)

(d)
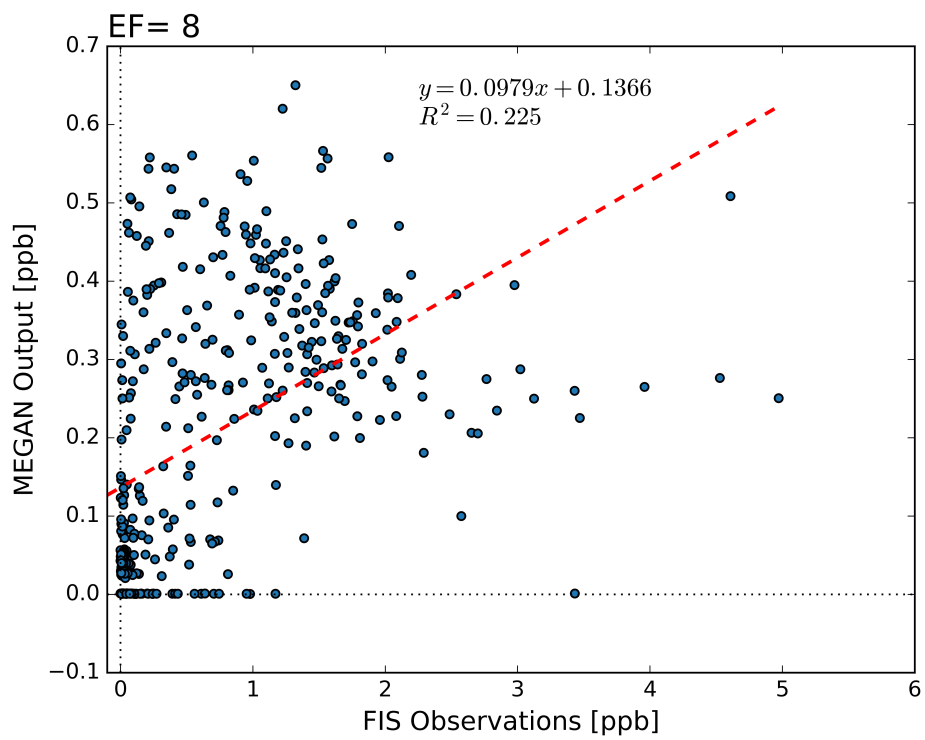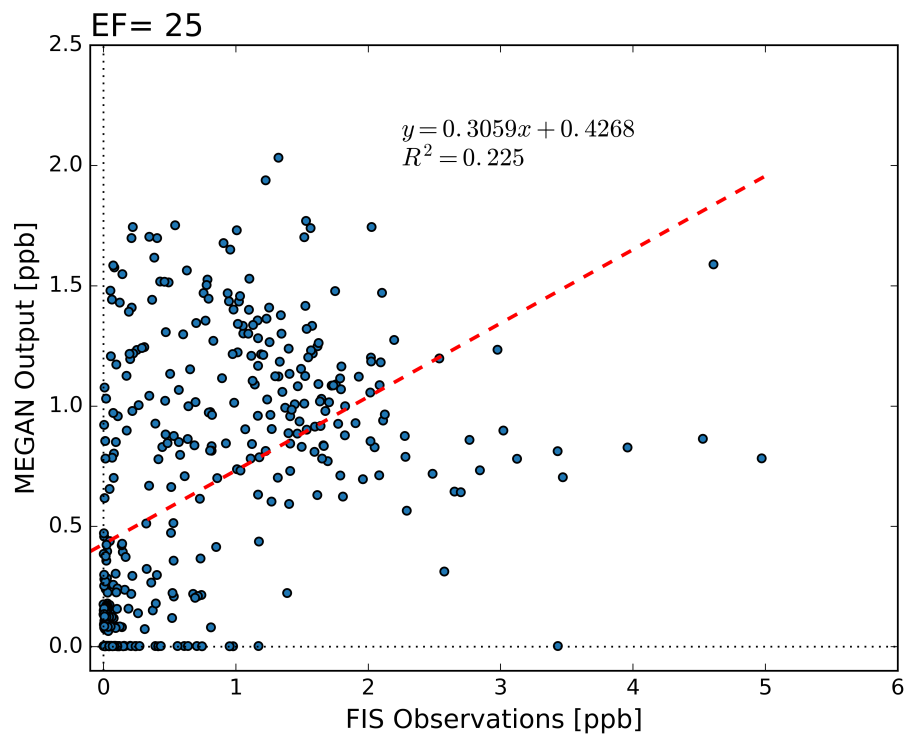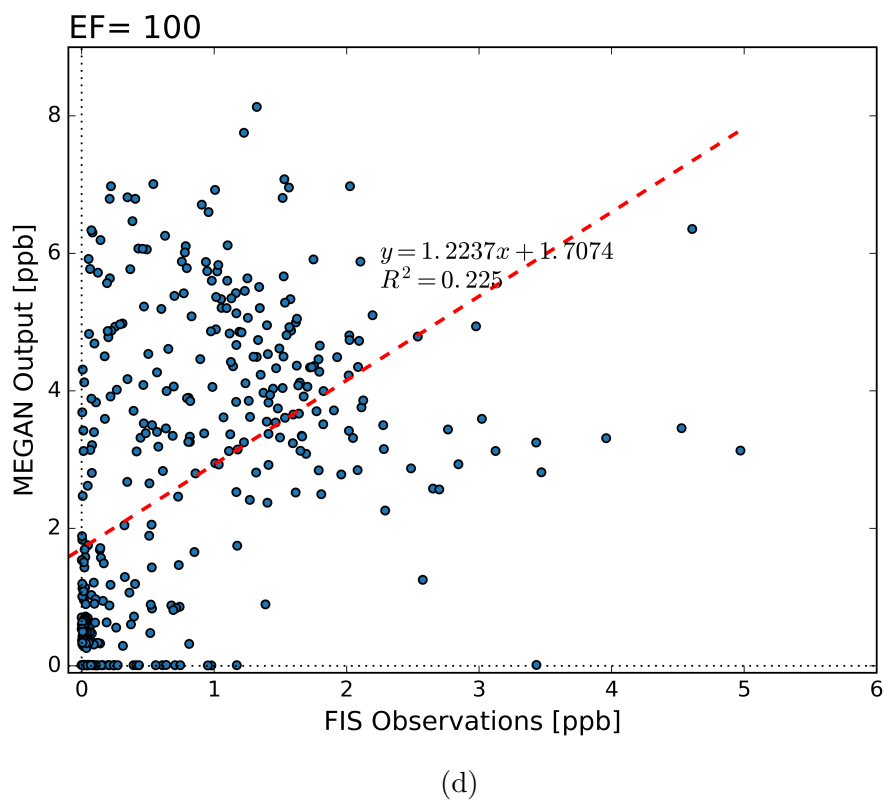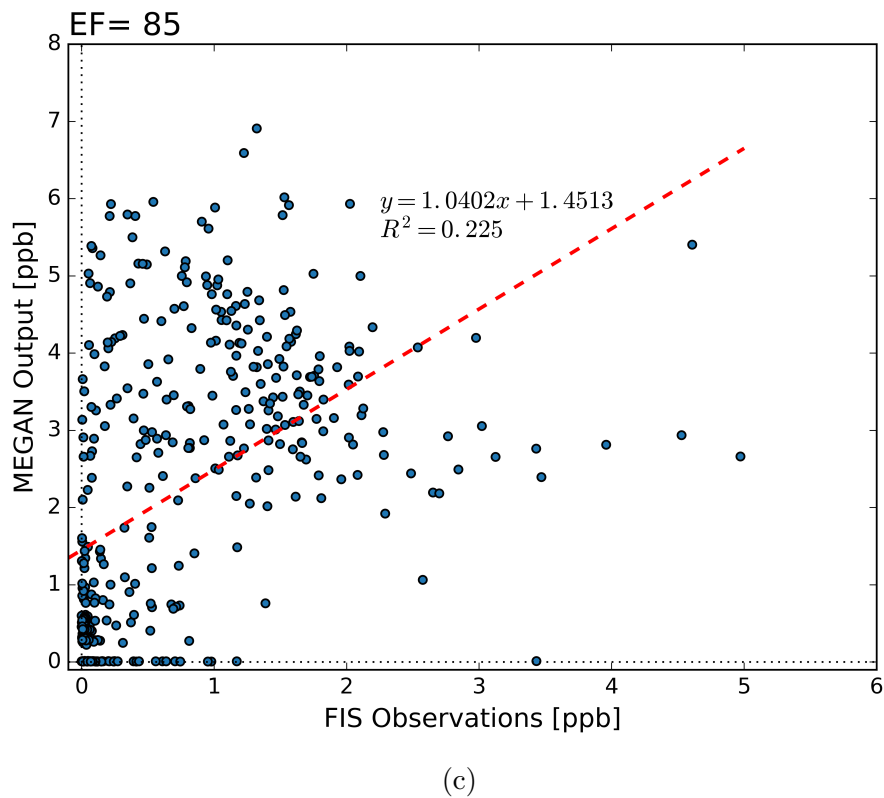
Figure 4.19: 2015 MEGAN model output for a variety of emission factors. Lines of best fit and R^2 values are shown on each plot. Points represent half-hourly averages.

The final sensitivity test was to understand the OH mechanism. This mechanism serves to simulate the loss of isoprene through reaction with OH. The challenge with modeling this reaction is that OH has a lifetime on the order of seconds, and no field measurements have been made anywhere in tropical Australia. As it is a byproduct of many photochemical reactions, the concentration of OH is assumed to follow a diurnal cycle that peaks at midday.

The effect of different OH reaction rates on isoprene concentrations is presented in Figure 4.20. Two plots are shown for each reaction rate: a short time series from Dec 2015 and a scatterplot comparing model output to FIS measurements for the entire year of 2015. The EF was set to 14 for this test and results are presented from the highest concentrations to lowest. Overall, the R^2 value increases with decreasing OH concentrations. The correlations also improve with decreasing OH, though they do not ever approach 1:1 as seen with the higher EF values. However, the intercept is closer to zero at the concentration of $2x10^6$ molec/cm^3. Another feature of the highly concentrated schemes is the presence of a double peak. Isoprene concentrations peak in the early morning and shortly before sunset, but are flattened during the daytime hours. This lessens as the concentration decreases.

Figures 4.21 and 4.22 show the resulting 2015 concentrations from each scenario. The 2015 S0 bias is -47%. Varying LAI to reflect the growing season (Figure 4.21b) shows little change in absolute value because the difference between maximum and minimum LAI is <2, However, an overall flattening of the isoprene response is observed due to peak LAI occurring in June and July, which is also the period of lowest emissions. Lowering the EF causes a substantial lowering of the final concentrations. As this worsened model bias, the EF was returned to its default value of 14 for S3. In S3, the concentration of OH was lowered until a point of best fit was achieved. This occurred at an OH concentration far below values reported in any study to date: 3×10^5 molec cm^{-3} (Vaughan et al., 2012).

(a)

(b)

(c)

(d)

(e)

(f)

(g)

(h)
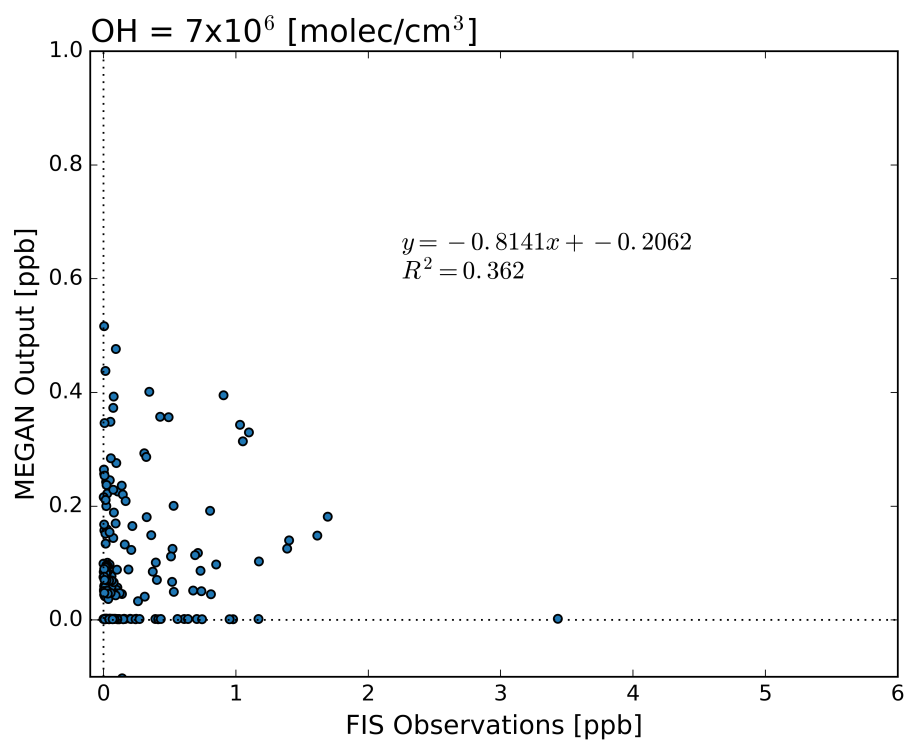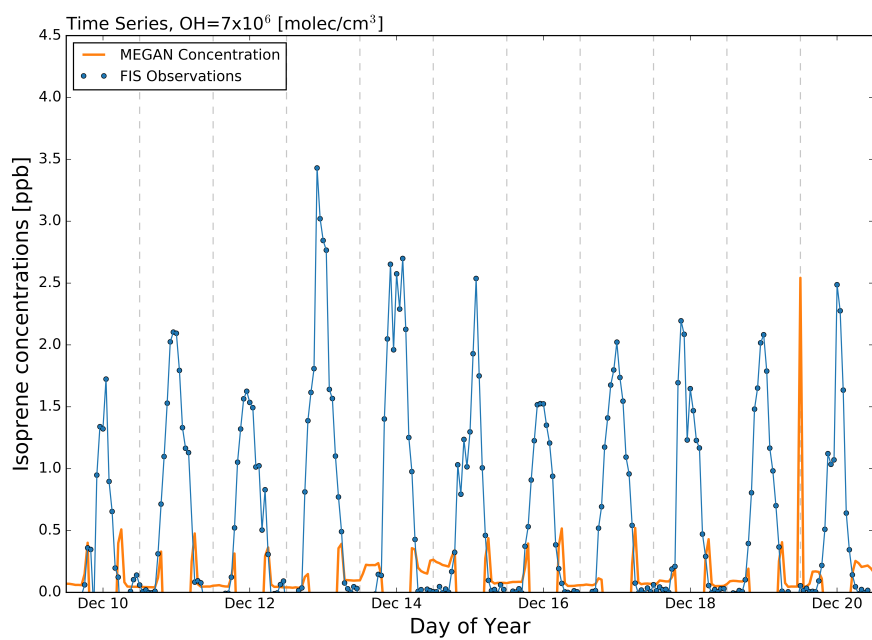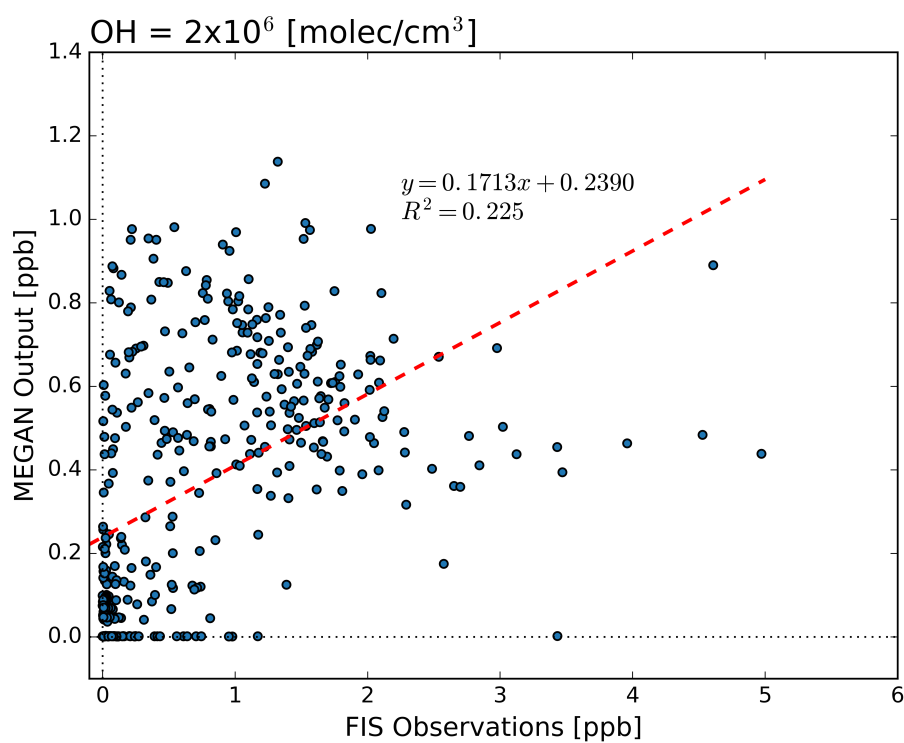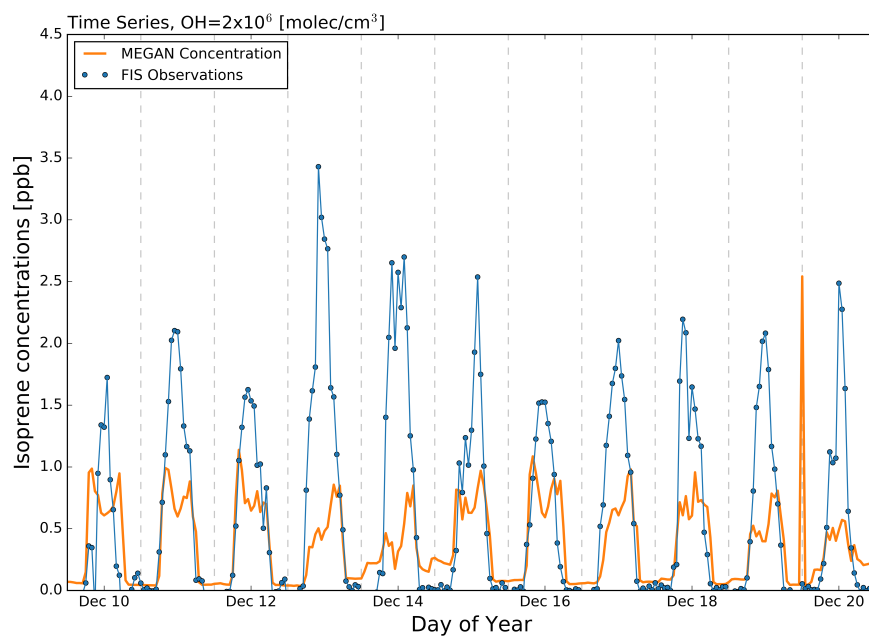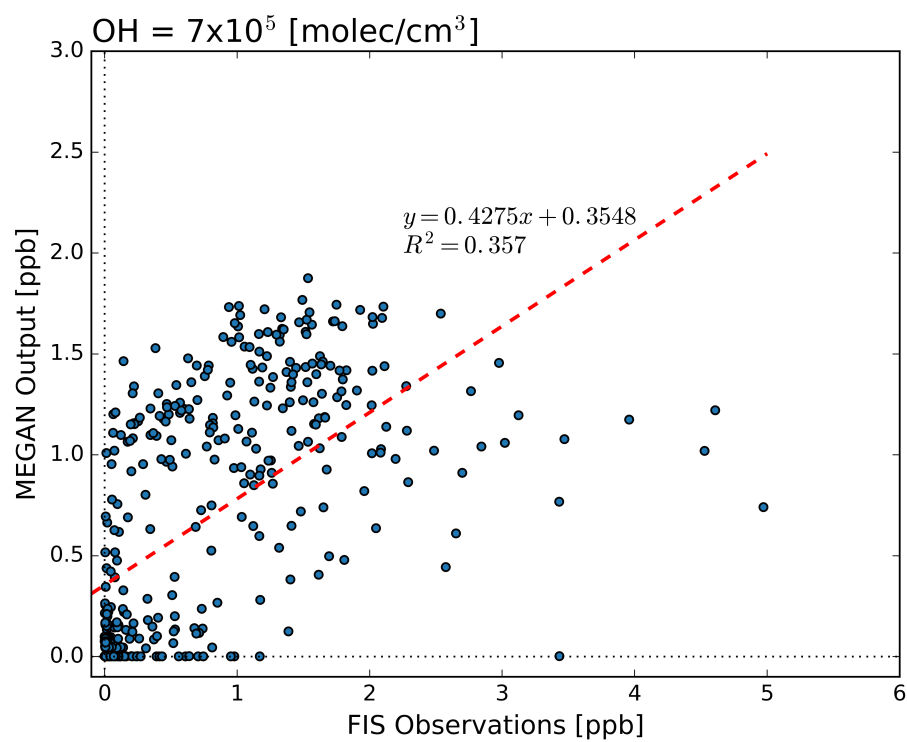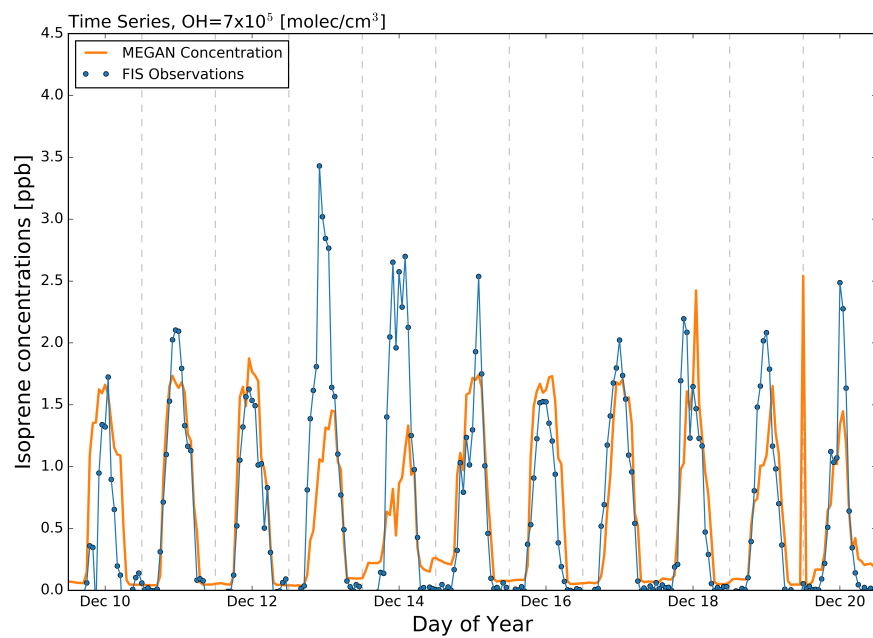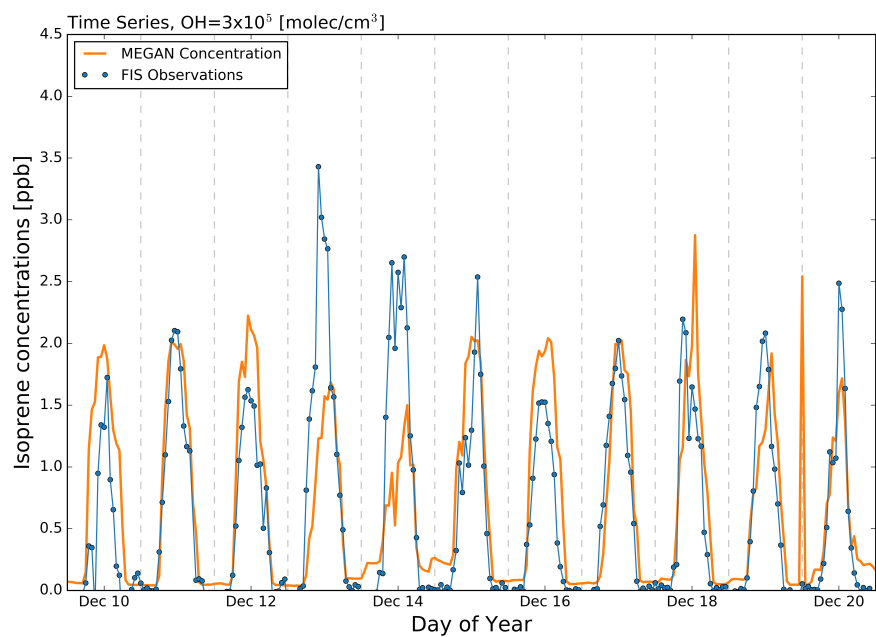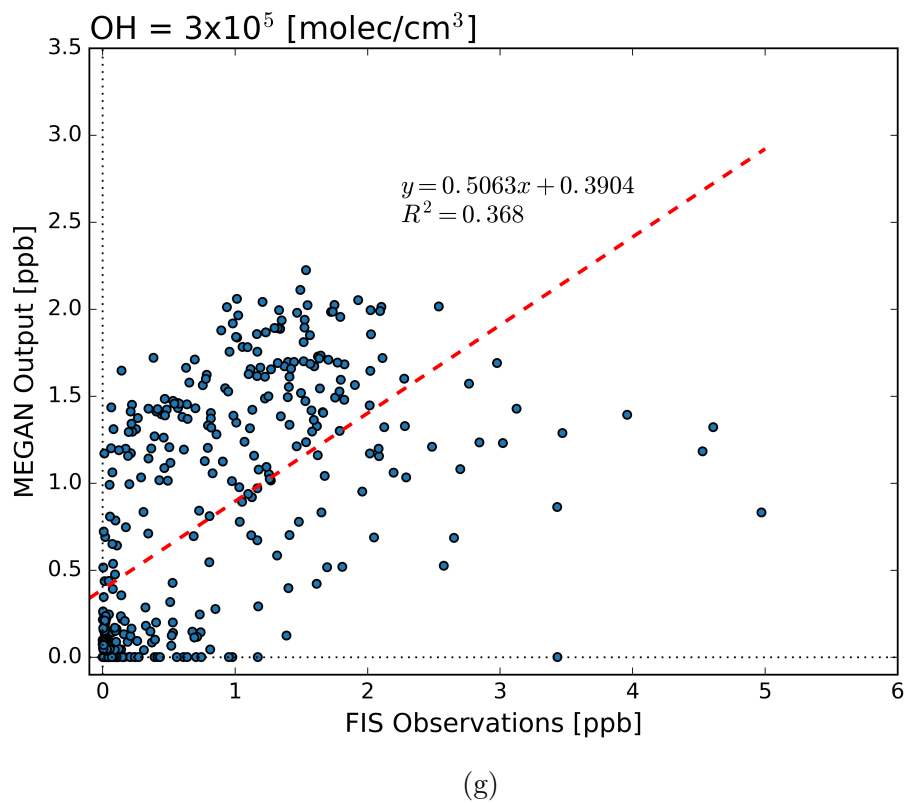
Figure 4.20: 2015 MEGAN model output across several OH emission factors. Lines of best fit and R^2 values are shown on each scatterplot. The timeseries plots show FIS output in blue and model output in orange. Model and FIS output are half-hourly averages.

At this concentration, model bias was reduced to 2%.
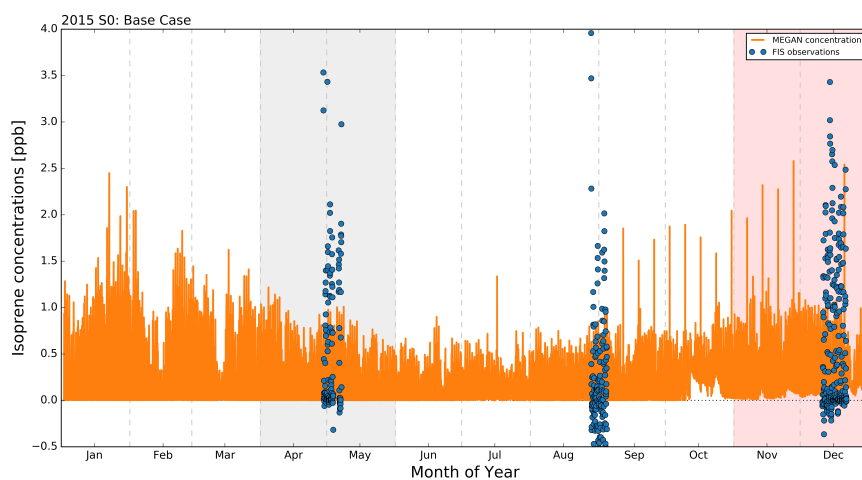
(a)
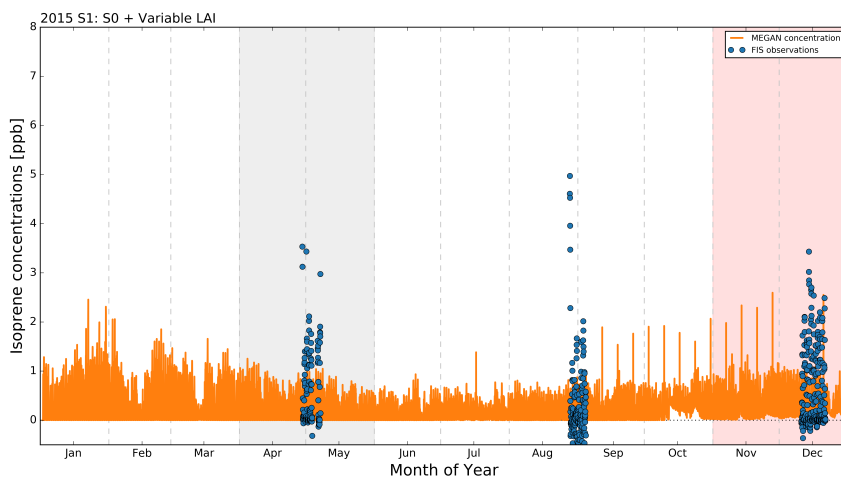
(b)

Figure 4.21: Year-long 2015 MEGAN output under S0 and S1 scenarios.

The bias for 2013 was -13% for S0, and improved to 6% in S3. However, this improvement only occurred when the EF was lowered to 10 (OH concentrations matched 2015 values). The reasons necessitating an interannual difference in EF remain unclear, but may have something to do with El Niño and the associated changes in cloudiness and rainfall patterns. Figure 4.8 plots the change in outbound solar radiation (OSR) over tropical Australia from 2013-mid 2016. It clearly shows the increased cloudiness over the tropics with the onset of El Niño.
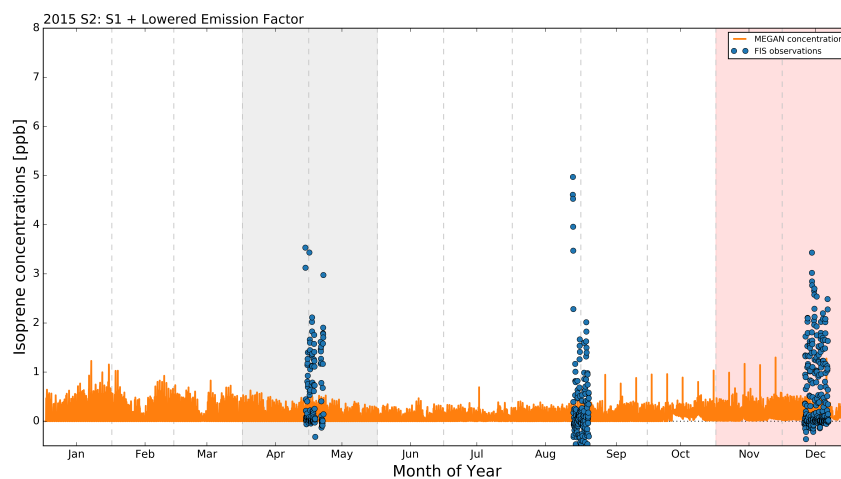
(a)
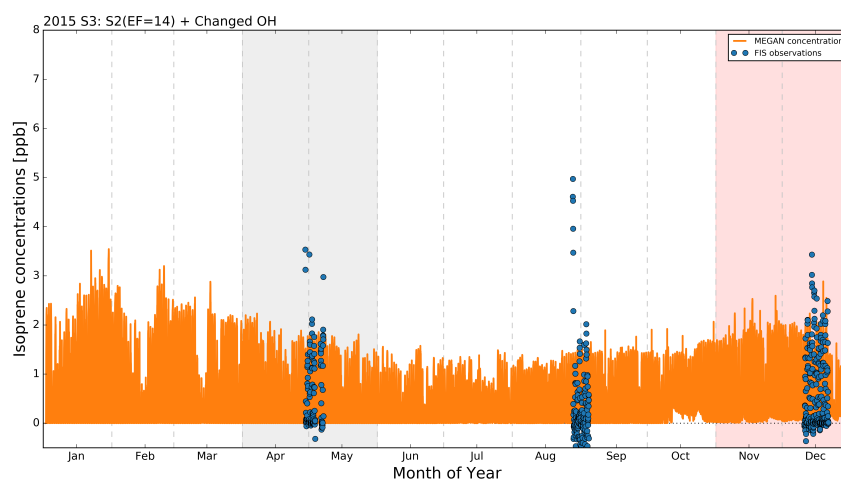
(b)

Figure 4.22: Year-long 2015 MEGAN model output under scenarios S2 and S3. Model output and FIS measurements are presented in half-hourly averages.

Langford et al. (2010) discussed the necessity of adding a diurnal factor to the EF in Borneo; but no study to date has specifically assessed interannual variability of emissions factors.

4.4   Comparison of Modelled Emissions to Space-Borne Observations of HCHO

In order to further evaluate model performance, emissions of both models were compared against the European Space Agency's Global Ozone Monitoring Experiment-2B (GOME-2B) satellite (De Smedt et al., 2008, 2012, 2015). The satellite passes overhead and retrieves formaldehyde (HCHO) column data at approximately 9:30 am local time every three days on average. These observations were compared to both MLC-CHEM and MEGAN calculations of vertical column density (VCD). MLC-CHEM provides HCHO VCDs as part of its output, so a direct comparison was made. Isoprene concentrations calculated from MEGAN were converted to VCDs using the equation described in Chapter 3 (Eq. 2.3). Satellite observations were averaged over a 2x2.5°area, and the supplemental input from GEOS-CHEM used in the models was spatially fitted to the same window.

4.4.1   Comparison Between MLC-CHEM and Satellite VCD

Figures 4.23 and 4.24 show analyses of MLC-CHEM HCHO VCD estimates compared to satellite observations across the entire measurement period. Though the model generated a VCD for every time step, only those from the 9:30 am time period are presented here in order to coincide with the estimated satellite overpass. The settings from S0 were used for this analysis as they provided the best overall fit to FIS observations.

A time series analysis is presented in Figure 4.23. The VCD columns cal-

culated by MLC-CHEM largely follow the concentrations presented in Section 4.2.1: annual maxima occur in the wet and DtW transition seasons, with annual minima in the dry season. In 2013 these VCD are overestimated and there is better fit between observations and model estimates in 2015. However, the model underestimates the VCD in the dry season in both years. Given that applying a variable LAI led to a strong inversion of the concentration pattern with annual maximum concentrations in the dry season, it is unlikely that its application would lead to a closer agreement between the model and observations during the dry season here.

A scatterplot showing the direct relationship between MLC-CHEM VCD calculations and satellite observations is shown in Figure 4.24. All three observation years show a bias in the lower portion of the plots, indicating the model underestimation during the dry season. This gives the plot a non-linear shape, though there is still a positive correlation between the two. However, that correlation is somewhat unbalanced, with a plot slope approaching 2 in 2013. The slope in 2015 is closer to 1, with the closest agreement between MLC-CHEM output and satellite observations occurring then.

4.4.2 Comparison Between MEGAN and Satellite VCD

Figures 4.25 and 4.27 show analyses of the estimated HCHO VCD as calculated by the MEGAN model against the GOME 2 satellite observations. Only the VCD from the 9:30 am (local) time period was used in these analyses. The settings from S2 were used since these settings provided the closest fit to observations and smallest overall model bias. An EF of 10 was used for the 2013 calculation, and in 2014 and 2015 the EF $= 7$. In the MEGAN model, the surface to column conversion is calculated as:
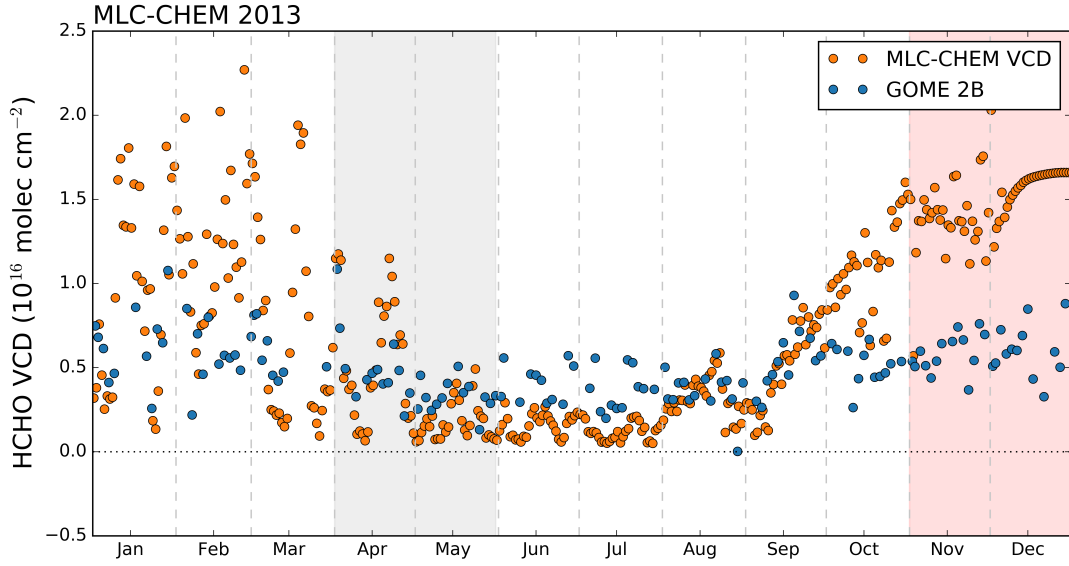
(a)
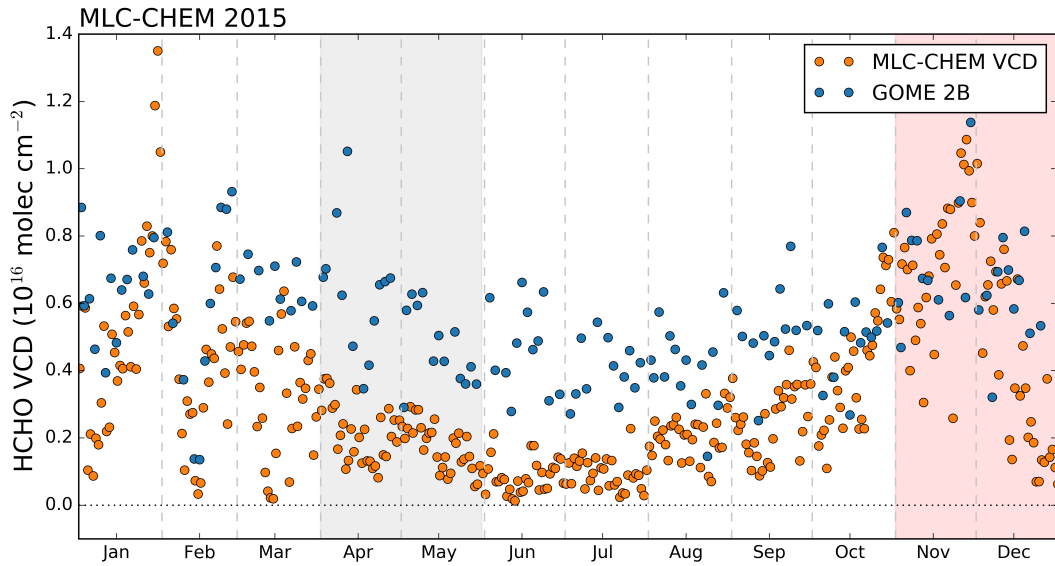
(b)

Figure 4.23: Time series of MLC-CHEM HCHO VCD compared to GOME-2B observations across the entire observation period. GOME-2B data is a daily observation from ∼9:30 LST, MLC-CHEM is presented as the half-hourly average of 9:00-9:30.

$$VCD = IsopMass_t(-\rho_{sfc}z_{scale}(exp(-\frac{z_{max}}{z_{scale}}) - exp(-\frac{z_{min}}{z_{scale}})),\qquad (4.10)$$
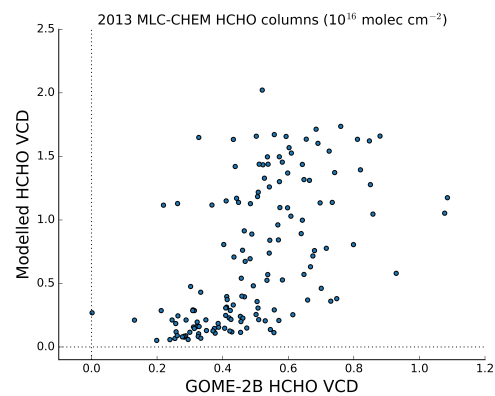
(a)
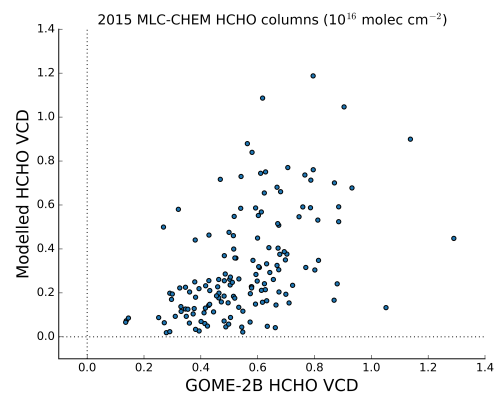
(b)

Figure 4.24: Comparison of MLC-CHEM HCHO VCD and GOME-2B observations. GOME-2B data is a daily observation from ∼9:30 LST, MLC-CHEM is presented as the half-hourly average of 9:00-9:30.

where $IsopMass_{(}t)$ is the mass of isoprene at time t, ρ_{sfc} is the density of air (2.463 x 10^{19} molec m^{-3}), z_{max} represents the upper boundary (10 x 10^5 m), and z_{scale} is the height of the troposphere (1.5 x 10^5), and z_{min} is the surface.

The time-series plots comparing MEGAN model HCHO estimates to GOME-2B observations is shown in Fig. 4.25. The 2013 plot shows a very close agreement between the model HCHO VCD estimates and the observations, though there is a slight underestimation of the model. Though it can only be compared in a general sense, as there is only one value reported per day, in any given season, the maximum modelled VCD overlaps with the minima of the observed VCD. This difference is $\sim$20-40% across all seasons. The years 2014 and 2015 show stronger model underestimations. The 2015 time series shows satellite observations and MEGAN VCD estimates tracking throughout the year, but the model consistently underestimates observations by $\sim$ 50%.

To further investigate this underestimation of MEGAN VCDs in 2015, an additional test of model performance was conducted. The annual EF was returned to its default value of 14, and estimated VCDs calculated from the updated emissions. The updated VCDs, shown in Figure 4.26, show a much closer agreement between GOME-2B observations and calculated VCD for the same time period. These findings show that, though the annual bias decreased from 18% to 2% when an EF = 7 was used, a higher EF is more appropriate for this time period throughout the year. Langford et al. (2010) indicated that an EF under circadian control improves agreement between observations and models in Borneo, and allows for greater specificity between plant functional types (Hewitt et al., 2011).

Figure 4.27 shows the correlation between GOME-2B satellite observations and MEGAN calculated VCD for the observation period. Unlike MLC-CHEM, the MEGAN results are closer to an x=y linear shape and lack the distinct dry season bias observed in the other model. However, the slopes are all <1, indicating
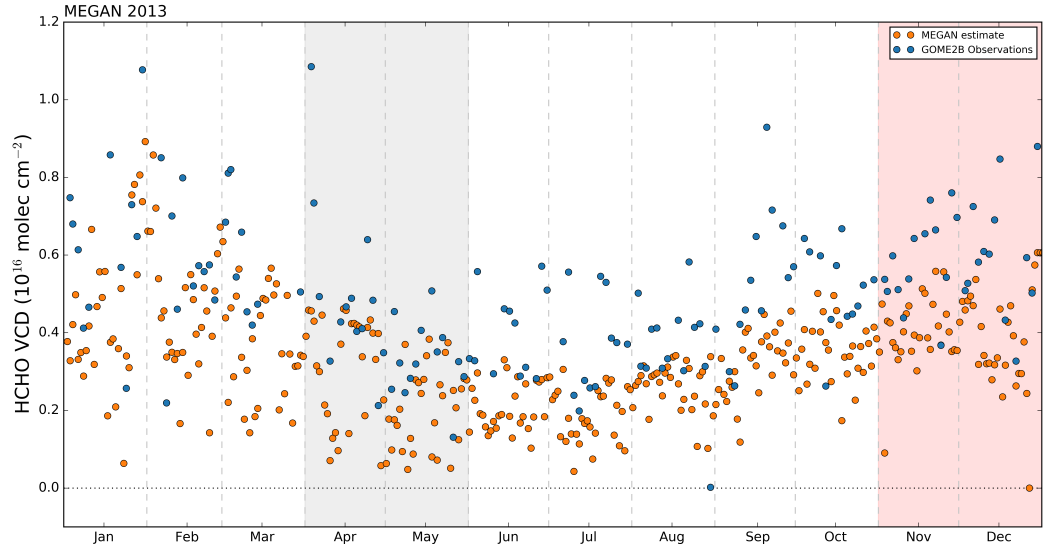
(a)
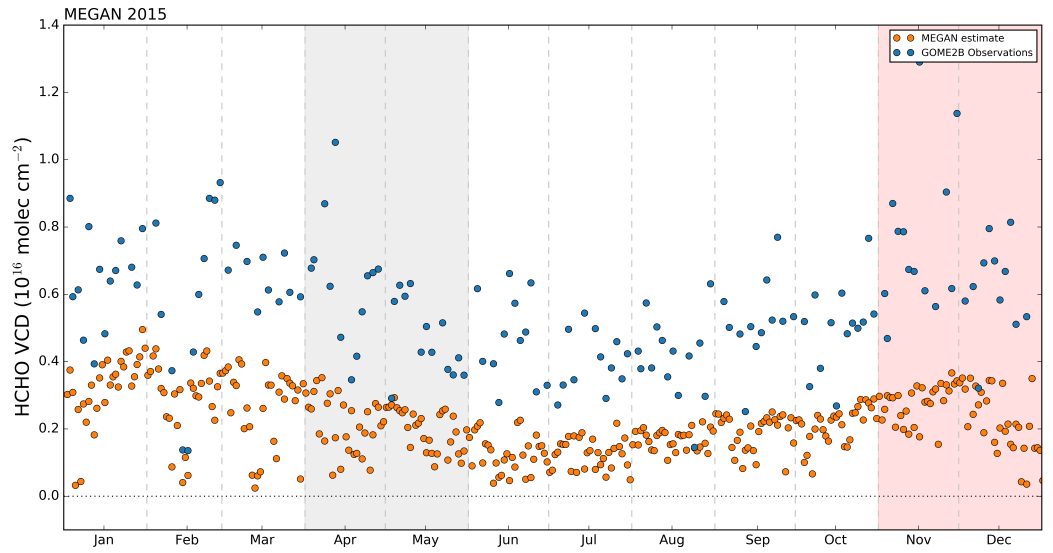
(b)

Figure 4.25: Time series of MEGAN HCHO VCDs compared to GOME-2B observations across the entire observation period. GOME-2B data is a daily observation from ∼9:30 LST, MEGAN is presented as the half-hourly average of 9:00-9:30.

the general under-estimation of MEGAN VCD values. The correction of this is observable in Figure 4.28, which shows the comparison for the year 2015 when the EF is raised to 14. Here, the slope approaches 0.5 and a clear linear shape
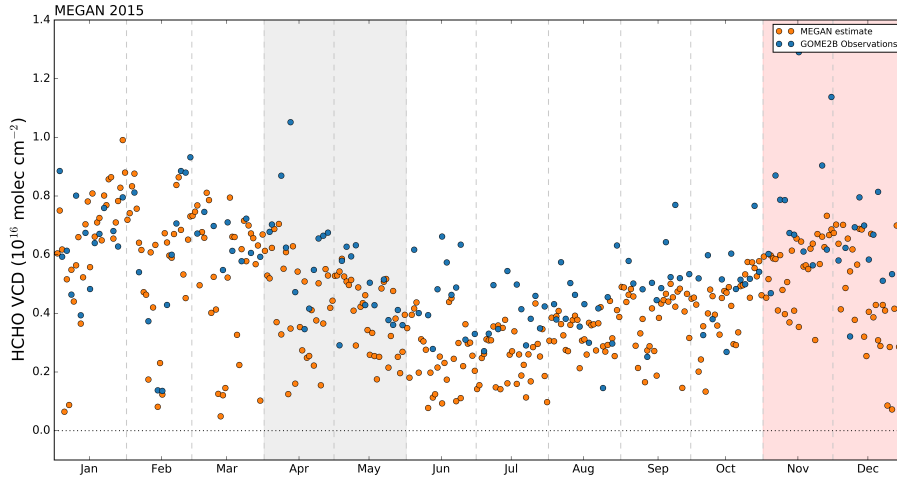
Figure 4.26: Time series of MEGAN HCHO VCD, calculated with an EF =14, compared to GOME-2B observations in 2015.GOME-2B data is a daily observation from ~9:30 LST, MEGAN is presented as the half-hourly average of 9:00-9:30.
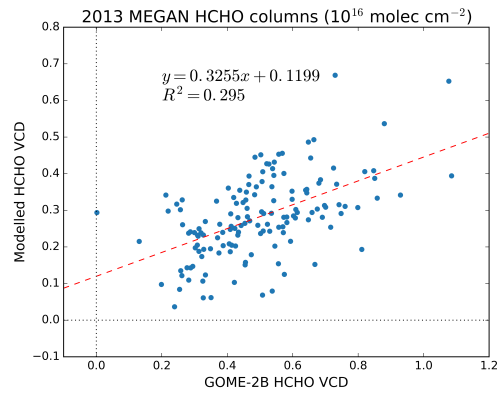
(a)
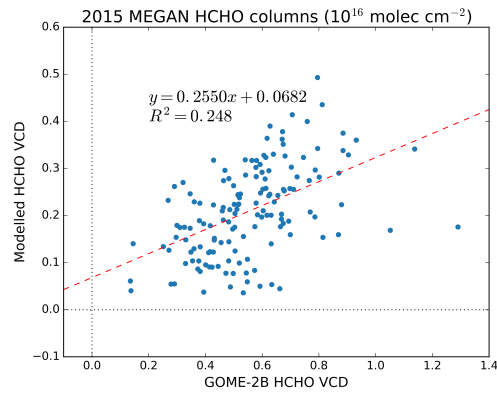
(b)

Figure 4.27: Comparison of MEGAN HCHO VCDs and GOME-2B observations.
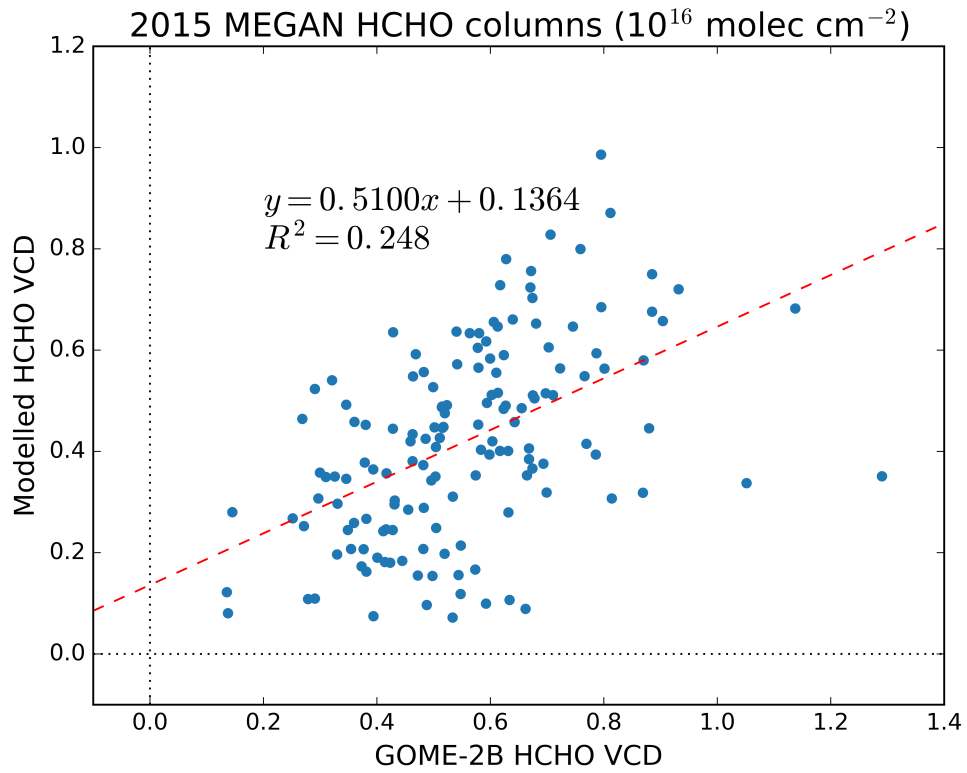
Figure 4.28: Comparison of MEGAN HCHO VCD, calculated with an EF=14, and GOME-2B observations. GOME-2B data is a daily observation from ~9:30 LST, MEGAN is presented as the half-hourly average of 9:00-9:30.

can be observed.

4.5   Summary of Key Results

The aim of this chapter was to compare measured isoprene concentrations with modelled outputs across several timescales to evaluate model performance and investigate drivers of isoprene emission. Both MLC-CHEM and MEGAN were described in Section 4.1. This description included a discussion of the emissions equations used in each model, sources of meteorological and supplemental data used as model input. Section 4.2 presented an extensive analysis of MLC-CHEM and MEGAN model performance under the base case scenario. First, an annual overview of both models is presented. Then each season is considered, focusing on a 10-day period for each model followed by a discussion of emission trends over the season. Both models tend to overpredict isoprene concentrations on days when the direct PAR is very high, and underpredict on overcast days when direct PAR is low. The models also showed a spike in concentrations in the morning during the WtD season (MLC-CHEM) and at the end of the dry season (MEGAN). They are attributed to changes in the solar declination angle with the change in seasons and the way boundary layer heights are calculated. This could be solved with further model calibration, though that was not the purpose of this research.

Following the description and base case analysis, sections 4.3.2 and 4.3.3 showed the results of model sensitivity analyses. In these analyses, FIS observations were compared against the base case scenario (S0) on an annual basis to show the relative influences of PAR and temperature. Then, the LAI was halved and doubled to show its relative importance in calculating emissions. Finally, the role of O_3 and NO_x in calculating isoprene concentrations in MLC-CHEM was investigated. It was determined that O_3 and NO_x had no effect on concentrations, thus allowing the use of constant values for these compounds in the 2015 input

files.

Following the initial tests, both models are tested under a variety of scenarios and the impact on model bias are discussed. Altering the LAI improves performance in the MEGAN model, but significantly changes the shape of the annual emissions in MLC-CHEM–annual maxima occur in the dry season and minima in the wet, which is the opposite of what was observed with the FIS. Changing the emission factor has no effect on MLC-CHEM, but further improves MEGAN agreement with observations in 2015. Finally, MEGAN performance is optimised when the amount of the OH radical available for removing isoprene is lowered. These changes improve bias in both models by $>10\%$.

Finally, Section 4.4 compares model output to GOME-2B satellite HCHO VCDs. The best-performing scenarios from the previous section were used to calculate model VCD estimates. MLC-CHEM calculates HCHO VCDs as part of its output, and the equation used to convert concentrations to HCHO VCDs in MEGAN is described. These VCDs were time-matched to satellite pass times. It is found that in MEGAN, the emission factors that yielded the lowest bias across all observation times differs from the factors that yield the best fit when the satellite passes over the site.

Chapter 5

Conclusions and Future Research Opportunities

The purpose of this thesis has been to provide a first look into seasonal isoprene concentration patterns in a pristine tropical rainforest environment and to compare those measurements to a modelled environment to further understanding of seasonal drivers. The main conclusions of my investigation are:

- The Fast Isoprene Sensor can be modified for long-term deployment in remote locations.

- Isoprene concentrations in tropical Australia follow a seasonal pattern, which is unique to that reported in other tropical forests. Where annual minima in the Amazon occur in the WtD season, the findings from this research indicate that the annual minima in the Daintree occurs in the dry season.

- The results of the model sensitivity testing indicate that in MEGAN, model-observation bias improves by more than 10% when LAI is varied to reflect the growing season and emission factors can be tailored to accommodate interannual variations. MLC-CHEM did not see the same improvements,

and further work is needed on this model in order to accurately describe the relationship between growing season and isoprene concentrations.

These findings and the establishment of this site for isoprene and other BVOC measurements provide a rich opportunity for further research. Though isoprene is a well-studied compound, several significant lines of questioning remain, particularly with regard to large-scale climate changes and subsequent foliar response.

5.1   Conclusions

Prior to this study, the FIS had never been deployed for remote, long-term operation in a tropical rainforest. This necessitated several hardware modifications which have since been implemented into newer instruments or are otherwise available as an option. First, the 4-channel timer (Omron H5S) that was used to control ozonizer power has been implemented into the main FIS unit. Second, the ozonizer that is available with the FIS unit is now modified to run on either 1 or 2 channels, to conserve oxygen. Third, a safety switch has been implemented that will shut the FIS off in the event of oxygen tanks losing pressure.

In addition to the hardware alterations, I needed to adapt the FIS calibration approach in order to account for changes in ozonizer performance in an un-air conditioned space. A comparison of this adaptation and the calibration method recommended by the manufacturer yielded a correlation of 1:1.02. My adaptation was further corroborated with samples collected using solid sorbent cartridges following USEPA method TO-17, which yielded two important results. First, I demonstrated that the FIS and solid sorbent cartridge correlations had a correlation of 1:1.15 in both daytime and early evening sampling. Second, I found that isoprene concentrations are at or near zero at night at the DRO.

In tropical latitudes, where temperatures are consistently warm with little

change to hours of daylight between summer and winter, there is an almost continuous growing season and seasonal isoprene emissions follow wet and dry seasons. In Chapter 3, I determined that isoprene concentrations in the Daintree also follow a seasonal cycle. Annual observed daytime maximum concentrations were highest (mean = 2 ppb) in the DtW season months (Nov-Dec) and lowest (mean= 1 ppb) minima in the dry season (Jun-Aug). This seasonality differs from both the Amazon and Borneo; Amazonian annual minima occurs in the WtD transition season, and there is little observable seasonality in Borneo (Langford et al., 2010; Palmer et al., 2007; Yañez Serrano et al., 2014). In addition to the timing of maxima and minima, the absolute value of concentrations differs as well. In the Amazon, there is a factor of 2–5 difference in daytime maximum concentrations between the wet and dry seasons, and no such difference in Borneo (Langford et al., 2010; Stavrakou et al., 2014). Collectively, these results indicate that further study is warranted to explicitly clarify the reasons behind the differences in emission profiles from tropical forests across the globe.

Understanding the differences in isoprene concentration patterns in tropical latitudes is essential to resolving model overpredictions in the tropics. Several studies have reported a 20% bias when using MEGAN in tropical ecosystems (Barkley et al., 2008; Marais et al., 2014; Stavrakou et al., 2014); and this study is the first to utilise MLC-CHEM for time scales >1 month. With the changes implemented in this study, I decrease that overprediction by more than 10%, and in some years, the annual model bias is reduced to single-digit percentages. However, I found that using MEGAN, model bias was minimised when different EFs were implemented for each year of data due to interannual variability. Further research is warranted to understand long-term climatic drivers such as El Niño and the Pacific Decadal Oscillation (PDO) affect isoprene emission rates on annual or multi-year scales.

Satellite data represents an important alternative method to quantify global

isoprene emissions, particularly in locations inaccessible for collecting surface measurements. In Chapters 3 and 4 I show that, when inversely modelled, GOME-2B satellite formaldehyde vertical column densities (HCHO VCD) provides a good fit with both observations and modelled output. However, I also found that when using MEGAN, the emission factors that yielded the best fit with the data across all observation times differs from the factors that yielded the best fit when the satellite passes over the site. This finding could be explored further by expanding the satellite component of this study to include a comparison of the DRO concentrations to observations from NASA's Ozone Monitoring Instrument (OMI) satellite, which has a flyover time of $\sim 13{:}00$ LST.

5.2 Areas for Future Research

Climate change has the potential to substantially alter the rates of BVOC emissions, which would in turn affect cloud cover, rainfall, and air quality patterns across the globe. Isoprene emissions are dependent upon the conditions under which a plant was grown, and regional changes in temperature, rainfall patterns, and CO_2 concentrations will affect the emission capacities of adult plants. Lab studies have shown that as CO_2 concentrations in air rises, isoprene emissions can decrease due to a decrease in dimethylallyl diphosphate, the substrate that serves as the basis for isoprene synthesis (Rosenstiel et al., 2003; Scholefield et al., 2004). In addition, isoprene serves as a precursor to SOA (Chung, 2002; Kroll et al., 2006). It is estimated that SOA formation from isoprene in the Amazon could contribute up to 1.6 Tg/year, up to 20% of the biogenic contribution to the global aerosol load (Lim et al., 2005). The SOA originating from isoprene oxidations products is hygroscopic in nature, and can serve as cloud condensation nuclei (CNN). This is important for global climate change as numbers of CCN can affect cloud formation and rainfall patterns. Since 70% of the global emis-

sions budget of isoprene originates in tropical latitudes, it is vital to continue to increase the understanding of isoprene emissions at all spatio-temporal scales in these regions, and applying that knowledge to global emissions models.

This research investigated isoprene concentrations on a canopy scale. Since it was the first study of its kind in the region, there are many ways to build on this research. For instance, though this work focused on isoprene concentrations, monoterpenes were observed on the solid sorbent cartridge samples collected in March 2018. Though the results were not reported here, I plan to include them in a future publication.

A second avenue of investigation for this research would be to further investigate nighttime concentrations at the DRO. Though several studies have reported variable isoprene concentrations overnight, the findings from the cartridge data show that the concentration at the DRO is at or near zero after dark. This finding deserves a more in-depth analysis to understand the paths of air parcels through the Daintree's complex topography in the afternoon and evening hours. An investigation of the back-trajectories of the air parcels with a Lagrangian model such as HYSPLIT would be ideal and could be enhanced by expanding the data set to include other seasons and collecting data throughout the night.

At a plant level, the Daintree Rainforest is home to nine of the 19 remaining primitive plant species on Earth, and there is a rich opportunity here to enhance understanding of the mechanism by which isoprene emission evolved in plants (Stork and Turton, 2008). The emissions patterns of trees and shrubs in the region is almost entirely unknown. Targeted species-specific, plant-level isoprene studies would fill a substantial data gap as well as provide insight into the evolution of isoprene emission as a trait. In addition, plant-level studies could perhaps provide clues to the function isoprene emission plays in plant health.

Beyond the Daintree Rainforest, the Wet Tropics of North Queensland would benefit from additional canopy-level BVOC studies. Coastal environments have

recently been identified as one of the last major ecosystems where isoprene emission patterns are poorly understood (Exton et al., 2014). Marine influences were an area of uncertainty for this research, as the crane tower is 1.5 km from the coast. However, the DRO's proximity to the ocean and the Great Barrier Reef makes it an ideal location to concurrently study coastal emissions and marine-land interactions. Many of the trees and shrubs in the region are endemic, sometimes found only in an area of a few square kilometers (Stork and Turton, 2008). These two elements could be responsible for substantial variation in emission patterns through the Wet Tropics region.

One of the outstanding challenges that spring from this research is understanding what role El Niño contributed to interannual variability observed in the measurements. It is currently unknown if ENSO, Pacific Decadal Oscillation (PDO), and Atlantic Equatorial Mode cycles affect global or regional BVOC emissions, and if so, what is the duration and long-term impact of these changes. Several studies quantify long-term isoprene emission patterns in the tropics on a regional scale, but intercontinental differences have not been addressed (Barkley et al., 2009, 2008; Geron et al., 2006; Marais et al., 2014; Stavrakou et al., 2014). Previous research has quantified interannual trends in HCHO column magnitudes that are attributable to anthropogenic influences, primarily over Asia and selected urban centers (De Smedt et al., 2015). Trending behavior was also observed over the Amazon, though this was related to land-use change (De Smedt et al., 2015).

A natural next step would be to build upon these research findings in tropical Australia by investigating the relationship between tropical isoprene emissions variability across multiple continents and long-term climatological patterns. This unquantified relationship could improve our understanding of and improve model performance in the tropics. This question could be addressed by taking advantage of satellite, aircraft, and meteorological data, as well as the availability of continuous observations from multiple platforms. While it would be a substantial

logistical challenge to concurrently collect in situ tropical BVOC emissions on a long-term scale in South America, Australasia, and Africa, this research would be possible with the utilisation of remote sensing tools and the integration of aircraft and ground-based measurements. I expect that these results could lead to improvements in emissions models and model drivers by creating parameterizations that are more nuanced and responsive to factors contributing to BVOC emissions in tropical latitudes.

Bibliography

U.S. Environmental Protection Agency. Method TO-17, 1999.

E. C. Apel, D. D. Riemer, A. Hills, W. Baugh, J. Orlando, I. Faloona, D. Tan, W. Brune, B. Lamb, H. Westberg, M. A. Carroll, T. Thornberry, and C. D. Geron. Measurement and interpretation of isoprene fluxes and isoprene, methacrolein, and methyl vinyl ketone mixing ratios at the PROPHET site during the 1998 Intensive. *Journal of Geophysical Research*, 107(D3), 2002. doi: 10.1029/2000jd000225.

R. Atkinson. Kinetics of the gas-phase reactions of oh radicals with alkanes and cycloalkanes. *Atmospheric Chemistry and Physics*, 3:2233–2307, 2003.

G.P. Ayers and R.W. Gillett. Isoprene emissions from vegetation and hydrocarbon emissions from bushfires in tropical Australia. *Journal of Atmospheric Chemistry*, 7:177–190, 1988.

B. Baker, J. Bai, C. Johnson, Z. Cai, Q. Li, Y. Wang, A. Guenther, J. Greenberg, L. Klinger, and C. Geron. Wet and dry season ecosystem level fluxes of isoprene and monoterpenes from a Southeast Asian secondary forest and rubber tree plantation. *Atmospheric Environment*, 39(2):381–390, 2005. doi: 10.1016/j. atmosenv.2004.07.033.

D. J. Barket, J. M. Hurst, T. L. Couch, A. Colorado, P. B. Shepson, D. D. Riemer, A. J. Hills, E. C. Apel, R. Hafer, B. K. Lamb, H. H. Westberg, C. T. Farmer, E. R. Stabenau, and R. G. Zika. Intercomparison of automated

methodologies for determination of ambient isoprene during the PROPHET 1998 summer campaign. *Journal of Geophysical Research-Atmospheres*, 106 (D20):24301–24313, 2001. doi: 10.1029/2000jd900562.

D. J. Barket, J.W. Grossenbacher, J.M. Hurst, P.B. Shepson, K. Olszyna, T. Thornberry, M.A. Carroll, J. Roberts, C. Stroud, J. Bottenheim, and T. Biesenthal. A study of the NOx dependence of isoprene oxidation. *Journal of Geophysical Research*, 109(D11):12, 2004.

M. P. Barkley, P. I. Palmer, I. De Smedt, T. Karl, A. Guenther, and M. Van Roozendael. Regulated large-scale annual shutdown of Amazonian isoprene emissions? *Geophysical Research Letters*, 36(4), 2009. doi: 10.1029/2008gl036843.

M. P. Barkley, T.P. Kurosu, K. Chance, I. De Smedt, M. Van Roozendael, A. Arneth, D. Hagberg, and A. Guenther. Assessing sources of uncertainty in formaldehyde air mass factors over tropical South America: Implications for top-down isoprene emission estimates. *Journal of Geophysical Research*, 117 (D13), 2012. doi: 10.1029/2011jd016827.

M.P. Barkley, P.I. Palmer, U. Kuhn, J. Kesselmeier, K. Chance, T.P. Kurosu, R.V. Martin, D. Helmig, and A. Guenther. Net ecosystem fluxes of isoprene over tropical South America inferred from Global Ozone Monitoring Experiment (GOME) observations of HCHO columns. *Journal of Geophysical Research*, 113(D20), 2008. doi: 10.1029/2008jd009863.

M. L. Bell, F. Dominici, and J.M. Samet. A meta-analysis of time-series studies of ozone and mortality with comparison to the national morbidity, mortality, and air pollution study. *Epidemiology*, 16(4):436–445, 2005.

M.L. Bell, A. McDermott, S.L. Zeger, J.M. Samet, and F. Dominici. Ozone and

short-term mortality in 95 US urban communities, 1987-2000. *Journal of the American Medical Association*, 292(19):2372–2378, 2004.

P. J. Bellingham. Cyclone effects on Australian rain forests: An overview. *Austral Ecology*, 33(4):580–584, 2008. ISSN 1442-9985.

I. Bey, D.J. Jacob, R.M. Yantosca, J. A. Logan, B. D. Field, A. M. Fiore, Q. Li, H. Y. Liu, L. J. Mickley, and M. G. Schultz. Global modeling of tropospheric chemistry with assimilated meteorology: Model description and evaluation. *Journal of Geophysical Research*, 106(D19):22073–23095, 2001.

F. Booker, R. Muntifering, M. McGrath, K. Burkey, D. Decoteau, E. Fiscus, W. Manning, S. Krupa, A. Chappelka, and D. Grantz. The ozone component of global change: Potential effects on agricultural and horticultural plant yield, product quality and interactions with invasive species. *Journal of Integrative Plant Biology*, 51(4):337–351, 2009. doi: 10.1111/j.1744-7909.2008.00805.x.

E. J. Bucsela, N. A. Krotkov, E. A. Celarier, L. N. Lamsal, W. H. Swartz, P. K. Bhartia, K. F. Boersma, J. P. Veefkind, J. F. Gleason, and K. E. Pickering. A new stratospheric and tropospheric no_2 retrieval algorithm for nadir-viewing satellite instruments: Applications to OMI. *Atmospheric Measurement Techniques*, 6(10):2607–2626, 2013. ISSN 1867-8548. doi: 10.5194/amt-6-2607-2013.

Australian Bureau of Meteorology. Record-breaking La Nina events. Report, 2012. URL `http://www.bom.gov.au/climate/enso/history/La-Nina-2010-12.pdf`.

S. Caldararu, P. I. Palmer, and D. W. Purves. Inferring Amazon leaf demography from satellite observations of leaf area index. *Biogeosciences*, 9(4):1389–1404, 2012. doi: 10.5194/bg-9-1389-2012.

J. Callies, E. Corpaccioli, M. Eisinger, and A. Lefebvre. GOME-2 MetOp's

second-generation sensor for operational ozone monitoriing. *ESA Bulletin*, 102: 28–36, 2000.

A. G. Carlton, C. Wiedinmyer, and Kroll J.H. A review of secondary organic aerosol (SOA) formation from isoprene. *Atmospheric Chemistry and Physics*, 9:4987–5005, 2009.

W.L. Chameides, W.L. Lindsay, J. Richardson, and Kiang C.S. The role of biogenic hydrocarbons in urban photochemical smog: Atlanta as a case study. *Science*, 241:1473–1475, 1988.

W.L. Chamides and J.P. Lodge. *Tropospheric ozone: Formation and Fate*. Surface level ozone exposures and their effects on vegetation. Lewis Publishers, Inc., Chelsea, MI, USA, 1992.

Chung-How Chi, Ryan W. McEwan, Chung-Te Chang, Chengyang Zheng, Zhijie Yang, Jyh-Min Chiang, and Teng-Chiu Lin. Typhoon disturbance mediates elevational patterns of forest structure, but not species diversity, in humid monsoon asia. *Ecosystems*, 18(8):1410–1423, 2015. doi: 10.1007/s10021-015-9908-3.

Serena H. Chung. Global distribution and climate forcing of carbonaceous aerosols. *Journal of Geophysical Research*, 107(D19), 2002. ISSN 0148-0227. doi: 10.1029/2001jd001397.

M. Claeys, B. Graham, G. Vas, W. Wang, R. Vermeylen, V. Pashynska, J. Cafmeyer, P. Guyon, M. O. Andreae, P. Artaxo, and W. Maenhaut. Formation of secondary organic aerosols through photooxidation of isoprene. *Science*, 303(5661):1173–6, 2004. ISSN 1095-9203 (Electronic) 0036-8075 (Linking). doi: 10.1126/science.1092805. URL `https://www.ncbi.nlm.nih.gov/pubmed/14976309`.

CSIRO. URL `http://keys.trin.org.au:8080/key-server/data/`

`0e0f0504-0103-430d-8004-060d07080d04/media/Html/taxon/Araucaria_`
`bidwillii.htm`.

T. J. Curran, L. N. Gersbach, W. Edwards, and A. K. Krockenberger. Wood density predicts plant damage and vegetative recovery rates caused by cyclone disturbance in tropical rainforest tree species of north Queensland, Australia. *Austral Ecology*, 33(4):442–450, 2008. doi: 10.1111/j.1442-9993.2008.01899.x.

N. Czoschke, M. Jang, and R.M. Kamens. Effect of acidic seed on biogenic secondary organic aerosol growth. *Atmospheric Environment*, 37(30):4287–4299, 2003. ISSN 13522310. doi: 10.1016/s1352-2310(03)00511-9.

Y. Dai, R. E. Dickinson, and Y-P. Wang. A two-big-leaf model for canopy temperature, photosynthesis, and stomatal conductance. *Journal of Climate*, 17:2281–2299, 2004.

V. Damian, A. Sandu, M. Damian, F. Potra, and G. R. Carmichael. The kinetic preprocessor KPP – a software environment for solving chemical kinetics. *Computers and Chemical Engineering*, 26:1567–1579, 2002.

K. G. S. Dani, I. M. Jamie, I. C. Prentice, and B. J. Atwell. Evolution of isoprene emission capacity in plants. *Trends in Plant Science*, 19(7):439–446, 2014. doi: 10.1016/j.tplants.2014.01.009.

I. De Smedt, J. F. Muller, T. Stavrakou, R. van der A, H. Eskes, and M. Van Roozendael. Twelve years of global observations of formaldehyde in the troposphere using GOME and SCIAMACHY sensors. *Atmospheric Chemistry and Physics*, 8:4947–4963, 2008.

I. De Smedt, M. Van Roozendael, T. Stavrakou, J. F. Muller, C. Lerot, N. Theys, P. Valks, N. Hao, and R. van der A. Improved retrieval of global tropospheric formaldehyde columns from GOME-2/MetOp-A addressing noise reduction

and instrumental degradation issues. *Atmospheric Measurement Techniques*, 5(11):2933–2949, 2012. doi: 10.5194/amt-5-2933-2012.

I. De Smedt, T. Stavrakou, F. Hendrick, T. Danckaert, T. Vlemmix, G. Pinardi, N. Theys, C. Lerot, C. Gielen, C. Vigouroux, C. Hermans, C. Fayt, P. Veefkind, J. F. Muller, and M. Van Roozendael. Diurnal, seasonal and long-term variations of global formaldehyde columns inferred from combined OMI and GOME-2 observations. *Atmospheric Chemistry and Physics*, 15(21):12519–12545, 2015. doi: 10.5194/acp-15-12519-2015.

R. E. Dickinson, M. Shaikh, R. Bryant, and L. Graumlich. Interactive canopies for a climate model. *Journal of Climate*, 11:2823–2836, 1998.

B. N. Duncan, A. I. Prados, L. N. Lamsal, Y. Liu, D. G. Streets, P. Gupta, E. Hilsenrath, R. A. Kahn, J. E. Nielsen, A. J. Beyersdorf, S. P. Burton, A. M. Fiore, J. Fishman, D. K. Henze, C. A. Hostetler, N. A. Krotkov, P. Lee, M. Lin, S. Pawson, G. Pfister, K. E. Pickering, R. B. Pierce, Y. Yoshida, and L. D. Ziemba. Satellite data of atmospheric pollution for U.S. air quality applications: Examples of applications, summary of data end-user resources, answers to FAQs, and common mistakes to avoid. *Atmospheric Environment*, 94:647–662, 2014. ISSN 13522310. doi: 10.1016/j.atmosenv.2014.05.061.

E. Dunne, I. E. Galbally, M. Cheng, P. Selleck, S. B. Molloy, and S. J. Lawson. Comparison of VOC measurements made by PTR-MS, adsorbent tubes–GC-FID-MS and DNPH derivatization–HPLC during the Sydney Particle Study, 2012: A contribution to the assessment of uncertainty in routine atmospheric VOC measurements. *Atmospheric Measurement Techniques*, 11(1):141–159, 2018. ISSN 1867-8548. doi: 10.5194/amt-11-141-2018.

K. M. Emmerson, I. E. Galbally, A. B. Guenther, C. Paton-Walsh, E. A. Guerette, M. E. Cope, M. D. Keywood, S. J. Lawson, S. B. Molloy, E. Dunne,

M. Thatcher, T. Karl, and S. D. Maleknia. Current estimates of biogenic emissions from Eucalypts uncertain for Southeast Australia. *Atmospheric Chemistry and Physics Discussions*, pages 1–26, 2016. doi: 10.5194/acp-2016-92.

EUMETSAT. GOME-2 factsheet. Darmstadt, Germany, 2015. URL `http://www.eumetsat.int`.

D. A. Exton, D. J. Smith, T. J. McGenity, M. Steinke, A. J. Hills, and D. J. Suggett. Application of a fast isoprene sensor (FIS) for measuring isoprene production from marine samples. *Limnology and Oceanography: Methods*, 8: 185–195, 2010.

D. A. Exton, T. J. McGenity, M. Steinke, D. J. Smith, and D. J. Suggett. Uncovering the volatile nature of tropical coastal marine ecosystems in a changing world. *Global Change Biology*, 21(4):1383–1394, 2014. doi: 10.1111/gcb.12764.

B. J. Finlayson-Pitts and J.N. Pitts. *Chemistry of the Upper and Lower Atmosphere–Theory, Experiments, and Applications*. Academic, San Diego, 2000.

E. V. Fischer, D. J. Jacob, R. M. Yantosca, M. P. Sulprizio, D. B. Millet, J. Mao, F. Paulot, H. B. Singh, A. Roiger, L. Ries, R. W. Talbot, K. Dzepina, and S. Pandey Deolal. Atmospheric peroxyacetyl nitrate (PAN): a global budget and source attribution. *Atmospheric Chemistry and Physics*, 14(5):2679–2698, 2014. doi: 10.5194/acp-14-2679-2014.

P. Forster, V. Ramaswamy, P. Artaxo, T. Berntsen, R. Betts, D.W. Fahey, J. Haywood, J. Lean, D.C. Lowe, G. Myhre, R. Nganga, G. Prinn, G. Raga, M. Schulz, and R. Van Dorland. *Changes in Atmospheric Constituents and in Radiative Forcing*. Cambridge University Press, Cambridge, United Kingdom and New York, NY, USA, 2007.

H. Fuchs, A. Hofzumahaus, F. Rohrer, B. Bohn, T. Brauers, H. P. Dorn, R. Haseler, F. Holland, M. Kaminski, X. Li, K. Lu, S. Nehr, R. Tillmann, R. Wegener, and A. Wahner. Experimental evidence for efficient hydroxyl radical regeneration in isoprene oxidation. *Nature Geoscience*, 6(12):1023–1026, 2013. doi: 10.1038/ngeo1964.

L. Ganzeveld. Manual for the stand-alone version of the Multi-Layer Canopy CHemistry Exchange model (MLC-CHEM). page 15, 2013.

L. Ganzeveld and J. Lelieveld. Impact of Amazonian deforestation on atmospheric chemistry. *Geophysical Research Letters*, 31(6), 2004. doi: 10.1029/ 2003gl019205.

L. Ganzeveld, J. Valverde-Canossa, G. K. Moortgat, and R. Steinbrecher. Evaluation of peroxide exchanges over a coniferous forest in a single-column chemistry-climate model. *Atmospheric Environment*, 40:68–80, 2006. ISSN 13522310. doi: 10.1016/j.atmosenv.2006.01.062.

L. Ganzeveld, L. Bouwman, E. Stehfest, D. P. van Vuuren, B. Eickhout, and J. Lelieveld. Impact of future land use and land cover changes on atmospheric chemistry-climate interactions. *Journal of Geophysical Research*, 115(D23), 2010. doi: 10.1029/2010jd014041.

L. N. Ganzeveld. Atmosphere-biosphere trace gas exchanges simulated with a single-column model. *Journal of Geophysical Research*, 107(D16), 2002a. ISSN 0148-0227. doi: 10.1029/2001jd000684.

L. N. Ganzeveld. Atmosphere-biosphere trace gas exchanges simulated with a single-column model. *Journal of Geophysical Research*, 107(D16), 2002b. doi: 10.1029/2001jd000684.

C. Geron, A. Guenther, J. Greenberg, H.W. Loescher, D. Clark, and B. Baker.

Biogenic volatile organic compound emissions from a lowland tropical wet forest in Costa Rica. *Atmospheric Environment*, 2002(36):3793–3802, 2002.

C. Geron, S. Owen, A. Guenther, J. Greenberg, R. Rasmussen, J. Huibai, Q. Li, and B. Baker. Volatile organic compounds from vegetation in southern Yunnan Province, China: Emission rates and some potential regional implications. *Atmospheric Environment*, 40(10):1759–1773, 2006. doi: 10.1016/j.atmosenv. 2005.11.022.

C. D. Geron, R. W. Daly, R. R. Arnts, A. B. Guenther, and F. L. Mowry. Canopy level emissions of 2-methyl-3-buten-2-ol, monoterpenes, and sesquiterpenes from an experimental *Pinus taeda* plantation. *Sci Total Environ*, 565: 730–41, 2016. ISSN 1879-1026 (Electronic) 0048-9697 (Linking). doi: 10. 1016/j.scitotenv.2016.05.034. URL `http://www.ncbi.nlm.nih.gov/pubmed/27232720`.

C.D. Geron, T.E. Pierce, and A.B. Guenther. Reassessment of biogenic volatile organic compound emissions in the Atlanta area. *Atmospheric Environment*, 29(13):1569–1578, 1995.

P.D. Goldan, W.C. Kuster, F.C. Fehsenfeld, and S.A. Montzka. The observation of a C5 alcohol emission in a North American pine forest. *Geophysical Research Letters*, 20(11):1039–1042, 1993.

M.S. Goldberg, R.T. Burnett, J. Brook, J.C. Bailar, M-F. Valois, and R. Vincent. Associations between daily cause-specific mortality and concentrations of ground-level ozone in Montreal, Quebec. *American Journal of Epidemiology*, 154(9):817–826, 2001.

J. P. Greenberg, A. B. Guenther, S. Madronich, W. Baugh, P. Ginoux, A. Druilhet, R. Delmas, and C. Delon. Biogenic volatile organic compound emissions in central africa during the Experiment for the Regional Sources and Sinks

of Oxidants (EXPRESSO) biomass burning season. *Journal of Geophysical Research: Atmospheres*, 104(D23):30659–30671, 1999. ISSN 01480227. doi: 10.1029/1999jd900475.

L. Gu, T. Meyers, S. G. Pallardy, P. J. Hanson, B. Yang, M. Heuer, K. P. Hosman, J. S. Riggs, D. Sluss, and S. D. Wullschleger. Direct and indirect effects of atmospheric conditions and soil moisture on surface energy partitioning revealed by a prolonged drought at a temperate forest site. *Journal of Geophysical Research*, 111(D16), 2006. ISSN 0148-0227. doi: 10.1029/2006jd007161.

L. Gu, A. Guenther, J. E. Shilling, H. Yu, M. Huang, C. Zhao, Q. Yang, S. T. Martin, P. Artaxo, S. Kim, R. Seco, T. Stavrakou, K. M. Longo, J. Tota, R. A. F. de Souza, O. Vega, Y. Liu, M. Shrivastava, E. G. Alves, F. C. Santos, G. Leng, and Z. Hu. Airborne observations reveal elevational gradient in tropical forest isoprene emissions. *Nature Communications*, 8, 2017.

A. Guenther, C.N. Hewitt, D. Erickson, R. Fall, C. Geron, T. Graedel, P. Harley, L. Klinger, M. Lerdau, W.A. McKay, T. Pierce, B. Scholes, R. Steinbrecher, R. Tallamraju, J. Taylor, and P. Zimmerman. A global model of natural volatile organic compound emissions. *Journal of Geophysical Research*, 100(D5):8873–8892, 1995.

A. Guenther, B. Baugh, G. Brasseur, J. Greenberg, P. Harley, L. Klinger, D. Serca, and L. Vierling. Isoprene emission estimates and uncertainties for the central african EXPRESSO study domain. *Journal of Geophysical Research: Atmospheres*, 104(D23):30625–30639, 1999. doi: 10.1029/1999jd900391.

A. Guenther, T. Karl, P. Harley, C. Wiedinmyer, P.I. Palmer, and C. Geron. Estimates of global terrestrial isoprene emissions using MEGAN (Model of Emissions of Gases and Aerosols from Nature). *Atmospheric Chemistry and Physics*, 6:3181–3210, 2006.

A. B. Guenther and A. J. Hills. Eddy covariance measurement of isoprene fluxes. *Journal of Geophysical Research-Atmospheres*, 103(D11):13145–13152, 1998. doi: 10.1029/97jd03283.

A. B. Guenther, P. R. Zimmerman, P. C. Harley, R. K. Monson, and R. Fall. Isoprene and monoterpene emission rate variability: Model evaluations and sensitivity analyses. *Journal of Geophysical Research: Atmospheres*, 98(D7): 12609–12617, 1993. doi: 10.1029/93jd00527.

A. B. Guenther, X. Jiang, C. L. Heald, T. Sakulyanontvittaya, T. Duhl, L. K. Emmons, and X. Wang. The Model of Emissions of Gases and Aerosols from Nature version 2.1 (MEGAN2.1): An extended and updated framework for modeling biogenic emissions. *Geoscientific Model Development*, 5(6):1471–1492, 2012. doi: 10.5194/gmd-5-1471-2012.

L. E. Gulden, Z.-L. Yang, and G.-Y. Niu. Interannual variation in biogenic emissions on a regional scale. *Journal of Geophysical Research*, 112(D14), 2007. ISSN 0148-0227. doi: 10.1029/2006jd008231.

H. Hakola, H. Hellén, and T. Laurila. Ten years of light hydrocarbons (C2–C6) concentration measurements in background air in Finland. *Atmospheric Environment*, 40(19):3621–3630, 2006. doi: 10.1016/j.atmosenv.2005.08.019.

D. T. Hanson, S. Swanson, L. E. Graham, and T. D. Sharkey. Evolutionary significance of isoprene emission from mosses. *American Journal of Botany*, 86 (5):634–639, 1999. doi: 10.2307/2656571.

P. C. Harley, M. E. Litvak, T. D. Sharkey, and R. K. Monson. Isoprene emission from velvet bean-leaves—interactions among nitrogen availability, growth photon flux-density, and leaf development. *Plant Physiology*, 105(1):279–285, 1994.

P.C. Harley and R.K. Monson. Ecological and evolutionary aspects of isoprene emission from plants. *Oecologia*, 118:109–123, 1999.

Peter Harley, Luanne Otter, Alex Guenther, and James Greenberg. Micrometeorological and leaf-level measurements of isoprene emissions from a southern African savanna. *Journal of Geophysical Research: Atmospheres*, 108(D13), 2003. doi: 10.1029/2002jd002592.

D.L. Hartmann, M. Klein Tank, A.M.G. andRusticucci, L.V. Alexander, S. Bronnimann, Y. Charabi, F.J. Dentener, E.J. Dlugokencky, D.R. Easterling, A. Kaplan, B.J. Soden, P.W. Thorne, M. Wild, and P.M. Zhai. *Climate Change 2013: The Physical Science Basis. Contribution of Working Group I to the Fifth Assessment Report of the Intergovernmental Panel on Climate Change.* Canbridge University Press, Cambridge, United Kingdom and New York NY, USA, 2014.

S. Hayward, C. N. Hewitt, J. H. Sartin, and S. M. Owen. Performance characteristics and applications of a proton transfer reaction-mass spectrometer for measuring volatile organic compounds in ambient air. *Environmental Science and Technology*, 36:1554–1560, 2002.

C. He, F. Murray, and T. Lyons. Seasonal variations in monoterpene emissions from Eucalyptus species. *Chemosphere: Global Change Science*, 2:65–76, 2000.

D. E. Heard. *Analytical Techniques for Atmospheric Measurement*. Blackwell Publishing, 2006.

D.A. Herbert, J.H. Fownes, and P.M. Vitousek. Hurricane damage to a Hawaiian forest: Nutrient supply rate affects resistance and resilience. *Ecology*, 80(3): 908–926, 1999.

C. N. Hewitt, K. Ashworth, A. Boynard, A. Guenther, B. Langford, A. R. MacKenzie, P. K. Misztal, E. Nemitz, S. M. Owen, M. Possell, T. A. M.

Pugh, A. C. Ryan, and O. Wild. Ground-level ozone influenced by circadian control of isoprene emissions. *Nature Geoscience*, 4(10):671–674, 2011. doi: 10.1038/ngeo1271.

Ed. Hewitt, C. *Reactive Hydrocarbons in the Atmosphere*. Academic Press, San Diego, CA, 1998.

R. Hill and A.B. Davis. Aborigines and fire in the wet tropics of Queensland, Australia: Ecosystem management across cultures. *Society & Natural Resources*, 12(3):205–223, 1999. doi: 10.1080/089419299279704.

R. Hill and A.B. Davis. Kuku-Yalanji rainforest aboriginal people and carbohydrate resource management in the wet tropics of queensland, australia. *Human Ecology*, 31(1):27–52, 2003.

A. J. Hills. *Fast Isoprene Sensor Operation Manual*. Hills Scientific, 2013.

A. J. Hills and P.R. Zimmerman. Isoprene measurement by ozone-induced chemiluminescence. *Analytical Chemistry*, 62:1055–1060, 1990.

R. Hoff and S. Christopher. Remote sensing of particulate pollution from space: Have we reached the promised land? *Journal of the Air & Waste Management Association*, 59(6):645–675, 2009. ISSN 1047-3289. doi: 10.3155/1047-3289.59. 6.645.

L. Huang, E. C. McDonald-Buller, G. McGaughey, Y. Kimura, and D. T. Allen. Annual variability in leaf area index and isoprene and monoterpene emissions during drought years in Texas. *Atmospheric Environment*, 92:240–249, 2014. ISSN 13522310. doi: 10.1016/j.atmosenv.2014.04.016.

K. Jardine, A. Yañez Serrano, A. Arneth, L. Abrell, A. Jardine, J. van Haren, P. Artaxo, L. V. Rizzo, F. Y. Ishida, T. Karl, J. Kesselmeier, S. Saleska, and T. Huxman. Within-canopy sesquiterpene ozonolysis in Amazonia. *Journal of Geophysical Research*, 116(D19), 2011. doi: 10.1029/2011jd016243.

K. J. Jardine, K. Meyers, L. Abrell, E. G. Alves, A. M. Yanez Serrano, J. Kesselmeier, T. Karl, A. Guenther, C. Vickers, and Jeffrey Q. Chambers. Emissions of putative isoprene oxidation products from mango branches under abiotic stress. *Journal of Experimental Botany*, 64(12):3369–3679, 2013.

H.E. Jeffries, R.M. Kamens, and K. Sexton. Early history and rationale for outdoor chamber work at the University of North Carolina. *Environmental Chemistry*, 10(4):349, 2013. doi: 10.1071/en13901.

T. Karl, T. J. Christian, R. J. Yokelson, P. Artaxo, W. Min Hao, and A. Guenther. The tropical forest and fire emissions experiment: Method evaluation of volatile organic compound emissions measured by PTR-MS, FTIR, and GC from tropical biomass burning. *Atmospheric Chemistry and Physics Discussions*, 7(3):8755–8793, 2007.

T. Karl, A. Hansel, L. Cappellin, L. Kaser, I. Herdlinger-Blatt, and W. Jud. Selective measurements of isoprene and 2-methyl-3-buten-2-ol based on NO^+ ionization mass spectrometry. *Atmospheric Chemistry and Physics*, 12(24): 11877–11884, 2012. doi: 10.5194/acp-12-11877-2012.

J. Kesselmeier, U. Kuhn, A. Wolf, M.S. Andrea, P. Ciccioli, E. Brancaleoni, M. Frattoni, A. Guenther, J. Greenberg, P. De Castro Vasconcellos, T. de Oliva, T. Tavares, and P. Artaxo. Atmospheric volatile organic compounds (VOC) at a remote tropical forest site in central Amazonia. *Atmospheric Environment*, 34:4063–4072, 2000.

A. Keto and K. Scott. *Tropical Rainforests of North Queensland, their Conservation and Significance*. Special Australia Heritage Publications No. 3. Australian Government Publishing Service, Canberra, 1986.

J. H. Kroll, N. Ng, S.M. Murphy, R.C. Flagan, and J.H. Seinfeld. Secondary

organic aerosol formation from isoprene photooxidation. *Environmental Science and Technology*, 40:1869–1877, 2006.

U. Kuhn, S. Rottenberger, T. Biesenthal, A. Wolf, G. Schebeske, P. Ciccioli, E. Brancaleoni, M. Frattoni, T. Tavares, and J. Kesselmeier. Isoprene and monoterpene emissions of Amazonian tree species during the wet season: Direct and indirect investigations on controlling environmental functions. *Journal of Geophysical Research*, 107(D20), 2002. doi: 10.1029/2001jd000978.

U. Kuhn, M. O. Andreae, C. Ammann, A.C. Araújo, E. Brancaleoni, P. Ciccioli, T. Dindorf, M. Frattoni, L.V. Gatti, L. Ganzeveld, B. Kruijt, J. Lelieveld, J. Lloyd, F.X. Meixner, A.D. Nobre, U. Poschl, C. Spirig, P. Stefani, A. Thielmann, R. Valentini, and J. Kesselmeier. Isoprene and monoterpene fluxes from Central Amazonian rainforest inferred from tower-based and airborne measurements, and implications on the atmopsheric chemistry and the local carbon budget. *Atmospheric Chemistry and Physics*, 7:2855–2879, 2007.

B. Langford, B. Davison, E. Nemitz, and C. N. Hewitt. Mixing ratios and eddy covariance flux measurements of volatile organic compounds from an urban canopy (Manchester, UK). *Atmos. Chem. Phys.*, 9:1971–1987, 2009.

B. Langford, P. K. Misztal, E. Nemitz, B. Davison, C. Helfter, T. A. M. Pugh, A. R. MacKenzie, S. F. Lim, and C. N. Hewitt. Fluxes and concentrations of volatile organic compounds from a South-East Asian tropical rainforest. *Atmospheric Chemistry and Physics*, 10(17):8391–8412, 2010. doi: 10.5194/acp-10-8391-2010.

J. Laothawornkitkul, J. E. Taylor, N. D. Paul, and C. N. Hewitt. Biogenic volatile organic compounds in the earth system. *New Phytol*, 183(1):27–51, 2009. doi: 10.1111/j.1469-8137.2009.02859.x.

W.F. Laurance, T.E. Lovejoy, H.L. Vasconcelos, E.M. Bruno, R.K. Didham, P.C.

Stouffer, C. Gascon, R.O. Bierregaard, S.G. Laurance, and E. Sampaio. Ecosystem decay of Amazonian forest fragments: A 22-year investigation. *Conservation Biology*, 16(3):605–618, 2002.

A. Lee, A.H. Goldstein, J.H. Kroll, N.L. Ng, V. Varutbangkul, R.C. Flagan, and J. H. Seinfeld. Gas-phase products and secondary aerosol yields from the photooxidation of 16 different terpenes. *Journal of Geophysical Research*, 111 (D17), 2006. doi: 10.1029/2006jd007050.

J. Lelieveld, T. M. Butler, J. N. Crowley, T. J. Dillon, H. Fischer, L. Ganzeveld, H. Harder, M. G. Lawrence, M. Martinez, D. Taraborrelli, and J. Williams. Atmospheric oxidation capacity sustained by a tropical forest. *Nature*, 452 (7188):737–40, 2008. doi: 10.1038/nature06870.

C. Leue, M. Wenig, T. Wagner, Oliver Klimm, U. Platt, and B. Jahne. Quantitative analysis of noxemissions from global ozone monitoring experiment satellite image sequences. *Journal of Geophysical Research: Atmospheres*, 106(D6): 5493–5505, 2001. ISSN 01480227. doi: 10.1029/2000jd900572.

R. Leuning, F. M. Kelliher, D. G. G. De Pury, and E.-D. Schulze. Leaf nitrogen, photosynthesis, conductance and transpiration: scaling from leaves to canopies. *Plant, Cell and Environment*, 18:1183–1200, 1995.

M. Liddell, 2013. URL `http://www.supersites.net.au/knb/metacat/lloyd.416.30/html`.

M. Liddell, 2014. URL `http://www.supersites.net.au/knb/metacat/lloyd.662.9/html`.

M. Liddell and S. Laurance, 2015. URL `http://www.supersites.net.au/knb/metacat/supersite.238.11/html`.

H-J. Lim, A.G. Carlton, and B.J. Turpin. Isoprene forms secondary organic

aerosol through cloud processing: model simulations. *Environmental Science and Technology*, 39:4441–4446, 2005.

Y.-J. Lim, A. Armendariz, Y.-S. Son, and J.-C. Kim. Seasonal variations of isoprene emissions from five oak tree species in East Asia. *Atmospheric Environment*, 45(13):2202–2210, 2011. doi: 10.1016/j.atmosenv.2011.01.066.

J. Llusia, J. Sardans, U. Niinemets, S. M. Owen, and J. Penuelas. A screening study of leaf terpene emissions of 43 rainforest species in Danum Valley Conservation Area (Borneo) and their relationships with chemical and morphological leaf traits. *Plant Biosystems*, 148(2):307–317, 2014. doi: 10.1080/11263504.2013.770803.

F. Loreto and S. Fineschi. Reconciling functions and evolution of isoprene emission in higher plants. *New Phytologist*, 206(2):578–82, 2015. doi: 10.1111/nph. 13242.

F. Loreto and J. P. Schnitzler. Abiotic stresses and induced BVOCs. *Trends Plant Sci*, 15(3):154–66, 2010. doi: 10.1016/j.tplants.2009.12.006.

A. R. MacKenzie, B. Langford, T. A. Pugh, N. Robinson, P. K. Misztal, D. E. Heard, J. D. Lee, A. C. Lewis, C. E. Jones, J. R. Hopkins, G. Phillips, P. S. Monks, A. Karunaharan, K. E. Hornsby, V. Nicolas-Perea, H. Coe, A. M. Gabey, M. W. Gallagher, L. K. Whalley, P. M. Edwards, M. J. Evans, D. Stone, T. Ingham, R. Commane, K. L. Furneaux, J. B. McQuaid, E. Nemitz, Y. K. Seng, D. Fowler, J. A. Pyle, and C. N. Hewitt. The atmospheric chemistry of trace gases and particulate matter emitted by different land uses in Borneo. *Philosophical Transactions of the Royal Society of London B: Biological Sciences*, 366(1582):3177–95, 2011. doi: 10.1098/rstb.2011.0053.

E. A. Marais, D. J. Jacob, T. P. Kurosu, K. Chance, J. G. Murphy, C. Reeves, G. Mills, S. Casadio, D. B. Millet, M. P. Barkley, F. Paulot, and J. Mao.

Isoprene emissions in Africa inferred from OMI observations of formaldehyde columns. *Atmospheric Chemistry and Physics*, 12(14):6219–6235, 2012. doi: 10.5194/acp-12-6219-2012. ACP.

E. A. Marais, D. J. Jacob, A. Guenther, K. Chance, T. P. Kurosu, J. G. Murphy, C. E. Reeves, and H. O. T. Pye. Improved model of isoprene emissions in Africa using OMI satellite observations of formaldehyde: implications for oxidants and particulate matter. *Atmospheric Chemistry and Physics Discussions*, 14 (5):6951–6979, 2014. doi: 10.5194/acpd-14-6951-2014.

C. A. Marandino, S. Tegtmeier, K. Krüger, C. Zindler, E. L. Atlas, F. Moore, and H. W. Bange. Dimethylsulphide (DMS) emissions from the western Pacific Ocean: a potential marine source for stratospheric sulphur? *Atmospheric Chemistry and Physics*, 13(16):8427–8437, 2013. ISSN 1680-7324. doi: 10. 5194/acp-13-8427-2013.

Dylan B. Millet, Daniel J. Jacob, K. Folkert Boersma, Tzung-May Fu, Thomas P. Kurosu, Kelly Chance, Colette L. Heald, and Alex Guenther. Spatial distribution of isoprene emissions from North America derived from formaldehyde column measurements by the OMI satellite sensor. *Journal of Geophysical Research*, 113(D2), 2008. ISSN 0148-0227. doi: 10.1029/2007jd008950.

P. S. Monks, C. Granier, S. Fuzzi, A. Stohl, M. L. Williams, H. Akimoto, M. Amann, A. Baklanov, U. Baltensperger, I. Bey, N. Blake, R. S. Blake, K. Carslaw, O. R. Cooper, F. Dentener, D. Fowler, E. Fragkou, G. J. Frost, S. Generoso, P. Ginoux, V. Grewe, A. Guenther, H. C. Hansson, S. Henne, J. Hjorth, A. Hofzumahaus, H. Huntrieser, I. S. A. Isaksen, M. E. Jenkin, J. Kaiser, M. Kanakidou, Z. Klimont, M. Kulmala, P. Laj, M. G. Lawrence, J. D. Lee, C. Liousse, M. Maione, G. McFiggans, A. Metzger, A. Mieville, N. Moussiopoulos, J. J. Orlando, C. D. O'Dowd, P. I. Palmer, D. D. Parrish, A. Petzold, U. Platt, U. Pöschl, A. S. H. Prévôt, C. E. Reeves,

S. Reimann, Y. Rudich, K. Sellegri, R. Steinbrecher, D. Simpson, H. ten
Brink, J. Theloke, G. R. van der Werf, R. Vautard, V. Vestreng, Ch Vla-
chokostas, and R. von Glasow. Atmospheric composition change – global and
regional air quality. *Atmospheric Environment*, 43(33):5268–5350, 2009. doi:
10.1016/j.atmosenv.2009.08.021.

R. K. Monson, N. Trahan, T. N. Rosenstiel, P. Veres, D. Moore, M. Wilkinson,
R. J. Norby, A. Volder, M. G. Tjoelker, D. D. Briske, D. F. Karnosky, and
R. Fall. Isoprene emission from terrestrial ecosystems in response to global
change: Minding the gap between models and observations. *Philos Trans A
Math Phys Eng Sci*, 365(1856):1677–95, 2007. doi: 10.1098/rsta.2007.2038.

R. K. Monson, R. T. Jones, T. N. Rosenstiel, and J. P. Schnitzler. Why only
some plants emit isoprene. *Plant Cell Environ*, 36(3):503–16, 2013. doi: 10.
1111/pce.12015.

J.-F. Muller, T. Stavrakou, S. Wallens, I. De Smedt, M. Van Roozendael, M.J.
Potosnak, J. Rinne, B. Munger, A. Goldstein, and A.B. Guenther. Global
isoprene emissions estimated using MEGAN, ECMWF analyses and a detailed
canopy environment model. *Atmospheric Chemistry and Physics*, 8:1329–1341,
2008.

R. B. Myneni, W. Yang, R. R. Nemani, A. R. Huete, R. E. Dickinson,
Y. Knyazikhin, K. Didan, R. Fu, R. I. Negron Juarez, S. S. Saatchi,
H. Hashimoto, K. Ichii, N. V. Shabanov, B. Tan, P. Ratana, J. L. Privette, J. T.
Morisette, E. F. Vermote, D. P. Roy, R. E. Wolfe, M. A. Friedl, S. W. Running,
P. Votava, N. El-Saleous, S. Devadiga, Y. Su, and V. V. Salomonson. Large
seasonal swings in leaf area of Amazon rainforests. *Proceedings of the National
Academy of Sciences*, 104(12):4820–4823, 2007. doi: 10.1073/pnas.0611338104.

U. Niinemets. Mild versus severe stress and BVOCs: thresholds, priming
and consequences. *Trends Plant Sci*, 15(3):145–53, 2010. ISSN 1878-4372

(Electronic) 1360-1385 (Linking). doi: 10.1016/j.tplants.2009.11.008. URL `https://www.ncbi.nlm.nih.gov/pubmed/20006534`.

Daintree Rainforest Observatory. DRO crane plot tree species list, 2014.

R. Ostertag, W.L Silver, and A.E. Lugo. Factors affecting mortality and resistance to damage following hurricanes in a rehabilitated subtropical moist forest. *Biotropica*, 37(1):16–24, 2005.

F. Pacifico, S. P. Harrison, C. D. Jones, and S. Sitch. Isoprene emissions and climate. *Atmospheric Environment*, 43(39):6121–6135, 2009. doi: 10.1016/j. atmosenv.2009.09.002.

P. Padhy and C. Varshney. Isoprene emission from tropical tree species. *Environmental Pollution*, 135(1):101–109, 2005a. doi: 10.1016/j.envpol.2004.10.003.

P. K. Padhy and C. K. Varshney. Emission of volatile organic compounds (VOC) from tropical plant species in India. *Chemosphere*, 59(11):1643–1653, 2005b. doi: 10.1016/j.chemosphere.2005.01.046.

P. I. Palmer, D. J. Jacob, K. Chance, R. V. Martin, R. J. D. Spurr, T. P. Kurosu, I. Bey, R. Yantosca, A. Fiore, and Q. Li. Air mass factor formulation for spectroscopic measurements from satellites: Application to formaldehyde retrievals from the Global Ozone Monitoring Experiment. *Journal of Geophysical Research: Atmospheres*, 106(D13):14539–14550, 2001. ISSN 01480227. doi: 10.1029/2000jd900772.

P. I. Palmer, D. J. Jacob, A. M. Fiore, and R. V. Martin. Mapping isoprene emissions over North America using formaldehyde column observations from space. *Journal of Geophysical Research*, 108(D6), 2003. ISSN 0148-0227. doi: 10.1029/2002jd002153.

P. I. Palmer, D. S. Abbot, T.-M. Fu, D. J. Jacob, K. Chance, T. P. Kurosu, A. Guenther, C. Wiedinmyer, J. C. Stanton, M. J. Pilling, S. N. Pressley,

B. Lamb, and A. L. Sumner. Quantifying the seasonal and interannual variability of North American isoprene emissions using satellite observations of the formaldehyde column. *Journal of Geophysical Research*, 111(D12), 2006. ISSN 0148-0227. doi: 10.1029/2005jd006689.

P. I. Palmer, M. P. Barkley, T. P. Kurosu, A. C. Lewis, J. E. Saxton, K. Chance, and L. V. Gatti. Interpreting satellite column observations of formaldehyde over tropical South America. *Philos Trans A Math Phys Eng Sci*, 365(1856): 1741–51, 2007. ISSN 1364-503X (Print) 1364-503X (Linking). doi: 10.1098/ rsta.2007.2042. URL `https://www.ncbi.nlm.nih.gov/pubmed/17513262`.

M. Pippin, S. Bertman, T. Thornberry, M. Town, M. A. Carroll, and S. Sillman. Seasonal variations of PAN, PPN, and O_3 at the upper Midwest PROPHET site. *Journal of Geophysical Research: Atmospheres*, 106(D20):24451–24463, 2001. doi: 10.1029/2001jd900222.

O. Pokorska, J. Dewulf, C. Amelynck, N. Schoon, M. Šimpraga, K. Steppe, and H. Van Langenhove. Isoprene and terpenoid emissions from *Abies alba*: Identification and emission rates under ambient conditions. *Atmospheric Environment*, 59:501–508, 2012. doi: 10.1016/j.atmosenv.2012.04.061.

M. J. Potosnak, B. M. Baker, L. LeStourgeon, S. M. Disher, K. L. Griffin, M. S. Bret-Harte, and G. Starr. Isoprene emissions from a tundra ecosystem. *Biogeosciences*, 10(2):871–889, 2013. doi: 10.5194/bg-10-871-2013.

M.J. Potosnak, L. LeStourgeon, S.G. Pallardy, K.P. Hosman, L. Gu, T. Karl, C. Geron, and A.B. Guenther. Observed and modeled ecosystem isoprene fluxes from an oak-dominated temperate forest and the influence of drought stress. *Atmospheric Environment*, 84:314–322, 2014. doi: 10.1016/j.atmosenv. 2013.11.055.

Shelley Pressley. Long-term isoprene flux measurements above a northern

hardwood forest. *Journal of Geophysical Research*, 110(D7), 2005. doi: 10.1029/2004jd005523.

T. A. M. Pugh, A. R. MacKenzie, B. Langford, E. Nemitz, P. K. Misztal, and C. N. Hewitt. The influence of small-scale variations in isoprene concentrations on atmospheric chemistry over a tropical rainforest. *Atmospheric Chemistry and Physics*, 11(9):4121–4134, 2011. doi: 10.5194/acp-11-4121-2011.

R.A. Rasmussen. Isoprene: Identified as a forest-type emission to the atmosphere. *Environmental Science and Technology*, 4(8):667–671, 1970.

R.A. Rasmussen and F.W. Went. Volatile organic material of plant origin in the atmosphere. *Proceedings of the National Academy of Sciences of the United States of America*, 53, 1965.

H.J.I. Rinne, A.B. Guenther, J.P. Greenberg, and P.C. Harley. Isoprene and monoterpene fluxes measured above Amazonian rainforest and their dependence on light and temperatures. *Atmospheric Environment*, 36:2421–2426, 2002.

T. N. Rosenstiel, M. Potosnak, K. L. Griffin, R. Fall, and R. K. Monson. Increased CO_2 uncouples growth from isoprene emission in an agriforest ecosystem. *Nature*, 421(6920):256–259, 2003. doi: 10.1038/nature01351.

Rupert Russell. *Daintree: Where the Rainforest Meets the Reef.* Weldon & The Australian Conservation Foundation, 1985.

M. Salby and H. Hendon. Intraseasonal behavior of clouds, temperature, and motion in the tropics. *Journal of the Atmospheric Sciences*, 51(15):18, 1994.

G.A. Sanadze. Nature of gaesous substances from the *Robinia pseudoacacia* leaves. *Rep. Akad. Nauk. Gruz SSR (Bulletin of the Academy of Sciences of the USSR)*, 19:83–86, 1957.

M. G. Sanderson, C. D. Jones, W. J. Collins, C. E. Johnson, and R. G. Derwent. Effect of climate change on isoprene emissions and surface ozone levels. *Geophysical Research Letters*, 30(18):4, 2003. doi: 10.1029/2003gl017642.

P.A. Scholefield, K.J. Doick, B.M. Herbert, C. N. Hewitt, J. P. Schnitzler, P. Pinelli, and F. Loreto. Impact of rising CO_2 on emissions of volatile organic compounds: Isoprene emission from *Phragmites australis* growing at elevated CO_2 in a natural carbon dioxide spring. *Plant, Cell & Environment*, 27: 393–401, 2004.

J. Schwender, J. Zeidler, R. Groner, C. Muller, M. Focke, S. Braun, F. W. Lichtenthaler, and H. K. Lichtenthaler. Incorporation of 1-deoxy-d-xylulose into isoprene and phytol by higher plants and algae. *FEBS Letters*, 414(1):129–134, 1997. doi: Doi10.1016/S0014-5793(97)01002-8.

D. J. Seidel, C. O. Ao, and K. Li. Estimating climatological planetary boundary layer heights from radiosonde observations: Comparison of methods and uncertainty analysis. *Journal of Geophysical Research*, 115(D16113):15, 2010. doi: 10.1029/2009D013680.

John H. Seinfeld and Spyros N. Pandis. *Atmospheric Chemistry and Physics: From Air Pollution to Climate Change*. Wiley-Blackwell, 1st edition, 1997.

John H. Seinfeld and Spyros N. Pandis. *Atmospheric Chemistry and Physics: From Air Pollution to Climate Change*. Wiley-Blackwell, 2nd edition, 2006. ISBN 978-0471720188.

B. Seok, D. Helmig, L. Ganzeveld, M. W. Williams, and C. S. Vogel. Dynamics of nitrogen oxides and ozone above and within a mixed hardwood forest in northern Michigan. *Atmospheric Chemistry and Physics*, 13(15):7301–7320, 2013. doi: 10.5194/acp-13-7301-2013.

D. Serça, A. Guenther, L. Klinger, L. Vierling, P. Harley, A. Druilhet, J. Greenberg, B. Baker, W. Baugh, C. Bouka-Biona, and J. Loemba-Ndembi. EXPRESSO flux measurements at upland and lowland Congo tropical forest site. *Tellus*, 53B:220–234, 2001.

T. D. Sharkey and F. Loreto. Water stress, temperature, and light effects on the capacity for isoprene emission and photosynthesis of kudzu leaves. *Oecologia*, 95(3):328–333, 1993. doi: 10.1007/Bf00320984.

T. D. Sharkey and R. K. Monson. The future of isoprene emission from leaves, canopies and landscapes. *Plant Cell and Environment*, 37(8):1727–40, 2014. doi: 10.1111/pce.12289.

T. D. Sharkey and S. S. Yeh. Isoprene emission from plants. *Annual Review of Plant Physiology and Plant Molecular Biology*, 52:407–436, 2001. doi: 10.1146/annurev.arplant.52.1.407.

T. D. Sharkey, A. E. Wiberley, and A. R. Donohue. Isoprene emission from plants: Why and how. *Annals of Botany*, 101(1):5–18, 2008. doi: 10.1093/aob/mcm240.

T.D. Sharkey, S. Yeh, A.E. Wiberley, T.G. Falbel, D. Gong, and D.E. Fernandez. Evolution of the isoprene biosynthetic pathway in kudzu. *Plant Physiology*, 137:700–712, 2005.

Thomas D. Sharkey. The future of isoprene research. *Bulletin of the Georgian National Academy of Sciences*, 3(3):8, 2009.

G. M. Silver and R. Fall. Enzymatic-synthesis of isoprene from dimethylallyl diphosphate in aspen leaf extracts. *Plant Physiology*, 97(4):1588–1591, 1991. doi: 10.1104/Pp.97.4.1588.

G.W. Staben and K.G. Evans. Estimates of tree canopy loss as a result of Cyclone

Monica, in the Magela Creek catchment northern Australia. *Austral Ecology*, 33:562–569, 2008.

T. Stavrakou, J. F. Muller, I. De Smedt, M. Van Roozendael, G. R. van der Werf, L. Giglio, and A. Guenther. Evaluating the performance of pyrogenic and biogenic emission inventories against one decade of space-based formaldehyde columns. *Atmospheric Chemistry and Physics*, 9(3):1037–1060, 2009.

T. Stavrakou, J. F. Müller, M. Bauwens, I. De Smedt, M. Van Roozendael, A. Guenther, M. Wild, and X. Xia. Isoprene emissions over Asia 1979-2012: Impact of climate and land-use changes. *Atmospheric Chemistry and Physics*, 14(9):4587–4605, 2014. doi: 10.5194/acp-14-4587-2014.

D. Stone, M. J. Evans, P. M. Edwards, R. Commane, T. Ingham, A. R. Rickard, D. M. Brookes, J. Hopkins, R. J. Leigh, A. C. Lewis, P. S. Monks, D. Oram, C. E. Reeves, D. Stewart, and D. E. Heard. Isoprene oxidation mechanisms: measurements and modelling of OH and HO_2 over a South-East Asian tropical rainforest during the OP3 field campaign. *Atmospheric Chemistry and Physics*, 11(13):6749–6771, 2011. doi: 10.5194/acp-11-6749-2011.

Nigel Stork and Eds. Turton, S. M. *Living in a Dynamic Tropical Forest Landscape*. Wiley-Blackwell, 2008. ISBN 978-1-4051-5643-1.

Nigel E. Stork. Australian tropical forest canopy crane: New tools for new frontiers. *Austral Ecology*, 32:4–9, 2008. doi: 10.1111/j.1422-9993.2007.01740.

R.K. Talukdar, J.B. Burkholder, A-M. Schmoltner, J.M. Roberts, R.R. Wilson, and A.R. Ravishankara. Investigation of the loss processes for peroxyacetyl nitrate in the atmosphere: UV photolysis and reaction with OH. *Journal of Geophysical Research*, 100(D7):163–173, 1995.

P. Tambunan, S. Baba, A. Kuniyoshi, H. Iwasaki, T. Nakamura, H. Yamasaki,

and H. Oku. Isoprene emission from tropical trees in Okinawa Island, Japan. *Chemosphere*, 65(11):2138–44, 2006. doi: 10.1016/j.chemosphere.2006.06.013.

D. Taraborrelli, M. G. Lawrence, J. N. Crowley, T. J. Dillon, S. Gromov, C. B. M. Groß, L. Vereecken, and J. Lelieveld. Hydroxyl radical buffered by isoprene oxidation over tropical forests. *Nature Geoscience*, 5(3):190–193, 2012. doi: 10.1038/ngeo1405.

A.B. Tawfik, R. Stockli, A. Goldstein, S. Pressley, and A.L. Steiner. Quantifying the contribution of environmental factors to isoprene flux interannual variability. *Atmospheric Environment*, 54(0):216–224, 2012. doi: 10.1016/j.atmosenv.2012.02.018.

D.T. Tingey, R. Evans, and M. Gumpertz. Effects of envrionmental conditions on isoprene emission from live oak. *Planta*, 152:565–570, 1981.

J.G. Tracey. *The vegetation of the humid tropical region of North Queensland.* CSIRO: Melbourne, 1982.

A. C. T. Turner. *Australian Agricultural Assessment 2001: National Land & Water Resources Audit.* Commonweath of Australia, 2001.

S.R. Turns. *An introduction to combustion-concepts and applications.* McGraw-Hill, Inc., New York, 1996.

S.M. Turton. Landscape-scale impacts of cyclone Larry on the forests of northeast Australia, including comparisons with previous cyclones impacting the region between 1858 and 2006. *Austral Ecology*, 33:409–416, 2008.

UNESCO. Wet Tropics of Queensland - UNESCO World Heritage Centre, 2014. URL `http://whc.unesco.org/en/list/486`.

S. Vaughan, T. Ingham, L. K. Whalley, D. Stone, M. J. Evans, K. A. Read, J. D. Lee, S. J. Moller, L. J. Carpenter, A. C. Lewis, Z. L. Fleming, and D. E.

Heard. Seasonal observations of OH and HO$_2$ in the remote tropical marine boundary layer. *Atmospheric Chemistry and Physics*, 12(4):2149–2172, 2012. ISSN 1680-7324. doi: 10.5194/acp-12-2149-2012.

C. E. Vickers, M. Possell, C. I. Cojocariu, V. B. Velikova, J. Laothawornkitkul, A. Ryan, P. M. Mullineaux, and C. Nicholas Hewitt. Isoprene synthesis protects transgenic tobacco plants from oxidative stress. *Plant, Cell and Environment*, 32(5):520–31, 2009. doi: 10.1111/j.1365-3040.2009.01946.x.

Y.-F. Wang, S.M. Owen, Q.-J. Li, and J. Peñuelas. Monoterpene emissions from rubber trees (*Hevea brasiliensis*) in a changing landscape and climate: chemical speciation and environmental control. *Global Change Biology*, 13(11):2270–2282, 2007. doi: 10.1111/j.1365-2486.2007.01441.x.

Edward L. Webb, Joshua O. Seamon, and Siaifoi Fa'aumu. Frequent, low-amplitude disturbances drive high tree turnover rates on a remote, cyclone-prone polynesian island. *Journal of Biogeography*, 38(7):1240–1252, 2011. doi: 10.1111/j.1365-2699.2011.02505.x.

F.W. Went. Organic matter in the atmosphere and its possible relation to petroleum formation. *Proceedings of the National Academy of Sciences of the United States of America*, 46:212–221, 1960.

A. E. Wiberley, A.R. Linskey, T.G. Falbel, and T.D. Sharkey. Development of the capacity for isoprene emission in kudzu. *Plant, Cell & Environment*, 28:898–905, 2005.

A.J. Winters, M.A. Adams, T.M. Bleby, H. Rennenberg, D. Steigner, R. Steinbrecher, and J. Kreuzwieser. Emissions of isoprene, monoterpene and short-chained carbonyl compounds from *Eucalyptus spp.* in southern Australia. *Atmospheric Environment*, 43(19):3035–3043, 2009. doi: 10.1016/j.atmosenv. 2009.03.026.

A. M. Yañez Serrano, A. C. Nolscher, J. Williams, S. Wolff, E. Alves, G. A. Martins, E. Bourtsoukidis, J. Brito, K. Jardine, P. Artaxo, and J. Kesselmeier. Diel and seasonal changes of biogenic volatile organic compounds within and above an Amazonian rainforest site. *Atmospheric Chemistry and Physics Discussions*, 14(21):29159–29208, 2014. doi: 10.5194/acpd-14-29159-2014.

Greg Yarwood, Gary Z. Whitten, and Sandhya Rao. Updates to the Carbon Bond 4 photochemical mechanism. Report, Lake Michigan Air Directors Consortium, 2005.

C. Zhang. Madden-julian oscillation. *Reviews of Geophysics*, 43(2), 2005. doi: 10.1029/2004rg000158.

W. Zimmer, N. Bruggemann, S. Emeis, C. Giersch, A. Lehning, Steinbrecher R., and J.-P. Schnitzler. Process-based modelling of isoprene emission by oak leaves. *Plant, Cell and Environment*, 23:585–595, 2000.